MASTER COPY

RANDOM VIBRATION ANALYSIS OF GRAVITY PLATFORMS SUBJECTED TO WIND-GENERATED WAVES AND EARTHQUAKES

A thesis submitted for the degree of

DOCTOR OF PHILOSOPHY

of the

UNIVERSITY OF SOUTHAMPTON

Faculty of Engineering and Applied Science

by Mario H. Chavez Gonzalez

September, 1979

UNIVERSITY OF SOUTHAMPTON

ABSTRACT

FACULTY OF ENGINEERING AND APPLIED SCIENCE
DEPARTMENT OF CIVIL ENGINEERING

Doctor of Philosophy

RANDOM VIBRATION ANALYSIS OF GRAVITY PLATFORMS SUBJECTED TO WIND GENERATED WAVES AND EARTHQUAKES

by Mario H. Chavez Gonzalez

In this work a methodology is proposed to perform the dynamical analysis of a concrete gravity platform, c.g.p., subjected to wind generated waves and earthquakes. Particular emphasis is put on the prediction of the so-called long-term structural responses, i.e. the probable responses during and beyond the structure proposed lifetime. The uncertainties on the properties of the material of the structure, the ones related to the supporting soil, as well as the ones associated to the mentioned environmental loads, are taken into consideration in the proposed methodology.

An important feature of the methodology is that it allows to carry out parametrical studies aiming to determine not only the structural responses of interest but also to define in a statistical sense the relative influence of each of the parameters in those responses. An application of the proposed methodology is presented.

A parametrical study on the maximum responses of a concrete gravity platform located in the North Sea was carried out. The parameters included were: Youngs modulus and critical damping of the reinforced concrete, soil media idealization and soil shear modulus, wave and seismic excitation. A seismic risk analysis for the platform site was performed because of the lack of seismic information of the North Sea region. The responses considered here were the deck displacement, the base shear force and the overturning moment.

The study showed that the uncertainties about the mentioned excitations provide the largest contribution in the dispersion values of the responses. The mean values of the long-term responses were about 30 % higher than the short-term ones for the considered case. This shows the importance of their computation as an important step in the assessment of the dynamical behaviour of this type of structures.

This work is dedicated to the memory of my late mother who made me understand the importance of mind training.

ACKNOWLEDGEMENTS

I would like to express my gratitude to Dr. C.A. Brebbia for his supervision and encouragement throughout the course of this study.

I also wish to thank Mr. B. Martinez R. and Dr. Ayala M. for their useful criticisms and revision of this work, as well as Drs. L. Esteva M. and H. Contreras for the helpful discussions I had with them. Many thanks are due to Mr. H. Sandoval R. for lending me his plotting subroutines. All these persons are from the Institute of Engineering of the UNAM, Mexico.

To my wife, Brigitte, I am indebted for her persevering efforts in pushing me through and for her neat typing of the thesis.

Finally, I would like to express my appreciation to the British Council, ANUIES, CONACYT and the Bank of Mexico for awarding me scholarships during different stages of this study.

TABLE OF CONTENTS

1. INTRODUCTION

1.1 The Problem

The search and exploitation of hydrocarbons in deeper waters, as in the North Sea, have brought interest in the analysis and design of the so-called gravity platforms. In particular, the concrete gravity platforms, c.g.p., which are structures made of concrete monoliths supported directly on the sea bed, have attracted the attention of a number of researchers. The reason for this is the wide range of problems which are required to be solved in order to provide with an appropriate design for this kind of structures.

In comparison with an onshore structure, a c.g.p. is set in an environment which, apart from contributing to the loading of the former, interacts with the c.g.p. to a high degree. Among other types of environmental loads on a c.g.p. the following ones should be mentioned: waves, currents, wind, floating ice, temperature gradients and earthquakes. Waves, earthquakes and floating ice could be considered of primary importance for the design of a c.g.p. because the amplitude of the forces associated to them. However, the wind and current loading and the loads associated to temperature gradients should also be considered in the final analysis of a c.g.p..

A rigorous structural analysis of a c.g.p. should be formulated as the analysis of a three-dimensional fluid-structure-soil system. The analysis of this system could, in principle, be performed by using finite element techniques; however, there are several aspects which do not favour this global approach. Among them, the following ones may be mentioned:

1) The different kinds of uncertainties surrounding the description of the properties of the components of the system, even when they are considered separately. For example, in relation with the waves, although there are some theories which propose certain mechanisms for the wind-generated waves, it has not been possible to confirm them fully as yet. As far as the soil is concerned, there is still a bulk of its properties to be better studied and determined, in particular the ones connected with its dynamic behaviour, which are of particular relevance in the dynamic analysis of a

c.g.p.. As for the structure itself, there is a lack of knowledge about the structural properties of the concrete, including the dynamic ones and others under the field condition at sea.

From the above paragraph, it can be concluded that the data which could be input to a rather sophisticated finite element code under these conditions, will be of poor quality, therefore, the results obtained from it will be alike, and would not reflect reality.

2) Due to the characteristics of each of the components of the system to be modelled, i.e. fluid, structure and soil, the number of degrees of freedom to be used must be very high. As a consequence, this brings increases of computational costs, assuming that the computer at hand is provided with the required storage.

3) From the last incise it follows that parametrical studies are ruled out (on economical grounds).

In this work a general methodology is proposed to perform the dynamical analysis of a c.g.p. subjected to wind-generated waves and ground motions. The other environmental loads could be treated in a similar way. Particular emphasis is put on the prediction of the so-called long-term structural responses, i.e. the probable responses during and beyond the structure proposed lifetime. The uncertainties on the environmental loads, about the properties of the material of the structure, as well as those of the supporting soil, are taken into consideration in the proposed methodology.

This work consists of the following chapters: Chapter 2 treats the idealization of the structure itself by using the finite element technique. The effect of shear deformation as well as flexural deformation are included in the computation of the stiffness of the elements. The main subject of Chapter 3 is the modelling of the soil environment. It includes a general discussion of the dynamic properties of soils and also of the condition of the soils found underlying the North Sea. The different kinds of soil-foundation interaction models are discussed. Finally one of them is chosen, taking into consideration the characteristics of the North Sea soils.

The determination of the probable seismic activity for a site located in the North Sea is performed in Chapter 4 . As this is a region of mild to low seismicity, the corresponding information

is rather scarce, therefore, it was necessary to use a seismic risk model to evaluate the probable activity at a chosen site in the region. The information from this model was drawn from different sources related to the seismic activity in the region of interest and other similar regions of the world.

In Chapter 5 the modelling of the wind-generated waves is presented. It is divided in two parts: in the first part, the characteristics of the waves, including the statistical ones as well as its spectral representation are introduced. In the second part, the determination of the wave loading on c.g.p. structures is introduced.

In Chapter 6 the main results of the previous chapters are utilized to obtain the expressions to compute the dynamic response of a c.g.p. resting on rigid and flexible soils when it is subjected to seismic loading and wave loading. The chapter starts with the formulation of the governing equation for a linear structural system on rigid and on flexible soil under a general dynamic load, and the introduction of the current techniques to solve that equation. The chapter ends with the application of the previous part to the derivation of expressions to compute the dynamic response of a c.g.p. under wave loading and seismic loading when it rests on rigid soil and flexible soil.

Chapter 7 deals with the determination of the expression which will provide with the long term statistics of the dynamic response of the c.g.p. under seismic load and wave load acting separately or simultaneously. The case of a single degree of freedom is treated first, followed by the multidegree of freedom one. Then the application of these results to the case of a c.g.p. under the mentioned environmental loads is presented. Finally the effect of the uncertainties of the dynamic properties of the c.g.p. as well as the uncertainties on the environmental loads on the long-term dynamic response are presented here.

In Chapter 8 as an example of the application of the methodology introduced in the previous chapters, a parametrical study of the maximum responses of a c.g.p. located in the North Sea was carried out. In particular the expected maximum deck displacement, base shear force and overturning moment when the

platform is subjected to seismic and wave loading, acting separately or simultaneously, were computed. The influence on these responses of the uncertainties about the values of the reinforced concrete elasticity modulus and its critical damping were included. The influence on the platform dynamic response of the properties of the soil media under the platform site was also taken into consideration by varying those properties within an appropriate range. Finally the uncertainties surrounding the seismic and wave excitation at the platform site were also considered.

In Chapter 9 the conclusions about the study and for the whole work are drawn.

In Chapter 10 a list of references is presented.

2. STRUCTURAL MODELLING

2.1 Introduction

The main feature of a concrete gravity platform, c.g.p. , is the ability to keep itself stable by virtue of its own weight without making use of special anchoring. A typical c.g.p. can be described as a framed superstructure supported by a large caisson whose base lies directly on the sea bed, fig 2.1. The caisson is usually made of a number of cylindrical cells with a height varying between one half and one third of the total water depth. The number of towers forming the columns of the frame is usually two or four. These towers are built as an extension of some of the cells forming the caisson. Finally, a deck supported by the towers completes the superstructure. The caisson and the towers are usually made of concrete, whereas the deck is built of steel.

In order to assess the dynamic behaviour of a c.g.p. subjected to wave and earthquake loading, fig. 2.2, it is essential to evaluate the dynamic properties of the platform. In general, the structural topology of the c.g.p. briefly described above is rather complex. Therefore, the structural idealization is a fundamental step towards the computation of the dynamic properties of the structure, i.e. its mass, stiffness and dissipative characteristics.

The description of a structural modelling technique and its use to idealize a c.g.p. is the main objective of this chapter. The topics included are the following ones: in Section 2.2 , the governing equations for an elastic body subjected to dynamic loading and related matter is presented; Section 2.3 starts with a discussion of the displacement based finite element method, f.e.m. , the section ends with the application of this method to a beam element type of discretization; the chapter ends with the idealization of a c.g.p. subjected to a general dynamic load by using the f.e.m. .

2.2 Governing equations

The dynamical analysis of any structure requires the computation of its inertial, elastic and damping properties [2.1]*. These properties can be represented as distributed over the spacial domain of definition or concentrated at discrete points of this domain. Once one of these

* A list of references is presented in Chapter 10

representations is chosen, the external loading is usually defined to match with the former.

The computing facilities available together with the finite element techniques such as those described in [2.2,2.3] have favoured the discrete modelling of structural properties. These properties are usually represented by coefficients arranged in a matricial form. Therefore, there will be mass $\underline{M}$, stiffness $\underline{K}$ and damping $\underline{C}$ matrices corresponding to the inertial, elastic and damping properties of the idealized structure respectively. These matrices are associated to vectors made of the discrete points (known as nodal points in the finite element method): accelerations $\ddot{\underset{\sim}{U}}$, displacements $\underset{\sim}{U}$, and velocities $\dot{\underset{\sim}{U}}$ respectively, through the equation of motion of the discretized structure [2.1] i.e.:

$$\underline{M}\ \ddot{\underset{\sim}{U}} + \underline{C}\ \dot{\underset{\sim}{U}} + \underline{K}\ \underset{\sim}{U} = \underset{\sim}{P} \qquad \ldots (2.1)$$

where a dot over $\underset{\sim}{U}$ means its derivative with respect to time, and $\underline{M}$, $\underline{K}$, $\underline{C}$ and $\underset{\sim}{P}$ are defined as follows:

Mass matrix:

The elements of the mass matrix $\underline{M}$ are called the mass influence coefficients m_{ij} ; they are defined in this case as the inertia force at a nodal point i due to a unit acceleration applied at nodal point j .

Stiffness matrix:

The elements of the stiffness matrix $\underline{K}$ are called the stiffness influence coefficients k_{ij} and defined as the force corresponding to nodal point i due to a unit displacement of nodal point j .

Damping matrix:

If a viscous damping mechanism is assumed, the elements of the damping matrix $\underline{C}$ called the damping influence coefficients c_{ij} are defined as the force corresponding to nodal point i due to a unit velocity of nodal point j .

Load vector:

An element P_i of load vector $\underset{\sim}{P}$ is simply defined as the external load applied to node i . In general P_i will be a function of the spatial coordinates and time.

2.3 The finite element method

In order to compute the mass, stiffness and damping matrices which are required in the equation of motion of the discretized structure, equation (2.1), the original structure has to be idealized. In the particular case of a concrete gravity platform this can be achieved satisfactorily by using the displacement-based finite element method (f.e.m.). A brief review of this method as generally applied to structural analysis is outlined in this section and its application to a c.g.p. is presented in the following one.

The f.e.m. can be considered as a particular form of the Ritz method of analysis, through which a continuum can be discretized in such a way that its displacement field can be approximated by a finite series of displacement functions. The latter, also known as interpolation functions, satisfy the geometric boundary conditions of the system. The continuum is divided into a finite number of small elements i.e. the so-called finite elements. Neighbouring finite elements are linked to each other by nodal points selected along the boundary of the elements; the displacements of the nodal points are taken as the degrees of freedom of the resulting system of finite elements.

The f.e.m. has the advantage over other methods of analysis that continua of complex shapes and with different material properties can be approximated as a system of finite elements of simple shapes and uniform or simply varying properties. To obtain the convergence and bounding of the solutions which are characteristic of a Ritz type of analysis, the interpolation functions used in the finite elements should include the rigid body displacements and lead to uniform strain states. Finally, those functions should maintain displacement compatibility along the boundary between elements and the external boundary.

Once the continuum has been divided into a finite set of finite elements, the mass, stiffness and damping properties of each of them may be computed; their corresponding external loads aretransformed to an element load. The contribution of each of the elements to the mass, stiffness and damping matrices of the whole discretized continuum is achieved by superposing the corresponding properties of the individual elements. This superposition

is obtained by simply adding the contribution of each of the elements coinciding at a nodal point. The vector of nodal loads can be calculated by following a similar procedure.

The mass properties of an element may be computed by evaluating the kinetic energy of the element expressed as the integral of the product of the unitary mass of the material and its nodal point velocities. This integration is carried out over the domain of definition of the displacement function selected. Similarly, the stiffness properties of an element may be calculated through the evaluation of the strain energy of the element. In this case the nodal point displacements are multiplied by the elastic constants of the material, and their product is integrated over the domain of definition.

The damping properties of an element could be evaluated by techniques similar to the above-mentioned ones for the element mass and stiffness, if reliable estimates of the internal damping characteristics of the material were available. Unfortunately, this is not the case, therefore, the usual practice is to express the element damping properties as a function of the element mass, the element stiffness, or a linear combination of both element properties [2.1]. Furthermore, another common practice is to define the damping properties as a function of the so-called fraction of critical damping (Section 6.7.1) based on tests of typical full-scale structures.

From the above discussion, it can be concluded that, from the practical point of view, the mass and stiffness matrices can be determined with a relatively high level of confidence, but this is not true for the damping matrix.

Concerning the external loads, they can be transformed into a load vector by evaluating the virtual work done by the loading acting through virtual displacements of the nodal points. In the case of distributed loads, the expression for the virtual work has to be integrated over the domain of definition.

The actual application of the f.e.m. for the computation of the mass $\underline{M}$ and $\underline{K}$ matrices and the nodal load vector $\underline{P}$ of a structure should include the following steps:

a) Divide the structure into a number of finite elements connected

by their nodal points. It is assumed that only beam elements [2.4] are required to discretize the structure and that the material behaves elastically.

b) Assume an interpolation function which, after some algebra, provides with an expression that links the displacements at any point of a typical element N , with its nodal displacements, i.e.:

$$u(x,t) = \underline{A}(x)\underset{\sim}{U}_N(t) \qquad \ldots (2.2)$$

where u is the displacement seeked, $\underline{A}$ is a matrix whose elements are functions of the coordinate x , and $\underset{\sim}{U}_N$ is a vector formed by the element nodal displacements, being a function of time.

c) The strain and stress vectors for the element are given by the following strain-displacement and strain-stress relations:

$$\underset{\sim}{\varepsilon} = \underline{B}(x)\underset{\sim}{U}_N(t) \qquad \ldots (2.3)$$

$$\underset{\sim}{\sigma} = \underline{D}\ \underset{\sim}{\varepsilon} \qquad \ldots (2.4)$$

where $\underset{\sim}{\varepsilon}$ is the vector of strains, $\underline{B}$ is a matrix which is formed by derivatives of $\underline{A}$, $\underset{\sim}{\sigma}$ is the vector of stresses and $\underline{D}$ is a matrix whose components are the material elastic parameters.

d) Evaluate the kinetic energy of the element, T , to obtain the corresponding mass matrix $\underline{M}_N$ i.e.:

$$T = \frac{1}{2}\int_{Vol} m\ \dot{\underset{\sim}{u}}^T\ \dot{\underset{\sim}{u}}\ dVol \qquad \ldots (2.5)$$

where m is the mass per unit of volume of the material and $u(x,t)$ has been expressed as a vector. Substituting equation (2.2) into equation (2.5):

$$T = \frac{1}{2}\dot{\underset{\sim}{U}}_N^T\ \underline{M}_N\ \dot{\underset{\sim}{U}}_N \qquad \ldots (2.6)$$

where

$$\underline{M}_N = \int_{Vol} m\ \underline{A}^T\ \underline{A}\ dVol \qquad \ldots (2.7)$$

e) Compute the strain energy U_s of the element to derivate its stiffness matrix $\underline{K}_N$ i.e.:

$$U_s = \frac{1}{2}\int_{Vol} \underset{\sim}{\varepsilon}^T\ \underset{\sim}{\sigma}\ dVol \qquad \ldots (2.8)$$

Substituting equations (2.3) and (2.4) into (2.8) gives:

$$U_s = \frac{1}{2} \underset{\sim}{U}_N^T \underline{K}_N \underset{\sim}{U}_N \quad \ldots (2.9)$$

where

$$\underline{K}_N = \int_{Vol} \underline{B}^T \underline{D} \underline{B} \, dVol \quad \ldots (2.10)$$

f) Compute the mass $\underline{M}$ and stiffness $\underline{K}$ matrices for the whole discretized structure. The elements of both matrices can be evaluated by performing the following operations:

$$m_{ij} = \sum_1^n (m_{ij})_N \quad \ldots (2.11)$$

$$k_{ij} = \sum_1^n (k_{ij})_N \quad \ldots (2.12)$$

where n takes the value of the number of elements connected at a node.

g) Apply the boundary conditions, i.e., impose the restrictions on the relevant degrees of freedom, accordingly to the previously-specified displacement conditions.

h) Compute the load vector $\underset{\sim}{P}$. This can be achieved by first evaluating the element load vectors $\underset{\sim}{P}_N$, and then superposing their components in the appropriate nodes. An individual $\underset{\sim}{P}_N$ is obtained by using the expression for the virtual work VW done by the external loads $P_d(x,t)$, i.e.:

$$VW = \int_0^{\ell} \delta \underset{\sim}{u}^T P_d(x,t) \, dx \quad \ldots (2.13)$$

where $\delta \underset{\sim}{u}$ is the vector of virtual displacements of the element, P_d is the distributed load as a function of x and time and ℓ is the length of the element. Substituting equation (2.2) into equation (2.13), the following result is obtained:

$$VW = \underset{\sim}{U}_N^T \underset{\sim}{P}_N(t) \quad \ldots (2.14)$$

where

$$\underset{\sim}{P}_N(t) = \int_0^{\ell} \underline{A}^T(x) \, P_d(x,t) \, dx \quad \ldots (2.15)$$

2.4 Structural modelling of a concrete gravity platform

As mentioned in the introduction, a typical concrete gravity platform (c.g.p.) is composed of three parts: a cellular caisson resting on the sea bed, several towers superposed to the caisson and a deck resting on the top of the towers (fig. 2.1). The caisson and towers are usually made of concrete whereas the deck is made of steel. The dimension and design strength of the caisson are such that for analysis purposes it could be considered as a rigid body, meanwhile the towers and deck are usually designed with flexible elements as opposed to the stiffness of the caisson. The c.g.p. to be studied in this work is the one shown in fig. 2.1. This structure is symmetric with respect to the planes xy and xz; therefore, if the dynamic loading acts at one of these planes, it is only necessary to analyze its effects on one half of the structure.

Taking the above paragraphs into consideration and assuming (for the sake of simplicity in the analysis) that the motion allowed to the structure only occurs in the x - y plane, the structural topology of the c.g.p. can be discretized by using beam elements for the towers and the deck and a rigid body for the caisson, as shown in fig. 2.3.

Due to the large diameter of the cross-section of the towers, apart from the bending stiffness and translational inertia, it is necessary to include the shear and rotational effects on the beam elements used [2.5] . In [2.4] the stiffness matrix of a prismatic beam element which includes the effect of shear deformation was presented; this element will be used in this work. In [2.6] the mass matrix of the prismatic beam element, which includes the translational inertia as well as the rotational one was proposed; this mass matrix will be used here.

In order to use the prismatic beam elements to represent the part of the towers whose cross-section changes with height, equivalent prismatic elements with inertia moments resulting from averaging the inertia moments of the ends of the real structure have to be computed first. An extra simplification of the formulation is to use a lumped mass matrix (a diagonal matrix) instead of a consistent one [2.4, 2.7] . By doing so, the computational effort

is substantially reduced, without losing accuracy in the final results obtained in a dynamical analysis [2.4, 2.7] .

The idealization of the deck by using beam elements is by no means the most exhaustive one; however, it is adequate to compute the displacement of the deck, whose maximum value is particularly relevant when assessing the overall dynamic behaviour of a c.g.p. .

Once $\underline{M}_N$ and $\underline{K}_N$ have been computed, the associated element damping matrix $\underline{C}_N$ can be evaluated by using the Rayleigh damping criteria [2.1] for example, i.e.:

$$\underline{C}_N = a_0\underline{M}_N + a_1\underline{K}_N \qquad \ldots (2.16)$$

where a_0 and a_1 are proportionality factors. In the case of $\underline{C}_N$ it is also computationally convenient to neglect its off-diagonal elements. The results of this practice have proved to be satisfactory, as reported in [2.8].

Once the element matrices $\underline{M}_N$, $\underline{K}_N$, and $\underline{C}_N$ have been computed for all the elements used, the global matrices $\underline{M}$, $\underline{K}$ and $\underline{C}$ for the whole structure can be evaluated by using equations (2.11) and (2.12), for the first two matrices and an equivalent expression for the latter. Finally the nodal load vector $\underset{\sim}{P}$ for the discretized structure can be computed by superposing appropriately, at each node, the nodal loads resulting from the application of equation (2.15) for the distributed loads to the external loads which are directly applied to those nodes. In this work it will be considered that the external loads are directly applied to the nodes.

3. SOIL MODELLING

3.1 Introduction

A common assumption about the dynamical analysis of a structure is to consider that its foundation is attached to a bedrock. This assumption implies that the base of the structure does not move when an external load is applied to the superstructure; or in the case of a seismic perturbation, the foundation will experience the same displacements as the surrounding soil. In many practical situations the above-mentioned assumption is not fulfilled, i.e. the soil is not rigid but shows a capability to strain under dynamic (or static) loading. As a consequence, the relative displacements (translation and rotational) between the foundation and the surrounding soil may occur during the loading process. This means that a soil-foundation interaction effect may occur. Due to this interaction effect the stiffness and damping characteristics of the structure are usually modified. The dynamic properties of the soil may also be affected by the presence of the structure.

From the previous paragraph it can be concluded that the influence of the soil on the dynamic analysis of a structure has to be taken into consideration when the field conditions require so. This can be achieved by including the soil flexibility properties in the mathematical model used to idealize the soil-structure system. A possible way of doing so is by splitting the original problem into two parts:

a) the study of the interaction between the soil medium and the foundation,

b) the study of the dynamic response of the soil-structure system.

This chapter is devoted to the description of part a) of the problem whereas part b) will be treated in Chapter 6. As mentioned above, the dynamic properties of the soil play an important role in the soil-foundation interaction (s.f.i.) effect; therefore, it is relevant to discuss those properties separately from the soil-foundation system. This is briefly presented in Section 3.2.1. In Section 3.2.2 the general features of the North Sea soils are commented upon, meanwhile in Section 3.2.3 the behaviour observed

on those soils when supporting a concrete gravity platform is introduced. The actual modelling of the soil-foundation system is the subject of Sections3.3.1 and 3.3.2. Finally in Section 3.3.3 the soil-foundation interaction model for a concrete gravity platform located in the North Sea is discussed.

3.2 Dynamic properties of North Sea soils

3.2.1 Generalities about the dynamic behaviour of soils

The soil is a two or three phase material made up of solids, water and/or air. The state of stress of a soil can be described only if the state of stress of each of its components is known. In practice this is rather difficult to ascertain and instead,a description of the behaviour of the whole mixture has been pursued.

The mechanical behaviour of soils is a function of their initial state as described by their void ratio, degree of saturation, and state of stress. Other factors which also have an influence on the soil behaviour are the stress path, stress rate and drainage conditions. However, experimental evidence has shown that a reduced number of parameters may describe the soil behaviour satisfactorily, such parameters being the following ones: strain rate, stress path, and state of effective stresses [31].

The soil changes its structure during the process of loading, and this effect is particularly noticeable during dynamic loading in which its non-linear behaviour is clearly shown. A typical stress-strain curve obtained during the cyclic loading of a soil sample shows that after a certain number of cycles, an increasingly permanent strain appears following each cycle (in fact even after a single loading cycle). However, if the amplitude of the dynamic load is less than a certain value, after a number of cycles, little or no additional permanent strain appears, and instead a hysteresis loop is developed. As there are different kinds of soils, to assess their dynamic behaviour, laboratory and in situ tests have to be carried out for each of them. Most of the experiments on the dynamic behaviour of soils have been performed on different types of soil samples (sands, clays, silty clays, etc.) under cyclic loading, by using simple shear, triaxial,resonant column, and torsion devices as shown in [32,33,34] . From such studies it

may be concluded [31] that the following parameters characterize the soil behaviour under dynamic loads: a) the shear modulus, G , for a small amplitude cyclic deformation; b) the stress-strain relationship for a large amplitude cyclic deformation; c) the strength during cyclic loading; and d) the internal damping of the soil. In the following paragraphs each of these parameters will be briefly commented upon.

a) The shear modulus, G , of soils under cyclic loading is smaller than the one observed under static loading; this decrease is a function of the ratio between the applied cyclic strain and the failure strain [33]. The shear modulus, G , can be obtained from the average slope of the stress-strain curve (a hysteresis loop) resulting from the small amplitude cyclic deformation test. The strain amplitude, initial effective stress, void ratio, and shear stress level are the main parameters, affecting the value of G for soils, but for cohesive soils additional parameters are involved [31]. The value of G for a given soil can be evaluated by using the following formulae which were proposed in [35,36,37] :

$$G = \frac{G_{max}}{1 + \gamma/\gamma_{max}} \qquad \ldots (3.1)$$

where G_{max} is the value of G for strain amplitudes lower than 10^{-4} ; γ is the strain amplitude associated to G and γ_{max} the maximum strain amplitude. In equation (3.1) the values of γ_{max} and G_{max} can be computed by the following expressions:

$$\gamma_{max} = \frac{\tau_{max}}{G_{max}} \qquad \ldots (3.2)$$

where

$$\tau_{max} = \{(\frac{1 + K_0}{2} \sigma'_v \ \mathrm{Sin}\Phi' + c' \ \mathrm{Cos}\Phi')^2 - (\frac{1 - K_0}{2} \sigma'_v)\}^{\frac{1}{2}} \qquad \ldots (3.3)$$

and K_0 = coefficient of lateral stress at rest; σ'_v = vertical

effective stress and c' , ϕ' static strength parameters in terms of effective stress. The value of G_{max} depends on the kind of soil under consideration i.e.:

i) for cohesive soils (clays):

$$G_{max} = 1230 \frac{(2.97 - e)^2}{(1 + e)} \sigma_m^{(0.5)} (OCR)^k \quad \ldots (3.4)$$

ii) for cohesionless soils with rounded grains (sands):

$$G_{max} = 2630 \frac{(2.17 - e)^2}{(1 + e)} \sigma_m^{(0.5)} \quad \ldots (3.5)$$

$(e < 0.8)$

iii) for cohesionless soils with angular grains (sands):

$$G_{max} = 1230 \frac{(2.97 - e)^2}{(1 + e)} \sigma_m^{(0.5)} \quad \ldots (3.6)$$

$(e > 0.6)$

where e represents the void ratio; σ_m is the mean effective stress in pounds/square inch; OCR is the consolidation ratio; and k is a function of the plasticity index of the particular soil.

The value of G can also be evaluated by using the average curves shear modulus -shear strain suggested in [38] . These curves were obtained by averaging the available experimental data on G . Finally, the value of G may also be determined by first performing field experiments leading to the velocity of the shear waves in the soil, V_s , and substituting its value in the expression:

$$G = \rho V_s^2 \quad \ldots (3.7)$$

where ρ is the mass density of the soil. The value of G computed through equation (3.7) corresponds to an amplitude strain of less than 10^{-4} ; therefore, it could be considered as the G_{max} for the soil under study.

b) Stress-strain relationship for large amplitude cyclic deformation. In general the main effect of the large amplitude cyclic deformation is a reduction in the shear capacity of soils. Stress-strain curves can be obtained by using the Rambert-Osgood

model calibrated with the observed experimental behaviour of soils under consideration [31].

c) The strength of soils during cyclic loading depends on: the stress level, the number of loading cycles and the strain at which the soil fails in a conventional undrained test [33] . It has also been reported [33] , that the strength after cyclic loading is a function of the peak cyclic strain experienced by the soil. In [39] it was found that the strength under seismic conditions may be approximated by the normal strength obtained during an undrained test. Loose saturated sands and silts are very susceptible to sudden loss of their shearing strength when subjected to cyclic loading i.e. to experience liquefaction [310] .

d) The internal damping of soils is produced by the friction between the soil grains when the soil is under dynamic loading. The amount of internal damping of soils under cyclic loading can be measured by the area of the hysteresis loops of the stress-strain curves developed during the loading. Among other parameters the internal damping of soils depends on: strain amplitude, effective stress, void ratio, and in the case of clays in the number of applied cycles [311] . The internal damping increases with strain amplitude, and decreases with increasing void ratio and the logarithm of the number of cycles [311] . The damping ratio (i.e. the ratio between the viscous and the critical dampings) is one of the parameters commonly used to represent the internal damping of soils. It can be computed by the following expression [38] :

$$\xi = \frac{\xi_{max} \ \gamma/\gamma_{max}}{1 + \gamma/\gamma_{max}} \qquad \ldots (3.8)$$

where ξ_{max} is the maximum damping ratio corresponding to very large strains. The value of ξ_{max} varies depending on the soil and drainage condition i.e.:

i) for clean, dry sands:

$$\xi_{max} = 33 \text{ percent} - 1.5 \log_{10} N \qquad \ldots (3.9)$$

ii) for clean, saturated sands:

$$\xi_{max} = 28 \text{ percent} - 1.5 \log_{10} N \quad \ldots (3.10)$$

iii) for saturated, cohesive soils:

$$\xi_{max} = 31 \text{ percent} - (3 + 0.03f)\, \bar{\sigma}_m^{(0.5)} + 1.5 f^{(0.5)} - 1.5 \log_{10} N \quad \ldots (3.11)$$

where N is the number of cycles; f is the frequency of applied cyclic load in cycles per second . The mean effective stress $\bar{\sigma}_m$ is given in Kg/cm^2. From equations (3.9) and (3.10) it can be observed that the damping ratio for sands is independent of f . The damping ratio ξ can also be evaluated by using the average curves proposed in [3.8]. These curves which relate ξ with the shear strain amplitude, γ , were obtained by averaging available experimental data on ξ (as the ones reported in [3.11, 3.12]) .

3.2.2 General features of North Sea soils

The sediments of geotechnical interest underlying the North Sea were laid down during the late or post-glacial period [3.13, 3.14, 3.15]. The North Sea soils consist mainly of alternating layers of clay and sand. The latter is the most common material to be found in the sea bed, except in sites as the Norwegian Channel where clay is the dominant material to be found; in other areas coarser materials are found [3.13].

In situ soil samplings have revealed that in many locations in the North Sea the layers of both clay and sand (or clayed silts and silty clays) are normally consolidated or overconsolidated (probably excepting in some cases, where the first layer under the mud line is not consolidated). For example, in the location of the Ekofisk tank, a uniform superficial layer of sand with a depth of about 25 meters produced some resistances varying between 70 and 500 Kg/cm^2. It has been suggested that the relative density of these layers, which in many cases is more than 100 percent, is due to the effect of passing waves which produce pressures on the sea floor [3.13] . The layers of overconsolidated

clays for the same Ekofisk site showed undrained strengths of about 5Kg/cm^2 or more [313] . Similar findings were reported in [315]for a site in the northern North Sea and in [313] for several sites.

In short, it can be said that most of the North Sea sites sampled up to now are made of a mantle of soft material, usually sand, overlying hard or moderately to heavy, overconsolidated soils, on many occasions being clays. Generally the strength of the soil layers increases with depth, the exception being some soft layers found near the sea bed.

3.2.3 Dynamic behaviour of North Sea soils supporting a concrete gravity platform

When a structure such as an offshore concrete platform is set on the sea bed, the soil underneath is subjected to static and cyclic loads. The static loads are associated with the submerged weight of the platform, and the cyclic loads with the horizontal forces and moments resulting from the wave action on the platform. The soil near the platform foundation is under alternate increasing and decreasing pressures generated by the passing waves. An increase occurs below the crests of waves and a decrease under the troughs.

The mentioned cyclic loads subject the soil underneath the platform foundation to alternating shear stresses of similar amplitudes but opposite directions [313] . A similar situation could arise if an earthquake occurred in the vicinity of the platform site. In this case the seismic waves would generate random seismic forces on the platform which in due course would produce shear stresses on the soil underneath the structure and on the surrounding soil as well.

Most of the studies on the cyclic behaviour of North Sea soils have been carried out on triaxial and/or simple shear devices, subjecting the soil samples to cyclic loading [313,314]. Centrifugal models have also been used [316] to that end. The main objective of these tests was to simulate the cyclic behaviour of soil samples located at the centre (simple shear) and at the edges (triaxial) of the platform foundation [34] . A fundamental problem of these experiments was the sampling techniques which, under the difficult environmental conditions

of the North Sea made the gathering of representative undisturbed samples almost an impossible task [3.17] . Other problems related to laboratory tests are: a) the difficulties arising during the sample preparation aiming at reproducing the unusual high densities of the sands and clays of the North Sea sediments; b) the effect of the boundary conditions resulting from the test devices utilized, which may not represent the field conditions [3.17, 3.18, 3.19] .

Because of the large cross-section of the concrete gravity platform foundation in contact with the sea bed, it has been suggested [3.18] that an undrained condition (i.e. a condition in which no significant drainage occurs in the soils during the loading) is the most likely to occur in the sea during storms or earthquake loadings. The main results observed during the cyclic loading of North Sea soils and soils of other regions under undrained conditions [3.4, 3.18, 3.19] may be summarized as follows:

For clays:

i) The shear modulus and failure shear stress are reduced by cyclic loading.

ii) At the same ratio of imposed cyclic loading, normally consolidated clays are more resistant than overconsolidated ones.

iii) Below a certain stress level, the behaviour of clays under cyclic loading is such that a hysteresis loop is produced. This stress level depends on the clay type, the overconsolidation ratio and the kind of cyclic loading.

iv) Sensitive normally consolidated clay can experience a build up of pore pressure and a decrease in the value of the effective stress; hence a shear failure occurs.

For sands:

The general behaviour of sands under cyclic loading is similar to that observed in clays [3.18] i.e. conclusions i) and iii) of clays apply directly to sands, and conclusion iv) corresponds to that observed in a loose sand. Another result drawn from those tests is that relatively dense sands experience an increase in their resistance when subjected to shear reversal, probably due to a preshearing effect [3.13] .

However, the results obtained on dense sands (as those found in the North Sea sediments) under undrained cyclic loading have to be taken with particular caution because only the amplitude

of the pore pressure observed at small strains can be relied upon [3.18]. This is so because in addition to the relative density of sands which have to be reproduced in the laboratory, other parameters such as the sand structure and the age of the deposit play an important role in considering cyclic behaviour [3.18].

3.3 Soil-foundation interaction models

The soil-foundation interaction (s.f.i.) effect, i.e. the generation of relative displacements between a foundation and the surrounding soil, may be observed when a dynamic perturbation is transmitted to a soil-foundation system a) through a superstructure and/or b) through the soil media. An example of the first case could be the dynamic loads generated by a turbo generator supported by a framed superstructure and transmitted to the foundation; the second case could arise when an earthquake occurs and the seismic waves are transmitted through the earth layers and reach the site where the structure of interest is located.

In any of the mentioned cases the soil surrounding the foundation of the structure would behave in a certain fashion depending on its dynamic properties (Section 3.2.1). At present, the models available to study the soil-foundation effects could be lumped into two kinds depending on the form in which the soil media is idealized. One is the so-called continuum approach and the other is the finite element approach. In the former approach the soil medium is usually idealized as a half-space (fig.3.1).With the finite element method approach the soil medium is modelled by a finite discrete region (fig.3.2).

As far as the foundation is concerned, a common assumption is to idealize it as a rigid solid; however, this assumption can be relaxed and the flexibility of the foundation can be taken into account. The main objective of the continuum and finite element method approaches as applied to s.f.i. problems is to model the inertia, stiffness and dissipative properties of the soil-foundation system, when a harmonic load is acting on the foundation. The main features of the continuum approach and the finite element method approach are presented in Sections 3.3.1 and 3.3.2 respectively.

3.3.1 The continuum modelling of a soil-foundation system

The continuum approach (which can be considered as the classical one) models the soil medium as a semi-infinite half-space [3.20] , a layer [3.21] or a layered half-space [3.22] . The soil material properties can be treated as linear elastic [3.20] , or viscoelastic ones [3.23], meanwhile the foundation is idealized as a massless rigid disc (fig.3.1) The continuum approach models lead to mixed boundary value problems. The kind of elastodynamic problem which results, depends on the assumptions made for the boundary conditions existing at the interface made up of the idealized foundation and the free surface of the half-space (Fig.3.1) If complete continuity of stresses and displacements is prescribed at the interface, a complete mixed boundary value problem arises [3.20] . When some of these continuity conditions (generally stresses) are modified, relaxed mixed boundary value problems appear [3.24].

Both complete or relaxed mixed boudary value problems have been formulated in such a way that they lead to integral equations [3.20,3.24], which have mainly been solved by using numerical techniques. Recently, [3.25] a formulation which uses potential theory has extended the capabilities of the continuum approach to include three dimensional models. In this formulation the superposition principle has been applied to point sources (loads) on the foundation surface. The resulting integral equations were approximated by sets of algebraic equations which were solved numerically [3.25] .

From the models described above, expressions relating the stress resultants of the area of contact or the applied harmonic external loads to the displacements of the foundations are obtained. These expressions are the impedance functions of the problem.

A number of solutions i.e. impedance functions for different types of loading and foundation shapes have been proposed but only some of them will be mentioned here. For a rigid circular foundation on an elastic half-space [3.20,3.24,3.26] ; for a rectangular foundation on an elastic half-space [3.27,3.28] ; for a strip footing on an elastic half-space [3.28,3.29] ; for the effect of layering of the soil medium [3.30,3.32] ; for embedded foundations [3.30,3.32] ; for three dimensional flat foundations of arbitrary shape [3.25].

The impedance functions are usually expressed as the addition of a real component and an imaginary component. Due to this mathematical representation, which resembles that obtained for the response of a linear spring-dashpot system, these components of impedance function have been associated to equivalent springs and viscous dampers respectively [3.33] . From the physical point of view the spring can be associated to the stiffness properties of the soil, and the damper to the energy dissipated by waves propagagating away from the foundation. This is known as the radiation damping property of soils. Both springs and dampers are a function of the soil medium properties, the geometrical characteristics of the foundation, and the frequency of the excitation.

As it was mentioned in Section 3.2.1, experiments have shown [334] that soils also dissipate energy through friction between the soil grains i.e. they have a material or internal damping. To take this into account for a particular soil foundation system, the equivalent damper should be computed as the sum of the contributions of the radiation and material dampings of that soil. Another possibility is to consider the material damping effect explicitely into the impedance function derivations [3.35].

For a circular disc resting on a half-space the expression for the impedance function associated to an external harmonic force, P_j , applied in the j direction (fig.3.1) is given by [3.24] :

$$P_j = K_j \left[k_j(a_0,\nu,D) + i a_0\ c_j(a_0,\nu,D)\right] u_j \quad . \ . \ . (3.12)$$

where P_j represents the amplitude of the force; K_j is the static stiffness of the disc in the j direction; k_j and c_j are dimensionless real-valued functions depending on the Poisson ratio, ν , loss ratio D of the half-space material and a dimensionless parameter a_0.

The following expressions

$$k_{j_s} = K_j \left[k_j(a_0,\nu,D)\right] \quad . \ . \ . (3.13)$$

$$c_{j_s} = K_j \left[a_0\ c_j(a_0,\nu,D)\right] \quad . \ . \ . (3.14)$$

represent the springs and viscous-dampers mentioned above, (Fig.3.3).

The static stiffness K_j is a function of the half-space material elastic properties and the characteristic dimension of the disc, (fig. 3.1). For example, the following expression of K_j corresponds to the horizontal, x, vertical, y, and rocking, θ, uncoupled displacements of the disc resting on an elastic half-space:

$$K_x = \frac{8Gr}{(2 - \nu)} \quad \ldots (3.15)$$

$$K_y = \frac{4Gr}{(1 - \nu)} \quad \ldots (3.16)$$

$$K_\theta = \frac{8Gr^3}{3(1 - \nu)} \quad \ldots (3.17)$$

where G is the shear modulus of the half-space material and r is the radius of the disc.

In equation (3.12) the dimensionless parameter a_0 is given by:

$$a_0 = \frac{\omega r}{V_s} \quad \ldots (3.18)$$

where ω is the frequency of the applied load and V_s represents the velocity of the shear waves for the half-space material (see equation (3.7)).

The loss ratio D represents the internal or material damping of the half-space material. It can be assumed to be linearly hysteretic in which case it can be defined as:

$$D = \frac{1}{4\pi} \frac{E_d}{E_s} \quad \ldots (3.19)$$

where E_d represents the energy dissipated per cycle by a soil sample under steady-state harmonic loading and E_s the maximum strain energy stored in the soil sample.

The inertial properties of the soil-foundation system can be represented by an equivalent mass (fig 3.3), which is equal to the mass of the foundation plus the mass of a certain volume of soil. This volume depends mainly on the characteristic dimension of the foundation and the direction of the applied loads (fig 3.1). The actual computation of the equivalent mass will be introduced in chapters 6 and 8.

Once an equivalent mass-spring-damper set has been obtained, a soil-foundation system can be treated as an equivalent lumped linear

system, whose analysis is straigthforward, as it will be shown in 6.2 and 6.3. Frequency-independent impedance functions have been proposed to simplify the analysis [3.32,3.36,3.37] . Satisfactory results have been obtained when such functions are used appropriately [3.37,3.38] .

The dynamic loading for the model of the continuum approach is usually specified at the free surface level (Fig.3.1). In the case of seismic excitation the input of the s.f.i. system is the so-called free field motion. However, for deeply embedded foundations the seismic excitation at different depths should be considered, in order to obtain better results [3.38] .

The following advantages and limitations of the continuum approach reported in different studies [3.38,3.39] will be mentioned:

The advantages are:

i) The real problem can be represented by a minimum of the relevant parameters of the s.f.i. phenomenon.

ii) It is fundamentally correct and leads to the recognition of the importance level of the s.f.i. effect.

iii) Three dimensional effects are automatically included in the analysis.

iv) A layered soil medium can be represented by this approach.

v) Both radiation damping and hysteretic damping of soils can be included in the analysis.

vi) Low computing costs make it suitable for simulation purposes.

The limitations are:

i) It is restricted to linear elastic or viscoelastic representations of the properties of the soil medium.

ii) It is limited to a number of foundation shapes for which the exact or approximated solution of the associated elastodynamic problem can be obtained.

3.3.2 The finite element modelling of a soil-foundation system

The finite element method (f.e.m.) approach models the soil medium as a finite region made up of small elements (Fig.3.2). The material and geometrical characteristics of each of the elements may differ from the characteristics of the rest of the elements forming the soil region. Thus, in principle, the f.e.m. allows the modelling of the soil media with material and geometrical

nonlinearities with relative ease.

As mentioned in Chapter 2, the f.e.m. applies the Ritz method to find an approximate solution to a particular set of governing equations and boundary conditions, i.e. the f.e.m. reduces the set of partial differential equations describing the motion of a continuum to a coupled set of ordinary time-dependent differential equations. According to the formulation of the f.e.m. approach utilized for the soil-foundation system, the method can be used to generate impedance functions (as those obtained by the continuum approach) [340], or to compute directly the displacements associated to the proposed degrees of freedom [341,342].

A number of finite element models has been proposed to solve s.f.i. problems by using three-dimensional solid elements [343], two-dimensional plane strain elements [340] or axisymmetric solid elements [341]. The last two models are the most widely used at the present time, due to economical and computer storage limitations [344].

The main difficulties found in the development of finite element models for solving s.f.i. problems arise from: a) the introduction of artificial boundaries to produce a finite region (fig.3.2),b) the size of the elements used (fig.3.2),c) the modelling of the damping of the system and d) the idealization of the nonlinear behaviour of soils.

The use of artificial boundaries in the model leads to the so-called box effect, i.e. the reflection on the artificial boundaries of the waves originated at the foundation which otherwise should propagate and dissipate freely in the soil medium. In order to eliminate the wave reflection phenomena which introduce artificial spurious waves in the response of the system, the artificial boundaries can be set far away from the foundation; if this is not possible (because of storage computer capabilities) it is recommended to use quiet [345] or transmitting boundaries [346,347,348]. However, the effectiveness of these kinds of boundaries for s.f.i problems has been questioned [339].

The size of the elements utilized is a function of the frequencies of the excitation which should be propagated through the discretized media. The value of one-fifth of the shortest excitation wavelength

has been suggested as the maximum size of a quadrilateral finite element [3.49] .

The modelling of the soil damping in finite element models is a subject of great controversy [3.50] . The fact that a properly performed finite element analysis should automatically include both hysteretic and radiation damping is generally accepted [3.51] , but there is disagreement concerning the way in which they should be implemented [3.50,3.51,3.52]. Some authors have introduced the soil material damping as a function of the strain that occurs in the finite elements [3.42] ; the radiation damping is accounted for through the size of the model [3.41] . Other authors have advocated the use of quiet boundaries to model the radiation damping and recommended the use of an appropriate material damping in the soil finite elements so that the hysteretic behaviour of soils can be taken into consideration [3.44,3.50]. Most of the f.e.m. codes for s.f.i. purposes provide with a single value of damping for all the elements per vibration mode, and a value within the interval limited by the values of the structure foundation damping and the damping of the soil media has to be adopted [3.42] . However, there are models as the one described in [3.53] which allow the use of a variable and different damping value for each element.

The idealization of the non-linear strain properties of soils is crucial for the analysis of s.f.i. effects when using the f.e.m. approach [3.42,3.51] . This is so because the stiffness and damping characteristics of a soil are strain dependent (Section 3.2.1). Due to the absence of any established criteria for describing an appropriate measurement of the strain of soils in two and three-dimensional conditions, the extension of a finite equivalent linear model [3.54] (originally developed for one-dimensional wave propagation applications) has been pursued [3.55,3.56] .

These models assume that the soil behaves as a linear-visco-elastic material with parameters G and ξ defined as a function of the maximum strain (as those proposed in [3.8]). Through an iterative scheme, the soil strains are computed for a set of shear modulus and damping values chosen for each iteration until they agree (within a tolerance limit) with the strain level assumed in the previous iteration. For one-dimensional problems the level of

strain is taken as a percentage of the computed peak strain (usually 0.66 of the peak strain), and for the two-dimensional case the level of strain has been chosen as a weighted fraction of the maximum principal shear strain [356] .

In s.f.i. systems subjected to seismic waves, two kinds of non-linearities have been observed [356] : the so-called primary non-linearities which occur in the whole of the soil region and are associated with the seismic motion, and the secondary non-linearities which are confined to the soil at the immediate vicinity of the foundation and related to the s.f.i. effects. The results obtained by using an equivalent linear model have shown that the secondary non-linearities of soils do not significantly affect the structural response of s.f.i. systems under seismic disturbances [356] . However, if a study of the potential deformation is being pursued, the secondary non-linearities should be taken into account [356] . The results of these linearization models have been questioned for the latter purpose [356] and also in more general lines in [344] . The criticism in both cases is about the validity of the iterative linear approximation to a non-linear problem, as well as the reliability of procedures used to estimate the parameters used in those models.

The excitation to the finite element model in a s.f.i. problem is generally specified at the base of the foundation or in the case of seismic disturbances at the base of the proposed mesh. The latter case requires the deconvolution of the surface recorded motion by using the one-dimensional wave propagation theory [349,353,357] . This theory implies that the surface motions are only produced by vertically propagating shear waves i.e. neglecting the contribution of surface waves as well as non-vertically incident body waves.

As a summary the following comments could be made with respect to the advantages and limitations of the f.e.m. approach as applied to s.f.i. problems [338,342] :

The advantages are:

i) The material and geometrical non-linearities (in the dynamical analysis) of the problem can be included.

ii) Complex geometrical shapes can be satisfactorily modelled.

The limitations are:

i) Due to computer storage capacity at present available, artificial boundaries for a finite soil region must be introduced in the model.

ii) There are still difficulties with the stress models used.

iii) The modelling of the radiation damping still appears to be unsatisfactory.

iv) The two-dimensional representation of a three-dimensional problem yields to an underestimation of structural responses.

3.3.3 Soil-foundation interaction model for a concrete gravity platform

In principle both procedures i.e. the continuum or the f.e.m. approaches could be utilized to study the s.f.i. effect on gravity platforms subjected to dynamic loads because, as it was shown in [3.38] the two methods should lead to similar results if they are used correctly to solve the same problem. This means that the selection of an approach for a particular application should be made by considering the characteristics of the soil-structure system to be analysed, the advantages and limitations of the methods (i.e. the continuum and f.e.m.) and the objectives of the study.

The soil-structure system under consideration consists of a massive concrete foundation supporting one or several towers and resting on the surface of a horizontally-layered soil medium. The system will be subjected to wave and (possibly) earthquake loading, and therefore the s.f.i. effects may be of importance on the overall dynamical behaviour of the system. As it was mentioned in Section 2.4 the foundation of an offshore concrete gravity platform consists of a circular or square caisson made up of a number of concrete cells [358]. The caisson is provided with concrete and steel skirts which, among other functions, prevent the generation of high contact pressures on the base of the caisson when this is lying on the sea-floor [358].

The characteristics of the soil medium to be found in typical sites of the North Sea were discussed in Sections 3.2.2 and 3.2.3. It was stated there that the general feature of the soil medium in the region was that of deep alluvial deposits, consisting of alternating horizontal layers of sand and clay. It was also commented about the consolidated or overconsolidated condition of those layers, as well as about the increase of the strength of the layers with depth. Concerning the values of the dynamical parameters of the sands and clays forming the layers, attention was drawn to the uncertainties in the values of those parameters, those uncertainties

being inherent in current soil sampling techniques and laboratory testing capabilities.

Measurements of the caisson-soil contact pressures developed on prototype offshore gravity platforms have shown that all the cells forming the caisson made contact with the sea-floor, and that the values of the recorded contact pressures were similar but not uniform throughout the caisson-soil interface [358] . It can also be concluded from these measurements that the base of the caisson has not been deformed.

Studies (analytical and experimental) of s.f.i. effects performed on prototype structures based inland have been reported [359,360]. In [359] the s.f.i. system was a multistorey concrete building resting on a soft-layered soil medium, subjected to forced vibration and micro-tremors. Among other conclusions reached in that study, it was stated that the total force acting at the interface soil-foundation, and the average motion observed were practically independent from the flexibility of the foundation (the analytical study compared the dynamical response of the building supported on a rigid and a flexible foundation). Therefore, the assumption of a rigid foundation could be used in s.f.i. studies aiming at predicting the overall dynamical response of the superstructure, but the same assumption would not be suitable to compute the relative deformation of structural elements near the foundation level [359]. In [360] experiments on a massive shaking table subjected to forced vibration and seismic excitations revealed that the s.f.i. non-linearities (usually of importance on small footings) were not shown in any appreciable degree.

Taking into account the following items: a) the characteristics of the offshore gravity platform -North Sea soil system described above, b) the advantages and limitations of the continuum and f.e.m. approaches to include s.f.i. effects, Section 3.3.1 and 3.3.2, c) the results of the s.f.i. studies on prototypes [358,359,360] and d) considering that the objective of this study is to predict the overall dynamic behaviour of an offshore gravity platform, it seems appropriate to use the continuum approach to compute the s.f.i. effects on the dynamical response of the system under consideration.

The model selected is the one which assumes a rigid circular foundation resting on the surface of a layered soil-medium. The assumption of a rigid foundation is generally fulfilled when comparing the rigidities of a concrete gravity platform and the soil in the North Sea bed [359]. Even if it was not the case, the results of the study reported in [3.59] support this assumption in terms of the aims of the present study expressed in above incise d). As far as the assumption of circular shape of the foundation is concerned, it agrees with one of the shapes proposed for the caisson cross-section, but if the foundation shape was rectangular or square, these shapes could be transformed to a circular one by using formulae as the ones presented in [3.36].

The effect of the layering of the soils under the North Sea will be taken into account by using available impedance functions which consider this soil condition. Furthermore, because the field condition prevailing on North Sea sites is that of deep alluvial deposits, which do not have a natural vertical boundary (i.e. a bedrock) at reasonable depths for modelling purposes, it may be concluded that the use of the continuum model can avoid the unwanted effects associated with the artificial boundary of the f.e.m. models necessary in cases like this one.

Another advantage resulting from the use of the continuum model for a structure with shallow embedment (as it is the case for an offshore gravity platform) is that when considering the seismic excitation, the free field motion can be applied at the base of the foundation directly, i.e. avoiding the deconvolution and related assumptions required when utilizing the f.e.m. approach.

The uncertainties about the soil dynamic parameters (Section 3.2.1) can be accounted for in an indirect fashion by varying the values of those parameters within a reasonable range. This technique should also be applied when using f.e.m. models [361]. Finally, the use of a continuum model allows to perform parametrical studies with great economies comparing with the costs involved when using a f.e.m. model for that purpose.

Two types of impedance functions will be utilized, one proposed in [362] for a rigid foundation on a layered viscoelastic soil medium in which the spring and dashpot elements are frequency dependent. The

other impedance functions to be used are the ones proposed in [3.23], which correspond to a rigid foundation on a viscoelastic half-space and are also frequency dependent. The former impedance functions will be taken from [3.23, 3.62] and the rest of the parameters necessary for the s.f.i. study will be introduced in Chapter 8.

4. SEISMIC LOADS

4.1 Introduction

Seismic loads are generated by the sudden random movement of the ground surrounding the foundation of a structure. This movement is transmitted to the structure as inertial forces acting on its elements. The amplitude of these forces mainly depend on the dynamical properties of the structure and the intensity of the earthquake.

A well-recognized feature of seismic events is the uncertainties about the sizes, locations and number of future earthquakes. Therefore the design of a structure in a region of potential seismic activity should incorporate those uncertainties. A rational way of doing so is by defining levels of intensity of the expected maximum ground motion parameters (such as acceleration, velocity, etc.) in a site for different time-spans (including the life-span of the structure). This is, to evaluate the seismic risk of the site where the structure will be built.

The seismic risk in a site can be obtained by using the so-called seismic risk models. Ideally, these models should synthesize all the seismological information available about the region in which the site is located as well as the present knowledge about the earthquake process itself. The output derived from those seismic risk models is usually presented as graphs or tables relating values of the ground motion parameters at the site of interest with periods of time, known as "return periods", and/or probabilities of exceedance.

Once the seismic risk for the site of interest has been obtained, the designer can analyse and assess the performance and economic implications of different designs under various levels of ground motion intensities.

In this chapter the following topics will be treated: in Section 4.2 a brief summary about the seismic phenomenon and its engineering implications is presented; in 4.3 some of the seismic risk models available are reviewed; in

4.4 expressions for a seismic risk model are presented, meanwhile in 4.5 the application of this model to a site located in the North Sea is produced and finally, in 4.6 the results of the application are discussed in terms of earthquake loads.

4.2 Generalities about seismic events

Before starting to deal with the determination of the seismic load, a brief summary of concepts and definitions associated with the earthquake phenomenon will be given in this section.

4.2.1 Origin of earthquakes

The earthquakes which are of interest for engineering purposes are considered to be of tectonic origin. This kind of earthquakes is generated when the crust of the Earth releases elastic energy through slips of geological faults. This energy is propagated in the form of seismic waves through the crust of the Earth which manifest themselves as a chaotic movement of the surface of the Earth. It is this random ground motion which produces damages to the structures located in the sites reached by the earthquakes if the structures have not been designed to withstand the former.

The point below the surface of the Earth where, presumably, a geological fault is first ruptured, is known as the focus of an earthquake. The depth of the focus below the surface of the Earth is called focal depth, and the distance from a site to the focus is named focal distance. As for the vertical projection of the focus on the surface of the Earth, it is known as the epicenter, and the distance from a site to the epicenter is called epicentral distance. The longitude of the ruptured fault is named fault length.

4.2.2 Modified Mercalli Intensity and Magnitude of an earthquake

The Modified Mercalli Intensity, I(MM), is a subjective descriptive measurement of the level of damage produced on man-made structures and superficial geologic environment by an earthquake in a site or region [4.1] . Depending on the level of damage caused by an earthquake in a site, a number which ranges

from I to XII is assigned to the I(MM) of that earthquake for that site. The lines separating regions which have experienced the same I(MM) are denominated isoseismal lines of an isoseismal map.

The Richter magnitude, M , is an objective measure of the energy released during an earthquake; it is defined as follows:

$$M = \log_{10} \frac{A}{A_0} \qquad \ldots (4.1)$$

where M is the magnitude of the earthquake, A the maximum amplitude recorded by a Wood-Anderson seismograph at a distance of 100 Km. from the epicenter, and A_0 an amplitude of 10^{-3} millimeters [41] . It is a general practice to produce an average value of M for an earthquake recorded in different seismological stations.

4.2.3 Seismic Energy, Strain and Moment

The following expression is widely used to compute the seismic energy E released during an earthquake [42] :

$$\log_{10} E = 11.8 + 1.5M \qquad \ldots (4.2)$$

the units of E in equation (4.2) are ergs. Another quantity of interest during seismic events is the seismic strain which occurs during the deformation process in the focal region. The seismic strain is related to the seismic energy of an earthquake by the expression [43] :

$$S = E^{\frac{1}{2}} \qquad \ldots (4.3)$$

The seismic moment, M_0 , is a measure of earthquake size, which mainly depends on the physical mechanism of the earthquake, and can be computed for large magnitudes with formula [44] :

$$\log_{10} M_0 = 19.9 + M \qquad \ldots (4.4)$$

4.2.4 Attenuation Law: Magnitude-Modified Mercalli Intensity

Due to the subjectivity of the Modified Mercalli Intensity Scale, the records of I(MM) constitute the only source of seismic

information for some sites or regions, especially for historical earthquakes occurred before the beginning of the century. While records of the magnitude M of earthquakes have been available for some regions since the early thirties, semi-empirical expressions -the so-called attenuation laws- relating the magnitude M of earthquakes with their I(MM) (and some of their geometrical characteristics) have been proposed for different regions in the world [45] . Those expressions are particularly useful to generate sets of data of M , from I(MM) records or vice-versa when required; for example, the following attenuation law:

$$M = \frac{2}{3} \; I(MM) + 1.4 \log_{10} h - 1.25 \qquad \ldots (4.5)$$

has been proposed for Northern Europe [46] ; in this expression h represents the focal depth of the earthquake.

4.2.5 Accelerograms

From an engineering point of view the basic information for estimating the seismic forces acting on structures is provided by the accelerograms, which are the time history of the ground acceleration. An accelerogram is composed of a random sequence of acceleration pulses and can be obtained by direct recording of the ground motion accelerations experienced at a site during an earthquake, by using an accelerograph; it can also be simulated by using an analog [47] or a digital computer [48] . The velocity and displacement records of a ground motion can be computed by integrating once and twice the associated accelerogram respectively.

It has been observed that the maximum responses of elastic structures subjected to seismic loads are mainly sensitive to the intensity and distribution in the frequency domain of the ground motions. It has also been concluded that the time distribution of the intensity and duration of earthquakes are of importance for the values of those maximum responses [49] . The intensity of a ground motion can be estimated from the values of the maximum acceleration (a_{max}), maximum velocity (v_{max}) and maximum displacement (d_{max}) of the respective records. These values of a_{max} , v_{max} and d_{max} provide the so-called ground spectra, when plotted on a special log paper. The ground spectra supply a

rough estimate of the frequency distribution of the ground motion [4.1, 4.2] .

Only very few regions in the world (for example California,U.S.) have enough accelerograms available to produce a satisfactory sample of the possible behaviour of structures located in those regions to future earthquakes. For regions in which the number of accelerograms is small or nonexistent (for example the U.K. where there are no accelerograms available) the computation of a_{max} , v_{max} and d_{max} relies on other estimates of the intensity of earthquakes, namely the Modified Mercalli Intensity I(MM) , and the Richter magnitude, M , of earthquakes.

A number of attenuation laws which relate the M (or I(MM)) and geometry parameters (usually the epicentral and focal distances) of earthquakes with their corresponding a_{max} , v_{max} and d_{max} has been suggested [45,410] .

Other estimates of ground motion intensity distribution are given by the Fourier Spectra, the Power Spectral Density Function and the Response Spectra. All of them require the accelerogram as a starting point in their computation as it will be made clear.

4.2.6 Fourier Spectra

The Fourier Spectra, (f.s.), of an accelerogram is defined as:

$$F(\omega) = \int_0^{t_1} a(t) \exp\left[-i\omega t\right] dt$$

$$= \int_0^{t_1} a(t) \cos(\omega t)\, dt - i \int_0^{t_1} a(t) \sin(\omega t)\, dt \qquad \ldots (4.6)$$

where $a(t)$ is the ground motion acceleration and t_1 its duration [42] . The modulus of the f.s. gives the Fourier amplitude spectra, i.e.:

$$|F(\omega)| = \left\{\left[\int_0^{t_1} a(t) \cos(\omega t)\, dt\right]^2 + \left[\int_0^{t_1} a(t) \sin(\omega t) dt\right]^2\right\}^{\frac{1}{2}} \qquad \ldots (4.7)$$

It has been shown [41] that when $|F(\omega)|$ is plotted as a function of the natural period or frequency of an undamped single degree of

freedom system, the f.s. represents an estimate of the final energy put into the system by the ground motion.

4.2.7 Power Spectral Density Function

The power spectral density function (p.s.d.f.), $G(\omega)$, is related to the Fourier amplitude spectrum as follows:

$$G(\omega) = \lim_{t_1 \to \infty} \frac{E\left[F(\omega)\right]^2}{t_1} \qquad \ldots (4.8)$$

where the expectation E is taken over a family of accelerograms, in which each of them is assumed to be a stationary stochastic process [411]. The plot of $G(\omega)$ as a function of the natural frequency ω provides an advantageous estimate of the energy content in a family of accelerograms. Equation (4.8) provides a way to compute the p.s.d.f. of real or simulated accelerograms which can be used as the seismic input to structural systems. Semi empirical expressions of p.s.d.f. resulting from studies on real earthquakes have been proposed; a widely used one is the so-called Kanai-Tajimi formula [412]:

$$G(\omega) = \frac{\left[1 + 4\xi_g^2 \left(\omega/\omega_g\right)^2\right] G_0}{\left[1 - \left(\omega/\omega_g\right)^2\right]^2 + 4\xi_g^2 \left(\omega/\omega_g\right)^2} \qquad \ldots (4.9)$$

in which ω_g and ξ_g represent the dominant natural frequency and damping of the ground respectively, and G_0 is a measure of the intensity of the ground motion. Equation (4.9) has been applied to a set of accelerograms recorded in the U.S. [413]; the resulting $G(\omega)$ is given by:

$$G(\omega) = \frac{0.01238\left(1 + \frac{\omega^2}{147.8}\right)}{\left(1 - \frac{\omega^2}{242}\right)^2 + \frac{\omega^2}{147.8}} \qquad \ldots (4.10)$$

4.2.8 Response Spectra

The response spectra (r.s.) are plots of maximum responses of single degree of freedom systems (s.d.f.) versus natural period or natural frequency [41,42]. The r.s. represent a measure of the

maximum value of the energy put into the s.d.f. system by an earthquake. This maximum energy produces maximum responses of the system, such as its maximum displacement S_d which can be computed by the following expression [4.2] :

$$S_d = \frac{1}{\omega'} \left| \int_0^{t_1} a(t)\, e^{-\omega' \xi (t-\tau)} \sin \omega' (t-\tau)\, d\tau \right|_{max} \quad \ldots (4.11)$$

where ω' and ξ represent the damped natural frequency and percentage of critical damping of the system, a(t) and t_1 the ground acceleration and its duration respectively. S_d is customarily used to derivate the maximum pseudo velocity of the system, S_v, and its maximum pseudo acceleration, S_a, i.e.:

$$S_v = \omega\, S_d \quad \ldots (4.12)$$

$$S_a = \omega^2\, S_d \quad \ldots (4.13)$$

S_a and S_v are reasonably good estimates of the maximum velocity and maximum absolute acceleration of the system [4.2]. The values of S_a , S_v and S_d , associated with different dampings of the s.d.f. systems, are usually plotted in a special logarithmic graph [4.1, 4.2].

There are several procedures to compute the r.s. depending on the information used for that purpose. One direct procedure is by computing S_d (equation (4.11)) for a family of s.d.f. systems using an accelerogram (real or simulated) as the input. There are two indirect techniques to compute the r.s.. One makes use of the ground spectra, the other one is based on attenuation laws.

The ground spectra are of particular relevance to the computation of the r.s. because they correlate satisfactorily with the latter. In particular the a_{max} correlates with the maximum responses of short natural period systems, meanwhile v_{max} and d_{max} correlate with intermediate and long natural period ones respectively. The ratio of the r.s. ordinate to the corresponding values of the ground spectra ordinate is called the spectral amplification factor.

Based on the existing relationship between the r.s. and the ground spectra, different techniques basically recommend to

multiply the values of the ground spectra by spectral amplification factors. The latter ones have been obtained by carrying out statistical studies on ground and response spectra computed from accelerograms recorded in the Californian region (U.S.) and elsewhere [4.14,4.15].

The other indirect technique to compute the r.s. is based on another statistical study performed on ground motions occurred on the West coast of the U.S.[4.16]. From this study attenuation laws for the S_v (and the ground spectra) were obtained. In fact, the study provided the expected value and the coefficient of variation of S_v (for different values of the percentage of the critical damping and natural period) as a function of the magnitude M and hypocentral distance R .

4.2.9 Relationship between response spectra and power spectral density function

In several studies the relationship existing between the response spectra and the power spectral density function has been pointed out. Among those studies the following can be mentioned:
a) In [49] it has been suggested (after [4.17]) that the undamped velocity response spectra represent an upper estimate of the Fourier amplitude spectra, and therefore (see Section 4.15) an upper estimate of the p.s.d.f.. In this case the expected p.s.d.f. can be computed by simply squaring the values of the corresponding expected undamped velocity response spectra, i.e.:

$$E\left[G(\omega)\right] = \{E\left[S_v\ (0,\omega)\right]\}^2 \frac{1}{t_0} \qquad \ldots\ (4.14)$$

In equation (4.14) the 0 inside the parenthesis represents the percentage of the critical damping of the system, ω its natural frequency, and t_0 the duration of the accelerogram.

b) An expression relating the p.s.d.f., $G(\omega)$ (expressed by equation (4.10)) with the average undamped pseudovelocity spectra, S_v, obtained from an ensemble of real (U.S.) and simulated accelerograms has been proposed in [4.13], i.e.:

$$E\left[G(\omega)\right] = \frac{0.237}{t_1} \{E\left[S_v\ (0,\omega,t_1)\right]\}^2 \qquad \ldots\ (4.15)$$

in which t_1 is the duration of the accelerograms ensemble; the 0 and the ω inside the parenthesis were defined previously; the t_1 used in that study was 18.6 sec.

c) In [4.18] a procedure to compute the p.s.d.f. from a r.s. has been proposed. This procedure is based on the random vibration analysis of ground motions applied to the determination of response spectra. After finding an approximate solution to the so-called first passage problem, the response spectra value, $y_{t_1,p}$, for an exceedance probability, p, and ground motion duration, t_1, are expressed as the product of the standard deviation of the response of the system $\sigma y(t_1)$ multiplied by a peak factor, $r_{t_1,p}$, i.e.:

$$y_{t_1,p} = \sigma y(t_1)\ r_{t_1,p} \qquad \ldots (4.16)$$

where y can be acceleration, velocity or displacement. The values of $r_{t_1,0.5}$ for typical accelerograms vary between 1.25 and 3.5 [4.18]. $\sigma y(t_1)$ is related to the p.s.d.f., $G(\omega)$, of the ground motion by the following expression:

$$\sigma y(t_1) = \left[G(\omega_n)\ \omega_n \left(\frac{\pi}{4\xi_{t_1}} - 1\right) + \int_0^{\omega_n} G(\omega)\ d\omega\right]^{\frac{1}{2}} \qquad \ldots (4.17)$$

where ω_n is the system natural frequency, and ξ_{t_1} represents an equivalent damping of the system, which can be obtained by:

$$\xi_{t_1} = \frac{\xi}{1 - \exp(-2\ \omega_n\ t_1)} \qquad \ldots (4.18)$$

in which ξ is the percentage of critical damping of the system.

Based on those results an estimate of the $G(\omega)$ can be computed from a given pseudovelocity spectrum S_v; the steps to be followed are [4.18]:

a) Divide the S_v values by a chosen peak factor $r_{t_1,p}$ at selected natural frequencies, ω_n; this leads to the $\sigma^2 y(t_1)$ spectrum; b) Use equation (4.17) iteratively to calculate the values of $G(\omega)$ at the proposed ω_n values. The procedure is reversible,

therefore a S_v spectrum may be obtained from a given $G(\omega)$.

4.2.10 Other techniques to obtain accelerograms and response spectra

As in the case of accelerograms availability for a region, there are some regions in which the files of I(MM) and/or M are incomplete (from a statistical point of view) or totally absent to derivate expressions relating them with the ground motion parameters a_{max}, v_{max}, and d_{max}. In such regions or sites the following techniques can be followed to produce a seismic input:

a) A historical set of accelerograms is chosen, and (if possible scaled in time and amplitude) it is considered as representative of the possible future earthquakes to occur in the site. The 1940 El Centro earthquake is widely used for this purpose because of the high value of the a_{max} which was recorded for this event [4.1].

b) A set of artificial accelerograms which includes different kinds of ground motion characteristics is selected and taken as a sample of the future earthquakes in the site [4.8,4.13].

c) A set of scaled standard or average response spectra is used [4.1]. These sets of response were obtained by averaging the response spectra of a sample of earthquakes which occurred in different sites in the U.S.

4.2.11 Accelerograms and Response Spectra on soft grounds

The techniques described in the last sections for obtaining the response spectra or accelerograms in a site are suitable for sites located on firm ground. If this is not so, the local soil should be taken into account. The local soil effect of softer soils is translated in a filtering of the ground motion, leading to an increase (or decrease) of the amplitude of the waves at certain frequencies and thus causing a dynamic amplification of the seismic waves.

Local soil effects become particularly relevant when the site is on a subsoil which is made of layers of rather different characteristics, and the earthquake has a moderate intensity and a large epicentral distance [4.19]. For short epicentral distances and stable soil behaviour the local soil effects are overshadowed

by the source mechanism of the earthquake [419] .

The practical outcome of the dynamic amplification of soils is that the seismic forces on a structure are larger, and act in a wider band of periods than the ones expected on the same structure on a firm ground [420] .

The procedure used for the determination of a response spectrum or accelerogram depends on the seismic and geotechnical information available for the site on a soft ground. Four main methods can be listed as follows: 1) A direct application of historical (or simulated) accelerograms, 2) A selection of an average response spectra, 3) The use of spectral amplification factors, 4) The application of numerical simulation models.

1) A set of historical or simulated accelerograms (Section 4.2.10), or their associated response spectra are chosen. This procedure is usually applied when there are no accelerograms for the site and the local geology is partially known.

2) Direct use of average or envelope response spectra (Section 4.2.10) obtained from regions with similar geology as that of the region in which the site is located. This procedure is followed when the regional geology is known.

3) A set of spectral amplification factors is used in combination with values of the maximum acceleration or ground spectra for the site. This technique can be applied when a_{max} and v_{max} or the ground spectra and the surface geology of the soil in a site are available. Sets of spectral amplification factors have been obtained from statistical studies of events occurred on the West coast of the U.S.; and, among other parameters, they take the type of soil and a probabilistic percentile level into account [421,422] .

4) The numerical simulation of local soil effects can be performed by using finite element [423] or finite-difference models [424] which directly compute the filtering effects of the subsoil when subjected to a reference ground motion. This technique requires detailed knowledge about the dynamic properties and geometry of the subsoil under the site

The main problem when applying the last technique arises from the difficulty of choosing the site where the reference ground motion should be applied. The uncertainties surrounding the

material properties, and mainly the ones attached to the earthquake characteristics should also be taken into consideration when deciding to use a 2D or 3D model instead of a 1D model. This is so because the application of the 2D and 3D models may become very expensive when performing statistical studies leading to the computation of the site accelerogram of response spectra [419].

As a general rule, whenever it is possible, a combination of techniques 3) and 4) should be used to determine the accelerograms or response spectra in a site.

4.3 Seismic risk models

In the previous section the current techniques to obtain accelerograms, response spectra or power spectral density functions were presented. Once obtained, any of them could be used as a seismic input to a structure located in a seismic region. Whichever representation of the ground motion is chosen, the final objective of the exercise is to produce a design seismic input. This input should include the possible future different ground motions on a site,each one with its own characteristics like frequency, content, intensity, duration, etc..

An example of a design seismic input could be the Californian average response spectra discussed previously (Section 4.2.10). Similar average response spectra could be computed and used as design spectra for other regions of the world, if a satisfactory sample of accelerograms recorded in sites of those regions were available. Unfortunately this is not the case for most sites, and use has to be made of the so-called seismic risk models.

The seismic risk models are mathematical models which combine the knowledge about the earthquake phenomena with the seismic information available for a region; they are used to compute the values of the maximum ground motion intensities on a site and their corresponding probabilities of exceedance and/or associated time spans called return periods.

4.3.1 Seismic information

The information available about the seismic activity in a region could be classified depending on its nature as geophysical,

statistical and miscellaneous. Each of them could be further specified as follows:

- The geophysical information includes: a) the geotectonic features of the region, b) the energy stored in the region and c) the regional strain.

- The statistical data can be associated to: a) the magnitude, M , of earthquakes occurred in the region, b) the epicentral distance and focal depths observed, c) the energy released in the region and other regions of the crust of the Earth, d) the recurrence of earthquakes in the region, e) the attenuation laws derivated from the earthquakes observed in the region and f) the record of ground motion intensities in the region such as I(MM) , a_{max} , etc..

Finally the miscellaneous information includes: a) the qualitative description of the earthquake history of the region, such as Isoseismal Maps, and b) similarities of earthquakes with related phenomena.

4.3.2 Size, number and location of seismic events

The whole of the seismic information should ideally be included in the seismic risk model in order to consider the uncertainty about the size , number and location of future earthquakes which may occur in the vicinity of a site.

The size of an earthquake can be associated to its magnitude, M . The probability distribution of the magnitude for a region can be calculated by using magnitude-frequency laws, such as the Richter law:

$$\log_{10} N = a - bm \qquad \ldots (4.19)$$

where N is the number of earthquakes per year in excess of magnitude m occurred in a region, and a and b are regional constants. The upper limit to the magnitudes in a region, m_1 , can be obtained by applying the analysis of extreme-value techniques to the record of magnitudes in that region [4.10,4.25]; the lower limit in a region m_0 is usually chosen from engineering considerations.

The number of earthquakes in a region can be computed by using stochastic models of earthquake occurrence. In [4.10] a comprehensive

discussion of the earthquake occurrence models currently available is presented. One of the models acceptable for engineering purposes is the Poisson process; this implies that the probability of the waiting times between events is independent of the time passed since the last event. The probability P_N that N earthquakes with a magnitude m>M will occur in a time interval (0,t) is given by:

$$P_N = \frac{\exp(-\nu_M t)\ (\nu_M t)^N}{N!} \qquad \ldots (4.20)$$

where ν_M is the mean rate of exceedance of earthquakes with magnitude M for a given volume of earth crust.

The location of an earthquake in a region can be taken into account by considering that a region can be divided into several seismic sources, and that their contribution to the intensities in the site are functions of the distance from the site to the source. The random characteristics of this distance can be represented by a probability distribution [426].

4.3.3 Seismic risk models available

Several seismic risk models have been proposed [426,427,428,429], all of them share the basic assumptions that the ground motion intensities, I , in a site are the result of the contributions of the seismic activity of a number of sources, into which a region has been divided i.e. a superposition principle is implicitely accepted in all the models. However these models differ in the way they handle the uncertainties attached to the geophysical, statistical and miscellaneous information available, as well as to the uncertainties related to the conceptual models of the earthquake process. In [427,429] the explicit handling of the mentioned uncertainties by using Bayesian statistics has been advocated. This technique consists in using statistical information to judge the likelihood of each of the assumptions made, and a posterior probability function is obtained. The generality of the Bayesian approach makes its application highly desirable whenever it is possible; this is fully discussed in [410]. A non-Bayesian approach is proposed in [426] and [428] in which the uncertainties connected to the assumptions made are dealt with directly i.e. any assumption can be changed if the data or the judgement of the

specialist (say a geologist) rule against it.

In Appendix B Cornell's seismic model [4.26] is briefly described; other models [4.28,4.29] are commented upon in the same appendix in relation to the former model.

From Appendix B, the following conclusions can be drawn: the seismic risk model proposed by Cornell [4.26] performs satisfactorily in general, but better results can be obtained from it if the uncertainties about the different parameters which intervene are taken into account, whenever it is possible.

For the purpose of this study, i.e. to obtain the seismic risk for a site in the North Sea (where, as it will be made clear in Section 4.4 , the seismic information is scarce) the Cornell's seismic risk model will be used.

In order to take into account the uncertainties about the attenuation law utilised, the one proposed in [4.16] will be used. This attenuation law implicitely takes into account the uncertainties about the actual and predicted values of the ground intensity [4.16] . The uncertainties about the seismic source zones, activity rate γ , b , and I(MM) values for the seismic region under consideration will be discussed in Section 4.4.

4.4 Application of a seismic risk model

In this section Cornell's seismic risk model [4.26] (Appendix B) will be applied to derivate expressions to evaluate the maximum expected ground intensity in a site. The expressions for the expected maximum response spectra and the expected maximum ground spectra will be obtained. The attenuation laws to be used are the ones proposed in [4.16], Section 4.2.8.

The region in which the site is located is discretized into several seismic sources. Each source is associated to the following geometrical shapes depending on geotectonic and geophysical considerations: a point source, fig. 4.1, a line source, fig 4.2 , and an areal source, fig. 4.3. The following derivations apply to any of the three types of seismic sources: - The attenuation law reads:

$$Y = b_1 \, 10^{b_2 M} \, (R + 25)^{-b_3} \qquad \ldots (4.21)$$

where Y represents the ordinate of the ground spectra (Section 4.2.5) or the pseudovelocity spectra, S_v, (Section 4.2.8), M is the random magnitude of the earthquake, R its random focal distance and b_i, $i = 1, 2, 3$ are parameters given in [416], table 4.1.

- The conditional probability that $Y \geq y$ for $R = r$ is given by:

$$P[Y \geq y|R = r] = [b_1 \, 10^{b_2 M} \, (R+25)^{-b_3} \geq y|R = r] \qquad \ldots (4.22)$$

where y and r are particular values of Y and R respectively.

- If M and R are assumed to be statistically independent, after some algebraic manipulations of equation (4.22) the following expression is obtained for $M > m_0$:

$$P[Y \geq y|R = r] = 1 - F_M\left[\frac{1}{2.3b_2} \, Ln\left\{\frac{y}{b_1}(r+25)^{b_3}\right\}\right] \qquad \ldots (4.23)$$

and by considering that $m_0 \leq m \leq \infty$ i.e. by using equation (A3):

$$P[Y \geq y|R = r] = \exp(\beta m_0) \, b_1^{\alpha} \, y^{-\alpha}(r+25)^{-\alpha b_3} \qquad \ldots (4.24)$$

where β is a regional constant, and $\alpha = \beta/(2.3b_2)$.

- The probability that $Y \geq y$, given that $M \geq m_0$, is obtained by substituting equation (4.24) into equation (A 6):

$$P[Y \geq y]_j = \int_{r_1}^{r_2} \exp(\beta m_0) \, b_1^{\alpha} \, y^{-\alpha}(r+25)^{-\alpha b_3} f_{R_j}(r)\,dr \qquad \ldots (4.25)$$

where $j = p, \ell, a$ refers to a point, line and areal source respectively, and $f_{R_j}(r)$ adopts the following form depending on the geometrical shape selected for the source, i.e.:

. for a line source, ℓ, fig.4.2: $f_{R_\ell}(r) = \dfrac{2r}{l(r^2 - d^2)^{\frac{1}{2}}}$ $\qquad \ldots (4.26)$

. for an areal source, a, fig.4.3: $f_{R_a}(r) = r = [h^2 + (x_0 + x)^2]^{\frac{1}{2}}$ $\qquad \ldots (4.27)$

Substituting equations (4.26) and (4.27) into equation (4.25), the

following expressions are obtained:

$$P[Y \geq y]_{\ell} = \exp(\beta m_0)\ b_1^{\alpha}\ y^{-\alpha}\ (\mathrm{Int})_{\ell} \qquad \ldots (4.28)$$

in which $(\mathrm{Int})_{\ell}$ stands for:

$$(\mathrm{Int})_{\ell} = \frac{2}{d^{(\alpha b_3 - 1)}} \int_0^{\sec^{-1}(\frac{r_0}{d})} \frac{\sec^2\theta\ d\theta}{(\sec\theta + \frac{25}{d})^{\alpha b_3}} \qquad \ldots (4.29)$$

r_0 , d , and θ are the line source geometry parameters (fig.4.2) when the geometry of the source is not symmetrical with respect to the site, $(\mathrm{Int})_{\ell}$ can still be calculated by superimposing equivalent symmetrical sources appropriately [4.26] ; and:

$$P[Y \geq y]_a = \exp(\beta m_0)\ b_1^{\alpha}\ y^{-\alpha}\ (\mathrm{Int})_a \qquad \ldots (4.30)$$

$$(\mathrm{Int})_a = 2\pi \int_{x_0}^{(x_f - x_0)} \frac{(x_0 + x)\ dx}{\{[h^2 + (x_0 + x)^2]^{\frac{1}{2}} + 25\}^{\alpha b_3}} \qquad \ldots (4.31)$$

where x , x_f and h are defined in fig.4.3;the factor 2π is due to the fact that an area covered by a complete circle is considered. If the areal source covers a segment of the circle, the corresponding $(\mathrm{Int})_a$ can be computed by multiplying equation (4.31) by the quotient $\gamma/2\pi$, fig.4.3. If the source is represented by a point, there is no uncertainty about the distance R i.e. R = r fig.4.1 therefore:

$$P[Y \geq y]_p = \exp(\beta m_0)\ b_1^{\alpha}\ y^{-\alpha}\ (\mathrm{Int})_p \qquad \ldots (4.32)$$

in which

$$(\mathrm{Int})_p = (r + 25)^{-\alpha b_3} \qquad \ldots (4.33)$$

- If the annual probability of exceedance is less or equal to 0.05, the distribution of Y_{max} is obtained by substituting equations (4.28), (4.30) and (4.32) into equation (B9) i.e.:

$$[1 - F_{Y_{max}}(y)]_j = \exp(\beta m_0)\ b_1^{\alpha}\ y^{-\alpha}\ (\mathrm{Int})_j\ \nu_j \qquad \ldots (4.34)$$

$j = p , \ell, a$

where ν_j is the mean rate of exceedance of earthquake per year for the source j.

- The average return period T_0 is given by:

$$T_{0_j} = \frac{1}{[1 - F_{max}(y)_j]}$$

$$= \frac{1}{\exp(\beta m_0)\ b_1\ y^{-\alpha}(Int)_j\ \nu_j} \quad \ldots (4.35)$$

- The T_{0_j} years intensity is obtained from equation (4.35):

$$y = [\exp(\beta m_0)\ (Int)_j\ \nu_j\ T_{0_j}]^{\frac{1}{\alpha}}\ b_1 \quad \ldots (4.36)$$

or substituting the value $\alpha = \beta/(2.3b_2)$

$$y = \exp(2.3m_0\ b_2)\ b_1[(Int)_j\ \nu_j\ T_{0_j}]^{\frac{2.3b_2}{\beta}} \quad \ldots (4.37)$$

- Finally the probability of the maximum value of $Y \geq y$ produced by the n sources at a site can be computed by using equation (A11); the associated T_0 years intensity is given by:

$$y = \sum_{k=1}^{n} \{\exp(2.3m_0 b_2)\ b_1\ [(Int)\ \nu T_0]^{\frac{2.3b_2}{\beta}}\}_k \quad \ldots (4.38)$$

In this case the subindex k may correspond to any of the three types of sources i.e. point, line or areal; the parameters involved in equation (4.38) may be different for each source. From the same equation it can be seen that the values of m_0, β, γ, b_1, b_2, b_3, as well as the geometry parameters implicit in the expressions for (Int) need to be known for each source. The value of the return period, T_0, is fixed by a code or chosen by the design engineer.

- In the case where the distribution of magnitudes in the region should correspond to equation (B4) i.e. when $m_0 \leq m \leq m_1$, it can be shown that for small probabilities of exceedance,

$$\left[1 - F_{max}(y)\right]_j = \{(1 - k)\nu + k\nu[\exp(\beta m_0)\, b_1^{\alpha}\, y^{-\alpha}\, (Int)]\}_j \quad \ldots (4.39)$$

$j = p, \ell, a.$

where k is given by equation (B5) and ν and (Int) correspond to the seismic sources with a focal distance less or equal to:

$$r_y = \left[\frac{b_1}{y}\ 10^{b_2 m_1}\right]^{\frac{1}{b_3}} - 25\ (Km) \quad \ldots (4.40)$$

in which y is a chosen value of Y, for example the value obtained by using equation (4.38).

The return period $(T_0)_j$ is given by:

$$(T_0)_j = \frac{1}{\left[1 - F_{Y_{max}}(y)\right]_j} \quad \ldots (4.41)$$

and for the n independent sources,

$$T_0 = \frac{1}{\sum_{j=1}^{n} \left[1 - F_{Y_{max}}(y)\right]_j} \quad \ldots (4.42)$$

4.5 Seismic risk in a site in the North Sea

The seismic risk for a site in the North Sea, fig. 4.4, will be obtained in this section. The seismic risk model to be used is the Cornell's model described in Appendix B. The expected maximum ground intensity parameters at the site to be computed are the ground spectra, the pseudovelocity spectra, and the power spectral density.

The site is located in a region of low to mild seismic activity, [425], but which nevertheless has experienced recent earthquakes with magnitudes of importance, such as the one occurred in April 1884 near Colchester with an $M = 5$ to 5.5 [431], fig.4.4, and the one occurred in June 1931 in the Doggers Bank, fig. 4.4, with an $M = 6$ [425]. Earthquakes have also occurred in or nearby the Norwegian channel, fig. 4.4, such as the one occurred not far from Bergen in January 1927 with an $M = 5.1$ to 5.7 and others mentioned in [432]. From the geological point of view there is some evidence which points out the seismic activity of the region. For example in [433],

it is suggested that the pockmarks found in different sites under the sea bed of the North Sea are the result of seismic disturbances acting on normal or underconsolidated sediments.

4.5.1 Seismic information for the site

The seismic information available for the region in which the site is located, fig. 4.4 , has been mainly collected for inland events, in the U.K. and the Continental shelf [46,425,434]. Offshore seismic information for the region is by enlarge scarce and most of it is confined to the Norwegian Coast [432] .

Both inland and offshore information are mainly of macroseismic origin i.e. computed from seismographs located at large distances from the epifocus.

In [46] and [425] information about the seismic activity in the European area during the period 1901-1955 has been gathered and processed to generate homogeneous data of the seismicity in the European area. From these references [46,425] the seismic information about Fennoscandia (i.e. Norway, Sweden and Finland), and the one associated to the United Kingdom and Ireland are of interest for this study because the North Sea includes parts of both regions.

In the next paragraphs the geophysical, statistical and miscellaneous information drawn from [46,425] and elsewhere relevant to this study will be presented.

Geophysical information

a) Geotectonic features of the region [46,425] : it is located in what could be considered the middle part of the Eurasian plate; the Caledonian Hercynian and Alpine orogenies are present in its faults and foldings, for example the Caledonian orogeny runs from Northern Norway to Western Ireland; the Great Glen fault is the only one in the U.K. which clearly correlates with detected seismic activity in the region; there is also some evidence of the relation between the seismic activity and the faulting in the Norwegian coast and the Oslo fjord [432].

b) Energy stored in the region [434], based on the assumption that the seismic events in Fennoscandia are due to post-glacial uplift of the region, an estimate of the value of the energy stored

during the period 1891-1920 was given; however its validity has been questioned in [4.32]. In the United Kingdom region, such studies have not been carried out as yet. Therefore there is not for the time being an answer about the value of the energy stored in the region of interest for this study.

c) Regional strain: its distribution in time can be observed in fig. 4 of [4.25], which shows that the largest amplitudes of the regional strain curves have been produced by largest events in Norway and the United Kingdom regions; i.e. events such as the earthquake occurred in the sea South of Oslo in October 1924 with an $M = 6.5$, and the ones already mentioned, one near Bergen in Norway in 1927, and in the South of the North Sea (near the Dogger Bank) in 1931. The space distribution of the regional strain can be appreciated through the map of seismic energy release (ΣE) given in [4.25] (the regional strain is related to the energy released by equation (4.3)). From this map, it can be seen that most of the regional strain (energy) is concentrated: a) in the South-western coast and the Oslo region in Norway; and b) in the United Kingdom along the Great Glen fault and a line passing through Birmingham, Nottingham and Hull.

Statistical information

a) Files of magnitude for the region: by applying equation (4.5) to the files of I(MM) in the seismic zones of Fennoscandia, U.K. and Ireland, the set of data for M shown in table 4.2 was obtained in [4.6]. The lower limit of the earthquake magnitudes in the region m_0, was taken as 4.1 in [4.6] (it usually varies between 3.5 and 4.5 in seismic risk studies [4.26]). The upper limit of the magnitudes observed in the region, m_0, were 6.25 and 6.3 for seismic zones of Fennoscandia, the United Kingdom and Ireland respectively [4.6,4.2]. These values were taken from the frequency magnitude graphs obtained in those references. In [4.35] a $m_0 = 5.72$ was obtained by applying the analysis of extreme -technique to the magnitudes of earthquakes occurred in the United Kingdom.

b) File of earthquakes depths, h: in [4.25] the average depths $\bar{h} = 50$ Km and 15 to 20 Km were found for earthquakes occurred in Fennoscandia, the U.K. and Ireland respectively.

c) Energy released in the region: in Table 13 of [46] the values of the total seismic energy in Fennoscandia and the United Kingdom and Ireland during the period 1901-1955 are given. Those values represented approximately 0.1% of the total energy released in the whole European area which was 7.9×10^{24} ergs for the same period of time.

d) Recurrence of earthquakes: the frequency-magnitude law expressed by equation (4.9) was used in [46,425] and [436]; by applying different fitting techniques to the magnitude data, the values of the coefficients a and b shown in table 4.3 were obtained in those references.

e) Attenuation laws: the lack of accelerograms in the region of interest has prevented the derivation of attenuation laws for ground spectra for the region. Other studies [435,436] have utilized laws proposed in [437] and [438] but in the present study the attenuation laws proposed in [416] , equation (4.21), will be used instead. The reason behind this choice is that the latter laws have the advantage that the coefficients of variation are provided for the expected values of the ground motion parameters to be computed, table 4.1 and that the S_v can be computed directly instead of using the ground spectra in combination with amplification factors, Section 4.2.8.

f) Records of I(MM), a_{max}, S_v, etc.: there are records of I(MM) for the region and they have been used to derivate the values of M, when records of the latter were not available for the period of time considered [46,423,435]. Samples of a_{max} are very reduced for the region in general and inexistent for the U.K. region [436].

Miscellaneous information

a) Qualitative description of an earthquake history: most of the information available for the inland parts of the region of interest is in the form of isoseismal and epicentral maps such as the ones presented in [425,435] and [436]. In fig.4.5 a map of isoseismals for the region of interest is presented and in fig. 4.6 the associated map of epicenters can be seen. Both maps are based on the ones proposed in [425] .

b) Similarities of earthquakes with related phenomena: the

information of earthquakes related to phenomena for the region is very reduced, such as the one proposed in [4.34] which was briefly discussed in incise b) of the geophysical information of this section.

4.5.2 Selection of seismic sources and their parameters β, m_0, ν, h, b_i, i = 1,2,3

In this section, the seismic information of the region where the site is located, which was described in the last section will be used to select the geometries of the sources as well as their associated parameters.

Division of the region in seismic sources:

From the geophysical information of the region and the isoseismal maps, figs. 4.5 and 4.6, the choice of sources shown in fig. 4.7 was made. The radius of the outer circle limiting the seismic region was chosen on the basis of the recommendation of [4.28] in which a distance of 300Km between the site and the potential seismic source is suggested. However in this study 500Km will be used in order to be able to include the Great Glen fault as well as part of the Norwegian epicenters, figs.4.4 and 4.6. The offshore sources resulted from the fact that very little information exists about the offshore seismic activity of the region. It is also due to the fact that the geological structure of the North Sea is not known in detail. Therefore the offshore parts of the region will be treated as if any future earthquake was equally likely to occur in any unit area of their sources.

The inland sources will also be considered as equally likely to generate an earthquake in any unit area, except the line source associated to the Great Glen. This is so because the period of observation 1901-1955 is too short (in the geological and statistical sense) and there is the possibility that the present seismicity of the different provinces may change in the future in such a way that "aseismic" regions may become active. The only source which can be chosen relying on the seismotectonic information available is the line source associated to the Great Glen, fig. 4.4 . Finally a point source will be associated to the epicenter of the Dogger Bank earthquake of 1931, figs 4.4 and 4.6 .

Determination of the average rate ν for each seismic source:

The average rate ν_j for each source was obtained by dividing the number of earthquakes with $M > 4.1$ observed in each source (on the basis of the epicentral map shown in fig. 4.6) by the period of time of observation i.e. 55 years. In table 4.4 the resulting ν_j are shown. For the ν_j associated to the seismic sources 1,5 and 7 in which no seismic event was observed during the time period 1901-1955, three different values were assumed: a low seismicity case $\nu_{1,5,7} = 0.018$ = observed ν_8 ; an intermediate seismicity $\nu_{1,5,7} = 0.127$ = observed ν_2 and a high seismicity case $\nu_{1,5,7} = 0.163$ = observed ν_4, table 4.4. These values were chosen in order to represent three levels of the possible seismic activity in the region on the basis of the activity observed in the 55 years' record.

Determination of the value of β:

The value of β can be obtained from $\beta = 2.3b$, [4.26], in which b is the parameter of the frequency-magnitude law, equation (4.9) . The value of b can be chosen from table 4.3; for this study the value $b = 0.96$, which is an average value of b for the seismic regions of Fennoscandia, the U.K. and Ireland [4.6] will be used. This value was chosen by taking into consideration the fact that it represents a regional value obtained from a larger sample of events than the samples used for the individual regions, as in [4.29].

Selection of the value of m_0:

The value $m_0 = 4.1$ will be used in this work. A value of 4.0 is usually chosen [4.26, 4.28] because it is considered to be the lowest limit of magnitude which can cause damage to engineering structures, but a lower value could be selected if it is considered appropriate.

Selection of geometrical parameters:

The depth of sources can be chosen from the average depths $\bar{h}$ discussed in Section 4.5 . The depths selected are shown in table 4.4. These values were chosen because they represent regional averages and because they minimize the value of $(Int)_a$, equation (4.31). For the point and line sources the values of their depths were taken directly from the catalog in [4.25]. The rest of the source geometrical parameters such as γ, d, and x_0 were obtained on the basis of fig. 4.3

Selection of values b_1, b_2, b_3:

The values of b_i $i=1, 2, 3$ to be used in the attenuation law equation (4.21) are the ones shown in table 4.1 [4.16] .

Selection of values of T :

The following values of the return period were chosen: 25, 50, 100, 200 and 500 years. The 25 and 50 year values may correspond to the life-span of the offshore platform, and the other values provide the lower probability levels of exceedance from which other levels of structural behaviour can be obtained.

With the parameters listed above and the seismic risk model discussed in 4.4 , a set of ground spectra, pseudovelocity spectra and their associated power spectral density functions were computed. The p.s.d.f. were calculated by using equation (4.17) and a peak factor equal to 3.5 (Section 4.2.9). These results are discussed in Chapter 8.

4.6 Resulting seismic loads

In general, the seismic loads acting on an inland structure are defined as the inertia forces resulting from the motion of the base of the structure during an earthquake. If the structure is assumed to be rigidly attached to the ground and if it has been discretized in such a way that its mass properties have been lumped (Section 2.4) the inertia force acting on nodal point i is expressed as follows:

$$F_i(t) = m_{ii}(\ddot{u}_i)_t = m_{ii}(\ddot{u}_i) + m_{ii}(\ddot{u}_g) \qquad \ldots (4.42)$$

where F_i is the resulting inertial force, m_{ii} is the lumped mass at nodal point i , $(\ddot{u}_i)_t$ is the total acceleration of m_{ii} ; $\ddot{u}_i$ is the acceleration of m_{ii} relative to the base of the structure and $\ddot{u}_g$ is the ground acceleration. According to the governing equation, equation (2.1), Section 2.2, the term $m_{ii}(\ddot{u}_i)$ corresponds to the element ii of the diagonal matrix resulting from the product $\underset{\sim}{M}\ \ddot{\underset{\sim}{U}}$; the term $m_{ii}(\ddot{u}_g)$ represents the ith component of the vector $\underset{\sim}{P}$ i.e.:

$$P_{s_i}(t) = - m_{ii}(\ddot{u}_g) \qquad \ldots (4.43)$$

where $P_{s_i}(t)$ is the effective seismic load acting on the ith nodal point of the discretized structure.

In Chapter 8 a number of p.s.d.f. of ground acceleration are presented. As shown in Section 4.2.7, they represent one of the forms to express the energy content of a set of accelerograms $\ddot{u}_g$; therefore they are implicitely included in equation (4.43). The actual use of those p.s.d.f. to define the seismic loads acting on a c.g.p. will be shown in Chapters 6 and 7 .

5. WAVE EXCITATION

5.1 Introduction

The wave loads are generated when sea waves incide over the surface of a structure placed in the sea environment. The difference in the relative motion between the fluid and the structure results in an interaction process. In this process the kinematic characteristics of the waves are usually modified by the presence of the structure. The waves which are of interest from the offshore design point of view are the so-called wind generated waves. The mechanisms underlying its generation are not completely explained as yet; however, a number of theories about them have been proposed [5.1, 5.2, 5.3]. A common assumption in those theories is the contribution of the wind in the wind-fluid energy transfer process; however, the way in which this energy acts on the fluid surface is different from one approach to the next. For example, the resonance model proposed in [5.1] assumes that the fluid surface motion is induced by pressure fluctuations in the wind, which are in random phase with the waves; meanwhile, the shear flow model [5.2] suggests that the waves modify the field of the air flowing at a certain distance over them. A mixed model based on both mentioned approaches was presented in [5.3], which assumed that the two mechanisms are complementary in the wave generation process.

The theories of wind wave generation discussed above have in common the assumption that a sea wave results from the random superposition of a number of waves which propagate in different directions and have different kinematic characteristics, i.e. a wind generated wave can be considered as a random process. From the above paragraph it can be concluded that the generation process of the wind waves is not fully explained as yet; therefore, the description of these waves has to resort on a combination of deterministic and non-deterministic theories to reach that end [5.4]. The classical hydrodynamic principles used to approximate the kinetic characteristics of the waves are discussed in Section 5.2.1; the random process utilized to formulate the non-deterministic characteristics of the sea waves is presented in Sections 5.2.2 to 5.2.4.

Once the kinematics of the wind generated waves is formulated, the fluid structure interaction which produces the wave loads can be studied. Depending on the combination of the wave and geometrical

structure parameters involved, the wave forces resulting are associated to different wave loading regimes, such as the so-called drag, inertia, diffraction and other wave loading regimes. The different wave loading regimes typical of concrete gravity platforms are discussed in Section 5.3.1. The drag, inertia and diffraction regimes are presented in Sections 5.3.2, 5.3.3 and 5.3.5 respectively. Finally, in Section 5.4 the expressions for wave loading used in this work are discussed.

5.2 Wave characteristics

5.2.1 Basic hydrodynamics

As it was briefly commented in the introduction, the wind generated waves can be considered as random processes; therefore, it is expected that their full description requires the use of a three-dimensional random process. However, as most of the reliable field data has been obtained for unidirectional waves, only this case will be presented in this work. Neglecting the randomness of the waves for a while, the simpler idealization of the waves is to represent them by simple harmonic waves. This idealization nevertheless is useful to establish the basic elements for the derivation of the kinematics of the sea waves; furthermore, the linear wave theory [5.5] can be used to this end (there are other higher order theories which could also be used); a brief summary of the linear wave theory [5.4, 5.5] is presented in this section.

The sea state is represented by simple harmonic waves based on the following assumptions:
a) the fluid is incompressible, b) the fluid is non-viscous, c) the waves are two-dimensional (fig.5.1), d) the waves are stationary in space and in time, e) Coriolis effect is neglected.
The equation of continuity of a fluid is given by:

$$\frac{D\rho}{Dt} + \rho \nabla . \underset{\sim}{\dot{v}} = 0 \qquad \ldots (5.1)$$

The equation of motion is expressed by:

$$\frac{D\underset{\sim}{\dot{v}}}{Dt} = \underset{\sim}{F_b} - \frac{1}{\rho} \nabla p \qquad \ldots (5.2)$$

where $\frac{D}{Dt}$ represents the total derivative of a variable, ρ is the fluid density, ∇ is the nabla vector and $\underset{\sim}{\dot{v}}$ is the vector of fluid particles velocities; $\underset{\sim}{F}_b$ represents the body forces and ∇p is the pressure gradient.

From assumption a), equation (5.1) is reduced to:

$$\nabla . \underset{\sim}{\dot{v}} = 0 \qquad \ldots (5.3)$$

and assumption b) implies:

$$\nabla \times \underset{\sim}{\dot{v}} = \underset{\sim}{0}$$

i.e.

$$\underset{\sim}{\dot{v}} = - \nabla \phi \qquad \ldots (5.4)$$

where ϕ is the velocity potential.

Substituting equation (5.4) into equation (5.3),

$$\nabla^2 \phi = 0 \qquad \ldots (5.5)$$

From fig.5.1, the boundary conditions (b.c.) associated to equation (5.5) are:

$$\dot{v}_y = - \left. \frac{\partial \phi}{\partial y} \right|_{y = -D} = 0 \qquad \ldots (5.6)$$

$$p \big|_{y = \eta} = 0 \qquad \ldots (5.7)$$

where $\dot{v}_y$ is the fluid particle velocity in the y direction and η is a particular value of the wave height. The last b.c. equation (5.7) has to be expressed in terms of the potential ϕ, in order to have a system of equations in which the variable is ϕ only.

Integrating equation (5.2) for the x and y directions plus assumption b) leads to Bernoulli's equation:

$$- \frac{\partial \phi}{\partial t} + \frac{1}{2} (\dot{v}_x^2 + \dot{v}_y^2) + \frac{p}{\rho} + gy = 0 \qquad \ldots (5.8)$$

where $\dot{v}_x$ is the fluid particle velocity in the x direction and g the acceleration of gravity; the other parameters were already

defined.

By considering the small amplitude wave theory, Airy Theory, which assumes that the amplitude of the surface wave is small compared to the length of the wave, or to the depth of the water where it propagates (see Fig.5.1) equation (5.8) is reduced to:

$$-\frac{\partial \phi}{\partial t} + \frac{p}{\rho} + gy = 0 \qquad \ldots (5.9)$$

Substituting equation (5.9) into equation (5.7) allows to express this b.c. as a function of ϕ i.e.:

$$\left.\frac{\partial \phi}{\partial t}\right|_{y = \eta} = \left.\frac{\partial \phi}{\partial t}\right|_{y = 0} = g\eta \qquad \ldots (5.10)$$

In short the system to be solved is:

$$\begin{aligned} &\nabla^2 \phi = 0 \\ \text{b.c.} \quad &\left.\frac{\partial \phi}{\partial y}\right|_{y = -D} = 0 \\ &\left.\frac{\partial \phi}{\partial t}\right|_{y = 0} = g\eta \end{aligned} \qquad \ldots (5.11)$$

The solution to the system of equations (5.11) is:

$$\phi = \frac{ag}{\omega} \frac{\cosh \kappa(y + D)}{\cosh (\kappa D)} \sin(\kappa x - \omega t) \qquad \ldots (5.12)$$

which is a progressive wave travelling in the positive direction of the x axis with a circular frequency ω, fig.5.1. In equation (5.12) a represents the amplitude of the harmonic wave, ω is its frequency, κ is the wave number, D is the total depth and x, y and t are the space and time coordinates respectively.

Another consequence of the small amplitude assumption is:

$$\left.\frac{\partial \phi}{\partial t}\right|_{y = 0} \doteq \left. -\frac{\partial \phi}{\partial y} \right|_{y = 0} \qquad \ldots (5.13)$$

and from equation (5.10):

$$\eta = \frac{1}{g} \frac{\partial \phi}{\partial t} \qquad \ldots (5.14)$$

Combining equations (5.13) and (5.14):

$$\frac{1}{g}\frac{\partial^2\phi}{\partial t^2} + \frac{\partial\phi}{\partial y} = 0 \qquad \ldots (5.15)$$

By substituting equation (5.12) into equation (5.15) and taking the deep water conditions, $D >> y$, into consideration, the following relations are derivated:

$$\omega^2 \doteq g\kappa$$

$$\omega = 2\pi f = \frac{2\pi c}{\lambda} = \kappa c \qquad \ldots (5.16)$$

$$c = \sqrt{g/\kappa} = \frac{\lambda}{T}$$

where f is the frequency of the wave in cycles per unit of time, c is the wave celerity, λ is the length of the wave and T is the wave period. The particle velocity in the x and y directions is obtained from the gradient of ϕ :

$$\dot{v}_x = -\frac{\partial\phi}{\partial x} = \frac{ag\kappa}{\omega}\,\frac{\cosh\kappa(y+D)}{\sinh(\kappa D)}\cos(\kappa x - \omega t) \qquad \ldots (5.17)$$

$$\dot{v}_y = -\frac{\partial\phi}{\partial y} = \frac{ag\kappa}{\omega}\,\frac{\sinh\kappa(y+D)}{\sinh(\kappa D)}\sin(\kappa x - \omega t) \qquad \ldots (5.18)$$

The particle accelerations in the x and y directions can be computed from equations (5.17) and (5.18):

$$\ddot{v}_x = ag\kappa\,\frac{\cosh\kappa(y+D)}{\sinh(\kappa D)}\sin(\kappa x - \omega t) \qquad \ldots (5.19)$$

$$\ddot{v}_y = -ag\kappa\,\frac{\sinh\kappa(y+D)}{\sinh(\kappa D)}\cos(\kappa x - \omega t) \qquad \ldots (5.20)$$

The particle trajectory r can be obtained from:

$$r_x = \int_0^t \dot{v}_x\,dt$$

$$= a\,\frac{\cosh\kappa(y+D)}{\sinh(\kappa D)}\sin(\kappa x - \omega t) \qquad \ldots (5.21)$$

$$r_y = \int_0^t \dot{v}_y \, dt$$

$$= - a \frac{\sinh \kappa(y + D)}{\sinh (\kappa D)} \cos (\kappa x - \omega t) \qquad \ldots (5.22)$$

From equations (5.21) and (5.22) it can be concluded that the particle trajectories describe circles with radii that tend to zero as y tends to D. If $y = 0$, equation (5.22) becomes:

$$r_y = \eta = - a \cos (\kappa x - \omega t) \qquad \ldots (5.23)$$

Substituting equation (5.12) into (5.9), the pressure p is obtained:

$$p(x,y,t) = \rho g \left[y + a \frac{\cosh \kappa(y + D)}{\sinh (\kappa D)} \cos (\kappa x - \omega t)\right]$$

$$y \leq 0 \qquad \ldots (5.24)$$

The main feature of Airy's wave theory is that a wave can be defined by using three independent parameters, namely, period (T), wave height (H) and mean water depth (D). All other parameters are functions of the above-mentioned ones. In [5.6] a classification of wave theories based on their behaviour to fulfill the boundary conditions is presented; among other conclusions it is mentioned that the Airy's wave theory is satisfactory in medium deep waters (i.e. 100-200 m. for example).

An average of the wave energy content over the wavelength and per unit area of the sea surface can be computed as a sum of the kinetic energy (KE) of orbital motion and potential energy (PE) of water level change. By using (5.18), (5.21) and (5.22) it can be shown that the average energy, $\overline{E}$, contained per unit area equals:

$$\overline{E} = \overline{PE} + \overline{KE}$$

$$= \tfrac{1}{4} \rho g a^2 + \tfrac{1}{4} \rho g a^2$$

$$= \tfrac{1}{2} \rho g a^2 \qquad \ldots (5.25)$$

5.2.2 Modelling of sea waves

From the coastal engineering point of view the main interest lies in the so-called wind generated waves; these waves contain larger amounts of energy which, at a certain time, will be transferred to the structures built up in the ocean environment. As mentioned in the introduction, the wind generated waves are rather complicated in nature; therefore, any mathematical representation of them should preserve this essentially random (non-deterministic) characteristic, fig.5.2.

Among other criteria for the mathematical modelling of wind generated waves, there are two which are widely accepted, namely [5.7] :

a) the random superposition of periodic wave patterns, and

b) the continuous juxtaposition of random impulses.

In criterion a), steady state solutions with a random phase are superposed, and in criterion b), transient solutions are sequentially added. Model a) has the advantage of using the sinusoidal wave representation derivated from Airy's wave theory, which makes its use simpler than the one associated to model b). In this section, only the former approach will be presented.

The representation of wind generated waves by using model a) was introduced in [5.8]. It assumes that the vertical movement of the particles, η , on the sea surface, generated by a unidirectional wind, can be represented by the superposition of N simple harmonic waves (as the ones obtained in equation (5.23)) of amplitude a_i ($i = 1,2, \ldots N$), frequency ω_i and random phase ε_i ; i.e.:

$$\eta(x,t) = \sum_{i=1}^{N} \eta_i(x,t)$$

$$= \sum_{\substack{i=1 \\ N \to \infty}}^{N} a_i \cos(\kappa_i x - \omega_i t + \varepsilon_i) \qquad \ldots (5.26)$$

with $0 \leq \omega_i \leq \infty$

$0 \leq \varepsilon_i \leq 2\pi$

The frequencies ω_i are uniformely spaced at intervals $\Delta\omega$, and the phase ε_i is random and uniformely distributed (i.e. the value of its probability density function is equal to $1/2\pi$).

If the abscissa x is kept constant in equation (5.26), the associated wave height will be a function of time only. From the frequency spacing condition the wave height will have a period $2\pi/\Delta\omega$. The average energy content per unit area of sea surface $(\overline{E})$ given in equation (5.25) shows that $\overline{E}$ is proportional to a . By analogy, in the case of equation (5.26) this definition can also be applied; but it will be associated to the amount of wave energy contained in a band frequency $\Delta\omega$ centered at ω_i i.e.:

$$\overline{E}(\omega_i)\Big|_{\Delta\omega} = \frac{1}{2}\rho g \sum_{\omega_i}^{\omega_i+\Delta\omega} a_i^2$$

$$= \rho g \; S_{\eta\eta}(\omega_i)\Delta\omega \qquad \ldots (5.27)$$

where $S_{\eta\eta}(\omega_i)$ is called the energy or power spectrum.

If the random process represented by equation (5.26) is assumed to be a zero mean, stationary, gaussian and ergodic process, it can be shown [59] that its mean square value is given by:

$$\langle \overline{\eta(t)^2} \rangle = R_{\eta\eta}(0)$$

$$= \int_0^\infty S_{\eta\eta}(\omega)\, d\omega \qquad \ldots (5.28)$$

Equation (5.28) implies that the amplitude a_i must tend to zero in order to produce a finite mean square value of the wave height. As a consequence, the formal definition for $S_{\eta\eta}(\omega)$ is:

$$S_{\eta\eta}(\omega_i) = \frac{1}{2}\sum_{\omega_i}^{\omega_i+\Delta\omega} \frac{a_i^2}{\Delta\omega} \qquad \ldots (5.29)$$

because $a_i^2 \to \infty$, when $N \to \infty$, whereas $a_i^2/\Delta\omega$ does not.

From equation (5.29):

$$\sum_{\omega_i}^{\omega_i+\Delta\omega} a_i = \sqrt{2\, S_{\eta\eta}(\omega_i)\Delta\omega} \qquad \ldots (5.30)$$

and substituting equation (5.30) into equation (5.26):

$$\eta(x,t) = \lim_{\substack{\Delta\omega \to 0 \\ n\Delta\omega \to \infty}} \sum_{i=0}^{\infty} \sqrt{2\, S_{\eta\eta}(\omega_i)\Delta\omega}\, \cos(\kappa_i x - \omega_i t + \varepsilon_i)$$

$$\ldots (5.31)$$

By analogy, the counterpart of equations (5.17) to (5.22) can be written as follows for this random representation of the sea waves:

$$\dot{v}_x = \lim_{\substack{\Delta\omega \to 0 \\ n\Delta\omega \to \infty}} \sum_{i=0}^{\infty} \omega\sqrt{2S_{\eta\eta}(\omega_i)\Delta\omega}\ \frac{\cosh \kappa_i(y+D)}{\sinh(\kappa D)} \cos(\kappa_i x - \omega_i t + \varepsilon_i) \quad \ldots (5.32)$$

$$\dot{v}_y = -\lim_{\substack{\Delta\omega \to 0 \\ n\Delta\omega \to \infty}} \sum_{i=0}^{\infty} \omega\sqrt{\quad\quad}\ \frac{\sinh \kappa_i(y+D)}{\sinh(\kappa D)} \sin(\kappa_i x - \omega_i t + \varepsilon_i) \quad \ldots (5.33)$$

$$\ddot{v}_x = \lim_{\substack{\Delta\omega \to 0 \\ n\Delta\omega \to \infty}} \sum_{i=0}^{\infty} \omega^2\sqrt{\quad\quad}\ \frac{\cosh \kappa_i(y+D)}{\sinh(\kappa D)} \sin(\kappa_i x - \omega_i t + \varepsilon_i) \quad \ldots (5.34)$$

$$\ddot{v}_y = -\lim_{\substack{\Delta\omega \to 0 \\ n\Delta\omega \to \infty}} \sum_{i=0}^{\infty} \omega^2\sqrt{\quad\quad}\ \frac{\sinh \kappa_i(y+D)}{\sinh(\kappa D)} \cos(\kappa_i x - \omega_i t + \varepsilon_i) \quad \ldots (5.35)$$

$$r_x = \lim_{\substack{\Delta\omega \to 0 \\ n\Delta\omega \to \infty}} \sum_{i=0}^{\infty} \sqrt{\quad\quad}\ \frac{\cosh \kappa_i(y+D)}{\sinh(\kappa D)} \sin(\kappa_i x - \omega_i t + \varepsilon_i) \quad \ldots (5.36)$$

$$r_y = -\lim_{\substack{\Delta\omega \to 0 \\ n\Delta\omega \to \infty}} \sum_{i=0}^{\infty} \sqrt{\quad\quad}\ \frac{\sinh \kappa_i(y+D)}{\sinh(\kappa D)} \cos(\kappa_i x - \omega_i t + \varepsilon_i) \quad \ldots (5.37)$$

Equations (5.32) to (5.37) provide the kinematics of the random representation of unidirectional wind generated waves.

5.2.3 Statistics of sea waves

The recording of the time history of sea surface elevation (fig 5.2) and the stochastic modelling of time series [5.9] provided the tools for a more realistic representation and understanding of sea waves. This led to the computation of practical results based on statistics of field data and theoretical studies. Some of these results will be mentioned in this section.

The statistical characterization of sea waves has been mainly concentrated in two wind generated wave parameters, namely height and period. A reason for this lies in the fact that the height is associated to the energy of a wave (Section 5.2) and the period is linked to the frequency of that wave.

A very important step toward the derivation of analytical expressions of the statistics of wave heights was given in [5.10, 5.11] . The main assumption in both papers is to represent the sea surface by a zero mean, ergodic gaussian process (equation (5.6)). Among other results they found out the following ones:

a) The process representing a wave height record can be narrow or wide band, depending on the value of the so-called spectral width parameter ε_0 . This parameter varies between 0 and 1 , and can be computed by:

$$\varepsilon_0^2 = \frac{m_0 m_4 - m_2^2}{m_0 m_4} \qquad \ldots (5.38)$$

where the nth spectral moment is

$$m_n = \int_0^\infty S_{\eta\eta}(\omega)\ \omega^n\ d\omega \qquad \ldots (5.39)$$

and $n = 0, 1, 2, \ldots$

$S_{\eta\eta}(\omega)$ = power spectral density of wave heights.

b) If the process is narrow band i.e. $\varepsilon_0 \to 0$ (which implies that the energy is mainly concentrated in a small frequency band of the associated energy spectrum), the maximum of surface elevation follows a Rayleigh probability density function, i.e.:

$$p(\eta_{max}) = \frac{\eta_{max}}{m_0} \exp\left[-\eta^2_{max}/2m_0 \right] \qquad \ldots (5.40)$$

Based on this result and taking into account that for a narrow frequency spectrum the wave height, H , is twice the maximum amplitude, the following statistics of wave height and wave period were obtained:

$$H_{mode} = 2\sqrt{m_0}$$

$$
\begin{aligned}
H_{r.m.s.} &= 2.828\ \sqrt{m_0} \\
\overline{H} &= 2.507\ \sqrt{m_0} \\
H_{\frac{1}{3}} &= 4.0\ \sqrt{m_0} \\
H_{\frac{1}{10}} &= 5.1\ \sqrt{m_0} \\
T_0 &= 2\pi\ \sqrt{m_0/m_2}
\end{aligned}
\qquad \ldots (5.41)
$$

where m_0, m_2 can be computed by using equation (5.39)

H_{mode} = most probable value of wave heights,

$H_{r.m.s.}$ = root-mean square value of wave heights,

$H_{\frac{1}{3}}$ = average of the highest one third of the waves, also known as significative wave heights, H_s ,

$\overline{H}$ = mean value of wave height,

$H_{\frac{1}{10}}$ = average of the highest one tenth of the waves, sometimes taken as the expected value of maximum wave height,

T_0 = average time between successive zero up-crossings (fig. 5.2).

c) If the process is broad-band i.e. $0 < \varepsilon_0 \leq 1$ (this means that the energy is distributed on a wide frequency band of the associated energy spectrum) the statistical distribution of the maxima of surface elevation is given by:

$$
p(x) = \frac{1}{\sqrt{2\pi}} \{\varepsilon_0 \exp\left[-x^2/2\,\varepsilon_0^2\right] + \sqrt{1-\varepsilon_0^2}\; x \exp\left[-x^2/2\right] \int_{-\infty}^{x\sqrt{1-\varepsilon_0^2}/\varepsilon_0} \exp\left[-t^2/2\right] dt \}
\qquad \ldots (5.42)
$$

where

$$x = \eta_{max}/\sqrt{m_0}$$

When $\varepsilon_0 \to 0$, the expression for $p(x)$ becomes a Rayleigh distribution (narrow band process), and for $\varepsilon_0 \to 1$, $p(x)$ is reduced to a Gaussian distribution. Based on these results the following statistics were obtained:

$$(H_{max})_{mode} = 2\sqrt{m_0}\left[\sqrt{2 \text{ Ln } N_0}\right]$$

$$\overline{H}_{max} = 2\sqrt{m_0}\left[\sqrt{2 \text{ Ln } N_0} + \frac{0.5772}{\sqrt{2 \text{ Ln } N_0}}\right] \quad \ldots (5.43)$$

where

$(H_{max})_{mode}$ = most probable value of maximum wave height,

$\overline{H}_{max}$ = mean value of maximum wave height,

$N_0 = \frac{T}{T_0}$ = number of zero upcrossings in the record (fig. 5.2),

T = the record duration and

T_0 was previously defined.

5.2.4 Empirical wave height spectra

Several empirical formulae (based on the analysis of wave amplitude records) have been proposed to express the power spectral density function of the wave heights, $S_{\eta\eta}$, as a function of the frequency, ω . The wind velocity W or the significant wave height H_s and significant wave period T_s are used in those expressions. The general equations for these spectral density functions are as follows [5.12] :

a) For wind velocity W :

$$S_{\eta\eta}(\omega) = \frac{A}{\omega^5} \exp\left[-B/W^4\ \omega^4\right] \quad \ldots (5.44)$$

where

A and B are empirical constants, W is the wind velocity at approximately 20 m. above sea level and ω is the frequency in rad./sec..

b) For significant wave height and period:

$$S_{\eta\eta}(\omega) = \frac{AH_s^2}{T_s^4\omega^5} \exp\left[-B/T_s^4\,\omega^4\right] \qquad \ldots (5.45)$$

T_s is usually expressed as a function of H_s. The empirical constants A and B can be computed by solving the system:

$$\begin{aligned} \frac{A}{4B} &= m_0 \\ \frac{A}{4}\sqrt{\frac{\pi}{B}} &= m_2 \end{aligned} \qquad \ldots (5.46)$$

where m_0 and m_2 -previously defined- should be computed for the particular sea state considered.

Two expressions for the computation of the power spectral density function of the wave heights are listed here:

1) Pierson and Moskowitz P-M [5.12] (fig. 8.13).

For fully developed seas (i.e. seas in which the fetch length and duration are long enough for a given velocity to produce the highest possible waves):

$$S_{\eta\eta}(\omega) = \frac{\alpha g^2}{\omega^5} \exp\left[-\beta(g/W\omega)^4\right] \qquad \ldots (5.47)$$

or

$$S_{\eta\eta}(\omega) = \frac{\alpha g^2}{\omega^5} \exp\left[-\frac{5}{4}\left(\frac{\omega}{\omega_{max}}\right)^{-4}\right] \qquad \ldots (5.48)$$

where the units of $S_{\eta\eta}(\omega)$ are $(m^2\text{-sec.})$ and,

$$\omega_{max} = (4\beta/5)^{\frac{1}{4}}\ (g/W),$$

α is a dimensionless constant = 0.0081 (for the North Sea),

β is a dimensionless constant = 0.74 (for the North Sea),

W is the wind velocity at a height of 19.5 m. above the sea surface,

g is the acceleration due to gravity and

ω_{max} is the frequency associated with the maximum value of $S\eta\eta(\omega)$.

2) Jonswap [5.13] (fig. 8.13).

This is similar to the P-M with an extra term called "overshoot", a term which takes the fetch limited condition into account.

$$S\eta\eta(\omega) = \frac{\alpha g^2}{\omega^5} \exp\left[-\frac{5}{4}\left(\frac{\omega}{\omega_{max}}\right)^{-4}\right] \gamma^{\exp\left[\frac{-(\omega-\omega_{max})^2}{2\sigma^2\,\omega_{max}^2}\right]} \quad \ldots (5.49)$$

where the units of $S\eta\eta(\omega)$ are $(m^2 - sec.)$, γ is the ratio of the maximum spectral energy level to the corresponding level of the P-M spectrum, usually called overshoot parameter, which is equal to 3.3 for the North Sea.

$$\sigma = \begin{cases} \sigma_a & \text{for } \omega \leq \omega_{max} \\ \sigma_b & \text{for } \omega > \omega_{max} \end{cases} \quad \ldots (5.50)$$

The average value of σ_a and σ_b in the North Sea are 0.07 and 0.09 respectively. The rest of the parameters were previously defined in relation to equation (5.48).

5.3 Wave loads

5.3.1 Wave loading regimes

The determination of the forces exerted by sea waves on structures represents a complicated task. The main difficulty lies in the fact that these forces are the result of an interactive process between the structure and the waves. In this process the former will usually modify the kinematics of the latter, with respect to the case in which no structure exists in the sea environment. Due to this characteristic

of the problem, the models used to determine the wave loads on structures have aimed at isolating the effects observed in the kinematics of the wave for specific combinations of wave and structure parameters.

A summary of the different loading regimes derived from analytical, field and laboratory experiments on the interaction flowing fluid-structure has been suggested in [5.14] . This summary is listed here:

a) $d/\lambda > 1$ . . . Condition near to pure reflection
b) $d/\lambda > 0.2$ . . . Diffraction increasingly predominant
c) $d/W_0 > 0.2$ . . . Inertia increasingly predominant
d) $d/W_0 < 0.6$ . . . Incipience of lift and drag
e) $d/W_0 < 0.2$ . . . Drag increasingly predominant

where d is the structure characteristic dimension, λ is the wave length, and W_0 is the wave orbit width parameter.

If the offshore structure is a concrete gravity platform placed on deep waters, the parameter "d" mentioned above could be the diameter of the caisson or the diameter of the towers. The parameters W_0 and λ correspond to the wave height and the wave length respectively.

For the caisson, the typical values of the ratio d/λ are larger than 0.2 ; therefore, the loads acting on the caisson are mainly produced by diffraction effects. For the towers, typical values of the ratios d/λ and d/W_0 are such that while portions of their length are subjected to loads produced by diffraction effects other parts are under loads associated to inertia and (sometimes) drag effects.

From the above paragraph it is clear that the loading regimes of interest for typical concrete gravity platforms are the diffraction, inertia and drag ones; therefore, in the following paragraphs, only those loading regimes will be discussed.

The actual determination of the forces resulting from any of the mentioned wave loading regimes implies the solution of the following problem: evaluate the forces acting on a body immersed in a non-uniform, unsteady, viscous fluid flow.

This problem is difficult to solve, because it requires, among other things, the finding of the kinematics of the boundary layer formed around the body [515] . This "boundary layer problem" is difficult to be solved even for simple geometrical shapes

immersed in a steady flow [5.7] . Therefore, the original problem has been idealized in such a way that its solution consists in the determination of the net force associated to the pressure and shear distribution on the surface of the object. This force is represented by the product of a coefficient (obtained experimentally) multiplied by a term which includes the structural characteristic parameters and the wave resulting kinematics.

5.3.2 Drag loads $(d/W_0) < 0.2$

The flow in a viscous fluid is characterized by the presence of normal (pressure) and tangential (shear) forces between adjacent infinitesimal layers of fluid. If a body is immersed in this fluid and kept stationary, the shear forces will cause an adhesion of the fluid particles close to the surface of the body. Due to this friction effect, a large velocity gradient field is generated around the body i.e. a boundary layer is produced [5.15] . In addition, a wake of flow is produced and consequently the pressure distribution around the body is not in equilibrium. The non-equilibrium resultant forces can be decomposed into two components: the drag force, acting parallel to the flow direction, and the lift force, which acts perpendicularly to the first. For symmetrical bodies the lift force is null [5.7] .

The drag force is composed of two parts: a form drag and a skin friction drag. The first is related to the fluid pressure forces over the body surface, and the second one is associated to the shearing forces which are a function of the fluid viscosity. The form drag is dominant in bluff shapes, such as cylinders, and for large numbers of Reynolds it is proportional to the square of the undisturbed velocity [5.15] . For streamlined shapes the skin friction is dominant.

The body shapes of a typical c.g.p. components are of the bluff type; therefore, in what follows, when the term drag is used, it will refer to the form drag. The actual determination of the drag force from a mathematical model includes the solutions of the boundary layer problem for a cylindrical shape immersed in an unsteady flow [5.7] . This problem is extremely complicated even when dealing with the same shape immersed in a steady flow; therefore its solution has required the experimental determination of a so-called drag coefficient which replaces an integral involving the flow velocity far and close to the boundary

layer [5.7] i.e. the expression for the drag force P_{drag} ,

$$P_{drag} = \rho \dot{v}^2 d \int_{-\infty}^{\infty} \{ \frac{\dot{v}_0}{\dot{v}} - \frac{\dot{v}_0^2}{\dot{v}^2} \} \, d\Omega \qquad \ldots (5.51)$$

(where ρ is the mass density of the fluid, $\dot{v}$ is the fluid velocity far from the body, $\dot{v}_0$ is the fluid velocity within the boundary layer, d is the diameter of the cylinder and Ω is the direction perpendicular to the surface of the boundary layer) can be substituted by the following expression [5.7] :

$$P_{drag} = \rho d \frac{\dot{v}^2}{2} K_d \qquad \ldots (5.52)$$

where K_d represents the integral in equation (5.51) and is called the drag coefficient; the other parameters have previously been defined. K_d has been determined experimentally for steady flow conditions; it depends on the shape of the structure and the number of Reynolds ($R_N = v_0 d/\gamma$, in which γ is the kinematic viscosity of the fluid).

The values of K_d obtained for cylinders show a great scatter; for example, in [5.16] , it is reported that K_d varies between 1.0 and 1.4 , meanwhile in [5.17] a value of $K_d = 0.5$ is recommended. Another author [5.18] has suggested $K_d = 1.0$ whereas in [5.19] a mean value of $\overline{K}_d = 1.05$ is proposed. In practice, the higher values of K_d are associated to slender members, which, combined with large values of the fluid velocities produce large drag forces.

5.3.3 Inertia loads $(d/W_0) > 0.2$

When a body is submerged into an unsteady, non-uniform, viscous fluid flow, in addition to the drag forces discussed in the previous section, an inertia force is observed. This inertia force is generated by the difference of relative velocities existing between the body and the fluid flow. The existence of this inertia force is confirmed when studying a simpler case such as the one associated to a vertical cylinder travelling with uniform velocity in a stationary fluid. By using potential flow theory (Section 5.2) the fluid velocity distribution can be found, and the total kinetic energy of the fluid per unit length of cylinder can be evaluated. This

kinetic energy is equal to a mass of fluid associated to the volume of the cylinder multiplied by the square of the velocity of the fluid [5.7] ; the mass of fluid into question is known as the "displaced mass". The total kinetic energy in the system is equal to the kinetic energy of the fluid plus the one generated by the movement of the cylinder. In this case it can be shown [5.7] that the mass involved is equal to the mass of the cylinder plus the displaced mass.

From the case described above, when considering a fix cylinder immersed in an accelerating fluid, the inertia force, P_{in} , required by the cylinder to keep its equilibrium position is equal to the mass of the cylinder, M_c , plus the displaced mass, M_f , multiplied by the fluid acceleration, $\ddot{v}$. For this case $M_c = M_f$ [5.7] ; therefore:

$$P_{in} = (M_c + M_f)\,\ddot{v}$$

$$= (2M_f)\,\ddot{v} \qquad \ldots (5.53)$$

$$= K_m \rho\ V_c\ \ddot{v}$$

where K_m is the so-called coefficient of inertia (equal to 2 in this theoretical case) and V_c is the volume of the cylinder. The other parameters were previously defined. The inertia coefficient K_m depends on the shape of the immersed part of the body and the flow characteristics around the body. Its theoretical evaluation becomes a difficult task even for relatively simple geometrical shapes; therefore, experiments have been carried out to compute K_m . For example, for cylinders the following values of K_m have been suggested: in [5.17] $K_m = 1.5$; in [5.18] $K_m = 2.0$; in [5.19] an average value $\bar{K}_m = 1.4$, and finally in [5.16] $0.5 < K_m < 2.5$.

5.3.4 Morison et al. equation

In what is -by now- a classical paper [5.20] Morison et al. suggested that the force exerted by a fluid on an accelerating cylinder could be computed as the superposition of a drag force plus an inertia force. The main assumption which is implicit in this formulation is that the characteristic dimension of the cylinder is such that the flow field is not disturbed by the presence of the immersed body.

Therefore, the total force per unit length, $P_w(t)$, of a fix cylinder immersed on an accelerating fluid can be computed by the following expression:

$$P_w(t) = K_m \rho \frac{\pi d^2}{4} \ddot{v} + \frac{1}{2} K_d \rho d \dot{v}|\dot{v}| \quad \ldots (5.54)$$

where all the terms have been previously defined when equations (5.52) and (5.53) were introduced. It is worthwhile to remark that the symbols $\ddot{v}$ and $\dot{v}$ stand for the fluid acceleration and velocity respectively as if no structure was immersed in the fluid. If in equation (5.54) the following terms are introduced:

$$V = (\frac{\pi d^2}{4}) \text{ x 1 meter}$$

$$C_m = K_m \rho V \quad \ldots (5.55)$$

$$C_d = \frac{1}{2} K_d \rho d$$

equation (5.54) can be rewritten as follows:

$$P_w(t) = C_m \ddot{v} + C_d \dot{v}|\dot{v}| \quad \ldots (5.56)$$

If the displacement of the cylinder is taken into consideration, it can be shown that equation (5.56) can be written as follows:

$$P_w(t) = C_m \ddot{v} - (K_m - 1) \rho V \ddot{u} + C_d \dot{v}|\dot{v}| \quad \ldots (5.57)$$

where $\ddot{u}$ is the body acceleration.

5.3.5 Diffraction loads $(d/\lambda) > 0.2$

When $d/\lambda > 0.2$, i.e. when the characteristic size of the body submerged in the sea is large compared to the length of the waves, the diffraction effects become important and dominate the resulting force regime [5.14] . For the case of plane waves propagating in a certain direction, diffraction occurs when the waves reach the body and the flow field is modified by the waves reflected on the body. This means that the resulting flow field is made up of the combination

of incident and reflected waves instead of incident waves only as it is assumed in the Morison equation.

Diffraction theory

Most of the mathematical models which have been used to study the diffraction effects on fluids [5.21, 5.22, 5.23] have the following assumptions in common: the fluid is considered inviscid, incompressible and irrotational; the resulting velocity field can be represented by the superposition of incident and diffracted velocity potentials i.e.:

$$\phi_t = \phi_i + \phi_d \qquad \ldots (5.58)$$

where ϕ_t is the resulting velocity potential and ϕ_i and ϕ_d represent the incident and diffracted velocity potentials respectively.

The potential ϕ_t is linear and satisfies the Laplace equation, $\nabla^2\phi_t = 0$, within the fluid region, as well as the following boundary conditions:

a) The kinematic condition on the sea floor:

$$\left.\frac{\partial \phi_t}{\partial y}\right|_{y = -D} = 0 \qquad \ldots (5.59)$$

b) The kinematic condition on the surface of the body:

$$\frac{\partial \phi_d}{\partial \Omega} = \begin{cases} 0 & \text{rigid body} \\ \dot{u} & \text{vibrating body} \end{cases} \qquad \ldots (5.60)$$

where Ω is the direction normal to the surface of the body;

c) The condition on the free surface:

$$\left.\frac{1}{g}\frac{\partial^2 \phi}{\partial t^2} + \frac{\partial \phi}{\partial y} = 0\right|_{y = 0} \qquad \ldots (5.61)$$

d) The radiation condition at a large distance from the body:

$$\left.\phi(r,\theta,y) = C(\theta)\, r^{-\frac{1}{2}}\, \frac{\cosh \kappa(y + D)}{\cosh (\kappa D)}\, \exp(i\kappa r) \to 0\right|_{r \to \infty} \qquad \ldots (5.62)$$

where r, θ, and y are the cylindrical coordinates of a point in the flow field.

The solution of the system of equations made up by the Laplace equation and the b.c. a), b), c) and d) yield to the velocity potential from which the pressure field can be computed i.e.:

$$p = -\rho \frac{\partial \phi}{\partial t} \qquad \ldots (5.63)$$

and by integrating equation (5.63) throughout the surface of the body, the acting hydrodynamical forces can be computed i.e.:

$$P_w = \int_s p \, ds \qquad \ldots (5.64)$$

where s represents the surface of the body.

Solutions to the diffraction problem

The solutions proposed forthe diffraction problem in different works [5.21, 5.22, 5.23, 5.24] can be divided into analytical, numerical and experimental; some of them will be described here.

Analytical solutions

The analytical solution to the diffraction problem stated by equations (5.58) - (5.62) represents a complex task and only a few solutions for simple body shapes have been obtained. For example, in [5.21] a solution was proposed for the diffraction problem of a single cylinder immersed in a fluid which propagates plane waves in a direction perpendicular to the longitudinal axis of the cylinder. The resulting horizontal force acting on a unitary length of cylinder is given by:

$$P_w(t) = \frac{2\rho g H}{\kappa} \frac{\text{Cosh } \kappa(y + D)}{\text{Cosh } (\kappa D)} A\left(\frac{\pi d}{\lambda}\right) \text{Cos } (\omega t - \beta) \qquad \ldots (5.65)$$

where

$$A\left(\frac{\pi d}{\lambda}\right) = \left[J_1'^2\left(\frac{\pi d}{\lambda}\right) + Y_1'^2\left(\frac{\pi d}{\lambda}\right)\right]^{-\frac{1}{2}} \qquad \ldots (5.66)$$

$$\tan \beta = \frac{J_1'\left(\frac{\pi d}{\lambda}\right)}{Y_1'\left(\frac{\pi d}{\lambda}\right)} \qquad \ldots (5.67)$$

In these expressions J'_1 and Y'_1 are respectively the derivatives of the Bessel functions of the first and second kind, of order one with respect to their arguments; the other parameters have already been defined.

Numerical solutions

Among the numerical solutions which have been suggested for the diffraction problem there are two which have a wide acceptance, namely, a) the source distribution method [5.22, 5.23, 5.25] and b) the finite element method [5.24].

a) The source distribution method makes use of the Green's theorem to express the velocity potential at points in the fluid region as function of sources located on the surface of the body. These sources are considered to act at the center of N small plane surfaces in which the surface of the body is divided. The mentioned sources pulsate with the same frequency as the known incident wave [5.5] and its strength is such that the boundary condition represented by equation (5.60) is satisfied. The sources produce a disturbance of the incident field associated to the scattered wave which includes local effects (i.e. the added mass), as well as diffraction of the incident wave. Details of the computational aspects of the method are described in [5.22, 5.23]. Once the diffracted potential ϕ_d is obtained, it can be linearly superposed to the incident potential ϕ_i and the pressure and forces follow by using equations (5.63) and (5.64) respectively.

For example in [5.23] the previously-described technique has been used to study the diffraction effects on circular cylinders resting on the bottom of the fluid, for different combinations of the geometric characteristics of the cylinders and the deep water regular waves. Among other results which were calibrated against experimental ones, the following diffraction coefficients for the resulting horizontal and vertical forces and the overturning moments on circular cylinders were obtained in [5.23] :

$$C_x = 1 + 0.75 \left(\frac{h}{2r}\right)^{\frac{1}{3}} \left(1 - 0.3\, \kappa^2 r^2\right) \qquad \ldots \quad (5.68)$$

$$C_y = \begin{cases} 1 + 0.74\ \kappa^2 r^2 \left(\frac{h}{2r}\right) & \text{for } \left\{1.48\ \kappa r \left(\frac{h}{2r}\right)\right\} < 1 \\ 1 + 0.5\ \kappa r & \text{for } \left\{1.40\ \kappa r \left(\frac{h}{2r}\right)\right\} > 1 \end{cases} \qquad \ldots \quad (5.69)$$

$$C_{ov} = 1.9 - 0.35\ \kappa r \qquad \ldots (5.70)$$

where C_x , C_y and C_{ov} are the coefficients for the horizontal and vertical forces and the overturning moment respectively; h and r are the height and radiusof the submerged cylinder. Equations (5.68) - (5.70) are valid for the following ranges:

a) the three equations for $h/d < 0.6$

b) equations (5.68) - (5.69) for $0.3 < h/2r < 2.3$

c) equation (5.70) for $0.6 < h/2r < 2.3$

However, it is suggested that its validity may be extended to a wider range of values of $h/2r$ and that for large values of $h/2r$ the values of C_x and C_{ov} tend to the value predicted by the theory proposed in [5.21].

By using the suggestion proposed in [5.23] about identifying the diffraction forces as the result of a diffraction coefficient multiplied by the corresponding Froude-Krylov force, expressions were obtained in [5.26] for the horizontal diffraction forces on a circular cylinder $P'_w(t)$, and on a caisson of square area $P''_{w_0}(t)$. Furthermore,expressions to evaluate the overturning moments in the caisson produced by the diffraction pressures on its sides, M_{w_1} , and on its top, M_{w_2} , were also obtained. These equations are:

$$P'_w(t) = C_x \left[\rho r \lambda \ell J_1(\pi d/\lambda)\right] \ddot{v} \qquad \ldots (5.71)$$

$$P''_{w_0}(t) = C_x \left[\rho g \gamma\ H \frac{\sinh(\kappa h_b)}{\kappa \cosh(\kappa D)}\right] \alpha \qquad \ldots (5.72)$$

$$M'_{w1}(t) = C_{ov}\left[\rho g \gamma\ H \frac{1}{\cosh(\kappa D)} \left\{ \frac{h_b}{\kappa} \sinh(\kappa h_b) + \frac{1}{\kappa^2}\ (1 - \cosh[\kappa h_b])\right\}\right] \alpha \qquad \ldots (5.73)$$

$$M'_{w2}(t) = C_y \left[\rho g \gamma\ H \frac{\cosh(\kappa h_b)}{\kappa \cosh(\kappa D)} \{\gamma\beta - \frac{1}{\kappa}\alpha\}\right] \qquad \ldots (5.74)$$

where

ℓ = length of the cylinder

α = $\sin\theta_1 - \sin\theta_2$

$$\beta = \text{Cos}\,\theta_1 + \text{Cos}\,\theta_2$$

$$\theta_1 = K\gamma - \omega t$$

$$\theta_2 = -K\gamma - \omega t$$

J_1 is the Bessel function of the first kind with respect to the argument;

γ is the length of the equivalent square section required to obtain the circular area of the caisson;

h_b is the height of the caisson;

The rest of the parameters were previously defined.

Other results obtained in [5.23] were: a) the interaction effect between cylinders is unimportant at radial distances larger than two cylinder diameters; b) the effect of currents in the North Sea on the hydrodynamical forces on offshore gravity platforms is negligible; c) as a consequence of b), the drag forces associated to the diffraction effect are very small compared to the inertial forces and therefore the former can be neglected; d) the difference on the hydrodynamical forces using the linear theory and the Stokes V order theory, is small for typical North Sea conditions.

b) The finite element method has also been used to solve the diffraction problem stated by equations (5.58) - (5.62). In this case both the fluid and the body are discretized by using standard two and three dimensional finite element techniques [5.24,5.27] . The fluid part of the domain is usually divided into different subdomains to separate the regions where the incident and the diffracted potentials apply. The coupling of finite elements with analytical and source distribution methods, [5.24] , and infinite elements [5.27] have also been proposed to solve wave diffraction problems. The results obtained with this technique agree within reasonable limits with the source distribution method results, but the computational costs are larger in the former.

Experimental results

Several experiments have been carried out to study the diffraction problems as the ones already mentioned above, reported in [5.23] . In general, the results obtained are in good agreement with some diffraction theory [5.21] predictions [5.22,5.23,5.25] . The main differences have been found in the vertical forces but this seems to be inherent to the models used [5.23] .

5.4 Wave forces used in this work

In Section 5.1, the wave loading regimes to which a concrete gravity platform could be subjected were mentioned. Due to the characteristic dimension and shape of its elements, the dominant loading regimes on a c.g.p. are the inertia and diffraction ones. The drag loading regime can be neglected for this type of structure because its contribution to the total hydrodynamic load is very small compared to the inertia and diffraction loads [5.9]. The inertia force to be used in this work corresponds to the inertia term of the Morison equation, expressions (5.6) or (5.7). It will be applied to compute the forces on the length of the towers which satisfy the condition $d/W_0 > 0.2$. The loads acting on the lower part of the towers and the caisson, which fall into the ratio $d/\lambda > 0.2$ will be computed by equations (5.22) - (5.23) i.e. through a diffraction coefficient multiplied by the corresponding Froude-Krylov force. The choice of those equations is based on the following reasons: a) the satisfactory agreement they provide when compared with experimental results [5.23]; b) the low computational cost compared with the full source distribution method or the finite element approaches [5.23] .

6. DYNAMIC RESPONSE OF A CONCRETE GRAVITY PLATFORM SUBJECTED TO SEISMIC AND WAVE LOADING.

6.1 Introduction

The dynamic response of a c.g.p. subjected to seismic loading and wave loading can be obtained by first formulating the governing equations for the cases under consideration and then applying numerical methods to solve those equations. The first part could be achieved by modelling the dynamic characteristics of the c.g.p. and its surrounding environment. The latter includes the idealization of the soil media. The modelling of the wave environment and representation of the seismic activity for the site where the structure is located are also necessary to establish the governing equations.

The modelling of the structure and the soil idealization were presented in Chapters 2 and 3 ; the seismic and wave loadings were the subjects of Chapters 4 and 5, respectively. Based on these chapters, the governing equations for a c.g.p. under those loadings are formulated in this chapter. The current techniques utilized to solve those equations are also presented herewith.

Taking into consideration that the c.g.p. is idealized as a linear structural system (see Chapter 2), the computation of the dynamic response for this system under arbitrary load, when its base rests on rigid soil and flexible soil is treated in 6.2 and 6.3 respectively. The particular case of a c.g.p. resting on a rigid soil and subjected to seismic load and wave load is presented in 6.4 . Finally, the case of a c.g.p. under the same types of loading but considering the flexibility of the soil is the subject of 6.5 .

6.2 Dynamic response of a linear structural system fixed to a rigid soil and subjected to an arbitrary load

The dynamic response of a linear system subjected to an arbitrary load may be obtained by solving the equation of dynamic equilibrium, which represents the forces acting on the system. Examples of these types of equations are the governing equations for a discretized structural system introduced in Section 2.2 i.e.:

$$\underline{M}\,\ddot{\underline{U}} + \underline{C}\,\dot{\underline{U}} + \underline{K}\,\underline{U} = \underline{P}(t) \qquad \ldots (6.1)$$

As it was mentioned in that section, $\underline{M}$, $\underline{C}$, and $\underline{K}$ stand for the mass, damping and stiffness properties of the structural system respectively; the vectors $\ddot{\underline{U}}$, $\dot{\underline{U}}$, $\underline{U}$ and $\underline{P}$ represent the acceleration, velocity and displacement of the system and external loading respectively. Equation (6.1) is valid for linear and nonlinear systems but in this case it will be associated to a linear structural system i.e. a system with linear dynamic properties and subjected to a load which can be described through a linear mathematical expression.

The solution of equation (6.1) can be achieved in the time domain or in the frequency domain. The choice of the domain in which the solution is obtained depends on several factors such as the characteristics of the dynamic properties of the system, the number of degrees of freedom used for the discretization and the time characteristics of the external loading. The accuracy and the cost of the procedure adopted should also be considered in the choice.

6.2.1 Modal superposition method

As the principle of superposition holds for a linear system, a numerical technique widely used to solve equation (6.1) is the so-called modal superposition method [6.1]. This technique is valid in both time and frequency domains. Through it, the response of the system expressed by the vector of displacements $\underline{U}$ is computed as follows:

$$\underline{U}(t) = \underline{R}\,\underline{Y}(t) \qquad \ldots (6.2)$$

where $\underline{R}$ is the modal matrix and $\underline{Y}$ is the vector of normal coordinates. $\underline{R}$ can be obtained by solving the eigenvalue problem associated to equation (6.1) i.e.:

$$|\underline{K} - \omega_s^2 \underline{M}|\, \underline{R}_s = 0 \qquad \ldots (6.3)$$

$$s = 1, 2, \ldots, n$$

The solution of equation (6.3) provides the undamped natural frequencies of the system, ω_s , and the associated modal vectors

$\underset{\sim}{R}_s$. The modal matrix $\underline{R}$ is formed by the vectors $\underset{\sim}{R}_s$; in equation (6.3) n stands for the number of degrees of freedom used to discretize the system. The elements of the normal coordinates vector, $\underset{\sim}{Y}$, are computed by solving the n simple degree of freedom system equations, resulting from the application of the orthogonality properties of $\underline{R}$ with respect to $\underline{M}$ and $\underline{K}$ i.e.:

$$\underline{M}^* = \underline{R}^T \underline{M} \underline{R} = \underline{I} \qquad \ldots (6.4)$$

$$\underline{K}^* = \underline{R}^T \underline{K} \underline{R} = \underline{\Omega}^2 \qquad \ldots (6.5)$$

and by assuming that:

$$\underline{C}^* = \underline{R}^T \underline{C} \underline{R} = \underline{\xi} \qquad \ldots (6.6)$$

where $\underline{I}$ is the identity matrix, $\underline{\Omega}^2$ and $\underline{\xi}$ are diagonal matrices whose elements are ω_s^2 and $2\xi_s \omega_s$ respectively. ξ_s is the fraction of critical damping for the sth mode [6.1] . This means that a system of n equations associated to n simple degree of freedom systems is obtained by substituting equation (6.2) into equation (6.1) and premultiplying it by $\underline{R}^T$ i.e.:

$$\underline{M}^* \ddot{\underset{\sim}{Y}} + \underline{C}^* \dot{\underset{\sim}{Y}} + \underline{K}^* \underset{\sim}{Y} = \underset{\sim}{P}^* \qquad \ldots (6.7)$$

or:

$$\ddot{Y}_s + 2\xi_s \omega_s \dot{Y}_s + \omega_s^2 Y_s = P_s^*(t) \qquad \ldots (6.8)$$

$$s = 1, 2, \ldots, n$$

where:

$$P_s^*(t) = \underset{\sim}{R}_s^T \underset{\sim}{P}(t) \qquad \ldots (6.9)$$

From the solution of equation (6.8) the elements Y_s of the vector $\underset{\sim}{Y}$ are obtained.

Once $\underline{R}$ and $\underset{\sim}{Y}$ are computed, the veetor of displacements $\underset{\sim}{U}$ can be calculated by using equation (6.2). A very important feature of the modal superposition method is that for most of the

structural systems considered in practice, the contribution of the high frequency modes to their dynamic response is very small [6.1] . Therefore, it is only necessary to solve $p (p \ll n)$ equations of the system represented by equation (6.8) to obtain a satisfactory degree of accuracy in the response.

6.2.2 Solution of the equation of motion in the time domain

The solution in the time domain of the sth equation of the system of equation (6.8) can be obtained by using any of the following methods: a) the Duhamel integral [6.1] , b) the step by step techniques [6.2] . The main features of these methods will be briefly discussed here.

a) The Duhamel Integral:

It can be shown [6.1] that the solution of equation (6.8) for an arbitrary loading $P_s^*(t)$ can be expressed by the convolution integral:

$$Y_s(t) = \int_0^t P_s^*(t)\, h_s(t - \tau)\, d\tau \qquad \ldots (6.10)$$

where

$$h_s(t - \tau) = \frac{1}{\omega_s'} \exp(-\xi_s \omega_s t) \sin \omega_s' t \qquad \ldots (6.11)$$

is the unit impulse response function and

$$\omega_s' = \omega_s (1 - \xi_s^2)^{\frac{1}{2}} \qquad \ldots (6.12)$$

is the damped natural frequency of the sth mode.

Equation (6.10) has to be numerically integrated by using methods such as the one proposed in [6.3] . A shortcoming of this method is that the integration interval used should be small for high frequencies, in order to obtain accurate solutions.

b) The step by step technique:

This name has been given to the numerical techniques which are based on the finite difference method [6.2] . An example of these kinds of techniques is the β method of Newmark [6.2] . In this method the displacement of the system represented by equation (6.8)

at time $(t + \Delta t)$ is expressed in terms of the value of its velocity and acceleration at time t, the value of its acceleration at time $(t + \Delta t)$ and certain coefficients. The scheme requires to make some assumptions concerning the behaviour of the system at time $(t + \Delta t)$; it is also necessary to know its initial conditions. Other similar techniques are described in [6.2] .

The main difficulties found when applying these kinds of techniques are related to the stability of the schemes used and the introduction of the so-called numerical damping on the system [6.2] .

6.2.3 Solution of the equation of motion in the frequency domain

The solution of equation (6.8) in the frequency domain may be obtained by using the so-called direct solution method in the frequency domain. With this method the response of the system expressed by its displacements is first computed in the frequency domain and then may be transformed to the time domain [6.1] . The procedure requires to express the velocity and the acceleration of the system and the time dependent load in the frequency domain; this can be achieved through the Fourier transform.

It can be shown [6.1] that the solution for the sth of equation (6.8) is given by:

$$Y_s(t) = \frac{1}{2\pi} \int_{-\infty}^{\infty} Y_s(\omega) \exp(i\omega t)\, d\omega \qquad \ldots (6.13)$$

where

$$Y_s(\omega) = H_s(i\omega)\, P_s^*(\omega) \qquad \ldots (6.14)$$

In equation (6.14) $Y_s(\omega)$ is the Fourier transform of $Y_s(t)$; $H_s(i\omega)$ represents the complex frequency response (c.f.r.) of the system and $P_s^*(\omega)$ stands for the Fourier transform of $P_s^*(t)$ i.e.:

$$Y_s(\omega) = \int_{-\infty}^{\infty} Y_s(t) \exp(-i\omega t)\, dt \qquad \ldots (6.15)$$

$$H_s(i\omega) = \frac{1}{\omega_s^2 \left[1 + \left(\frac{\omega}{\omega_s}\right)^2 + 2i\xi_s \frac{\omega}{\omega_s}\right]} \qquad \ldots (6.16)$$

$$P_s^*(\omega) = \int_{-\infty}^{\infty} P_s^*(t) \exp(-i\omega t)\, dt \qquad \ldots (6.17)$$

It is convenient to keep in mind that $H_s(i\omega)$ and $h_s(t)$ form a Fourier couple and that the former can also be written as follows:

$$H_s(i\omega) = |H_s(i\omega)| \exp(i\Psi) \quad \ldots (6.18)$$

$$|H_s(i\omega)| = \frac{1}{\omega_s^2} \left\{ \left[1 - \left(\frac{\omega}{\omega_s}\right)^2 \right]^2 + 4\xi_s^2 \left(\frac{\omega}{\omega_s}\right)^2 \right\}^{-\frac{1}{2}} \quad \ldots (6.19)$$

and

$$\Psi = \tan^{-1} - \frac{2\xi_s \frac{\omega}{\omega_s}}{1 - \frac{\omega}{\omega_s}} \quad \ldots (6.20)$$

In equation (6.18) $|H_s(i\omega)|$ is the amplitude of the c.f.r. and Ψ the phase angle. If equation (6.14) is replaced in equation (6.13) the term $\frac{P_s^*(\omega)}{2\pi}$ defines the amplitude per unit of frequency of the load component at frequency ω .

In practice equations (6.13) and (6.14) are only solved for a reduced number of frequencies ω_i . This is valid because outside a certain frequency band the contribution of the terms $\frac{P_s^*(\omega)}{2\pi}$ in those equations is nil. Once equation (6.13) has been solved for the chosen number of normal coordinates p , the displacement U_s can be computed through equation (6.2).

From the above paragraphs, it can be seen that the direct solution method in the frequency domain could be applied directly to equation (6.2) if this is convenient for the analysis at hand. In this case equation (6.14) is related to the original discretized system, i.e. to the displacements $\underset{\sim}{U}$ instead of the normal coordinates Y_s , therefore, the resulting expression is:

$$\{-\omega^2 \underline{M} + i\omega \underline{C} + \underline{K}\} \underset{\sim}{U}(\omega) = \underset{\sim}{P}(\omega) \quad \ldots (6.21)$$

where $\underset{\sim}{U}(\omega)$ and $\underset{\sim}{P}(\omega)$ are the Fourier transforms of $\underset{\sim}{U}(t)$ and $\underset{\sim}{P}(t)$ respectively. Equation (6.21) represents a system of n complex algebraic equations. After this system of equations has been solved the solution in the time domain can be achieved through the following equation:

$$\underset{\sim}{U}(t) = \frac{1}{2\pi} \int_{-\infty}^{\infty} \underset{\sim}{U}(\omega) \exp(i\omega t) d\omega \quad \ldots (6.22)$$

To avoid the solution of the whole system of equations (6.21) and (6.22), (which for some cases is computationally expensive) the modal superposition technique can also be applied; in this case the expression corresponding to equation (6.2) is:

$$\underset{\sim}{U}(\omega) = \underline{R}\ \underset{\sim}{Y}(\omega) \qquad \ldots (6.23)$$

where $\underline{R}$ is the modal matrix discussed in Section 6.2.1 and $\underset{\sim}{Y}(\omega)$ is the vector of normal coordinated in the frequency domain. Once equation (6.23) is substituted in equation (6.21) and the result premultiplied by $\underline{R}^T$ the solution in the time domain can be determined through equations (6.14), (6.23) and (6.22).

6.3 Dynamic response of a linear structural system resting on a flexible soil and subjected to an arbitrary load

The dynamic response of a linear structural system resting on a flexible soil (in what follows, this system will be referred to as a soil-structure system, i.e. s.s.s.) under an arbitrary load may be computed by combining the dynamic properties of the structure, the corresponding properties of its soil-foundation system and the dynamic load. If the structure is modelled as proposed in 2.4 and the soil-foundation system is represented by an impedance function as the one presented in 3.3 , the governing equations for the s.s.s. can be formulated for the load under consideration.

It can be shown [6.4] that by considering the dynamic equilibrium of both the discretized structure and the idealized soil-foundation subsystems, the governing equations for the s.s.s. can be written as follows:

$$\underline{M}_0\ \ddot{\underset{\sim}{U}}_0 + \underline{C}_0\ \dot{\underset{\sim}{U}}_0 + \underline{K}_0\ \underset{\sim}{U}_0 = \underset{\sim}{P}_0(t) \qquad \ldots (6.24)$$

In this equation $\underline{M}_0$, $\underline{C}_0$ and $\underline{K}_0$ represent the mass, damping and stiffness of the s.s.s. and $\ddot{\underset{\sim}{U}}_0$, $\dot{\underset{\sim}{U}}_0$, $\underset{\sim}{U}_0$ are the acceleration, velocity and displacement of the system respectively. $\underset{\sim}{P}_0$ is the vector of applied loads. Equation (6.24) is similar to equation (6.1), however, the vector and matrices of the former have extra elements which take the flexibility of the soil into account.

Therefore the vector $\ddot{\underset{\sim}{U}}_0$ (as well as $\dot{\underset{\sim}{U}}_0$ and $\underset{\sim}{U}_0$) is formed by the degrees of freedom of the structure resting on rigid soil, $\underset{\sim}{U}_0^s$, plus the degrees of freedom of the idealized foundation, $\underset{\sim}{U}_0^f$. Accordingly to this, the matrices $\underline{M}_0$, $\underline{C}_0$ and $\underline{K}_0$ as well as $\underset{\sim}{P}_0(t)$ have elements which correspond to those degrees of freedom.

From (6.24) it follows that $\underset{\sim}{U}_0^s$ consists of the relative displacements of the nodal points with respect to the foundation as well as the slopes associated to those displacements. Therefore, the dimension of $\underset{\sim}{U}_0^s$, n^s is equal to $2n$, where n is the total number of nodes used to discretize the structure. If the degrees of freedom considered for the idealized foundation are its horizontal translation, u_0 , and its rocking θ_0 , and their interaction is neglected, see fig. 3.2, the explicit form of equation (6.24) is given by:

$$\left[\begin{array}{c|c|c} \underline{M} & \underset{\sim}{B}_1 & \underset{\sim}{B}_2 \\ \hline \underset{\sim}{B}_1^T & m_0^t & m_0' \\ \hline \underset{\sim}{B}_2^T & m_0' & I_0^t \end{array}\right] \left\{\begin{array}{c} \ddot{\underset{\sim}{U}}_0^s \\ \hline \ddot{u}_0 \\ \hline \ddot{\theta}_0 \end{array}\right\} + \left[\begin{array}{c|c|c} \underline{C} & \underset{\sim}{0} & \underset{\sim}{0} \\ \hline \underset{\sim}{0}^T & c_{xs} & 0 \\ \hline \underset{\sim}{0}^T & 0 & c_{\theta s} \end{array}\right] \left\{\begin{array}{c} \dot{\underset{\sim}{U}}_0^s \\ \hline \dot{u}_0 \\ \hline \dot{\theta}_0 \end{array}\right\}$$

$$+ \left[\begin{array}{c|c|c} \underline{K} & \underset{\sim}{0} & \underset{\sim}{0} \\ \hline \underset{\sim}{0}^T & k_{xs} & 0 \\ \hline \underset{\sim}{0}^T & 0 & k_{\theta s} \end{array}\right] \left\{\begin{array}{c} \underset{\sim}{U}_0^s \\ \hline u_0 \\ \hline \theta_0 \end{array}\right\} = \left\{\begin{array}{c} \underset{\sim}{P}_0^s(t) \\ \hline P_{u_0}(t) \\ \hline P_{\theta_0}(t) \end{array}\right\} \quad \ldots \quad (6.25)$$

In equation (6.25), $\underline{M}$, $\underline{C}$ and $\underline{K}$ are the mass, damping and stiffness matrices for the structure on a rigid soil respectively. In the same equations, the products $\underset{\sim}{B}_1\ddot{u}_0$ and $\underset{\sim}{B}_2\ddot{\theta}_0$ represent the inertial forces of the translational and rotational degrees of freedom, due to the foundation horizontal displacement and its rotation about an axis through the center of gravity of the foundation. It can easily be shown that:

$$\underset{\sim}{B}_1^T = \begin{bmatrix} m_{11} & 0 & m_{33} & 0 & \cdots & m_{2n-1,2n-1} & 0 \end{bmatrix} \quad \ldots (6.26)$$

$$\underset{\sim}{B}_2^T = \begin{bmatrix} m_{11}h_1 & m_{22} & m_{33}h_2 & m_{44} & \cdots & m_{2n-1,2n-1}h_n & m_{2n,2n} \end{bmatrix} \quad \ldots (6.27)$$

where m_i represents the ith lumped mass, h_i the height of its associated node with respect to the center of gravity of the foundation, and n is the number of nodes. It can also be shown [6.4] that:

$$m_0^t = \sum_{i=1}^{n} m_{jj} + m_0 \quad \ldots (6.28)$$

$$m_0' = \sum_{i=1}^{n} m_{jj}h_i \quad \ldots (6.29)$$

$$I_0^t = \sum_{i=1}^{n} I_{0i} + I_0 + \sum_{i=1}^{n} m_{jj}h_i^2 \quad \ldots (6.30)$$

$$j = 2i - 1$$

where m_0 and I_0 are the equivalent mass and mass moment of inertia of the soil-foundation subsystem respectively. The contribution of the soil to m_0 and I_0 can be computed by using equation (8.17) and (8.18) respectively. I_{0i} stands for the ith centroidal moment of inertia of the masses of the structure. c_{js} and k_{js} ($j=x,\theta$) in equation (6.25) can be computed by using equations (3.14) and (3.13) respectively.

The elements of $\underset{\sim}{P}_0^s$ represent the nodal loads acting on the structure. Concerning P_{u_0} and P_{θ_0}, they stand for the horizontal load and the moment applied at the center of gravity of the foundation.

From equation (6.25) it can be seen that the extra elements of $\underline{C}_0$ and $\underline{K}_0$ are frequency dependent ones; due to this, the solution of equation (6.24) is relatively complex compared with the solution of equation (6.1). The methods currently in use to solve equation (6.24) are the modal superposition method and the direct solution method, both introduced in 6.2 .

As the modal superposition method is strictly applicable to time invariable systems which have classical normal modes [6.5] ,

some assumptions with respect to $\underline{K}_0$ and $\underline{C}_0$ have to be made in order to apply it to solve equation (6.24). With the direct solution method the system of equations (6.24) is expressed in the transformed field (Fourier or Laplace), and the resulting set of algebraic equations (as many as the number of degrees of freedom considered) has to be solved for each frequency of excitation. Finally in order to obtain the solution in the time domain the use of the inverse Fourier (or Laplace) transform is required in the latter method. An outline of both methods for solving equation (6.24) is given in 6.3.1 and 6.3.2 .

6.3.1 Modal superposition method applied to soil-structure systems

As mentioned above, the modal superposition method is strictly applicable to systems which do not change their dynamic properties with time. This is not the case for the s.s.s. represented by equation (6.24), in which both $\underline{C}_0$ and $\underline{K}_0$ have some elements which are frequency dependent. However, experiments with prototypes [6.6,6.7] have shown the existence of orthogonal modes of vibration in s.s.s. . This evidence, as well as the availability of frequency independent impedance functions [6.6,6.9,6.10] have encouraged the development of approximate modal superposition methods to be used for the dynamic analysis of s.s.s. .

The approximate modal superposition methods proposed in different works [6.6,6.11,6.12,6.13] make the following assumptions with respect to $\underline{K}_0$. It is assumed that its elements k_{js} (equation 3.13) are time invariant but that the value they adopt are functions of a chosen frequency. This frequency is usually taken as the fundamental undamped natural frequency of the s.s.s. [6.13]. As this frequency is not known at the outset, some iterations have to be performed on equation (6.31); the undamped natural frequency of the superstructure attached to a rigid soil could be taken as the iteration starting frequency [6.13] . Another possibility with respect to the elements k_{js} of $\underline{K}_0$ is to use frequency independent impedance functions [6.6] .

Whichever way has been adopted with respect to the soil stiffness elements k_{js} , the s.s.s. undamped natural frequencies, ω_s^0 , and the associated modal shapes, $\underset{\sim}{R}_s^0$, can be computed by solving

the following eigenvalue problem:

$$\left| \underline{K}_0 - \omega_s^{0\,2} \quad \underline{M}_0 \right| \quad \underset{\sim}{R}_s^0 = \underset{\sim}{0} \qquad \ldots (6.31)$$

Once equation (6.31) has been solved, the s.s.s. represented by equation (6.24) can be transformed into an equivalent system of N uncoupled single degree of freedom systems resting on a rigid soil by following the procedure outlined in Section 6.2 .

The modal damping associated to each normal coordinate should include the contributions of the damping of the structure (section 2.4) as well as the soil damping (Sections 3.2 and 3.3). Several suggestions have been made to estimate the modal damping of s.s.s. For example, in [6.6, 6.11, 6.12, 6.13] the Jacobsen energy ratio criterion [6.14] was applied to calculate a weighted modal damping. In [6.12] the modal dampings of a s.s.s. were computed by matching the modulus of the transfer functions of the exact solution and the modal solution. In [6.13] the classical method of modal analysis was used to compute the weighted modal dampings. The assumption made in the latter proposal is equivalent to the Jacobsen energy criteria used in [6.6, 6.11] ; therefore, it will be briefly presented here.

The method suggested in [6.13] assumes that the fraction of critical damping of the equivalent single degree of freedom systems, ξ_s^0 , can be expressed by equation (3.19), i.e.:

$$\xi_s^0 = \frac{1}{4\pi} \quad \frac{E_d}{E_s} \qquad \ldots (6.32)$$

where E_d represents the energy dissipated per cycle when the s.s.s. vibrates with a frequency ω_s^0 and modal shape $\underset{\sim}{R}_s^0$; E_s is the maximum strain energy stored in the system, i.e.:

$$E_d = \pi \, \omega_s^0 \, \underset{\sim}{R}_s^{0\,T} \quad \underline{C}_0(\omega_s^0) \, \underset{\sim}{R}_s \qquad \ldots (6.33)$$

and

$$E_s = \frac{1}{2} \; \omega_s^{0\,2} \, \underset{\sim}{R}_s^{0\,T} \quad \underline{K}_0(\omega_1^0) \, \underset{\sim}{R}_s^0$$

$$= \frac{1}{2} \; \omega_s^{0\,2} \, \underset{\sim}{R}_s^{0\,T} \quad \underline{M}_0 \; \underset{\sim}{R}_s^0 \qquad \ldots (6.34)$$

Notice that in equation (6.34) it is assumed that the elements k_{js} of $\underline{K}_0$ have been computed for the fundamental undamped natural frequency of the s.s.s. . However, equation (6.33) refers to the sth modal frequency of the system.

The modal vector $\underset{\sim}{R}^0_s$ can be partitioned into two vectors, one associated to the structure degrees of freedom, $\underset{\sim}{R}^s_s$, and the other related to the foundation degrees of freedom, $\underset{\sim}{R}^f_s$. By expressing $\underset{\sim}{R}^s_s$ as a linear combination of the modal shapes of the same structure attached to a rigid soil $\underset{\sim}{R}_s$ and substituting equations (6.33) and (6.34) into equation (6.32) the following result is obtained [6.13] :

$$\xi^0_s = \sum_{i=1}^{n} \beta_{is}\, \xi_s + \lambda_s \qquad \ldots (6.35)$$

where $s = 1, 2, \ldots N$

$$\beta_{is} = \frac{(\underset{\sim}{R}^T_i \; \underline{M} \; \underset{\sim}{R}^s_s)}{(\underset{\sim}{R}^T_i \; \underline{M} \; \underset{\sim}{R}_i)\;\; (\underset{\sim}{R}^{0\,T}_s \; \underline{M}_0 \; \underset{\sim}{R}^0_s)} \; \frac{\omega_i}{\omega^0_s} \qquad \ldots (6.36)$$

$$\lambda_s = \frac{1}{2\omega_s} \; \frac{\underset{\sim}{R}^{f\,T}_s \; \underline{C}^f_0 \; (\omega^0_s) \; \underset{\sim}{R}^f_s}{\underset{\sim}{R}^{0\,T}_s \; \underline{M}_0 \; \underset{\sim}{R}^0_s} \qquad \ldots (6.37)$$

In equations (6.35) and (6.36) ξ_s and ω_i are the fraction of critical damping and the undamped natural frequency of the structure resting on a rigid soil respectively; the matrix $\underline{C}^f_0(\omega^0_s)$ of equation (6.37) includes the elements c_{js} of the impedance function (see equation (3.14))which represents the soil damping. From equation (6.35) it can be seen that the fraction of critical damping for the sth mode of the s.s.s. is expressed as the combination of the fraction of critical damping of the structure on a rigid soil and the damping associated to the soil foundation system.

Once the undamped natural frequencies, ω^0_s , and the fraction of critical damping, ξ^0_s , of the s.s.s. have been computed by using equations (6.31) and (6.35) respectively, the following system of equations is obtained by considering the orthogonal properties of $\underline{M}_0$, $\underline{K}_0$ with respect to $\underline{R}^0_s$ and by assuming that the product $\underline{R}^{0\,T}_s \; \underline{C}_0 \; R^0_s$ gives a diagonal matrix whose elements are

$2\xi_s^0\ \omega_s^0$,

$$\ddot{Y}_s^0 + 2\xi_s^0\ \omega_s^0\ \dot{Y}_s^0 + {\omega_s^0}^2\ Y_s^0 = P_s^0(t) \quad \ldots (6.38)$$

$$s = 1, 2, \ldots N$$

where $P_s^0(t)$ results from the product $\underline{R}_s^{0T}\ \underline{P}_0$.
This system of equations is similar to equation (6.8) but the former refers to a s.s.s. . Equation (6.38) can be solved by any of the numerical methods presented in Sections 6.2.2 and 6.2.3 . Finally the dynamic response of the s.s.s. can be determined by using the following expression:

$$\underset{\sim}{U}_s^0(t) = \underline{R}_s^0\ \underset{\sim}{Y}_s^0(t) \quad \ldots (6.39)$$

In equation (6.39) the matrix $\underline{R}_s^0$ is formed by the vectors $\underset{\sim}{R}_s^0$; the comments made with respect to the modal superposition method in Section 6.2.1 are also valid here.

6.3.2 Direct solution method applied to soil-structure systems

The direct solution method in the frequency domain introduced in Section 6.2.3 can also be utilized to solve equation (6.24). In this case the system of equations to be solved in the frequency domain is:

$$\{-\omega^2\ \underline{M}_0 + i\omega\ \underline{C}_0 + \underline{K}_0\}\ \underset{\sim}{U}_0(\omega) = \underset{\sim}{P}_0(\omega) \quad \ldots (6.40)$$

where $\underset{\sim}{U}_0(\omega)$ and $\underset{\sim}{P}_0(\omega)$ are the Fourier transforms of $\underset{\sim}{U}_0(t)$ and $\underset{\sim}{P}_0(t)$ respectively. As mentioned in Section 6.2.3 this system of N complex algebraic equations has to be solved for each excitation frequency. The solution of equation (6.24) in the time domain can be obtained by an expression similar to equation (6.22) i.e.:

$$\underset{\sim}{U}_0(t) = \frac{1}{2\pi} \int_{-\infty}^{\infty} \underset{\sim}{U}_0(\omega)\ \exp(i\omega t)\ d\omega \quad \ldots (6.41)$$

An important feature when the method is used to calculate the dynamic response of a s.s.s. such as the one represented by equation (6.24), is the fact that it is not necessary to make extra assumptions with respect to the matrices $\underline{C}_0$ and $\underline{K}_0$. This means

that the actual values of their elements c_{js} and k_{js} respectively are used in the evaluation of $\underset{\sim}{U}_0(\omega)$ for a given frequency. This can be of great importance when the impedance function utilized varies drastically with frequency. However, the direct solution method applied through equations (6.40) and (6.41) can be expensive, because the computational effort increases as the cube of the number of degrees of freedom (N) of the s.s.s. .[6.15] . This shortcoming of the direct solution methods can be improved if the modal superposition in the frequency domain (equation (6.23)) is used as shown in Section 6.2.3.

6.4 Dynamic response of a c.g.p. resting on a rigid soil

The dynamic response of a c.g.p. attached to a rigid soil and subjected to wave load and seismic load may be computed by solving the equations of motion for this type of structure. If the discretization of the c.g.p. is carried out by using the scheme introduced in 2.4 , the resulting governing equation will be expression (6.1) The vector $\underset{\sim}{U}$ of this equation consists of $2n$ degrees of freedom, n being the total number of nodes after applying the boundary conditions and 2 the number of degrees per node, i.e. u_t , u'_t where the subindex t means that both the displacement and the slope at a node include the bending and snear deformations.

Concerning the matrices $\underline{M}$, $\underline{C}$ and $\underline{K}$ of equation (6.1), their elements correspond to the degrees of freedom included in $\underset{\sim}{U}$ and can be computed as mentioned in Chapter 2. In this case $\underline{M}$ will be formulated as a lumped matrix (sections 2.3 and 2.4) and $\underline{K}$ results a banded matrix. $\underline{C}$ can be obtained by using equation (2.23), but here it will be assumed that it is such that equation (6.6) holds. The elements of $\underset{\sim}{P}$ of equation (6.1) can be evaluated accordingly with sections 2.3 and 2.4 for the type of load considered.

Once matrices $\underline{M}$, $\underline{C}$ and $\underline{K}$ as well as $\underset{\sim}{P}(t)$ are evaluated for the c.g.p. under consideration, its dynamic response may be computed by using the procedures outlined in 6.2 .

6.4.1 Solution for seismic loading

The right hand side of equation (6.1) represents a general dynamic load acting on a linear structural system. When this load is the result of a seismic perturbation i.e. an earthquake,

the term $\underset{\sim}{P}(t)$ of equation (6.1) is made of the so-called seismic loads. This type of loading was discussed in Chapter 4 , and the particular case of an inland structure subjected to an earthquake was presented in Section 4.6 . As it was shown in that section for the discretized structure, the resulting seismic load for its lumped mass is given by equation (4.43) i.e.:

$$P_{s_i} = - m_{ii} \ddot{u}_g \qquad \ldots (6.42)$$

where m_{ii} is the ith lumped mass and $\ddot{u}_g$ is the ground acceleration in the direction indicated in fig.2.2. Equation (6.42) is a part of the associated inertia force, the other part being given by the product $m_{ii} \ddot{u}_{ii}$, where $\ddot{u}_{ii}$ is the acceleration of the ith mass with respect to the foundation of the structure.

In the case of an offshore structure such as a c.g.p. subjected to an earthquake, the resulting inertia forces are generated from the acceleration of a mass formed by the mass of the structure plus the mass of the displaced fluid. This is so because, as it was mentioned in Section 5.3.3 with relation to the inertia wave loading on a submerged body, the inertia force acting on an accelerating body is equal to the mass of the body plus the mass of the displaced fluid, multiplied by the acceleration of the body. Therefore, in the case of an earthquake acting on a c.g.p. the seismic load is given by:

$$P_{s_i} = - (m_{ii} + m^d_{ii}) \ddot{u}_g \qquad \ldots (6.43)$$

where m_{ii} and $\ddot{u}_g$ were previously defined and m^d_{ii} represents the mass of the displaced fluid associated to the ith node. The other contribution to the resulting inertia force is given by the product $(m_{ii} + m^d_{ii}) \ddot{u}_i$, where $\ddot{u}_i$ is again the relative acceleration of the ith mass with respect to the foundation of the structure.

From the above paragraph it follows that for the case under consideration the governing equations are:

$$\underline{\hat{M}} \, \underset{\sim}{\ddot{U}} + \underline{C} \, \underset{\sim}{\dot{U}} + \underline{K} \, \underset{\sim}{U} = - \underline{\hat{M}} \, \underset{\sim g}{\ddot{U}} \qquad \ldots (6.44)$$

where

$$\hat{\underline{M}} = \underline{M} + \underline{M}^d \qquad \ldots (6.45)$$

The terms involved in equations (6.44) and (6.45) have been defined previously except for the matrix $\underline{M}^d$ and the vector $\ddot{\underset{\sim}{U}}_g$. $\underline{M}^d$ represents the mass of the displaced fluid, being a diagonal matrix whose elements are equal to m^d_{ii} for the translational degrees of freedom in the direction of the ground motion, and nil for the other degrees of freedom. The components of $\ddot{\underset{\sim}{U}}_g$ are equal to $\ddot{u}_g$ for the translational degrees of freedom in the direction of the ground motion and nil for the others.

Equation (6.44) can be solved by using any of the procedures presented in 6.2 . It may be noticed that the drag forces associated to the velocities of the structure have been neglected in the formulation of equation (6.44). The validity of this assumption is based on the discussion presented in Section 5.4 .

6.4.2 Solution for wave loading

The wave loading on a c.g.p. was discussed in Chapter 5. The different types of wave loading regimes to which this kind of offshore structure may be subjected were commented upon in that chapter. In Section 5.4 it was concluded that the main wave loading regimes for a c.g.p. are the inertia and diffraction ones. Another conclusion was that the drag loads acting on the c.g.p. structural elements could be neglected without noticeably affecting the accuracy of the value of the total computed wave loading. Finally, expressions for the inertia and diffraction wave loading regimes were introduced in 5.3.3 through 5.3.5 .

The wave nodal loads on the discretized structure can be computed as follows. If its ith node belongs to beam elements which satisfy the ratio $d/W_0 > 0.2$ (where d is the diameter of the elements and W_0 the wave height), the wave inertia load acting on the node can be evaluated by using equation (5.57), i.e.:

$$P_{w_i}(t) = K_m \rho V_i \ddot{v}_i - (K_m - 1) \rho V_i \ddot{u}_i \qquad \ldots (6.46)$$

where, as mentioned in 5.3.4 , K_m is the coefficient of inertia for the immersed body, ρ the mass density of the fluid, V_i the tributary volume of the beam elements ending at the ith node, $\ddot{v}_i$ is the acceleration of the water particles at that node as if no body existed and $\ddot{u}_i$ is the relative acceleration of that node with respect to the structure foundation.

The second term of the right hand side of equation (6.46) is the displaced mass mentioned in Section 6.4.1 , i.e. $m^d_{ii}\ddot{u}_i$. This term can be added to the associated term $m_{ii}\ddot{u}_i$ of the corresponding row of equation (6.1); therefore, the final expression of the wave inertia load is:

$$P'_{w_1}(t) = K_m \rho V_i \ddot{v}_i \qquad \ldots (6.47)$$

If the ith node of the idealized structure corresponds to beam elements in which the relation $d/\lambda > 0.2$ is satisfied (where λ is the wave length), the associated diffraction force can be evaluated by using equation (5.71). For the horizontal diffraction force on the caisson, equation (5.72) should be used. Finally the overturning moments produced by the diffraction forces and acting at the center of gravity of the caisson, can be evaluated by using equations (5.73) and (5.74).

From the above paragraphs it follows that the governing equations for the case under consideration are:

$$\underline{\bar{M}}\ \ddot{\underset{\sim}{U}} + \underline{C}\ \dot{\underset{\sim}{U}} + \underline{K}\ \underset{\sim}{U} = \underset{\sim}{P}_w \qquad \ldots (6.48)$$

where

$$\underline{\bar{M}} = \underline{M} + \underline{V}(K_m - 1)\rho \qquad \ldots (6.49)$$

$$\underset{\sim}{P}_w = \begin{Bmatrix} P'_{w_1} \\ \vdots \\ P'_{w_n} \end{Bmatrix} \qquad \ldots (6.50)$$

The elements of equations (6.47)-(6.49) have already been defined except for $\underline{V}$ and $\underset{\sim}{P}_w$. $\underline{V}$ is a diagonal matrix whose elements are

the volumes, V_i (i=1,...n) associated to each nodal point. The elements of $\underset{\sim}{P}_w$ can be emputed by using equations (6.47) or (5.71) depending on the node under consideration, i.e. if the inertia or diffraction regime apply, respectively. Notice that the components of $\underline{\overline{M}}$, equation (6.48), are arranged in such a way that the correspond to their respective wave nodal loads. Again, the solution of equation (6.48) can be achieved by utilizing the methods presented in 6.2 .

6.5 Dynamic response of a c.g.p. resting on a flexible soil

The dynamic response of a c.g.p. resting on a flexible soil and subjected to seismic loading can be obtained by solving the associated governing equations. If the structural modelling of the c.g.p. is made as described in Chapter 2, and if the interaction between its foundation and the surrounding soil is idealized by impedance functions as discussed in Chapter 3, the dynamic response of the c.g.p. can be computed by solving equation (6.24) for the type of load under consideration.

As already mentioned in 6.3 , equation (6.24) includes the degrees of freedom of the structure, $n^s = 2n$, plus those associated to its idealized soil-foundation, n^f . Therefore, the dimension of the vector $\underset{\sim}{U}_0$ (also of $\dot{\underset{\sim}{U}}_0$ and $\ddot{\underset{\sim}{U}}_0$) in this equation is equal to $N = n^s + n^f$. The degrees of freedom n^s of $\underset{\sim}{U}_0$ correspond to the relative displacements of the nodal points with respect to the foundation, and the associated slopes at these nodal points.

In this work $\underset{\sim}{U}_0^f$ consists of the foundation horizontal translation and its rocking with respect to the axis z , accordingly to fig. 3.3 . The coupling between these two degrees of freedom is neglected in the formulation. The contribution of the vertical impedance, fig. 3.3 is not included in the present formulation. Both effects could be considered in equation (6.24) without representing major complications for its solution.

Concerning the matrices $\underline{M}_0$, $\underline{C}_0$ and $\underline{K}_0$ of equation (6.24) they can be computed for the c.g.p. based on 2.4 and 3.3 and accordingly with equation (6.25). The vector $\underset{\sim}{P}_0(t)$ in the

same equation has to be evaluated accordingly with equation (6.25) and the type of load being considered. The actual solution of equation (6.24) may be obtained by using the techniques presented in 6.3 .

6.5.1 Solution for seismic load

The expressions for the seismic loads which may occur in a c.g.p. resting on flexible soils are basically the same as for the c.g.p. resting on a rigid soil. Therefore, the discussion about them introduced in 6.4.1 is valid here, i.e. the elements of vector $\underset{\sim}{P}^{s}_{0}(t)$ in equation (6.25) are given by:

$$P^{s}_{0_i}(t) = -(m_{ii} + m^{d}_{ii})\,\ddot{u}_g \qquad \ldots (6.51)$$

and the expressions corresponding to P_{u_0} and P_{θ_0} are given by:

$$P_{u_0} = -\left[m^{t}_{0} + (m^{t}_{0})^{d}\right]\ddot{u}_g \qquad \ldots (6.52)$$

$$P_{\theta_0} = \sum_{\substack{i=1 \\ j = 2i-1}}^{n} (m_{jj} + m^{d}_{jj})\, h_i\, \ddot{u}_g \qquad \ldots (6.53)$$

where all the elements included in equations (6.50) to (6.52) were defined in 6.4.1 and 6.4.2 . Concerning the elements of $\underline{M}_0$ in equation (6.25) for the case under consideration, they include the contribution of the displaced mass for the nodes which correspond to the submerged part of the c.g.p. . Therefore, instead of m_{jj} , they should read $m_{jj} + m^{d}_{jj}$ in equation (6.26) through to (6.30), $j=2i-1 (i=1,\ldots n)$. The solution of equation (6.24) for seismic load can be achieved by substituting equations (6.51)-(6.53) into the former one and applying any of the methods introduced in 6.3 .

6.5.2 Solution for wave loading

The wave loading for this case can be obtained by following 6.4 because the comments expressed there also applied to a c.g.p. resting on flexible soil. Therefore, the components of the vector $\underset{\sim}{P}_0(t)$ are as follows for this case:

$$\underset{\sim}{P}^{s}_{0}(t) = \begin{Bmatrix} P'_{w_1} \\ P'_{w_n} \end{Bmatrix} \qquad \ldots (6.54)$$

$$P_{u_0}(t) = P_{w_2} \quad \text{(associated to } m_0\text{)} \qquad \ldots (6.55)$$

$$P_{\theta_0}(t) = M'_{w_1} + M'_{w_2} \qquad \ldots (6.56)$$

where the elements of $\underset{\sim}{P}^{s}_{0}$ were defined in relation to equation (6.50). P_{w_2} in equation (6.55) can be computed by using equation (5.72). M'_{w_1} and M'_{w_2} are given by equations (5.73) and (5.74) respectively. Again, the elements m_{jj} included in equations (6.26) through to (6.30) for $j=2i-1(i=1,\ldots n)$ should read in this case $(m_{jj} + m^{d}_{jj})$ for the appropriate nodes. The solution of equation (6.24) for wave loading can be performed by using any of the schemes presented in 6.3 .

7. STATISTICS OF THE RESPONSE OF A CONCRETE GRAVITY PLATFORM UNDER SEISMIC AND WAVE LOADS ACTING SEPARATELY OR SIMULTANEOUSLY

7.1 Introduction

In Chapter 6 the current techniques to solve the governing equations of a discretized c.g.p. resting on rigid (and flexible) soil and subjected to seismic and wave loads were presented. The solution of these equations provides with the time history of the nodal displacements or other linearly-related structural responses. The random nature of the mentioned loads plus the assumption about the linearity of the systems lead to responses which are also random variables. Furthermore, the statistical characteristics of the responses can be derivated from those of the loading. This latter feature is very useful in the assessment of the safety of a structure, because the application of probabilistic methods to this end follows immediately. For example, the second-moment probabilistic structural safety analysis and design method [7.1] requires the knowledge of the mean and variance of a structural response; these are used in combination with the variance of the random structural resistance and yield an estimate of the expected value of the structural response.

The present chapter will be devoted to the derivation of expressions to compute the statistics of the structural response of the discretized c.g.p. (Chapter 2) under seismic loading (Chapter 4) and wave loading (Chapter 5) acting separately or simultaneously. Due to the type of loading considered in this work, special emphasis will be given to obtain expressions associated to the statistics of peak responses, in particular its mean and variance.

In 7.2 the statistics of the response of a linear structural system subjected to a single application of a stationary load is treated. The long term statistics of the response of the same system but now under the action of two stationary loads acting simultaneously is the subject of 7.3 . In 7.4 expressions for the extreme value statistics of the response of a c.g.p. under seismic and wave loading and acting separately and simultaneously are presented. Finally, the influence of the uncertainties in the

knowledge of the dynamic properties of the c.g.p. on the statistics of its structural response is introduced in 7.5 .

7.2 Statistics of the response of a linear system subjected to Stationary loading

7.2.1 Single degree of freedom system

In Chapter 6 the current techniques utilized to solve the equations of motion of a linear structural system were introduced. There, it was shown that the solution of the equation of motion of a single degree of freedom system subjected to a dynamic load can be expressed as the convolution of the unit impulse response function of the system, $h(t - \tau)$ and its dynamic load, $P(t)$, i.e. equation (6.10). Furthermore, the same solution could be achieved in the frequency domain by multiplying the complex frequency response of the system, $H(i\omega)$, and the Fourier transform of the load, $P(\omega)$, as shown by equation (6.14). Since both $h(t - \tau)$ and $H(i\omega)$ represent the time invariant dynamic properties of the linear system in those equations, and considering that the load is a random stationary process, the statistical properties of its response, $Y(t)$, uniquely depend on the statistical properties of the dynamic load $P(t)$ [7.2] .

It can be shown [7.2] that if the dynamic load $P(t)$ is a Gaussian ergodic process with a zero mean value, the response $Y(t)$ will also be a process with the same characteristics as $P(t)$. The statistics of a Gaussian ergodic process can be completely defined once its autocorrelation function $R(\tau)$ (or its associated power spectral density function) is computed [7.2]. This is so because the parameter of the probability density function of a stationary normally distributed random variable is its variance which, for a zero mean value process, is equal to the autocorrelation function evaluated at $\tau = 0$ [7.2] , i.e. for the response of the system $Y(t)$,

$$R_{yy}(\tau) = E\left[Y(t)\ Y(t+\tau)\right] \qquad \ldots (7.1)$$

$$S_{yy}(\omega) = \int_{-\infty}^{\infty} R_{yy}(\tau)\ \exp(-i\omega\tau)d\tau \qquad \ldots (7.2)$$

$$\sigma^2 y = R_{yy}(0) = \int_{-\infty}^{\infty} S_{yy}(\omega)d\omega \qquad \ldots (7.3)$$

$$p\,[\dot{y}(t)] = \frac{1}{\sqrt{2\pi}\,\sigma y}\,\exp\left(-\frac{y^2}{2\,\sigma^2 y}\right) \qquad \ldots (7.4)$$

where R_{yy} , S_{yy} , $\sigma^2 y$ stand for the autocorrelation function, the power spectral density function and the variance of the random variable, $Y(t)$. E represents the expectance of what is inside the rectangular parenthesis; equation (7.4) is the probability density function of $Y(t)$.

Another statistics of practical interest for the Gaussian ergodic processes represented by $Y(t)$ is that the probability density function of the peak amplitudes approaches the Rayleigh distribution, and as a consequence, the mean and the standard deviation of the extreme value of $Y(t)$ are given by [7.3] :

$$\overline{Y}_T = \sigma y\,\{(2\mathrm{Ln}\nu T)^{\frac{1}{2}} + \frac{0.5772}{(2\mathrm{Ln}\nu T)^{\frac{1}{2}}}\} \qquad \ldots (7.5)$$

$$\sigma y_T = \left(\frac{\pi}{\sqrt{6}}\right)\frac{\sigma y}{(2\mathrm{Ln}\nu T)^{\frac{1}{2}}} \qquad \ldots (7.6)$$

where σy is the standard deviation of $Y(t)$, i.e. the square root of $\sigma^2 y$, and

$$\nu = \frac{1}{2\pi}\left\{\frac{\int_{-\infty}^{\infty}\omega^2\,S_{yy}(\omega)\,d\omega}{\int_{-\infty}^{\infty}S_{yy}(\omega)\,d\omega}\right\}^{\frac{1}{2}} \qquad \ldots (7.7)$$

and T is the time-interval of the process $Y(t)$.

7.2.2 Multidegree of freedom system

The statistics of the response of a multidegree of freedom system as the one represented by equations (6.1) and (6.24) can be obtained from expressions similar to equations (7.1) to (7.7) if it is assumed that the components of the loading vector are Gaussian ergodic processes. For the displacements, $\underset{\sim}{U}$, of the lumped masses or any linearly-related response, their statistics can be obtained by using the following expressions:

$$\underline{R}_{uu}(\tau) = E\left[\underset{\sim}{U}(t)\,\underset{\sim}{U}^T(t+\tau)\right] \qquad \ldots (7.8)$$

$$\underline{S}_{uu}(\omega) = \frac{1}{2\pi} \int_{-\infty}^{\infty} \underline{R}_{uu}(\tau) \exp(-i\omega\tau) d\tau \quad \ldots (7.9)$$

$$\underline{\sigma}^2_{uu} = \underline{R}_{uu}(0) = \int_{-\infty}^{\infty} \underline{S}_{uu}(\omega) d\omega \quad \ldots (7.10)$$

$$\underline{\bar{u}}_T = \underline{\sigma}_{uu} \{(2\mathrm{Ln}\underline{\nu}T)^{\frac{1}{2}} + \frac{0.5772}{(2\mathrm{Ln}\underline{\nu}T)^{\frac{1}{2}}}\} \quad \ldots (7.11)$$

$$\underline{\sigma u}_T = (\frac{\pi}{\sqrt{6}}) \frac{\underline{\sigma}_{uu}}{(2\mathrm{Ln}\underline{\nu}T)^{\frac{1}{2}}} \quad \ldots (7.12)$$

where $\underline{R}_{uu}(\tau)$, $\underline{S}_{uu}(\omega)$, $\underline{\sigma}^2_{uu}$, $\underline{\sigma}_{uu}$ are the correlation matrix, the cross spectral density function (c.s.d.f.) matrix, the covariance matrix and the standard deviation matrix of the displacements, $\underset{\sim}{U}(t)$, respectively. Equations (7.11) and (7.12) provide with the mean and the covariance matrices of the extreme value of the displacements $\underset{\sim}{U}(t)$; the matrix $\underline{\nu}$ in the same equations is computed from:

$$\underline{\nu} = \frac{1}{2\pi} \left\{ \frac{\int_{-\infty}^{\infty} \omega^2 \underline{S}_{uu}(\omega) d\omega}{\int_{-\infty}^{\infty} \underline{S}_{uu}(\omega) d\omega} \right\}^{\frac{1}{2}} \quad \ldots (7.13)$$

In this case the term T stands for the duration of the loading $\underset{\sim}{P}(t)$. A typical element of the covariance matrix, equation (7.10), can be computed as follows: assuming that the solution to equation (6.1) or (6.24) is expressed by equation (6.2) (i.e. using the modal superposition method) the displacement u_ℓ can be calculated by

$$u_\ell(t) = \sum_{j=1}^{n} r_{\ell j} Y_j(t) \qquad \ell = 1,2,\ldots,m \quad \ldots (7.14)$$

where $r_{\ell j}$ is the modal amplitude of the ℓth mass in the jth mode and corresponds to the ℓth row, jth column of the modal matrix $\underline{R}$. The cross correlation function for the responses u_ℓ and u_m is:

$$R_{u_\ell u_m}(\tau) = E\left[u_\ell(t)\, u_m(t+\tau)\right]$$

$$= E\left[\sum_{j=1}^{n} \sum_{k=1}^{n} r_{\ell j}\, r_{mk}\, Y_j(t)\, Y_k(t+\tau)\right]$$

$$= \sum_{j=1}^{n} \sum_{k=1}^{n} r_{\ell j}\, r_{mk}\, E\left[Y_j(t)\, Y_k(t+\tau)\right] \qquad \ldots (7.15)$$

Substituting equation (6.10) into equation (7.15), it can be shown that the latter can be written as:

$$R_{u_\ell u_m}(\tau) = \sum_{j=1}^{n} \sum_{k=1}^{n} r_{\ell j}\, r_{mk} \int_{-\infty}^{\infty} \int_{-\infty}^{\infty} h_j(\tau_1)\, h_k(\tau_2) \times R_{p_j^* p_k^*}(\tau - \tau_1 + \tau_2)\, d\tau_1\, d\tau_2 \qquad \ldots (7.16)$$

where τ_1 , τ_2 are dummy time variables and

$$R_{p_j^* p_k^*}(\tau) = E\left[P_j^*(t)\, P_k^*(t+\tau)\right] \qquad \ldots (7.17)$$

is the cross correlation of loads P_j^* and P_k^* which can be computed by using equation (6.9).

Substituting equation (7.16) into the appropriate element of equation (7.9) and considering the relationship between $h_s(t)$ and $H_s(i\omega)$ (mentioned in 6.2.3), the c.s.d.f. for displacements u_ℓ and u_m is obtained:

$$S_{u_\ell u_m}(\omega) = \sum_{j=1}^{n} \sum_{k=1}^{n} r_{\ell j}\, r_{mk}\, H_j^*(i\omega)\, H_k(i\omega)\, S_{p_j^* p_k^*}(\omega) \qquad \ldots (7.18)$$

where $H(i\omega)$ is given by equation (6.18) and $H^*(i\omega)$ is its complex conjugate. The c.s.d.f. for loads $P_j^*(t)$ $P_k^*(t)$ i.e. $S_{p_j^* p_k^*}(\omega)$ is given by:

$$S_{p_j^* p_k^*}(\omega) = \frac{1}{2\pi} \int_{-\infty}^{\infty} R_{p_j^* p_k^*}(\tau) \exp(-i\omega\tau)\, d\tau \qquad \ldots (7.19)$$

Finally, substituting equation (7.19) into the corresponding element of equation (7.10) leads to the covariance of the displacements u_ℓ and u_m , i.e.

$$\sigma^2 u_\ell u_m = \int_{-\infty}^{\infty} \{ \sum_{j=1}^{n} \sum_{k=1}^{n} r_{\ell j}\, r_{mk}\, H_j^*(i\omega)\, H_k(i\omega)\, S_{p_j^* p_k^*}(\omega)\, d\omega \qquad \ldots (7.20)$$

Expressions of the same form as equations (7.18) and (7.20) can be

obtained for the statistics of other structural responses of interest which can be expressed as a linear superposition of the normal coordinates $Y_s(t)$; i.e. if $a(t)$ is the response of interest, the condition is that $a(t)$ can be expressed as follows:

$$a(t) = \sum_{s=1}^{n} b_s Y_s(t) \qquad \ldots (7.21)$$

where the b_s's are known coefficients which link $a(t)$ with $Y_s(t)$. It can be shown that in this case the covariance of the response $a(t)$ is given by:

$$\sigma^2 aa = \int_{-\infty}^{\infty} \{ \sum_{j=1}^{n} \sum_{k=1}^{n} b_j \, b_k \, H_j^*(i\omega) \, H_k(i\omega) \, S_{p_j^* p_k^*}(\omega) \} d\omega \qquad \ldots (7.22)$$

The limits of the integrals in equations (7.20) or (7.22) range from $-\infty$ to $+\infty$; however, the actual dynamic loading is usually restricted to a band of frequencies of practical engineering interest, let us say from ω_i to ω_f . Therefore, those limits can be changed as follows: $-\infty$ to ω_i and $+\infty$ to ω_f , without loosing accuracy in the final result of the integration.

7.3 Long term statistics of the extreme value of the response of a linear system subjected to stationary loads acting simultaneously

7.3.1 Single degree of freedom system under a single type of loading

Equations (7.5) and (7.6) provide with the mean and the standard deviation of the extreme value of the response $Y(t)$ for a single application of the load; therefore, the term T in those equations refers to the duration of such loading. However, if the load is acting for a number of times during a period of time T_0 with $T_0 >> T$, equations (7.5) and (7.6) will not yield the extreme statistics of $Y(t)$ for T_0 . In this case those statistics could be obtained by following [7.4] i.e.:

$$\overline{Y}_{T_0} = \overline{Y}_T + p \, \sigma y_T \qquad \ldots (7.23)$$

$$\sigma y_{T_0} = q \, \sigma y_T \qquad \ldots (7.24)$$

where $\overline{Y}_{T_0}$ and σy_{T_0} are the mean and the standard deviation of the extreme value of $Y(t)$ for the period of time T_0 ; $\overline{Y}_T$ and σy_T represent the mean and the standard deviation of the response $Y(t)$ for the load acting during time T . The parameters p and q in equations (7.23) and (7.24) are the mean and the standard deviation of the normalized variate, $\Phi = (y_{T_0} - \overline{Y}_T)/\sigma y_T$, respectively.

The former two parameters are function of the power spectral density function of $Y(t)$, $S_{yy}(\omega)$, the occurrence rate of the loading, ν_p , the period of time T_0 and the instantaneous intensity distribution of $Y(t)$. If it is assumed that the load forms a filtered Poisson process i.e.: a) that the load occurrences during the length of time T_0 follow a Poisson process, b) that the load intensities at various occurrences are statistically independent and c) identically distributed random variables;the parameters p and q can be computed as follows:

$$p = \frac{\int_{-\infty}^{\infty} y \, f_{y_{T_0}}(y)dy - \overline{Y}_T}{\sigma y_T} \qquad \ldots (7.25)$$

$$q = \frac{\{\int_{-\infty}^{\infty} y^2 \, f_{y_{T_0}}(y)dy - (\overline{Y}_T + p\sigma y_T)^2\}^{\frac{1}{2}}}{\sigma y_T} \qquad \ldots (7.26)$$

where the expression for the probability density function $f_{y_{T_0}}$ is derivated in Appendix C . The rest of the parameters in equations (7.25) and (7.26) were previously defined.

7.3.2 Single degree of freedom system under two different types of loads acting simultaneously

In the case of two loads acting simultaneously on a single degree of freedom system during a time interval T_0 such that $T_0 >> T$, where T is the duration of each loading, the extreme statistics of its response $Y(t)$ can be evaluated with expressions similar to equations (7.23) and (7.24). Accepting assumptions a), b) and c) of Section 7.3.1 and making the following extra ones: d) there is a linear superposition of load effects, i.e. $Y(t) = Y_1(t) + Y_2(t)$,

e) the responses $Y_1(t)$ and $Y_2(t)$ associated to the loads $P_1(t)$ and $P_2(t)$ are statistically independent the mean and the standard deviation of the extreme value of $Y(t)$ can be computed by [7.4] :

$$\overline{Y}_{T_0} = \sum_{i=1}^{2} \overline{Y}_{T_i} + p\left(\sum_{i=1}^{2} \sigma^2 y_{T_i}\right)^{\frac{1}{2}} \quad \ldots (7.27)$$

$$\sigma y_{T_0} = q\left(\sum_{i=1}^{2} \sigma^2 y_{T_i}\right)^{\frac{1}{2}} \quad \ldots (7.28)$$

where

$$p = \frac{\sum_{i=1}^{2} p_i \, \sigma^2 y_{T_i}}{\sum_{i=1}^{2} \sigma^2 y_{T_i}} \quad \ldots (7.29)$$

$$q = \frac{\sum_{i=1}^{2} q_i \, \sigma^2 y_{T_i}}{\sum_{i=1}^{2} \sigma^2 y_{T_i}} \quad \ldots (7.30)$$

In equations (7.27) to (7.30) the parameters $\overline{Y}_{T_i}$, $\sigma_{y_{T_i}}$, p_i and q_i for $i=1,2$ are associated to the responses of the system under loads P_i , $i=1,2$. The parameters p_i and q_i are evaluated by using equations (7.25) and (7.26).

7.3.3 Multidegree of freedom system under a single type of loading

The computation of the long-term statistics of a multidegree of freedom system under a single type of loading can be obtained by following the procedures underlined in Section 7.3.1 . The results obtained there can also be applied to the present case in which the statistics of the extremes of the response $\underset{\sim}{U}(t)$ are seeked i.e.:

$$\overline{\underset{\sim}{U}}_{T_0} = \overline{\underset{\sim}{U}}_{T} + \underset{\sim}{p}^{T} \, \underline{\sigma u}_{T} \quad \ldots (7.31)$$

$$\underline{\sigma u}_{T_0} = \underset{\sim}{q}^{T} \, \underline{\sigma} \, u_T \quad \ldots (7.32)$$

where $\underline{\bar{U}}_T$ and $\underline{\sigma u}_T$ are computed from equations (7.11) and (7.12) respectively, $\underset{\sim}{p}^T$ and $\underset{\sim}{q}^T$ are made with the p's and q's parameters corresponding to each degree of freedom. This means that once the vectors $\underset{\sim}{p}$ and $\underset{\sim}{q}$ are evaluated by using equations (7.25) and (7.26) with $u_{ij}(t)$ instead of $y(t)$ as parameters, a typical extreme value statistics of the response u_{jj} for a time interval T_0 can be calculated as follows:

$$(\bar{u}_{jj})_{T_0} = (\bar{u}_{jj})_T + p_j(\sigma u_{jj})_T \qquad \ldots (7.33)$$

$$(\sigma u_{jj})_{T_0} = q_j(\sigma u_{jj})_T \qquad \ldots (7.34)$$

7.3.4 Multidegree of freedom system under two different types of loads acting simultaneously

When two types of loading are acting simultaneously on a multidegree of freedom system, the extreme statistics of its response $\underset{\sim}{U}(t)$ could be computed by following the assumptions made in Section 7.3.2 . Therefore, the expressions equivalent to equations (7.27) and (7.28) are in this case the following ones:

$$\underline{\bar{U}}_{T_0} = \sum_{i=1}^{2} (\underline{\bar{U}}_T)_i + \underset{\sim}{p}^T \left(\sum_{i=1}^{2} (\underline{\sigma}^2 u_T)_i\right)^{\frac{1}{2}} \qquad \ldots (7.35)$$

$$\underline{\sigma}\, u_{T_0} = \underset{\sim}{q}^T \left(\sum_{i=1}^{2} (\underline{\sigma}^2 u_T)_i\right)^{\frac{1}{2}} \qquad \ldots (7.36)$$

where $(\underline{\bar{U}}_T)_i$ and $(\underline{\sigma}\, u_T)_i$ $i=1,2$ are computed for the associated load P_i , $i=1,2$ from equations (7.11) and (7.12) , the elements of the vectors $\underset{\sim}{p}$ and $\underset{\sim}{q}$ are evaluated for each degree of freedom using equations (7.29) and (7.30) respectively with parameters $u_{ij}(t)$ instead of $Y_i(t)$. It can be shown that the expressions corresponding to the extreme value statistics of the jth degree of freedom are given by:

$$(u_{jj})_{T_0} = \sum_{i=1}^{2} ((\bar{u}_{jj})_T)_i + p_{ij}\left[\sum_{i=1}^{2} (\sigma^2 u_{jj})_T\right]_i^{\frac{1}{2}} \qquad \ldots (7.37)$$

$$(\sigma u_{jj})_{T_0} = q_{ij}\left[\sum_{i=1}^{2}(\sigma^2 u_{jj})_T\right]_i^{\frac{1}{2}} \qquad \ldots (7.38)$$

where $((\bar{u}_{jj})_T)_i$ and $((\sigma^2 u_{jj})_T)_i$ stand for the mean and variance of the displacement of the jth node when the structure is under a type of load i for a time T . It should be noticed that p_{ij} and q_{ij} i=1,2 in equations (7.37) and (7.38) are associated to the loads P_i , i=1,2 and to the jth degree of freedom.

7.4 Statistics of the response of a c.g.p. subjected to seismic and wave loading

With the expressions already presented in 7.3 of this chapter plus the onesintroduced in chapters 4 to 6 the evaluation of the statistics of the response of a c.g.p. under seismic and/or wave loading could be obtained in a straightforward manner. This is so because the c.g.p. has been discretized in such a way that the governing equations for the structure supported on a rigid or flexible soil, i.e. equations (6.1) and (6.24) respectively, correspond to multidegree of freedom systems. Concerning the loading, in Chapters 4 and 5 it was seen that both seismic and wave loading could be assumed to be Gaussian stationary processes, and that their occurrences could be associated to the Poisson process. From a physical point of view these types of loadings can be considered as statistically independent. Therefore, both types of loading satisfy the assumptions made in Sections 7.2.1 , 7.3.1 , and 7.3.2 .

From the above paragraphs, it can be concluded that the expressions presented in Sections 7.2.2 , 7.2.3 and 7.2.4 can be utilized to evaluate the statistics of the response of a c.g.p. under seismic and wave loading acting separately or simultaneously. However, equation (7.19) has to be determined for the type of load considered.

7.4.1 Statistics of the response of a c.g.p. : seismic loading

In this section, equation (7.19) will be derivated for the seismic loading. Equation (4.43) provides the expression for the seismic loading acting on a lumped mass. From this equation and the definition of the generalized load, equation (6.9), it can be concluded that the jth generalized load associated to the discretized structure is given by:

$$P^*_{sj}(t) = -\sum_{i=1}^{n} r_{ij} \; m_{ii} \; \ddot{u}_g \qquad \ldots (7.39)$$

It can be shown that by substituting equation (7.39) into equation (7.17) and this one into (7.19), the cross-spectral density function $S_{p^*_j p^*_k}(\omega)$ is given by:

$$S_{p^*_j p^*_k}(\omega) = \sum_{i=1}^{n} \sum_{\ell=1}^{n} r_{ij} \; r_{\ell k} \; (m_{ii} m_{\ell\ell}) \; S_{\ddot{u}_g} \qquad \ldots (7.40)$$

where $S_{\ddot{u}_g}$ is the power spectral density of the ground acceleration, examples of which can be seen in figs. 8.9 to 8.12.

Once $S_{\ddot{u}_g}$ is computed and equation (7.40) is evaluated, the latter can be substituted into equation (7.20) and then it is possible to carry on with the calculation of the statistics of interest for the c.g.p. under consideration following Sections 7.2.2 , 7.3.3 and 7.3.4 .

7.4.2 Statistics of the response of a c.g.p. : wave loading

Here the expressions for the cross-spectral density function for wave loading, equation (7.19), will be derivated. In particular, the case of the inertia load (Section 5.3.3) will be treated in detail. As the case of the diffraction load (Section 5.3.5)can be obtained in a similar way, the resulting expressions will only be quoted. The inertia wave load for the ith lumped mass is given by:

$$P_{w_i} = C_{m_i} \ddot{v}_i \qquad \ldots (7.41)$$

and the jth associated generalized wave load by:

$$P^*_{w_j} = \sum_{i=1}^{n} r_{ij} \; C_{m_i} \ddot{v}_i \qquad \ldots (7.42)$$

substituting equation (7.42) into equation (7.17) gives:

$$R_{p^*_j p^*_k}(\tau) = E\Big[\sum_{i=1}^{n} \sum_{\ell=1}^{n} r_{ij} \; r_{\ell k} \; C_{m_i} \; C_{m_\ell} \; \ddot{v}_i(t) \; \ddot{v}_\ell(t+\tau)\Big] \qquad \ldots (7.43)$$

and putting (7.43) into (7.19) leads to:

$$S_{p_j^* p_k^*}(\omega) = \sum_{i=1}^{n} \sum_{\ell=1}^{n} r_{ij}\, r_{\ell k}\, C_{m_i} C_{m_\ell}\, \omega^2 T_1 S_{\eta\eta}(\omega) \quad \ldots (7.44)$$

where r_{ij} is the modal amplitude of the ith mass in the jth mode,

$$T_1 = \frac{\cosh \kappa(y_i + D) \cosh \kappa(y_\ell + D)}{\sinh^2 (\kappa D)} \quad \ldots (7.45)$$

and $S_{\eta\eta}(\omega)$ is the power spectral density function of wave heights which can be computed by equations (5.48) or (5.49).

For the diffraction forces the corresponding expression is:

$$S_{p_j^* p_k^*}(\omega) = \sum_{i=1}^{n} \sum_{t=1}^{n} r_{ij}\, r_{tk}\, C'_{d_i}\, C'_{d_t}\, \omega^2\, T_1 S_{\eta\eta}(\omega) \quad \ldots (7.46)$$

where

$$C'_{d_i} = C_{x_i}\, \rho\, r_i\, \ell_i\, \lambda\, J_1(\pi d_i/\lambda) \quad \ldots (7.47)$$

$$C'_{d_t} = C_{x_t}\, \rho\, r_t\, \ell_t\, \lambda\, J_1(\pi d_t/\lambda) \quad \ldots (7.48)$$

Having computed expressions (7.44) and (7.46) the computation of the statistics of the response of interest of the c.g.p. can be carried out accordingly to Sections 7.2.2 , 7.3.3 and 7.3.4 .

7.4.3 Statistics of the response of a c.g.p. : seismic and wave loading acting simultaneously

The computation of the statistics of the response of a c.g.p. subjected to seismic loading and wave loading acting simultaneously can be achieved by applying the expressions presented in Section 7.3.4. Those expressions require the previous computation of the parameters included in equations (7.35) and (7.36) for each type of loading, i.e. the ones associated to the seismic loading and the ones to the wave loading, the derivation of which was presented above, i.e. in Sections 7.4.1 and 7.4.2 respectively.

7.5 Statistics of the response of a c.g.p. considering uncertainties on its dynamic properties and on the excitation forces

The expressions presented above to evaluate the statistics of the response of a c.g.p. subjected to seismic loading and wave loading include only the uncertainties on both types of excitations. However, there are other uncertainties associated to the imperfect knowledge of the dynamic properties of the structure under consideration. For example, the uncertainties concerning the stiffness and damping characteristics of the structural materials.

In this section, a scheme to take those uncertainties into consideration when evaluating the statistics of the response of a c.g.p. is presented. In [7.5] a procedure was suggested to compute an estimate of the nth statistical moments of the distribution of a function of random variables in terms of the first few moments of the later variables. The procedure consists in approximating the nth moment of the function from the Taylor expansion of the function about the expectation of the random variables [7.5] .

The case of a two-point estimate is of particular interest here because it allows to introduce the mentioned uncertainties in the computation of the mean and the coefficient of variation of the response of interest. It can be shown [7.5] that if this structural response, Y , is expressed as follows

$$Y = Y(k,c,e) \qquad \ldots (7.49)$$

where k,c, and e are random variables which stand for the stiffness, the damping of the structure and the applied excitation respectively, the mean $\bar{Y}$ and the coefficient of variation V_y of the function Y are given by:

$$\bar{Y} = \frac{\bar{Y}(k)\ \bar{Y}(c)\ \bar{Y}(e)}{\bar{Y}^2(k,c,e)} \qquad \ldots (7.50)$$

$$V_y = \{[1 + V_y(k)]^2\ [1 + V_y(c)]^2\ [1 + V_y(e)]^2 - 1\}^{\frac{1}{2}} \qquad \ldots (7.51)$$

where

$$\bar{Y}(k) = \tfrac{1}{2}\{Y(\bar{k} + \sigma k, \bar{c}, \bar{e}) + Y(\bar{k} - \sigma k, \bar{c}, \bar{e})\} \quad \ldots (7.52)$$

$$\bar{\bar{Y}}(k,c,e) = Y(\bar{k}, \bar{c}, \bar{e}) \quad \ldots (7.53)$$

$$V_y(k) = \left| \frac{\{Y(\bar{k} + \sigma k, \bar{c}, \bar{e}) - Y(\bar{k} - \sigma k, \bar{c}, \bar{e})\}}{\{Y(\bar{k} + \sigma k, \bar{c}, \bar{e}) + Y(\bar{k} - \sigma k, \bar{c}, \bar{e})\}} \right| \quad \ldots (7.54)$$

$Y(\bar{k} \pm \sigma k, \bar{c}, \bar{e})$ and $V_y(k)$ are the mean value and the coefficient of variation of the response $Y(k,c,e)$ evaluated for $k = \bar{k} \pm \sigma k$, $c = \bar{c}$ and $e = \bar{e}$ respectively. The expressions for $\bar{Y}(c)$, $V_y(c)$ and $\bar{Y}(e)$, $V_y(e)$ are similar to (7.52) and (7.54) but using the mean values and the standard deviations of the corresponding parameters. Finally $Y(\bar{k}, \bar{c}, \bar{e})$ in equation (7.53) corresponds to the mean value of the response evaluated for the mean value of parameters k, c, and e.

The set of equations (7.50)-(7.51) and (7.31) to (7.34) can be used to obtain the statistics of the degrees of freedom of interest. A similar procedure could be followed to compute the statistics of other responses of the c.g.p. .

8. PARAMETRICAL STUDIES ON THE MAXIMUM RESPONSES OF A CONCRETE GRAVITY PLATFORM

8.1 Introduction

In order to implement the methodology introduced in the previous chapters to obtain the maximum responses of a c.g.p. under seismic and wave loading, a computer program written in Fortran was developed. A block diagram of the program is shown in fig. 8.1.

As an example of the type of results which can be obtained with the program, the maximum expected responses of a c.g.p. under the mentioned environmental loads were computed. It was assumed that the return period of interest was 50 years. The maximum responses calculated include the effect of the imperfect knowledge on the properties of the structural material and the uncertainties surrounding the seismic and wave excitations. The uncertainties associated to the properties of the soil media were taken into consideration by varying those properties within an appropriate range.

The topology of the c.g.p. selected for the study is shown in fig. 2.2. This geometry corresponds to a platform with two towers or could be associated to one half of a symmetric c.g.p. with four towers, fig. 2.1. The platform site, located in the North Sea, is shown in fig. 4.4.

The geometrical characteristics of the c.g.p. under consideration and the uncertainties on the properties of the structural material are discussed in 8.2 . The properties of the soil media for the selected site, which characterize its dynamic behaviour are the subject of 8.3 . The uncertainties about the values of the seismic and wave excitations for the site shown in fig. 4.4 are introduced in 8.4 and 8.5 respectively.

In 8.6 a parametrical study of the influence of the uncertainties about E_c , ξ_c as well as the idealization of the soil media on the free vibration characteristics of the c.g.p. was carried out. In 8.7 the effect of the mentioned parameters, as well as the uncertainties about the seismic and wave excitations on some characteristic dynamic responses of the c.g.p. were examined. The platform dynamic responses selected were the maximum values of deck displacement, base shear force and overturning moment.

In particular, the first two statistical moments of these

responses when the platform is under seismic and wave loads acting separately or simultaneously were computed. In addition, the influence of the caisson storage mass on the mentioned responses of the platform was studied in 8.8 .

8.2 Selected concrete gravity platform and the uncertainties about the properties of its structural material

The c.g.p. selected for this study is shown in fig. 2.2; as it can be observed, this topology corresponds to a platform with two towers or to one half of a symmetric platform with four towers, fig. 2.1. The general characteristics of the platform are the ones already mentioned in Chapter 2, i.e. it consists of a caisson, two or more towers and a deck. The platform site has been located in the North Sea, fig. 4.4. As far as the uncertainties about the properties of the platform structural material are concerned, the variability of the elasticity modulus, E_c , and the percentage of critical damping, ξ_c , will be considered.

8.2.1 Geometry of the platform under study

The caisson is a reinforced concrete structure with rectangular shape in plant view and a height of about one third of the water depth. The towers are also reinforced concrete structures having tapered shape for the lower two thirds of their height and a constant diameter in the upper third. The deck is made of steel girders and usually has a rectangular shape in plant. Some details of the geometry of the platform are given in Table 8.1.

The structural discretization of the c.g.p. was performed accordingly with 2.4, i.e. the caisson was considered as a rigid block and the towers and deck were represented by beam elements, fig. 2.3. Seven elements of constant length were used to represent each tower, and the deck was idealized by one beam element whose stiffness was considered several times larger than the stiffness associated to the former elements.

8.2.2 Uncertainties about the reinforced concrete elasticity modulus, E_c

From statistical studies [8.1] it has been found that the

value of E_c varies according to a number of parameters, i.e. it should be considered as a random variable. The results of these studies are such that the histograms of E_c can be adjusted to a normal distribution pattern. The following values of its mean and coefficient of variation, C.V. , have been reported in [8.1] :

$$\overline{E}_c = 2.2 \times 10^6 \quad \text{to} \quad 3.6 \times 10^6 \ (\text{Ton/m}^2)$$

$$\text{C.V. of } E_c = 0.10 \quad \text{to} \quad 0.25 \qquad \ldots (8.1)$$

In this work the lower limits of $\overline{E}_c$ and C.V. will be used as a conservative measure of the E_c value which can be achieved in practice.

8.2.3 Uncertainties about the critical damping, ξ_c , of the reinforced concrete

The value of ξ_c is also a random variable as it has been shown in [8.2] . In this reference, a study of the value of ξ_c on real multistorey buildings was performed. The histograms obtained from experimental results were adjusted to lognormal or gamma distribution patterns, and the following values of ξ_c were found:

$$\xi_c = 0.0426$$

$$\sigma_{\xi_c} = 0.0323 \qquad \ldots (8.2)$$

for small deformations, and:

$$\xi_c = 0.0663$$

$$\sigma_{\xi_c} = 0.1799 \qquad \ldots (8.3)$$

for large deformations.

In this work the values associated to the small deformations will be used, because only the linear elastic behaviour will be considered for this type of structures.

8.3 Dynamic parameters of the soil media under the platform site

In order to apply the soil structure interaction model discussed in 3.3.3., the following properties of the soil at the platform site

are required: mass density, ρ_s , shear modulus, G_s , and internal damping, ξ_s . The shear wave velocity of the soil, V_s , is nearly associated to shear modulus as it was shown in equation (3.7). Finally, the contribution of the soil to the equivalent mass of the soil-foundation system has to be determined. The soil data reported in [8.3] for a site located in the North Sea will be assumed to be the soil properties existing at the platform site (fig. 4.4).

The soil media found up to a depth of 40 meters from the mud line are layers of sand, clay and silty clay with variable thickness. Four layers are clearly distinguished in this type of soils: a) a layer of sand about three meters deep (medium dense) with a negligible shear strength; b) a layer of silty clay about 20 meters deep, whose undrained shear strength varies from 0.25 to 1.0 Kg/cm^2; c) a seven meter layer of sand with an undrained shear strength of about 4 Kg/cm^2, d) a layer of silty clay of about 11 meters with an undrained shear strength of 4 Kg/cm^2.

On the basis of the characteristics of the soil medium described above, two different idealizations will be considered for it: a layer over a half space and a half space. For the former idealization, a layer of 23 meters deep was used. These idealizations of the soil media will be selected considering that enough information is available to compute their associated equivalent dampers and springs [8.4 - 8.5] .

8.3.1 Mass density of the soil, ρ_s

In order to determine ρ_s for the two soil idealizations, a weighted average of the soil densities reported in fig. 7 of [8.3] was taken. These weights were obtained as the ratio of the depth of the selected layer to the sum of the depths of all the layers. The resulting mass densities were as follows:

a) for the layer over a half space:

$$\rho_s = 0.178 \ (\text{Ton-sec}^2)/\text{m}^4 \qquad \ldots (8.4)$$

b) for the half space:

$$\rho_s = 0.163 \ (\text{Ton-sec}^2)/\text{m}^4 \qquad \ldots (8.5)$$

8.3.2 Soil shear modulus, G_s

The values of G_s for the layer over the half space and the half space were computed by using equation (3.6), i.e. it was assumed that $G = G_{max}$, taking into account that sand is the predominant material in the soil media under study. The void ratios, e , for each idealization were calculated by using weighted averages (as the ones used to compute ρ_s) of the voild ratios of the layers. The value of e for each layer was computed for the data on humidity content, W , reported in fig. 7 of [8.3] and the following expression [8.6] :

$$e = S_s \times W \qquad \ldots (8.6)$$

where an $S_s = 2.7$ was assumed as a typical value for sands. The following void ratios resulted frome these computations:

a) for the layer over the half space:

$$e = 1.280 \qquad \ldots (8.7)$$

b) for the half space:

$$e = 1.043 \qquad \ldots (8.8)$$

The mean effective stress, σ_m , appearing in equation (3.5) was calculated by using the following expression [8.6]:

$$\sigma_m = \frac{2}{3}\ \sigma_v \text{ (pounds/sq. inch)} \qquad \ldots (8.9)$$

where σ_v , the soil vertical stresses, can be computed as follows:

$$\sigma_v = \frac{3}{4}\ (2\ r_{0eq})\gamma' + 0.43\ \frac{W_{TOTAL}}{A_{eq}} \qquad \ldots (8.10)$$

where r_{0eq} is the equivalent radius of the foundation, γ' is the absolute density of the soil, W_{TOTAL} is the total weight applied to the foundation and A_{eq} is the equivalent area of the foundation (see Table 8.1). The following values of σ_m were obtained:

a) for the layer over a half space:

$$\sigma_m = 37.84 \text{ (Ton/m}^2\text{)} \qquad \ldots (8.11)$$

b) for the half space:

$$\sigma_m = 33.07 \ (\text{Ton/m}^2) \qquad \ldots (8.12)$$

Finally, by substituting the values of e and σ_m for each idealization, the following values of G are obtained:
a) for the layer over a half space:

$$G = 7{,}490 \ (\text{Ton/m}^2) \qquad \ldots (8.13)$$

b) for the half space:

$$G = 11{,}603 \ (\text{Ton/m}^2) \qquad \ldots (8.14)$$

The following values of G_s will be used in this work: 5,000 , 7,500 , 10,000 and 15,000 (Ton/m^2). These values were selected in order to include the ones associated to both soil media idealizations.

8.3.3 Shear wave velocity, V_s

The values of V_s for the soil idealization can be obtained by substituting the assumed values of ρ_s and G_s into equation (3.7). The results were:
a) For the layer over a half space:

$$V_s = 214 \ \text{m/sec}^2 \qquad \ldots (8.15)$$

b) for the half space:

$$V_s = 255 \ \text{m/sec}^2 \qquad \ldots (8.16)$$

8.3.4 Soil internal damping, ξ_s

A value of 0.05 for the hysteretical damping of both idealizations was assumed. This value was selected considering that the data given in [8.4] is restricted to this value. However, this value agrees reasonably well with reports of experimental data on this kind of soils onshore [8.7] .

8.3.5 Soil Poisson modulus, ν_s

The ν_s used in this work was 0.25 in order to allow the use of the results of [8.4].

8.3.6 Equivalent mass for the soil-foundation interaction model used

The contribution of the soil media to the inertial properties of the equivalent soil-foundation system, fig. 3.3 , can be computed by applying the following expressions reported in [8.8] (based on [8.9]):

$$m_0 = 0.095\ (M_{foundation})/Bx \qquad \ldots (8.17)$$

$$I_0 = 0.240\ (I_{foundation})/B\theta \qquad \ldots (8.18)$$

where m_0 and I_0 are the mass and mass moment of inertia of the virtual volume of soil and

$$Bx = \frac{2 - \nu_s}{8} \frac{M_{foundation}}{\rho (r_{0eq})^3} \qquad \ldots (8.19)$$

$$B_\theta = \frac{3(1 - \nu_s)}{8} \frac{I_{foundation}}{\rho (r_{0eq})^5} \qquad \ldots (8.20)$$

By substituting the values of parameters included in equations (8.19) and (8.20) the following m_0 and I_0 were obtained:
a) for the layer over the half space:

$$m_0 = 2{,}486\ (\text{Ton-sec}^2)/\text{m} \qquad \ldots (8.21)$$

$$I_0 = 4.937 \times 10^6\ (\text{Ton-sec}^2 - \text{m}) \qquad \ldots (8.22)$$

b) for the half space:

$$m_0 = 2{,}277\ (\text{Ton-sec}^2)/\text{m} \qquad \ldots (8.23)$$

$$I_0 = 4.523 \times 10^6\ (\text{Ton-sec}^2 - \text{m}) \qquad \ldots (8.24)$$

8.4 Seismic excitation at the platform site

The seismic excitation at the platform site represented by the p.s.d. function of ground acceleration, S_{aa} , was obtained by applying the seismic risk model discussed in 4.4 to the seismic information presented in 4.5 . Different S_{aa}'s and their associated pseudovelocity response spectra (Section 4.2.8-4.2.9) as well as their related ground spectra were computed for several

values of the return period.

8.4.1 Expected maximum ground acceleration, a_{max}, ground velocity, v_{max}, and ground displacement, d_{max}, at the platform site for different return periods

The value of the expected a_{max}, v_{max} and d_{max} for the platform site are presented in figs. 8.2, 8.3 and 8.4 respectively. From these figures, it can be seen that the expected values and the dispersion of those parameters increase as the value of T_0 is longer, the increase being more important for a_{max} and v_{max}. The values obtained are similar to the ones reported in [8.10] for other seismic risk studies in sites of the region.

8.4.2 Expected ground and pseudovelocity spectra, S_g, S_v, at the platform site for return periods of 50 and 500 years

The expected S_g and S_v at the platform site are shown in figs. 8.5 to 8.8. The spectra resulting for return periods of 50 and 500 years and a structural critical damping, ξ, equal to 0.05, are shown in figs. 8.5 and 8.6 respectively. The spectra for the same return periods but for a $\xi = 0.02$ are shown in figs. 8.7 and 8.8. The comments made in 8.4.1 about the expected values of a_{max}, v_{max} and d_{max} can also be applied here.

8.4.3 Expected power spectral density function of ground acceleration, S_{aa}, at the platform site for return periods of 50 and 500 years

From the S_v shown in figs. 8.5 to 8.8 and by applying to them equation(4.17), the p.s.d functions shown in figs. 8.9 to 8.12 were obtained. As it would be expected, both the mean value and the standard deviation of S_{aa} increase for a longer T_0. It can also be observed that the maximum value of S_{aa} occurs within a band of frequencies limited by 5 and 6 (rad/sec).

8.5 Wave excitation at the platform site

In order to introduce the uncertainties surrounding the wave excitation, the uncertainties about the value of the wind velocity at 19.5 m. above sea level, $W_{19.5}$, which is one of the parameters

of the power spectral density function of wave heights, $S_{\eta\eta}$, equation (5.44)), will be evaluated here. This can be done by evaluating the mean value, $\overline{W}_{19.5}$, and the standard deviation, $\sigma W_{19.5}$, for the platform site shown in fig. 4.5 .

8.5.1 Expected maximum velocity, $W_{19.5}$, at the platform site for a return period of 50 years

In [8.11], it has been suggested that as for the peak gust velocities, their associated mean velocities appear to follow the extreme value distribution, i.e.:

$$P_W[w] = \exp\{-\exp[-\alpha(w - z)]\} \quad \ldots (8.25)$$

where w is a particular value of W and α and z are the parameters of the distribution; α provides a measure of its dispersion and z is the mode (most probable value) of the distribution. The mean and the standard deviation of the distribution are given by:

$$\overline{w} = z + 0.5777/\alpha \quad \ldots (8.26)$$

$$\sigma w = 1.282/\alpha \quad \ldots (8.27)$$

In [8.12] the most probable values of the height of the highest wave, H_{max}, and its zero upcrossing period, T_z, occurring on British waters during a 12-hour storm were presented. These values correspond to a 50 year return period. The values of H_{max} and $T_{z_{max}}$ for the considered site can be drawn from figs. 1 and 2 of [8.12] respectively. Those values are $H_{max} \doteq 26$ m. and $T_{z_{max}} \doteq 13.4$ sec.. A possible way of computing the most probable value of $W_{19.5}$ associated to H_{max} and to $T_{z_{max}}$ is by using Table 3-VII of [8.13] . In this table, the values of several of the parameters characterizing the waves for a fully developed sea are presented. Among others, H_{max}, $T_{z_{max}}$ and $W_{19.5}$ are included. For example, from the mentioned table, to the H_{max} and $T_{z_{max}}$ quoted above correspond a $(W_{19.5max}) \doteq 25.7$ m./sec. and a $(W_{19.5max}) = 20.6$ m./sec. respectively. Those values of $W_{19.5max}$ can be considered as the parameter z in equation (8.26).

As for the quotient $1/\alpha$ in the same equations, from studies reported in [8.11] for the extreme mean/hourly wind speed over the British Isles, it can be assumed to be equal to ten per cent of the parameter z mentioned above.

From the above considerations and by using equations (8.26) and (8.27), the mean value and the standard deviation of $W_{19.5max}$ can be evaluated. The results of this computation are shown in Table 8.2.

8.5.2 Expected power spectral density functions of wave heights, $S_{\eta\eta}$, at the platform site for a return period of 50 years

By following 7.5 the computation of the expected $S_{\eta\eta}$ and $\overline{S}_{\eta\eta} \pm \sigma S_{\eta\eta}$ at the platform site for a return period of 50 years was performed by substituting the corresponding values of the highest $W_{19.5}$ (Table 8.2) in equations (5.47) and (5.49). These equations represent the P-M and Jonswap p.s.d.f. of wave heights for a fully developed sea respectively. The resulting $S_{\eta\eta}$'s p.s.d. functions are shown in fig. 8.13. From this figure it can be observed that the maximum value of $S_{\eta\eta}$ occurs within a band of frequencies limited by 0.25 and 0.375 (rad/sec). It can also be observed that the dispersion is large as in the case of seismic excitation.

8.6 Influence of the uncertainties about E_c, ξ_c, as well as the soil idealization on the free vibration characteristics of the concrete gravity platform

The influence of E_c and ξ_c as well as the soil idealization on the free vibration characteristics of the c.g.p. were studied by solving equation (6.31). The mean values and the mean values plus and less a standard deviation of E_c and ξ_c were used by following 7.5 . The effect of the soil idealization was introduced by considering the two soil idealizations mentioned in 8.3 i.e. a half space and a layer over a half space. The effect of G_s was introduced by varying its value accordingly to the values selected in 8.3.2.

8.6.1 Expected fundamental frequency, ω_1^0

The expected fundamental frequency as a function of soil shear modulus is shown in fig. 8.14 . From this figure, it can be

observed that the influence of the uncertainties about E_c on ω_1^0, as measured by $\sigma\omega_1^0$, is more important for increasing values of G_s. This result reveals that the structural stiffness coefficients dominate the solution of equation (6.31) as the soil stiffness increases. As far as the soil idealization influence on the value of ω_1^0, it can be asserted that the frequencies obtained with the layer are higher for about five percent than the ones calculated with the half space idealization, except for a $G_s = 10{,}000$ (Ton/m^2). For this particular value of G_s the soil stiffness on both idealizations are practically the same.

8.6.2 Expected critical damping, ξ_1^0, associated to the fundamental mode

The resulting expected ξ_1^0 is presented in fig. 8.15 as a function of soil shear modulus. There, it is observed that as in the case of the uncertainties about E_c, the influence of the uncertainties about ξ_c is more important as the soil becomes more rigid. This is shown by the coefficient of variation of ξ_1^0, which increases from 1.37 for a $G_s = 5{,}000$ (Ton/m^2) to 1.83 for $G_s = 15{,}000$.

The uncertainties about E_c do not contribute in any appreciable degree to the computed expected value of ξ_1^0 for the values of G_s considered in this work.

The influence of the soil idealization on the value of ξ_1^0 is shown by the larger value of this parameter obtained for the layer idealization. This is so because a larger amount of energy is dissipated by the layer than by the half space. This effect is more important for low values of G_s. As it would be expected, the value of ξ_1^0 tends to ξ_c for increasing values of G_s.

8.6.3 Expected complex frequency response, $H_1(\omega)$, associated to the fundamental mode

In order to illustrate the influence of the uncertainties about E_c, ξ_c and the soil idealization on the expected $H_1(\omega)$, the variation of $|H_1(\omega)|$ with frequency is presented in figs. 8.16 and 8.17. From these two figures, it can be observed that the expected maximum value of $|H_1(\omega)|$ decreases as the soil becomes more rigid. In addition, this reduction in $|H_1(\omega)|$ corresponds to a higher natural frequency, as it would be expected.

8.7 Influence of the uncertainties about E_c and ξ_c as well as soil idealization on the maximum responses of the concrete gravity platform when it is subjected to seismic and wave loads acting separately or simultaneously

In order to study the influence of the uncertainties about E_c, ξ_c and the soil idealization on the maximum responses of the c.g.p. when it is under seismic and wave loading, the mean values and the mean values plus and less a standard deviation of the structural parameters as well as the excitation were used accordingly to 7.5 and Chapter 6. Equation (7.20) was only used to compute the autocovariance of u The results of the expected deck displacement, u, base shear force, V, and overturning moment, M, are shown in figs. 8.18 to 8.61.

From the analysis of the figures mentioned above, it can be asserted that the first mode of vibration (rocking) was predominant for the three responses; therefore, it was only necessary to superpose the responses associated to the first three modes of vibration of the system. Due to this, the study mainly dealt with the results associated to the first mode i.e. first generalized load, first generalized coordinate, etc. .

The pattern followed for the study can be synthesized as follows:

a) analysis of the responses in the frequency domain,

b) analysis of the responses as a function of G_s,

c) analysis of the C.V. associated to each of the parameters considered.

With the results obtained in a) , the influence of the soil idealization and the type of excitation on the p.s.d. functions of the responses can be studied. From the results of b) , the influence of the soil idealization, parameter G_s , and the type of excitation on the expected values (and the dispersions) of the responses can be analyzed. The short and long term responses (for a return period of 50 years) can also be compared by using this type of results. Finally, with the results obtained in c) , the relative influence of the different parameters on the C.V.'s of the responses can be analyzed. Here only the study on u is presented.

The Jonswap p.s.d.f. (fig. 8.13) of wave heights was used to compute the responses associated to the wave excitation. The P-M

spectra (fig. 8.13) was utilized in some cases in order to be compared with the Jonswap results. As mentioned in 8.5.1, it was assumed that these spectra correspond to a twelve hour storm (a fully developed sea) and a return period of 50 years; the mean rate of occurrence of the storm, ν_p (Section 7.3.1) is assumed to be equal to 2/year.

The p.s.d.f. of ground acceleration, S_{aa}, shown in figs. 8.9 and 8.10 were used in the study for the seismic excitation. A return period of 50 years and a mean rate of occurrence, ν_p, (Section 7.3.1) of 0.163/year (Table 4.4) was utilized for this study.

8.7.1 Expected deck displacement, u

The results of this study concerning deck displacement, u, are shown in figs. 8.18 to 8.39. In figs. 8.18 to 8.30, the results associated to wave excitation are introduced; the ones related to seismic excitation are shown in figs. 8.31 to 8.38. Finally, in fig. 8.39, the expected deck displacement is shown as a function of G_s when both types of excitations are acting simultaneously on the platform.

a) Analysis of the expected u for wave excitation in the frequency domain

In figs. 8.18 to 8.20, the p.s.d.f. of the first generalized load for wave excitation, $S_{p,W}$, as a function of frequency is presented. By comparing both fig. 8.18 and fig. 8.19, it can be observed that for the same type of soil and the same values of G_s, the peaks of S_{p,W_-} for $W^+_{19.5}$ is about 75 % higher than the peak obtained for $W_{19.5}$.

It can also be observed that both peaks occur at the frequency of their associated $S_{\eta\eta}$'s (fig. 8.13). From figs. 8.18 and 8.20, it can be asserted that for the same values of G_s and $W_{19.5}$ but with a different soil idealization, the maximum value of $S_{p,W}$ is about 5 % higher for the half space soil representation than for the layer one.

In figs. 8.21 to 8.23, the p.s.d.f. of the first generalized coordinate for wave excitation, $S_{y,W}$, as a function of frequency is shown. From these figures, it can be asserted that, in general, the behaviour of $S_{y,W}$ is as the one described above for $S_{p,W}$

i.e. the comments about figs. 8.18 - 8.19 can be applied to figs. 8.21-8.22 . However, the peak value of $S_{y,W}$ for the half space idealization is about 30 % higher than the value obtained from the layer idealization, figs. 8.21-8.23. The latter result is due to the smaller damping of the system associated to the half space idealization (fig. 8.15).

In figs. 8.24-8.28, the p.s.d.f. of deck displacement for wave excitation, $S_{u,W}$, as a function of frequency, are presented. From figs. 8.24, 8.26, and 8.27, it can be observed that for the same soil idealization and the same value of G_s , the peak value of $S_{u,W}$ for $\overline{W}_{19.5}$ is about 50 % smaller and higher than the values of the $S_{u,W}$ peaks associated to $W^{+}_{19.5}$ and $W^{-}_{19.5}$ respectively. (About the same ratio between the peak values of the corresponding $S_{\eta\eta}$ is observed in fig. 8.13.) It can also be noticed from these figures, that the peaks occurred at the same frequencies as for the respective $S_{\eta\eta}$ spectra. From figs. 8.24-8.25, it can be concluded that for the same value of all the parameters and soil idealization but for different values of G_s , a reduction in the value of the maxima of $S_{u,W}$ occurs as the soil becomes more rigid. This is a result of a reduction in the value of $|H_1(\omega)|^2$ as well as an increase in the value of ω_1^0 for G_s = 15,000 (Ton/m^2), when compared with the values of the same parameter for G_s = 5,000 (see figs. 8.16-8.17).

In figs. 8.24-8.28, it can be observed that for the same values of all the parameters but for a different soil idealization, the $S_{u,W}$ are practically independent from the soil idealization. This is so in spite of the higher value of the first generalized coordinate for the half space representation, (figs. 8.21-8.23). Nevertheless, the amplitudes of the modal shapes associated to the half space idealization are smaller than the ones associated to the layer idealization.

b) Analysis of the expected u for wave excitation as a function of G_S

In fig. 8.29, the expected deck displacement, u_W , as a function of soil shear modulus, G_s , for both soil idealizations is presented. From this figure, it can be asserted that the mean values of u_W are particularly the same ones for the layer and the half space soil idealizations. The C.V. is about 2 for all the values of G_s . It can also be observed that the mean value of u_W is smaller for an

increasing value of G_s . For the same fig. 8.29, the value of u_W for G_s = 5,000 (Ton/m) obtained by using the P-M p.s.d.f. (fig. 8.13) was identified with a mark: X . This value is about 20% smaller than the one obtained for the Jonswap spectra.

In fig. 8.30, the expected short and long term displacements, u_W , for wave excitation are shown. This figure corresponds to a layer soil idealization. The short term displacement is associated to a 12 hour storm and the long term displacement to the same storm and to a return period of 50 years. From this figure, it can be observed that the expected value for the long term u_W is about 35 % higher than the short term u_W for all the values of the G_s considered in this study. It can also be observed that the C.V. for both short and long term u_W's is about 2. Finally, for both cases there is a reduction in the value of u_W for an increasing value of G_s .

a) Analysis of the expected u for seismic excitation in the frequency domain

In figs. 8.31-8.33, the p.s.d.f.'s of the first generalized coordinate for seismic excitation, $S_{y,Q}$, as a function of frequency are shown. All these curves correspond to $G_s = 5{,}000(\text{Ton/m}^2)$. Similar curves for $S_{y,Q}$ were obtained when considering higher values of G_s .

By comparing figs. 8.31-8.32, it can be observed that the peak value of $S_{y,Q}$ for S^{+}_{aa} is about three times higher than the value obtained for S^{-}_{aa} . Both peaks occur at the fundamental frequency of the system, $\omega_1^0 = 1.83$(rad./sec).

From figs. 8.32-8.33, it can be asserted that for the same value of all the parameters but with a different soil idealization, the peak value of $S_{y,Q}$ is about three times higher for the half space soil idealization than for the layer one. It can also be observed that the peak of $S_{y,Q}$ in the half space soil idealization occurs at $\omega_1^0 = 1.73$ (rad./sec.).

This high value of $S_{y,Q}$ is due to the combination of lower values of ω_1^0 and ξ_1^0 compared to the ones obtained for the layer idealization.

The p.s.d.f.'s of deck displacement for seismic excitation, $S_{u,Q}$, as a function of frequency, ω, are shown in figs. 8.34-8.36.

From figs. 8.34-8.35, it can be observed that for this response, two peaks are present: one at $\omega_1^0 = 1.832$ (rad./sec.) and the second at $\omega_2^0 = 3.36$ (rad./sec.). The peak occurring at ω_2^0 is higher than the other one. This is due to the higher damping associated to the rocking mode of vibration, $\xi_1^0 = 0.076$, compared to the damping associated to the second mode, $\xi_2^0 = 0.0426$. The values of the peaks of $S_{u,Q}$ for S_{aa}^+ (fig. 8.35) are about three times higher than the peaks of $S_{u,Q}$ obtained for $\bar{S}_{aa}$ (fig. 8.34). This is due to the fact that the values of S_{aa}^+ are about three times higher than the ones associated to $\bar{S}_{aa}$ (see fig. 8.9).

From fig. 8.35 compared to fig. 8.36, it can be seen that by keeping the values of all the parameters constant and varying the soil idealization, the first peak of $S_{u,Q}$ occurs at $\omega_1^0 = 1.73$ (rad./sec.) for the half space idealization. It can also be seen that the value of the second peak of $S_{u,Q}$ is about the same for both soil idealizations, but the value of the first peak obtained for the half space idealization is about twice the corresponding one to the layer soil representation. This is due to the smaller damping associated to the first mode (rocking) for the half space idealization, $\xi_1^0 = 0.0466$.

b) Analysis of the expected u for seismic excitation as a function of G_s

In fig. 8.37, the expected deck displacement for seismic excitation, u_Q, as a function of G_s for both soil idealizations is shown. From the figure, it can be observed that the values of u_Q are about 5 % higher for the half space idealization than for the layer one. It can also be seen that the value of u_Q increases for an increasing G_s. In addition, the C.V. is about 3 for all the values of G_s considered.

In fig. 8.38, the expected short and long term deck displacements for seismic excitation, u_Q, are shown. The short term response is associated to an earthquake of 15 secs of duration and the long term to the same earthquake but for a return period of 50 years and a mean reccurrence rate of 0.163/year. From fig. 8.38, it can be seen that the values for the long term deck displacements are about 30 % higher than the ones associated to the short

term ones. For both cases, the value of u_Q increases for a higher value of G_s. Finally, it can be observed that the C.V. for both u_Q's is about 3.

In fig. 8.38, the expected deck displacement for seismic and wave excitation acting simultaneously, $u_{Q,W}$, is displayed as a function of G_s. By comparing this figure with fig. 8.29, it can be seen that $u_{Q,W}$ behaves basically as u_W, except that the values of the former are higher (3 %) than the ones associated to the latter. The comments expressed about u_W also apply to $u_{Q,W}$ and they will not be reported here.

8.7.2 Expected base shear force, V

The results of the study on V are shown in figs. 8.40 8.50. The results about V for wave excitation are presented in figs. 8.41-8.45; the corresponding results for seismic excitation can be seen in figs. 8.46-8.49.

The expected value of V when both types of excitation are acting simultaneously on the platform is shown in fig. 8.50. The p.s.d.f. of V was computed accordingly with equation (7.22) where the coefficient b_j was calculated as follows:

$$b_j = (\omega_j^0)^2 \sum_{i=1}^{n} m_{ii} (r_s^s)_{ij} \qquad \ldots (8.28)$$

$j = 1,2, \ldots, p$ (p = last mode of vibration considered)

$i = 1,3,\ldots, N$ (i.e. the i's associated to the translational degrees of freedom)

where $(r_s^s)_{ij}$ is the amplitude of the jth modal shape associated to the ith nodal point; the other parameters were already defined in Chapter 6. Equation (7.22) is only valid for a structure resting on a rigid soil. For the case under consideration, the p.s.d.f. of the base shear force associated to the soil equivalent spring displacement has to be considered. It can be shown that the general expression of the term associated to the latter p.s.d.f. is given by:

$$\int_{-\infty}^{\infty} \{ \sum_{j=1}^{N} \sum_{k=1}^{N} (r_s^f)_{xj} (r_s^f)_{xk} H_j^*(i\omega) H_k(i\omega) S_{p_j^* p_k^*}(\omega) k_{xs}^2 \} d\omega \qquad \ldots (8.29)$$

where $(r_s^f)_{xi}$ (i = j,k) is the amplitude of the i modal shape associated to the equivalent mass translational displacement, and k_{xs} can be computed with equation (3.13). The rest of the terms were already defined in relation with equation (7.22).

a) Analysis of the expected V for wave excitation in the frequency domain

In figs. 8.40-8.44, the p.s.d.f. of base shear force for wave excitation $S_{V,W}$ as a function of frequency is presented. From figs. 8.40, 8.42 and 8.43, it can be observed that, as for $S_{u,W}$, for the same soil idealization and the same value of G_s, the peak value of $S_{V,W}$ for $\bar{W}_{19.5}$ is about 50 % smaller and higher than the values of the $S_{V,W}$ peaks corresponding to $W^+_{19.5}$ and $W^-_{19.5}$ respectively.

The same ratios result from considering the values of the respective $S_{\eta\eta}$ spectra. From figs. 8.40 and 8.41, it can be seen that when the soil becomes more rigid and the values of the rest of the parameters are kept constant, the values of $S_{V,W}$ are smaller. This is due to the smaller $|H_1(\omega)|^2$ associated to G_s =15,000 (Ton/m^2) compared to the one related to G_s = 5,000 (Ton/m^2) (figs. 8.16-8.17).

From figs. 8.40 and 8.44, it can be observed that for all the parameters kept at the same value and only varying the soil idealization, the resulting $S_{V,W}$'s are practically the same for both the half space and the layer soil idealizations. The reason behind this was expressed above in 8.7.1.

b) Analysis of the expected V for wave excitation as a function of G_s

The expected V for wave excitation as a function of G_s for both soil representation is shown in fig. 8.45. From this figure, it can be concluded that the mean values of V_W for the half space idealization are higher for about 5 % than the ones obtained for the layer idealization, except for G_s = 10,000 (Ton/m^2) where the mean values coincide. This comes from the fact that the equivalent soil stiffness for both idealizations coincide for this value of G_s. The C.V. is about 0.9 for both soil idealization.

It can also be observed in fig. 8.45 that for a P-M p.s.d.f.

of wave heights, the resulting mean value of V_W is about 25 % smaller than the one calculated with the Jonswap one and the layer idealization. The V_W associated to P-M has been marked with an X in fig. 8.45.

Finally, from this figure, it can be observed that the value of V decreases for an icreasing value of G_s. This is so because the caisson displacements are smaller for a higher value of G_s.

a) Analysis of the expected V for seismic excitation in the frequency domain

In figs. 8.46-8.48, the p.s.d.f. of base shear force for seismic excitation, $S_{V,Q}$, is presented as a function of frequency. By comparing figs. 8.46 and 8.47, it can be seen that for all the parameters being the same except the intensity of the seismic excitation, the peak value of $S_{V,Q}$ for S^+_{aa} is about 4 times the one obtained for $\bar{S}_{aa}$. This result is so because the ratio between S^+_{aa} and $\bar{S}_{aa}$ for $\omega = \omega_1^0$ is as well about 4.

From figs. 8.47-8.48, it can be asserted that if all the parameters are kept constant but the soil idealization is different, the peak of $S_{V,Q}$ is about 2.5 times higher for the half space soil idealization. This is due to the smaller system damping and soil stiffness associated to this soil idealization than the ones related to the layer soil idealization.

b) Analysis of the expected V for seismic excitation as a function of G_S

In fig. 8.49, the expected V for seismic excitation, V_Q, as a function of G_s for both idealizations is presented. According to this figure, it can be observed that the mean values of V_Q for the half space soil idealization are about 15 % higher than the ones obtained for the layer soil idealization. It can also be seen from fig. 8.49 that the values of V_Q increase for growing values of G_s. This is a result of several combined effects i.e. for a higher value of G_s, the values of ω_1^0 are also higher (fig. 8.14); the value of the associated ξ_1^0 diminishes (see fig. 8.15) and the value of S_{aa} corresponding to the mentioned $\omega = \omega_1^0$ is higher than ω_1^0 values associated to a growing G_s within the range of studied here (see fig. 8.9).

It can also be observed from fig. 8.49 that the dispersion in the values of V increases for an increasing G_s, in this case the C.V. being of about 2.3.

The expected base shear force for seismic and wave excitation acting simultaneously $V_{Q,W}$ is shown in fig. 8.50. By comparing fig. 8.45 to 8.50 it can be concluded that the influence of the wave excitation dominates the behaviour of the expected $V_{Q,W}$. However, the mean values of $V_{Q,W}$ are about a 5 % higher than the ones of V_W showing the contribution of the seismic excitation. In general, the comments expressed about V_W also apply to $V_{Q,W}$.

8.7.3 Expected overturning moment, M

The results of the study on M are shown in figs. 8.51-8.61. The results concerning M for wave excitation are introduced in figs. 8.51-8.56; the corresponding ones to seismic excitation are presented in figs. 8.57-8.60. Finally, the results obtained when both excitations are acting simultaneously are shown in fig. 8.61.

The p.s.d.f. of M was computed by using equation (7.22), with a coefficient b_j equal to:

$$b_j = (\omega_j^0)^2 \sum_{i=1}^{N} m_{ii} \, (r_s^s)_{ij} \, h_i \qquad \ldots (8.30)$$

$j = 1,2,\ldots,p$ (p = last mode of vibration considered)

$i = 1,3,\ldots,N$ (i associated to the translational degrees of freedom only)

where all the parameters have been defined in relation to equation (8.30), except h_i which is the height of the nodal point i with respect to the center of gravity of the foundation.

As in the case of V, there is an extra term associated to the soil rocking stiffness which has to be added to the right hand side of equation (7.22) i.e.

$$\int_{-\infty}^{\infty} \{ \sum_{j=1}^{N} \sum_{k=1}^{N} (r_s^f)_{\theta j} \, (r_s^f)_{\theta k} \, H_j^*(i\omega) \, H_k(i\omega) \, S_{p_j^* p_k^*}(\omega) \, k_{\theta s}^2 \} d\omega \qquad \ldots (8.31)$$

in this expression $(r_s^f)_{\theta i}$ $(i = j,k)$ is the amplitude of the ith modal shape associated to the equivalent mass displacement; $k_{\theta s}$ can be computed with equation (3.13).

a) Analysis of the expected M for wave excitation in the frequency domain

In figs. 8.51-8.55, the p.s.d.f. of overturning moment for wave excitation $S_{M,W}$ is shown as a function of frequency. Accordingly to figs. 8.51, 8.53 and 8.54, it can be seen that for the same soil idealization and the same value of G_s, the peak value of $S_{M,W}$ for $\bar{W}_{19.5}$ is about 50 % smaller and higher than the values of the $S_{M,W}$ associated to $W^{+}_{19.5}$ and $W^{-}_{19.5}$ respectively. This is because the ratios of the associated $S_{\eta\eta}$ are the same as the mentioned ones.

By comparing figs. 8.51-8.52, it can be concluded that (as for $S_{u,W}$ and $S_{V,W}$) the values of $S_{M,W}$ are smaller for a higher value of G_s. This is so because they are related to a $|H_1(\omega)|^2$ smaller than the associated to a softer soil. From figs. 8.51-8.55, it can be observed that for a different soil idealization but the rest of the parameters having the same values, the resulting $S_{M,W}$'s are very similar for both soil idealizations.

b) Analysis of the expected M for wave excitation as a function of G_s

The expected M for wave excitation as a function of G_s for both soil representations is shown in fig. 8.56. From this figure, it can be asserted that the values of M_W for both soil idealizations are practically the same for all the range of G_s values studied here. The reason behind this result is that in spite of having smaller $k_{\theta s}$ and ξ_1^0 for the half space idealization than for the layer, the amplitudesof their associated modal shapes are also smaller. The C.V. is about 1.06 with a slight reduction of its value for increasing calue of G_s.

The mean value of M_W obtained for a layer idealization of the soil and a P-M p.s.d.f. of wave heights is also shown in fig. 8.56. This result has been marked with an * X in fig. 8.56. The mean value M_W for the P-M spectra is about 25 % smaller than the one obtained with the Jonswap spectra. Finally, from fig. 8.56, it can be asserted that there is a reduction of M_W for increasing values of G_s. This is so because the amplitude of the foundation rotation for a harder soil is smaller than for a softer soil.

a) Analysis of the expected M for seismic excitation in the frequency domain

In figs. 8.57-8.59, the p.s.d.f. of overturning moment for seismic excitation, $S_{M,Q}$, is presented as a function of frequency. From figs. 8.57 and 8.58, it can be seen that (as for $S_{V,Q}$) for different intensities of seismic excitation and keeping the other parameters constant, the peak value of $S_{u,Q}$ for S^{+}_{aa} is about 4 times the one obtained for $\overline{S}_{aa}$. The reason for this result was given above, related to $S_{V,Q}$.

When figs. 8.50 and 8.59 are compared, the comments made about figs. 8.47-8.48 can be applied to the former two, but now, in relation to M.

b) Analysis of the expected M for seismic excitation as a function of G_s

In fig. 8.60, the expected M for seismic excitation, M_Q, for both idealizations is presented as a function of G_s. From this figure, it can be seen that the mean values of M_Q for the half space soil idealization are about 20 % higher than the ones obtained for the layer soil idealization. It can also be seen that as for V_Q, the values of M_Q increase for increasing values of G_s. The reason for this was commented upon with relation to V_Q. From the same fig. 8.60, it can be observed that the dispersion of M_Q increases for a larger value of G_s; the C.V. is about 2.3 as in the case of V_Q.

The expected overturning moment for seismic and wave excitations acting simultaneously, $M_{Q,W}$, is shown in fig. 8.61. The comments expressed about $V_{Q,W}$ also apply to $M_{Q,W}$; therefore, they will not be repeated here.

c) Analysis of the C.V. associated to each of the parameters considered

The analysis of the C.V.'s associated to each of the parameters considered will be discussed here. Those C.V.'s were computed by applying equation (7.54). The C.V.'a for responses u_W and u_Q were calculated with equation (7.51). The results reported here correspond to the layer soil idealization. For the half space soil idealization, similar results were obtained. The values of G_s utilized are the ones already mentioned in analyses type a) and b) above.

The results of the study can be seen in Table 8.3. The results concerning u_W are discussed first followed by the ones associated to u_Q .

Influence of the uncertainties about E_c , ξ_c and about the wave excitation, W , on u_W

From Table 8.3, it can be observed that the influence of the uncertainties about W largely dominate, followed by the ones about E_c , the uncertainty corresponding to ξ_c is negligible.

The influence of E_c on u_W decreases as the value of G_s increases; this is a consequence of the higher values of ω_1^0 obtained for a harder soil, which yield smaller values of u_W.

The influence of ξ_c on u_W is nil for the whole range of G_s. This can be explained by the fact that the contribution of ξ_c to the critical damping first mode , ξ_1^0 , is negligible when compared to the contribution of the soil damping (see equation (6.35)).

As expected, the influence of W on u_W remains at the same level for all the G_s's considered here, because $S_{\eta\eta}$ is independent of G_s . The influence of E_c , ξ_c and W on u_W diminishes with an increasing G_s , showing the influence of E_c on the final response under consideration.

Influence of the uncertainties about E_c , ξ_c and the seismic excitation, Q , on u_Q

From Table 8.3, it can be concluded that the uncertainties on the seismic excitation largely dominate, followed by the ones related to ξ_c , the last influence being the uncertainties associated to E_c.

The influence of E_c on u_Q does not show a definite trend; however, it reaches a maximum for $G_s = 10{,}000$ (Ton/m^2)

The influence of ξ_c on u_Q decreases for an increasing G_s . This behaviour can be explained as follows. While the mean value of $u_Q(\xi_c)$ increases with an increasing G_s , the value of the differences between $[u_Q(\bar{\xi}_c + \sigma\xi_c) - u_Q(\bar{\xi}_c - \sigma\xi_c)]$ remains almost the same for the range of G_s's considered here; therefore, when equation (7.59) is applied, the ratios indicated in that equation diminish for an increasing G_s .

The influence of the uncertainties about Q on u_Q remain at about the same level for all the values of G_s considered here.

Finally, the influence of E_c , ξ_c and Q on u_Q diminishes for an increasing value of G_s . This is so because that is the trend of ξ_c (discussed above) whose contribution is important in the final value of the C.V. of u_Q.

8.8 Influence of caisson storage mass on the free and forced vibration responses of the concrete gravity platform

A study of the influence of the caisson storage mass, m_{cs}, on the free and forced vibration responses of the selected c.g.p. was carried out. This analysis is limited to the expected long term responses, and was performed by using the mean values of E_c, ξ_c, S_{aa} and $S_{\eta\eta}$ (see figs. 8.2, 8.4 and 8.5). The soil was idealized as a layer over a half space and G_s was varied in the same range as in the previous studies. The study consists in varying both the caisson storage mass and G_s while keeping the values of the other parameters constant.

The experiment aimed at simulating a real situation in which by a planned or unforeseen action, the caisson storage mass takes a value within the proposed range, i.e. $0.25\ m \leqslant m_{cs} \leqslant m$, where m is the mass of a full caisson. The results of the study are presented in figs. 8.62-8.72.

8.8.1 Expected fundamental frequency ω_1^0

In fig. 8.62, the variation of the expected fundamental frequency ω_1^0 with m_{cs} as a function of G_s is presented. From this figure, it can be observed that ω_1^0 for $m_{cs} = 0.25$ is higher (about 2.5 %) than the ω_1^0 obtained for the full caisson. This pattern is kept through all the G_s's considered in this study. As it would be expected, the lower value of ω_1^0 corresponds to an $m_{cs} = m$. The results which have been described reveal that the variation of m_{cs} has an almost negligible influence on the value of the mass moment of inertia of equivalent foundation, and therefore, on the fundamental frequency of the system which is associated to rocking mode.

8.8.2 Expected critical damping, ξ_1^0, associated to the fundamental mode

In fig. 8.62, the variation of the expected ξ_1^0 with m_{cs} as a function of G_s is presented. From this figure, it can be concluded that the variation of m_{cs} does not affect the value of the expected ξ_1^0. However, it can be observed from this figure that the higher damping is associated to the larger m_{cs}. The reason for this is that for a smaller m_{cs} the ω_1^0 increases and the ratios in equations (6.36) and (6.37), where ω_1^0 is involved, are smaller than for $m_{cs} = m$.

8.8.3 Expected deck displacements, u

The results obtained from the study are presented in figs. 8.64, 8.65 and 8.66. In these figures, the values of the expected u_W, u_Q and $u_{Q,W}$ as a function of G_s are shown respectively.

From fig. 8.64, it can be seen that for the softer soil, the u_W for $m_{cs} = m$ is about 5 % larger than the one for $m_{cs} = 0.25$ m, and that this difference almost vanishes for the harder soil. The reason for this behaviour of u_W is that the amplitude of the rocking displacement of the foundation is larger for the maximum value of m_{cs} which implies a lower ω_1^0 and therefore a larger wave loading intensity (see fig. 8.13). However, this effect vanishes as the soil becomes stiffer i.e. for a soil with a larger equivalent rocking spring.

In fig. 8.65, the variation of u_Q with m_{cs} can be seen. Here, as in the case of u_W, the larger values of u_Q for the whole range of G_s are associated to $m_{cs} = m$; however, the minimum values of u_Q for all the m_{cs}'s occur for the softer soil This is explained by the fact that the lower ω_1^0's (see fig. 8.62) are associated to this soil, and therefore the lower values of $\overline{S}_{aa}$ (see fig. 8.9) are associated as well. The opposite occurs for the harder soil as shown in the same figure. The relative differences between the highest value of u_Q ($m_{cs} = m$) and the minimum one ($m_{cs} = 0.25$ m) at $G_s = 15{,}000$ (Ton/m) is about 2.5 %.

In fig. 8.66, the variation of deck displacement for seismic and wave excitation, $u_{Q,W}$, is presented as a function of m_{cs}. Comparing this figure with fig. 8.64, it can be concluded that the behaviour of $u_{Q,W}$ is very similar to the one observed for u_W, except that the values of the former are about 3 % higher than the values associated to the latter, due to the contribution of the displacements associated to the seismic excitation. The comments made about u_W also apply to $u_{Q,W}$, therefore, they will not be repeated here.

8.8.4 Expected base shear force, V

The results concerning the variation of V with m_{cs} can be seen in figs. 8.67, 8.68, and 8.69, which correspond to V_W,

V_Q and $V_{Q,W}$ respectively. By comparing fig. 8.66 with fig. 8.64, it can be observed that the trend in the behaviour of V_W is similar to the one presented for u_W. However, for the former, the differences between the higher and the smaller values of V_W are of about 8 % and remain of the same value for the whole range of G_s's. The reason for this behaviour of V_W is that its value is largely dominated by the contribution of the shear force associated to the foundation displacement. The values of the soil equivalent stiffness (K_{xs} and $k_{\theta s}$) are the same for different values of m_{cs} and a given G_s; in addition, the ratios between the equivalent foundation displacements for different m_{cs}'s are the same as for their associated shear forces. Therefore, as the ratios between foundation displacements remain the same for the range of G_s considered here, the ratios of the associated shear forces do so as well. Larger shear forces are associated to larger m_{cs}'s because their corresponding ω_1^0's are smaller, i.e. closer to the peak value of $S_{\eta\eta}$ (see fig. 8.13).

The results of the analysis for V_Q are presented in fig. 8.68. From figs. 8.65 and 8.68, it can be concluded that the behaviour of V_Q is similar to the one observed for u_Q due to the reasons given for the behaviour of the latter. As in the case of V_W, the resulting V_Q is closely related to the behaviour of the equivalent foundation displacements. However, the highest values of V_Q are associated to harder soils, for which the ω_1^0's are higher, i.e. closer to maximum values of S_{aa} (see fig. 8.9). It can also be observed from fig. 8.68 that the differences between V_Q for $m_{cs} = m$ and the one associated to $m_{cs} = 0.25\ m$ and about 16 % for the whole range of G_s considered here.

The results of the study on $V_{Q,W}$ are shown in fig. 8.69. By comparing figs. 8.67 and 8.69, it can be observed that $V_{Q,W}$ behaves basically as V_W, except that the values of the former are about 3 % higher than those the latter. This increase is due to the contribution of the V_Q's to the final values of $V_{Q,W}$. The comments made about V_W also apply to $V_{Q,W}$, therefore they will not be repeated here.

8.8.5 Expected overturning moment, M

The results of the study on the expected overturning moment, M, are introduced in figs. 8.70-8.72. The values of the overturning moment due to wave excitation, M_W, are presented in fig. 8.70; the moments related to the seismic excitation, M_Q, are shown in fig. 8.71; finally, the moments resulting from both types of excitation acting simultaneously are shown in fig. 8.72.

By comparing figs. 8.70-8.72 with 8.67-8.68, it can be concluded that the behaviour of M is very close to the one observed for V. As the comments made about V_Q, V_W and $V_{Q,W}$ can also be applied to M_W, M_Q and $M_{Q,W}$ respectively, they will not be repeated here and only a few observations concerning M will be made here.

For example, as far as M_W is concerned, it can be seen from fig. 8.70 that the difference of the values of M_W for an m_{cs}=m and the M_W's associated to a m_{cs} = 0.25 m is of about 2 % for the whole range of G_S considered here. This is due to the ratio obtained for the rotational displacements of the equivalent foundation.

From fig. 8.71, it can be seen that the ratio of M_Q for m_{cs} = m and for m_{cs} = 0.25 m is about 5 % for the softer soil, and that for the harder soil it is about 7 %. Finally, in fig. 8.72, it can be observed that the ratio of the mentioned differences are of about 2 % and 3 % respectively. Again, the influence of the seismic excitation is reflected by the higher ordenates of fig. 8.72 when compared to the ones of fig. 8.70.

9. CONCLUSIONS

In this chapter, the main conclusions which can be drawn from the study as well as the future work on the subject will be commented upon.

One conclusion is that with the methodology proposed in this work the computation of a c.g.p. dynamic responses when it is subjected to wave and earthquake loading can be performed in a straightforward manner. The methodology allows the inclusion of the main parameters which contribute to the dynamic behaviour of the platform. Furthermore, the uncertainties surrounding the values of those parameters can be taken into account in a rational manner with relative ease. This is of particular importance when designing the c.g.p. structures, because the particularly hazardous environment in which they are set calls for a special care concerning its possible behaviour.

The computation of estimates of the maximum expected dynamic responses of the platform is an important step forward to this end. With the methodology suggested in this work, the determination of those estimates for different return periods can be achieved. Another important feature of the proposal is that the uncertainties about relevant structural parameters as well as the uncertainties related to the environmental loading can be considered at a reasonably economical computing cost. This allows to carry out parametrical studies aiming to determine not only the structural responses of interest but also to define in a statistical sense the relative influence of each of the parameters used in those responses.

The application carried out in Chapter 8 is an example of the type of studies which can be performed by using the proposed methodology. In that chapter, the analysis of the influence of the uncertainties about the structure properties (E_c , ξ_c) as well as the ones associated to the wave and seismic excitations (W,Q) and also the related soil idealization and soil shear modulus, G_s , on the structural responses of a c.g.p. was performed.

From the results commented upon in Chapter 8, the following conclusions may be made about the influence of the parameters

mentioned above on the platform fundamental frequency, ω_1^0 (rocking), its associated critical damping, ξ_1^0 , deck displacement, u , base shear force, V , and overturning moment, M .

1. The influence of the uncertainties about E_c on ω_1^0 , as measured by $\sigma\omega_1^0$, is more important for increasing values of G_s . The values of ω_1^0 obtained with the layer are higher for about five percent than the ones calculated with the half space idealization.

2. The influence of the uncertainties about ξ_c on ξ_1^0 is more important as the soil becomes more rigid. The uncertainties about E_c do not contribute to the computed expected value of ξ_1^0 for the values of G_s considered in this work. The influence of the soil idealization on the value of ξ_1^0 is shown by the higher value of this parameter obtained for the layer idealization.

3. The mean values of u_W are almost the same ones for the layer and the half space soil idealizations. In addition, the mean value of u_W is smaller for an increasing value of G_s . A high coefficient of variation, C.V. (of about 2) is obtained for all the values of G_s .

4. The values of u_Q are about five percent higher for the half space idealization than for the layer one. Those values of u_Q increase for an increasing G_s . In addition, the C.V. is about 3 for all the values of G_s considered. The values for the long term deck displacements are about 30 % higher than the ones associated to the short term ones. For both cases, the value of u_Q increases for a higher value of G_s . The C.V. for both u_Q's is about 3 .

5. The mean value of $u_{Q,W}$ behaves basically as u_W , except that the values of the former are higher (3 %) than the ones associated to the latter, showing the influence of seismic excitation.

6. The mean values of V_W for the half space idealization are higher for about 5 % than the ones obtained for the layer idealization, except for G_s = 10,000 (Ton/m^2) where they coincide. The value of V_W decreases for an increasing value of G_s .

7. The mean values of V_Q for the half space soil idealization are about 15% higher than the ones obtained fro the layer soil idealization. The values of V_Q increase for growing values of G_s. The dispersion in the values of V increases for an increasing G_s, in this case the C.V. being of about 2.3.

8. The influence of the wave excitation dominates the behaviour of the expected $V_{Q,W}$. However, the mean values of $V_{Q,W}$ are about a 5% higher than the ones of V_W, showing the contribution of the seismic excitation.

9. The expected values of M_W for both soil idealizations are the same for all the range of G_s values studied here. There is a reduction of M_W for increasing values of G_s. The C.V. is about 1.06 with a slight reduction of its value for increasing values of G_s.

10. The mean values of M_Q for the half space soil idealization are about 20% higher than the ones obtained for the layer soil idealization. The values of M_Q increase for increasing values of G_s.

11. The influence of the wave excitation dominates the behaviour of the expected $M_{Q,W}$. Nevertheless, the mean values of $M_{Q,W}$ are about a 5% higher than the ones of M_W, showing the contribution of the seismic excitation.

As for the future work which could be interesting to perform, the following points could be mentioned:

a) To include other parameters (apart from the wind velocity) concerning the wave excitation modelling. For example the wave direction occurring at a given site.

b) As soon as more seismic information is available about the region, try to include it in the seismic risk model used. This may be done in the context of bayesian statistics, for example.

c) In the light of new information about the diffraction forces on gravity platforms, particularly the ones occurring on prototypes, use a more sophisticated analytical modelling of these types of forces.

d) To improve the structural modelling of the concrete gravity platform. In particular to include more degrees of freedom for each node used to discretize the towers and the deck.

10. REFERENCES

2.1 Clough R.W. and Penzien J., 1975. "Dynamics of Structures". Mc Graw Hill, New York.

2.2 Brebbia C.A. and Connor J.J., 1975. "Fundamentals of Finite Element Techniques". Butterworths, London.

2.3 Zienkiewics O.C., 1971. "The Finite Element Method in Engineering Science". Mc Graw Hill, London.

2.4 Przemieniecki J.S., 1968. "Theory of Matrix Structural Analysis". Mc Graw Hill, New York.

2.5 Hurty W.C. and Rubinstein M.F., 1964. "Dynamics of Structures". Prentice-Hall, Englewood Cliffs, N.J..

2.6 Archer J.S., 1965. "Consistent Matrix Formulation for Structural Analysis Using Finite Element Techniques". J. Am. Inst. Aeron. Astron. 3.

2.7 Bathe K.J. and Wilson E.L., 1976. "Numerical Methods in Finite Element Analysis". Prentice-Hall, Englewood Cliffs,N.J.

2.8 Thomson W.T. et al., 1974. "A Numerical Study of Damping". Earth. Eng. and Struct. Dyn., Vol. 3.

3.1 Faccioli E. and Resendiz D., 1976. "Soil Dynamics: Behaviour Including Liquefaction". In C. Lomnitz and E. Rosenblueth (editors),"Seismic Risk and Engineering Decisions". Elsevier, Amsterdam.

3.2 Seed H.B. and Lee K.L., 1966. "Liquefaction of Saturated Sands During Cycle Loading". Proc. ASCE 92 (SM6).

3.3 Thiers G.R. and Seed H.B., 1969. "Strength and Stress-Strain Characteristics of Clays Subjected to Seismic Loading Conditions". Vibration Effects of Earthquakes on Soils and Foundations ASTM Special Technical Publication 450.

3.4 Andersen K.M., 1976. "Behaviour of Clay Subjected to Undrained Cyclic Loading". Proc. of the Conf. on Behaviour of Offshore Structures, Norwegian Inst. of Tech..

3.5 Hardin B.O. and Richart E., 1963. "Elastic Wave Propagation in Granular Soils". Proc. ASCE 89 (SM1).

3.6 Hardin B.O. and Black W.L., 1968. "Vibration Modulus of Normally Consolidated Clay". Proc. ASCE 94 (SM2).

3.7 Hardin B.O. and Black W.L., 1969. Closure to "Vibration Modulus of Normally Consolidated Clay". Proc. ASCE 95 (SM6).

3.8 Seed H.B. and Idriss I.M., 1970. "Soil Moduli and Damping Factors for Dynamic Response Analysis". Report EERC 70-10, Earthquake Engineering Research Center, University of California, Berkeley, California.

3.9 Seed H.B. and Chan K.L., 1966. "Clay Strength Under Earthquake Loading Conditions". Proc. ASCE 92(SM2).

3.10 Seed N.B., 1968. "Landslides During Earthquakes Due to Liquefaction". Proc. ASCE 94 (SM5).

3.11 Hardin B.O. and Drnevich V.P., 1972. "Shear Modulus and Damping in Soils: Measurements and Parameter Effects". Proc. ASCE 98 (SM6).

3.12 Hardin B.O. and Drnevich V.P., 1972. "Shear Modulus and Damping in Soils: Design Equations and Curves". Proc. ASCE 98 (SM7).

3.13 Bjerrum L., 1973. "Geotechnical Problems Involved in Foundations of Structures in the North Sea". Geotechnique, 23, No. 3.

3.14 Løken T., 1976. "Geology of Superficial Sediments in the Northern North Sea". Proc. of the Conf. on Behaviour of Offshore Structures, Norwegian Inst. of Tech..

3.15 Milling M.E., 1975. "Geological Appraisal of Foundation Conditions, Northern North Sea". Oceanology International 75, Brighton, 1975.

3.16 Rowe P.W. et al., 1976. "Model Study of Offshore Gravity Structures Founded in Clay". Proc. of the Conf. on Behaviour of Offshore Structures, Norwegian Inst. of Tech..

3.17 Procter D.C., 1976. "Requirements of Soil Sampling for Laboratory Testing". In "Offshore Soil Mechanics" by Lloyds'

Register of Shipping and Cambridge University Eng. Dept..

3.18 Hoeg K., 1976. "Foundation Engineering for Fixed Offshore Structures". Proc. of the Conf. on Behaviour of Offshore Structures, Norwegian Inst. of Tech..

3.19 Wood D.M., 1976. "Cyclic Loading of Soil Samples". In "Offshore Soil Mechanics" by Lloyds' Register of Shipping and Cambridge University Eng. Dept..

3.20 Bielak J., 1971. "Earthquake Response of Building-Foundation Systems". Report No. EERL 71-04, EERL, Cal. Inst. of Tech..

3.21 Bycroft G.N., 1956. "Forced Vibrations of a Rigid Circular Plate on a Semi-Infinite Space and an Elastic Stratum". Phil. Trans. Roy. Soc.,London.

3.22 Luco J.E., 1974. "Impedance Functions for a Rigid Foundation on a Layered Medium". Nucl. Eng. Des. 31(2).

3.23 Veletsos A.S. and Verbic B., 1973. "Vibration of Viscoelastic Foundations". Int. J. of Earthquake Eng. and Struct. Dyn. Vol. 2.

3.24 Veletsos A.S. and Wei Y.T., 1971. "Lateral and Rocking Vibration of Footings". Proc. ASCE 97 (SM9).

3.25 Wong H.L., 1975. "Dynamical Soil Interaction". Report No. EERL 75-01, Cal. Inst. of Tech..

3.26 Luco J.E. and Westman R.A., 1971. "Dynamic Response of Circular Footings". Proc. ASCE 97 (EM5).

3.27 Elorduy J. , Nieto J.A. and Szekely E.M., 1967. "Dynamic Response of Bases of Arbitrary Shape Subjected to Periodic Vertical Loading". Proc. Intl. Symp. on Wave Propagation and Dynamic Properties of Earth Materials, New Mexico.

3.28 Luco J.E. and Westman R.A., 1972. "Dynamic Response of a Rigid Footing Bonded to an Elastic Half-Space". J. Appl. Mech., Vol. 39 E(2).

3.29 Oien M.A., 1971. "Steady Motion of a Rigid Strip Bonded to an Elastic Half-Space". J. Applied Mech., Vol. 38, E(2).

3.30 Kashio J., 1970. "Steady State Response of a Circular Disc Resting on Layered Medium". Ph.D. Thesis, Rice University.

3.31 Tajimi H., 1969. "Dynamic Analysis of a Structure Embedded in an Elastic Stratum". Proc. Fourth World Conf. in Earthquake Eng. , Santiago, Chile.

3.32 Novak M. and Sachs K., 1973. "Torsional and Coupled Vibrations of Embedded Footings". Int. J. of Earthquake Eng. and Struct. Dyn., Vol. 2.

3.33 Hsieh T.K., 1962. "Foundation Vibrations". Proc. Inst. Civil Engineers, 22.

3.34 Dobry R., 1971. "Soil Properties and the One Dimensional Theory of Earthquake Amplification". D. Sc. Dissertation, M.I.T..

3.35 Veletsos A.S. and Nair V.V.D., 1975. "Seismic Interaction of Structures on Hysteretic Foundations". Proc. ASCE 101 (ST1).

3.36 Richart Jr., F.E., Hall J.R. and Woods R.D., 1970. "Vibration of Soils and Foundation". Prentice-Hall, Inc.,New Jersey.

3.37 Novak M., 1974. "Effect of Soil on Structural Response to Wind and Earthquake". Int. J. of Earthquake Eng. and Struct. Dyn., Vol. 3.

3.38 Hall J.R. and Kissenpfenning P., 1976. "Special Topics on Soil-Structure Interaction". Nuclear Eng. and Design 38.

3.39 Novak M., 1977. "Theme Report on Topic 4 Foundation and Soil-Structure Interaction". Proc. 6th World Conf. Earthquake Eng., New Dehli.

3.40 Luco J.E. et al., 1974. "The Dynamic Modelling of the Half-Plane by Finite Elements". Nuclear Eng. and Design 31.

3.41 Ghosh S.V. and Wilson E.L., 1969. "Dynamic Stress Analysis of Axisymetric Structures Under Arbitrary Loading". Report EERC 69-10, Coll. of Eng., University of California, Berkeley.

3.42 Seed H.B. et al., 1975. "Soil-Structure Interaction Analyses for Seismic Response". Proc. ASCE 101 (GT5).

3.43 Bathe K.J. et al., 1973. "SAP IV - A Structural Analysis Program for Static and Dynamic Response of Linear Systems". Report EERC 73-11, Coll. of Eng., Univ. of Cal., Berkeley.

3.44 Hadjian A.H., 1976. "Soil-Structure Interaction - An Engineering Evaluation". Nuclear Eng. and Design 38.

3.45 Lysmer J. and Kuhlmeyer R.L., 1969. "Finite Dynamic Model for Infinite Media". Proc. ASCE 95 (EM4).

3.46 Waas G., 1972. "Linear Two-Dimensional Analysis of Soil Dynamics Problems in Semi-Infinite Layered Media". Ph.D. Thesis, Univ. of Cal., Berkeley.

3.47 Kausel E. and Roesset J.M., 1975. "Dynamic Stiffness of Circular Foundations". Proc. ASCE 101 (EM6).

3.48 Lysmer J. et al., 1975. "FLUSH - A Computer Program for Approximate 3-D Analysis of Structure-Soil-Structure Interaction". Report EERC 75-30, Coll. of Eng., Univ. of Cal., Berkeley.

3.49 Idriss I.M. et al., 1973. "QUAD-4: A Computer Program for Evaluating the Seismic Response of Soil Structures by Variable Damping Finite Element Procedures". Report EERC 73-16, Coll. of Eng., Univ. of Cal., Berkeley.

3.50 Hadjian A.H., 1976. Discussion to "Soil-Structure Interaction Analysis for Seismic Response" by Seed H.B. et al., Proc. ASCE 102 (GT4).

3.51 Hall J.R. et al., 1976. Discussion to "Soil-Structure Inter-Action Analysis for Seismic Response". Proc. ASCE 103 (GT4).

3.52 Seed H.B. et al., 1977. Closure to "Soil-Structure Interaction Analysis for Seismic Response". Proc. ASCE 103 (GT4).

3.53 Lysmer J. et al., 1974. "LUSH: A Computer Program for Complex Response Analysis of Soil-Structure Systems". Report EERC 74-4, Coll. of Eng., Univ. of Cal., Berkeley.

3.54 Seed H.B. and Idriss I.M., 1969. "Influence of Soil Conditions and Ground Motions During Earthquakes". Proc. ASCE 95 (SM1).

3.55 Constantopoulos I.V. et al., 1973. "A Comparison of Linear and Exact Nonlinear Analysis of Soil Amplification". Proc. 5th World Conf. Earthquake Eng., Rome.

3.56 Kausel E. et al., 1976. "Nonlinear Behaviour in Soil-Structure

Interaction". Proc. ASCE 102 (GT11).

3.57 Schnable P.B. et al., 1972. "SHAKE - A Computer Program for Earthquake Response Analysis of Horizontally Layered Sites". Report EERC 72-12, Coll. of Eng., Univ. of Cal., Berkeley.

3.58 Frimann Clausen C.J., 1976. "The Condeep Story" in P. George and D. Wood (editors),"Offshore Soil Mechanics". Cambridge Univ. Eng. Dept., Lloyds' Register of Shipping.

3.59 Wong H.L. et al., 1977. "Contact Stresses and Ground Motion Generated by Soil-Structure Interaction". Earthquake Eng. and Struct. Dyn. ,Vol. 5.

3.60 Tajimi H. et al., 1977. "Dynamic Response of Large-Scale Shaking Table Foundation and its Surrounding Ground". Preprints 6th World Conf. in Earthquake Eng., New Dehli.

3.61 Valera J.E. et al., 1977. "Seismic Soil-Structure Interaction Effects at Humboldt Bay Power Plant". Proc. ASCE 103 (GT10).

3.62 Luco J.E., 1976. "Vibrations of a Rigid Disc on a Layered Viscoelastic Medium". Nuclear Eng. and Design 36.

4.1 Housner G.W., 1970. "Strong Ground Motion". In R.L. Wiegel (editor), "Earthquake Engineering". Prentice-Hall, Englewood Cliffs, N.J..

4.2 Newmark N.M. and Rosenblueth E., 1971. "Fundamentals of Earthquake Engineering". Prentice-Hall, Englewood Cliffs, N.J..

4.3 Benioff H., 1955. "Earthquake and Rock Creep". Bull. Seismol. Soc. Am., 45.

4.4 Lomnitz C., 1974. "Global Tectonics and Earthquake Risk". Elsevier, Amsterdam.

4.5 Ambrasey N.N., 1973. "Dynamics and Response of Foundation Materials in Epicentral Regions of Strong Earthquakes". Proc. 5th World Conf. Earthquake Eng.,Rome.

4.6 Karnik V.I.T., 1968. "Seismicity of the European Area. Pt.1". Academia, Prague.

4.7 Bycroft G.N., 1960. "White Noise Representation of Earthquakes". Proc. ASCE 86 (EM2).

4.8 Rascón O. and Chávez M., 1973. "On an Earthquake Simulation Model". Proc. 5th World Conf. Earthquake Eng., Rome.

4.9 Cornell C.A., 1969. "Design Seismic Inputs". Seminar on Seismic Design of Nuclear Power Plants, Cambridge, Mass., M.I.T. Press.

4.10 Esteva L., 1976. "Seismicity". In C. Lomnitz and E. Rosenblueth (editors), "Seismic Risk and Engineering Decisions". Elsevier, Amsterdam.

4.11 Rosenblueth E., 1964. "Probabilistic Design to Resist Earthquakes". Proc. ASCE 90 (EM5).

4.12 Tajimi H., 1960. "A Statistical Method of Determining the Maximum Response of a Building Structure during an Earthquake". Proc. 2nd. World Conf. Earthquake Eng., Tokyo.

4.13 Housner G.W. and Jennings P.C., 1964. "Generation of Artificial Earthquakes". Proc. ASCE 90 (EM1).

4.14 Newmark N.M. and Hall W.J., 1969. "Seismic Design Criteria for Nuclear Reactor Facilities". Proc. 4th. World Conf. Earthquake Eng., Santiago:2,B-4.

4.15 Newmark N.M. et al., 1973. "Seismic Design Criteria for Nuclear Power Plants". Proc. ASCE 99 (PO2).

4.16 McGuire R.K., 1974. "Seismic Structural Response Risk Analysis, Incorporating Peak Response Regressions on Earthquake Magnitude and Distance". M.I.T. Dept. Civil Eng. Rept. :R74-51.

4.17 Hudson D.E., 1962. "Some Problems in the Application of Spectrum Techniques to Strong Motion Earthquake Analysis". Bull. Seismol. Soc. Am., 52.

4.18 Vanmarcke E.H., 1976. "Structural Response to Earthquakes". In C. Lomnitz and E. Rosenblueth (editors), "Seismic Risk and Engineering Decisions". Elsevier, Amsterdam.

4.19 Ibid. 3.1

4.20 Ibid. 3.54

4.21 Seed H.B. et al., 1976. "Relationships of Maximum Acceleration, Maximum Velocity, Distance from Source, and Local Site Conditions for Moderately Strong Earthquakes". Bull. Seismol. Soc. Am., 66.

4.22 Mohraz B., 1976. "A Study of Earthquake Response Spectra for Different Geological Conditions". Bull. Seismol. Soc. Am., 66.

4.23 Ibid. 3.49

4.24 Idriss I.M. and Seed H.B., 1968. "Seismic Response of Horizontal Soil Layers". Proc. ASCE 94 (SM4)

4.25 Karnick V.I.T., 1971. "Seismicity of the European Area. Pt. 2". Academia, Prague.

4.26 Cornell C.A., 1968. "Engineering Seismic Risk Analysis". Bull. Seismol. Soc. Am., 58.

4.27 Esteva L., 1968. "Bases para la formulación de Decisiones de Diseño Sísmico". Natl. Univ. México, Inst. of Eng. Rept. 182.

4.28 Der Kiureghian A. and Ang H.S., 1977. "A Fault-Rupture Model for Seismic Risk Analysis". Bull. Seismol. Soc. Am., 67.

4.29 McGuire R.K., 1977. "Effects of Uncertainty in Seismicity on Estimates of Seismic Hazard for the East Coast of the United States". Bull. Seismol. Soc. Am., 67.

4.30 Esteva L., 1969. "Seismicity Prediction: A Bayesian Approach". Proc. 4th World Conf. Earthquake Eng., Santiago:1,A-1.

4.31 Scott R.F., 1977. "The Essex Earthquake of 1884". Int. J. Earthquake Eng. Struct. Dyn., 5.

4.32 Kvale A., 1960. "Norwegian Earthquakes in Relation to Tectonics". Årbok for Universitetet I Bergen. Mat. -Naturv. Serie, No. 10.

4.33 Redding J., 1976. "Glacial Genesis of North Sea Soils". In P. George and D. Wood (editors), "Offshore Soil Mechanics". Cambridge Univ. Eng. Dept., Lloyds' Register of Shipping.

4.34 Båth M., 1953. "Seismicity of Fennoscandia and Related Problems". Gerl. Beitr. z. Geoph. B. 63, H3.

4.35 Lilwall R.C., 1976. "Seismicity and Seismic Hazard in Britain". Seismol. Bull. Inst. Geol. Sci., No. 4, 9pp.

4.36 Burton P.W., 1977. "Assessment of Seismic Hazard in the U.K.". Proc. SECED. Conf. on Instrumentation for Ground Vibration and Earthquakes, Keele Univ..

4.37 Esteva, L., 1967. "Criteria for the Construction of Spectra for Seismic Design". Third Panamerican Symposium on Structures, Caracas, Venezuela.

4.38 Esteva L. and Rosenblueth E., 1964. "Espectros de Temblores a Distancias Moderadas y Grandes". Bol. Soc. Mex. Ing. Sísmica 2(1).

4.39 Esteva L. and Villaverde R., 1973. "Seismic Risk, Design Spectra and Structural Reliability". Proc. 5th. World Conf. Earthquake Eng., Rome.

5.1 Phillips O.M., 1957. "On the Generation of Waves by Turbulent Wind". J. Fluid Mech. 2(5).

5.2 Miles J.W., 1957. "On the Generation of Surface Waves by Shear Flows". J. Fluid Mech. 3(2).

5.3 Miles J.W., 1960. "On the Generation of Surface Waves by Turbulent Shear Flows". J. Fluid Mech. 7(3).

5.4 Kinsman B., 1965. "Wind Waves". Prentice-Hall, Englewood Cliffs, N.J..

5.5 Lamb H., 1945. "Hydrodynamics". 6th edition. Dover Publ. New York.

5.6 Dean R.G., 1970. "Relative Validities of Water Wave Theories". Proc. ASCE 96 (WW1).

5.7 Myers J.J. et al. (editors), 1969. "Handbook of Ocean and Underwater Engineering". Mc Graw Hill, New York.

5.8 Denis S.M. and Pierson W.J., 1963. "On the Motion of Ships on Confused Seas". Transs. SNAME.

5.9 Rice S.O., 1944-45. "Mathematical Analysis of Random Noise". In "Selected Papers on Noise and Stochastic Processes", edited by N. Wax. Dover Publ., New York, 1954.

5.10 Longuet-Higgins M.S., 1952. "On the Statistical Distribution of the Heights of Sea Waves". J. Marine Res., 11.

5.11 Cartwright D.E. and Longuet-Higgins M.S., 1956. "The Statistical Distribution of the Maximum of a Random Function". Proc.R.Soc.,Ser A.

5.12 Pierson W.J. and Moskowitz L., 1964. "A Proposed Spectral Form for Fully Developed Wind Seas Based on the Similarity Theory of S.A. Kitaigorodskii". J. Geophys. Res., 69.

5.13 Chakrabarti S.K. and Snider R.H., 1975. "Modelling of Wind Waves with JONSWAP Spectra". Proc. Modelling 75.

5.14 Hogben N., 1974. "Fluid Loading of Offshore Structures, a State of Art Appraisal: Wave Loads". R. Inst. of Naval Arch..

5.15 Streeter V.L., (editor), 1961. "Handbook of Fluid Dynamics". Mc Graw Hill, New York.

5.16 Wiegel R.L., 1964 . "Oceanographical Engineering". Prentice-Hall, Englewood Cliffs, N.J..

5.17 Reid R.O. and Bretschneider C.L., 1964. "The Design Wave in Deep Water or Shallow Water, Storm Tide, and Forces on Vertical Piling and Large Submerged Objects". Tex. A & M Dept. Oceanog. Tech. Rept..

5.18 Goda Y., 1964. "Wave Force Experiments on a Vertical Circular Cylinder: Experiments and a Proposed Method of Wave Force Computation". Port Harbour Tech. Res. Inst. Tech. Rept. 8., Yokosuka, Japan.

5.19 Wilson B.W. and Reid R.O., 1963. "A Discussion of Wave Force Coefficients for Offshore Pipelines". J. ASCE 89 (WW1).

5.20 Morison J.R. et al., 1950. "The Force Exerted by Surface Waves on Piles". Petrol. Trans. Am. Inst. Mining Metal Engineering.

5.21 Mac Camy R.C. and Fuchs R.W., 1954. "Wave Forces on Piles: A Diffraction Theory". U.S. Army Corps Engrs. Beach Erosion Board. Tech. Memo . 69.

5.22 Garrison C.J. and Rao V.S., 1971. "Interaction of Waves with Submerged Objects". J. ASCE 97 (WW2).

5.23 Hogben N. and Standing R.G., 1975. "Experience in Computing Wave Loads on Large Bodies". Proc. 7th. OTC Conf., Houston.

5.24 Zienkiewics O.C. et al., 1977. "The Coupling of the Finite Element Methods and Boundary Solutions Procedures". Int. J. Num. Meth. in Engr. 11.

5.25 Garrison C.J. and Chow P.Y., 1972. "Wave Forces on Submerged Bodies". J. ASCE 98 (WW3).

5.26 Nataraja R. and Kirk C.L., 1977. "Dynamic Response of a Gravity Platform UnderRandom Wave Forces". Proc. 9th. OTC Conf., Houston.

5.27 Zienkiewics O.C. and Bettes P., 1977. "Diffraction and Refraction of Surface Waves Using Finite and Infinite Elements". Int. J. Num. Meth. in Eng. 11.

6.1 Ibid. 2.1

6.2 Ibid. 2.6

6.3 Dempsey K.M. and Irvine H.M., 1978. "A Note on the Numerical Evaluation of Duhamel's Integral". Int. J. of Earthquake Eng. and Struct. Dyn., Vol. 6.

6.4 Bielak J. and Chávez M., 1974 . "Efectos de Interacción Estructura-Subsuelo en el Análisis Dinámico de Estructuras Masivas de Turbogeneradores". Informe a la CFE. Inst. de Ing. UNAM.

6.5 O'Kelly M.E.J., 1964. "Vibration of Viscously Damped Linear Dynamic Systems". Ph.D. Thesis. Cal. Inst. of Tech..

6.6 Ibid. 3.37

6.7 Ibid. 3.39

6.8 Ibid. 3.59

6.9 Ibid. 3.23

6.10 Ibid. 3.36

6.11 Roesset J.M. et al., 1973. "Modal Analysis for Structures with Foundation Interaction". Proc. ASCE 99(ST3).

6.12 Tsai N.C., 1974. "Modal Damping for Soil-Structure Interaction". Proc. ASCE 100 (EM2)

6.13 Bielak J., 1975. "Modal Analysis for Building-Soil Interaction". Informe E 17. Inst. de Ingeniería, UNAM, México.

6.14 Jacobsen L.S., 1960. "Damping in Composite Structures". Proc. 2nd. World Conf. Earthquake Eng., Tokyo.

6.15 Choprá A.K. and Gutierrez J.A., 1974. "Earthquake Analysis of Multistorey Buildings Including Foundation Interaction". Int. J. of Earthquake Eng. and Struct. Dyn., Vol. 3.

7.1 Ang A.H.S. and Cornell C.A., 1974. "Reliability Bases of Structural Safety and Design". Proc. ASCE 100 (ST9).

7.2 Papoulis A., 1965. "Probability, Random Variables and Stochastic Processes". Mc Graw Hill Inc..

7.3 Davenport A.G., 1961. "The Application of Statistical Concepts to the Wind Loading of Structures". Proc. of the Institution of Civil Engineers, London.

7.4 Der Kiureghian A., 1978. "Second Moment Combination of Stochastic Loads". J. ASCE 104 (ST10).

7.5 Rosenblueth E., 1975. "Point Estimates for Probability Moments". Proc. Nat. Acad. Sci. USA Vol. 72, No. 10.

8.1 Tichý M. and Vorlicěk, 1972. "Statistical Theory of Concrete Structures". Irish Univ. Press, Shannon, Ireland.

8.2 Haviland R., 1976. "A Study of the Uncertainties in the Fundamental Translational Periods and Damping Values for Real Buildings". M.I.T. Dept. Civil Eng. Dept.: R76-12.

8.3 Wood D.M., 1976. "Development of Blanche Field Northern North Sea". In"Offshore Soil Mechanics" by Lloyds' Register of Shipping and Cambridge University Eng. Dept..

8.4 Ibid. 3.62

8.5 Ibid. 3.23

8.6 Lambe T.W. and Whitman R.V., 1969. "Soil Mechanics", Wiley, New York.

8.7 Whitman R.V., 1969. "Soil-Structure Interaction", Seminar on Seismic Design of Nuclear Power Plants, Cambridge, Mass., M.I.T. Press

8.8 Flores Berrones R., 1977. "Parametros de Diseño en Cimentaciones de Maquinaria". Informe 389. Inst. de Ingeniería, UNAM, México.

8.9 Whitman, R.V., 1973. "Notes in Soil Dynamics"., M.I.T.

8.10 Ibid. 4.35

8.11 Ibid. 7.3

8.12 Draper L., 1972. "Extreme Wave Conditions in British and Adjacent Waters". Proc. 13th. Coastal Eng. Conf., Vancouver.

8.13 Silvester R., 1974. "Coastal Engineering, I , Generation, Propagation and Influence of Waves", Elsevier, Amsterdam.

LIST OF SYMBOLS

a	amplitude of the harmonic wave
a_0	proportionality factor, equation (2.23)
a_1	proportionality factor, equation (2.23)
$a(t)$	ground motion acceleration; structural response
a_i	amplitude of simple harmonic wave
$\underline{A}$	matrix used in equation (2.2)
A_0	amplitude of 10^{-3} millimeters; maximum amplitude recorded by a Wood-Anderson seismograph at a distance of 100 Km. from the epicentre
b	parameter used in equation (4.19)
b'_s	coefficient used in equation (7.22)
$\underline{B}$	matrix formed by derivates of $\underline{A}$
$\underset{\sim}{B}_1$	vector used in equation (6.25)
$\underset{\sim}{B}_2$	vector used in equation (6.25)
c	wave celerity
c'	static strength parameter in terms of effective stress
c_{ij}	damping influence coefficient
c_j	dimensionless real-valued function depending on the Poisson ratio
c_{js}	soil-foundation equivalent damping
c_{xs}	equivalent viscous damper in the x direction
$c_{\theta s}$	equivalent viscous damper in rocking
C_m	coefficient used in equation (3.56)
C_{ov}	diffraction coefficient for the overturning moment
C_x	diffraction coefficient for the horizontal forces
C_y	diffraction coefficient for the vertical forces
$\underline{C}$	structural damping matrix
$\underline{C}^*$	generalized damping matrix
$\underline{C}_N$	damping matrix of the nth finite element
$\underline{C}_0$	damping matrix of the soil-structure system
d	line source geometrical parameter; diameter of the cylinder
D	loss ratio; total depth of water
$\underline{D}$	matrix of the material elastic properties
e	void ratio

E, E_c expectance; seismic energy; Young's modulus of elasticity of the material, Young's modulus of reinforced concrete

E_d energy dissipated by a soil

E_s maximum strain energy stored in the soil

$\bar{E}$ average energy

f frequency in cycles per sec.

$f_I(i)$ cumulative power spectral density function

$|F(\omega)|$ Fourier spectra

$\underset{\sim}{F}_b$ body forces

g acceleration of gravity

G shear modulus of elasticity of the material

G_{max} value of G for strain amplitudes lower then 10^{-4}

$G(\omega)$ power spectral density function

G_0 measure of the intensity of the ground motion

h defined in fig. 4. ; height of submerged part of a cylinder

h_b height of the caisson

h_i height of the ith node with respect to the center of gravity of the foundation

$h_s(t-\tau)$ unit impulse response function

H wave height

$H_{\frac{1}{3}}$ average of the highest one third of the waves, also known as significative wave heights, H_s

$H_{\frac{1}{10}}$ average of the highest one tenth of the waves, sometimes taken as the expected value of maximum wave height

$(H_{max})_{mode}$ most probable value of wave heights

$H_{r.m.s.}$ root-mean square value of wave heights

H_s significant wave height

$H_s(i\omega)$ complex frequency response of the system

$\bar{H}$ mean value of wave height

$\bar{H}_{max}$ mean value of maximum wave height

$|H_s(i\omega)|$ amplitude of the complex frequency response

i nodal point

i^T transpose of matrix of i

$\bar{i}$ mean of variable i

I ground motion intensities

$I(MM)$ Modified Mercalli Intensity

$I(x)$ moment of inertia of a cross-section

I_0 ith centroidal moment of inertia of a mass

$\underline{I}$ identity matrix

J_1' derivate of the Bessel functions of the first kind, of order one

k function of the plasticity index of a particular soil

k_{ij} element of $\underline{K}$

k_j dimensionless real-valued function used in equation (3.12)

k_{js} soil-foundation equivalent stiffness

k_{xs} equivalent stiffness of the soil in the x direction

$k_{\theta s}$ equivalent stiffness of the soil in rocking

K_d drag coefficient

K_j static stiffness of the disc in the j direction

K_m coefficient of inertia

K_0 coefficient of lateral stress at rest

$\underline{K}$ structure stiffness matrix

$\underline{K}_N$ stiffness matrix of the nth finite element

$\underline{K}_0$ stiffness of soil-structure system

$\underline{K}^*$ structure stiffness matrix

$\bar{K}_d$ mean value of K_d

$\overline{KE}$ kinetic energy

ℓ length

Ln natural logarithm

m mass per unit of vlolume

m_i ith lumped mass

m_{ij} element of $\underline{M}$

m_n nth spectral moment

$m(x)$ mass per unit length

m_0 lower limit of magnitude in a seismic region; mass of the foundation

m_0' mass used in equation (6.25)

M magnitude of the earthquake

M_c mass of a cylinder

M_f displaced mass

M_{wi} diffraction overturning moments

$\underline{M}$ structure mass matrix

$\underline{M}^*$ generalized mass matrix

$\underline{M}_N$ mass matrix of the nth finite element

$\underline{M}_0$ mass of the soil-structure system

$\underline{M}^d$ mass of the displaced fluid

$\bar{\underline{M}}$ defined in equation (6.49)

$\hat{\underline{M}}$ defined in equation (6.45)

N number of cycles

N_0 $= \frac{T}{T_o}$ = number of zero up crossings in a record

OCR consolidation ratio

p probability of excedence; parameter of equation (7.23)

p_d distributed load

$p_d(x,t)$ external loads

p_i ith applied load

p(t) dynamic load

P_{drag} drag force

$P_{ei}(t)$ effective seismic load acting on the ith nodal point of the discretized structure

P_{in} inertia force

$P_s^*(t)$ dynamic load

$P_s^*(\omega)$ = $P(\omega)$ = Fourier transform of applied load

P_{u_0} horizontal load applied at the center of gravity of the foundation

$P_w(t)$ wave load

$P'_w(t)$ horizontal diffraction forces on a circular cylinder

$P''_w(t)$ horizontal diffraction forces on a caisson of square area

P_{θ_0} overturning moment applied at the center of gravity of the foundation

P_N probability of occurrences of earthquakes

$\overline{PE}$ average potential energy

$\underset{\sim}{P}(t)$ structure load vector

$\underset{\sim}{P}_N$ element load vector

$\underset{\sim}{P}_0$ vector of applied loads for soil-structure system

$P(\omega)$ Fourier transform of P(t)

q parameter of equation (7.24)

r radius of the disc; line source geometrical parameter; particle trajectory; cyclindrical coordinate of a point in the flow field; radius of the submerged cylinder

$r_{\ell j}$ element of modal matrix $\underline{R}$

$r_{t_1,p}$ peak factor used in equation (4.16)

r_x displacement of water particles in the x direction

r_y displacement of water particles in the y direction

R random focal distance of the earthquake

R_{ii} autocorrelation function of i

$R_{\eta\eta}(0)$ autocorrelation function of wave height

$R(\tau)$ autocorrelation function

$\underline{R}$ modal matrix of a structural system on a rigid soil

$\underline{R}^{\theta}_{s}$ modal matrix of a structural system on a flexible soil

$\underset{\sim}{R}_s$ sth modal vector associated to $\underline{R}$

$\underset{\sim}{R}^{0}_{s}$ sth modal vector associated to $\underline{R}^{\theta}_{s}$

$\underset{\sim}{R}^{s}_{s}$ modal vector associated to the structure degrees of freedom

$\underset{\sim}{R}^{f}_{s}$ modal vector associated to the foundation degrees of freedom

s surface of the body

S seismic strain

S_a pseudo-acceleration response spectra

S_d displacement response spectra

S_{ii} power spectral density function of i

S_v pseudo-velocity response spectra

$S_{\eta\eta}(\omega)$ power spectral density function of wave heights

t time

t_0 duration of the accelerogram

t_1 duration of the accelerogram ensemble

T kinetic energy of the element; wave period; duration of a process

T_0 return period; time between succesive zero upcrossings

T_s significant wave period

u displacement of the structure

u_t nodal displacement which includes bending and shear deformations

u'_t nodal slope which includes bending and shear deformation

u_0 horizontal translation of the foundation

$\ddot{u}_g$ ground acceleration

$\ddot{u}_i$ acceleration of m_{ii} relative to the base of the structure

U structural displacment

U_s strain energy

$\underline{U}^T$ used in equation (7.11)

$\underset{\sim}{U}_N$ vector formed by the element nodal displacements

$\underset{\sim}{U}_0$ displacement of the soil-structure system

$\underset{\sim}{U}_0^f$ vector of displacement of the foundation

$\underset{\sim}{U}_0^s$ vector of nodal displacements of the structure

$\underset{\sim}{U}(\omega)$ Fourier transform of U(t)

$\dot{\underset{\sim}{U}}$ vector of nodal velocities of the structure on a rigid soil

$\dot{\underset{\sim}{U}}_0$ vector of nodal velocities of the soil-structure system

$\ddot{\underset{\sim}{U}}$ vector of nodal acceleration of the structure on a rigid soil

$\ddot{\underset{\sim}{U}}_g$ vector of ground acceleration

$\ddot{\underset{\sim}{U}}_0$ vector of nodal acceleration of the soil-structure system

v_i fluid particle velocity at the ith node as if no body existed

$\dot{v}$ fluid velocity

$\dot{v}_x$ fluid particle velocity in the x direction

$\dot{v}_y$ fluid particle velocity in the y direction

$\dot{v}_0$ fluid vector within the boundary layer

$\underline{\dot{v}}$ vector of fluid particle velocity

$\ddot{v}$ fluid acceleration

$\ddot{v}_i$ acceleration of the water particles at the ith node as if no body existed

$\ddot{v}_x$ fluid particle acceleration in the x direction

$\ddot{v}_y$ fluid particle acceleration in the y direction

V_c volume of the cylinder

V_i tributary volume of the beam elements ending at the ith node

V_s velocity of the shear waves in the soil

V_y coefficient of variation of y

VW virtual work

w wave orbit width parameter

$W_{19.5}$ wind velocity at a height of 19.5 m. above the sea surface

x horizontal axis; coordinate

x_f defined in fig. 4.3

x_0 defined in fig. 4.3

y vertical axis; coordinate

$Y_s(t)$ generalized coordinate

$Y_s(\omega)$ Fourier transform of $Y_s(t)$

$Y_{t_1,p}$ response spectra value ; equation (4.16)

Y_1' derivate of the Bessel function of the second kind, of order one

$\overline{Y}^T$ mean of the response of Y(t)

$\overline{Y}_{T_0}$ mean of the extreme value of Y(t)

$\underset{\sim}{Y}$ vector of normal coordinates

$\underset{\sim}{Y}(\omega)$ vector of normal coordinates in the frequency domain

α a dimensionless number; equation (5.47), and (4.24)

β a regional seismic constant used in equations (4.24) and (5.47)

γ strain amplitude; activity rate; parameter of equation (5.14); kinematic viscosity of a fluid; equivalent length for the foundation

ε_i random phase of simple harmonic wave

ε_0^2 spectral width parameter, used in equation (5.38)

$\underset{\sim}{\varepsilon}$ vector of strains

η a particular value of the wave height; vertical movement of the particles on the sea surface

$\overline{\eta(t)^2}$ mean square value of η

θ rocking displacement; line source geometrical parameter

θ_0 rocking of the foundation

λ wave length

κ wave number

ν Poisson ratio; parameter of equation (7.7); occurrence rate

ν_g mean rate of excedence of earthquakes per year for source j

ν_i mean occurrence rate of i

ν_M mean rate of excedence of earthquakes with magnitudes M for

ξ damping ratio; percentage of critical damping

ξ_c value of reinforced concrete fraction of critical damping

ξ_g damping of the ground

ξ_s fraction of critical damping for the sth mode on the soil

ξ_s^0 fraction of chitical damping for the soil-structure system

ξ_t equivalent damping of the system,used in equation (4.18)

$\underline{\xi}$ generalized damping, used in equation (6.6)

ρ mass density of the soil; fluid density

σ_a parameter of equation (5.49)

σ_b parameter of equation (5.49)

σ_m mean effective stress in pounds/square inch

$\sigma_{y(t_i)}$ standard deviation of the response of the system

σ_i^2 variance of i

$\underline{\sigma_{ii}}$ standard deviation matrix

$\underline{\sigma_{ii}^2}$ covariance matrix

$\bar{\sigma}_m$ mean effective stress

τ shear stress

τ_1 dummy time variable

τ_2 dummy time variable

$\bar{\tau}$ mean duration

ϕ velocity potential; normalized variate

ϕ_d diffracted velocity potential

ϕ_i incident velocity potential

ϕ_t total velocity potential

ϕ' static strength parameter of soils

ω frequency in rad./sec.

ω_g dominant natural frequency of the ground

ω_i ith undamped natural frequency

ω_{max} parameter of equation (5.48)

ω' damped natural frequency

ω_s' damped natural frequency of the soil-structure system

ω_s^0 undamped natural frequency of the soil-structure system

$\Delta\omega$ increment of frequency

Ω domain of a variable; direction perpendicular to the surface of the boundary layer

$\underline{\Omega^2}$ diagonal matrix whose components are the square of the undamped frequency

ψ phase angle

δ virtual displacement

∇ Laplace operator

$\frac{D}{Dt}$ total derivative

$E[\,.\,]$ expectance of .

$P(.)$ probability density function of (.)

$\frac{\partial}{\partial t}$ partial derivative with respect to time

$\dot{z}$ derivative of z with respect to time

$\underline{i}^T$ transpose of matrix i

LIST OF TABLES

LIST OF FIGURES

8.20 P.s.d.f. of the first generalized load for wave excitation, $S_{p,W}$, as a function of frequency, ω

8.21 P.s.d.f. of the first generalized coordinate for wave excitation, $S_{y,W}$, as a function of frequency, ω

8.22 P.s.d.f. of the first generalized coordinate for wave excitation, $S_{y,W}$, as a function of frequency, ω

8.23 P.s.d.f. of the first generalized coordinate for wave excitation, $S_{y,W}$, as a function of frequency, ω

8.24 P.s.d.f. of deck displacement for wave excitation, $S_{u,W}$, as a function of frequency, ω

8.25 P.s.d.f. of deck displacement for wave excitation, $S_{u,W}$, as a function of frequency, ω

8.26 P.s.d.f. of deck displacement for wave excitation, $S_{u,W}$, as a function of frequency, ω

8.27 P.s.d.f. of deck displacement for wave excitation, $S_{u,W}$, as a function of frequency, ω

8.28 P.s.d.f. of deck displacement for wave excitation, $S_{u,W}$, as a function of frequency, ω

8.29 Deck displacement for wave excitation, u_W, as a function of soil shear modulus, G_s

8.30 Short and long term deck displacement for wave excitation, u_W, as a function of soil shear modulus, G_s

8.31 P.s.d.f. of the first generalized coordinate for seismic excitation, $S_{y,Q}$, as a function of frequency, ω

8.32 P.s.d.f. of the first generalized coordinate for seismic excitation, $S_{y,Q}$, as a function of frequency, ω

8.33 P.s.d.f. of the first generalized coordinate for seismic excitation, $S_{y,Q}$, as a function of frequency, ω

8.34 P.s.d.f. of deck displacement for seismic excitation, $S_{u,Q}$, as a function of frequency, ω

APPENDIX B

Cornell's seismic risk model [4.26]

The Cornell's seismic risk model makes the following assumptions:

a) The seismic region in which the site is located can be divided into n sources based on the tectonics, geology and earthquake history of the region. The shape of the sources has to be assimilated to a point, a line or an area depending on their specific characteristics figs. 4.1, 4.2, 4.3 respectively;

b) The earthquake generating mechanism is concentrated in a point;

c) The isoseismals produced by earthquakes are circular;

d) There is equal likelihood of earthquake occurrence along or over a line or areal source respectively;

e) The occurrence of earthquakes can be represented by a Poisson process;

f) The occurrence rate remains constant in time.

Some of the assumptions can be altered if the information available in a specific case allows it, but this will usually imply increased mathematical complexities [4.26].

As it has been mentioned in the text, the final objective of a seismic risk model is to compute the maximum ground motion intensities in a site and their return periods. To do so, the following steps are implied:

1) An attenuation law for the desired ground motion intensity at the site, I, is selected i.e. $I = f(M, R, C_j)$ . . . (B1) in which f stands for function of, M is the earthquake random magnitude, R its random focal distance, and C_j (j = 1, 2, 3) are regional constants. From equation(B1) the following expression can be derivated:

$$M = g(I,R,C_j)$$

where g reads 'function of'.

2) Assuming probabilistic independance between M and R, the conditional probability that the intensity I will be equal or exceed a value i, when an earthquake occurs at R = r can be expressed as follows:

$$P[I \geq i | R = r] = P[M \geq g\ (i, r, C_j)]$$

$$= 1 - F_M\ [g\ (i, r, C_j)] \qquad \ldots (B2)$$

where $F_M[m]$ is the cumulative distribution function (c.d.f.) of magnitudes and $g\ (i, r, C_j)$ was defined previously.

3) In order to compute the complementary distribution function of M i.e. $1 - F_M(m)$, the Richter Magnitude frequency law, equation (4.19), is used. Two cases may be considered: a) when $m_0 \leq m \leq \infty$; and b) when $m_0 \leq m \leq m_1$; where m_0 and m_1 are the lower and upper limits of the magnitude in a region.

For case a) the following equation is obtained:

$$1 - F_M(m) = e^{-\beta(m - m_0)} \qquad m_0 \leq m \leq \infty \qquad \ldots (B3)$$

in which β is a regional constant which varies between 1.5 and 2.3 [426] ; and for case b) :

$$1 - F_M(m) = (1 - k) + ke^{-\beta(m - m_0)} \qquad m_0 \leq m \leq m_1 \qquad \ldots (B4)$$

where:

$$k = \left[1 - e^{-\beta(m_1 - m_0)}\right]^{-1} \qquad \ldots (B5)$$

4) The c.d.f. of I , $F_I(i)$ given that $M \geq m_0$ is:

$$1 - F_I(i) = P[I \geq i]$$

$$= \int_{r_1}^{r_2} P[I \geq i | R = r]\ f_R(r)\ dr \qquad \ldots (B6)$$

where $P[I \geq i | R = r]$ is obtained by combining equations(B2) with equations(B3) or(B4), depending on the distribution of magnitudes considered, and $f_R(r)$ is the probability density function of R and r_1 and r_2 the limits of r .

5) The probability distribution of $I_{max}(t)$ for a period of time of t years can be obtained by using equation (4.20) for N = 0 i.e.:

$$P\left[I_{max}(t) \leq i\right] = P_N(0)$$

$$= \exp(-p_i \nu t) \qquad \ldots (B7)$$

where ν_M in equation (4.20) has been multiplied by $p_i \nu$ in which p_i, the probability that an event with $m \geq m_0$ occurs is given by equation (B6) and ν is the mean rate of exceedance of earthquakes per year. For $t = 1$ year,

$$F_{I_{max}}(i) = P\left[I_{max}(1) \leq i\right]$$

$$= (1 - p_i \nu) \qquad \ldots (B8)$$

6) If the annual probability of excedence is ≤ 0.05 the distribution of I_{max} can be approximated by:

$$1 - F_{I_{max}}(i) = 1 - \exp(-p_i \nu)$$

$$= (1 - p_i \nu)$$

$$= p_i \nu \qquad \ldots (B9)$$

7) The average return period T_0 for $I \geq i$ is defined as:

$$T = \frac{1}{1 - F_{I_{max}}(i)}$$

$$= \frac{1}{p_i \nu} \qquad \ldots (B10)$$

8) The T_0 years intensity can be obtained from equation (B10) when p_i is given explicitely.

9) The contribution of the n independent sources to the intensity in a site leads to the probability of the maximum value of $I \leq i$ at the site i.e.:

$$F_{I_{max}}(i) = \prod_{j=1}^{n} F_{I_{max_j}}(i)$$

$$= \prod_{j=1}^{n} \exp(-p_i \nu)_j$$

$$= \exp(-\sum_{j=1}^{n} (p_i \nu)_j) \qquad \ldots (B\,11)$$

This result is drawn from the property of the Poisson process that says: a process made up of independent Poisson processes is a new Poisson process with average arrival rate equal to the sum of the individual rates.

10) The return period T_0 for I_{max} at the site follows from equation (B11).

Other seismic risk models

The seismic risk model proposed in [4.28] makes the same assumptions as Cornell's model except for assumptions b) and c) of the latter. This is so because the former model assumes that the total energy released during an earthquake is distributed along the ruptured zone, the slip length of which can be calculated from a semi-empirical expression which includes the magnitude of the earthquake and regional constants. It was found [4.28] that the value of the slip length affects the values of the ground motion parameters to be computed. Finally the uncertainties due to the attenuation law and the slip length expressions used were taken into consideration following the criterion underlined in [4.10,4.39] i.e. by assuming that the actual intensity is equal to the product of a random coefficient by the intensity predicted by the model. The application of the model [4.28] to a site in San Francisco, U.S. showed that the ground intensities computed with Cornell's model underestimate the actual values by a factor or two, when compared with the ones obtained by using the proposed model [4.28] specially for earthquakes of large magnitudes (the magnitudes reported in [4.28] varied from M = 7 onwards).

In [4.29] the Cornell's seismic risk model was applied taking the uncertainties in seismic source zone, activity rate ν, b value and I(MM)max value into consideration. The technique used to include the uncertainties about the mentioned parameters was done in a Bayesian context [4.10,4.27] i.e. posteriori distributions of the parameters were calculated on the basis of their associated functions and their a priori distributions. The scheme was applied

to compute the seismic risk of sites in the Eastern Coast of the U.S. and among other the following conclusions were drawn:

a) The inclusion of the uncertainties of γ and I(MM)max values caused that the I(MM) values predicted for low risks (low probability of excedence) to be insensitive to the sources used to represent the seismicity at sites located in the East Coast of the U.S.;

b) The absence of geologic or tectonic evidence which would limit the size of events in a region makes it logical and conservative to assume a uniform distribution on the I(MM)max, between the I(MM)max observed and I(MM) = XII;

c) The risks associated with a deterministic risk criterion (i.e. based on the maximum observed value in a site) vary by factors of ten or more for sites considered depending on the geometry source used.

APPENDIX C

Derivation of the probability density function $f_{y_{T_0}}$

From the assumptions made in 7.3.1 about the process $y(t)$, it follows that the cumulative distribution function of y_{T_0}, $F_{y_{T_0}}(y)$, can be expressed as [7.4] :

$$F_{y_{T_0}} = P(Y_{T_0} < y)$$

$$= \sum_{n=0}^{\infty} P(Y < y \mid N = n) \quad P(N = n) \qquad \ldots (C1)$$

where N is the random number of occurrences of the load during the period of time, T_0,

$$P(N = n) = \frac{(\nu T_0)^n \exp(-\nu T_0)}{n!} \qquad \ldots (C2)$$

ν is the mean occurrence rate of the load and

$$P(Y < y \mid N = n) = [F_Y(y)]^n \qquad n = 1,2,3\ldots$$

$$P(Y < y \mid N = n) = 0. \quad y < 0. \quad n = 0 \qquad \ldots (C3)$$

$$P(Y < y \mid N = n) = 1. \quad y > 0. \quad n = 0$$

Substituting equations (C2) and (C3) into (C1) yields:

$$F_{y_{T_0}} = \exp\{-\nu T_0 [1 - F_Y(y)]\} + [H(y) - 1] \exp(\nu T_0) \qquad \ldots (C4)$$

where the step function, $H(y)$, is nil for $y < 0$ and one for $y > 0$. From equation (C4) the probability density function $f_{y_{T_0}}(y)$ is obtained, i.e.:

$$f_{y_{T_0}} = \nu T_0 \, f_{y_T}(y) \exp\{-\nu T_0 [1 - F_{y_T}(y)]\}$$

$$+ \delta(y) \exp(-\nu T_0) \qquad \ldots (C5)$$

where the probability density and the cumulative distribution functions, $f_{y_T}(y)$ and $F_{y_T}(y)$ of the process y during time T are Raleigh distributed, i.e.:

$$f_{y_T}(y) = \frac{y}{\sigma_y^2} \exp\left(-\frac{y^2}{2\sigma_y^2}\right) \qquad \ldots (C6)$$

$$F_{y_T}(y) = \int_0^y \frac{y_1}{\sigma_y^2} \exp\left(-\frac{y_1^2}{2\sigma_y^2}\right) dy_1 \qquad \ldots \text{(C7)}$$

where y_1 is a dummy variable; in equation (C5) $\delta(y)$ is the Dirac delta function associated to a spike of unit area at $y = 0$. By substituting equations (C6) and (C7) into equation (C5) the following result is obtained:

$$f_{y_{T_0}}(y) = \nu T_0 \left[\frac{y}{\sigma_y^2} \exp\left(-\frac{y^2}{2\sigma_y^2}\right) \exp\left\{-\nu T_0 \exp\left(-\frac{y^2}{2\sigma_y^2}\right)\right\}\right] \qquad \ldots \text{(C8)}$$

The actual evaluation of p and q, equations (7.25) and (7.26) respectively, can be carried out by substituting equation (C8) into them.

Expected ground motion parameter y	Period T sec.	b_1	b_2	b_3	Coefficient of variation of y
a_{max} cm/sec^2		472.3	0.278	1.301	0.548
v_{max} cm/sec.		5.64	0.401	1.202	0.696
d_{max} cm		0.393	0.434	0.885	0.883
	0.1	10.090	0.233	1.341	0.651
	0.15	45.350	0.197	1.408	0.639
	0.2	31.450	0.226	1.323	0.577
	0.3	27.780	0.290	1.416	0.560
	0.4	11.630	0.333	1.309	0.628
	0.5	5.740	0.356	1.197	0.591
2.54 S_v cm/sec.	0.6	2.350	0.415	1.171	0.609
	0.8	1.245	0.415	1.020	0.635
ξ = 0.05	1.0	0.432	0.399	0.704	0.703
	1.5	0.132	0.439	0.574	0.837
	2.0	0.122	0.466	0.675	0.941
	3.0	0.0934	0.485	0.709	1.007
	4.0	0.0728	0.520	0.788	1.191
	5.0	0.0706	0.557	0.938	1.193
	6.0	0.1045	0.483	0.806	1.173
	8.0	0.1475	0.435	0.767	0.976

Table 4.1 Values of coefficients b_i, i=1,2,3 for the attenuation law $y = b_1 \, 10^{b_2 M} (R + 25)^{-b_3}$ and values of the coefficient of variation of y [4.16]

Seismic zone / Magnitude M	3 Fennoscandia	10 U.K. & Ireland	3 Fennoscandia	10 U.K. & Ireland
	depth $h \leq 50$ Km.		depth $h > 50$ Km.	
4.1 - 4.6	24	18	0	0
4.7 - 5.1	26	5	0	0
5.2 - 5.6	7	5	1	0
5.7 - 6.2	1	1	0	2
6.3 - 6.7	1	0	0	0
6.8 - 7.2	0	0	0	0
7.3 - 7.7	0	0	0	0
7.8 - 8.2	0	0	0	0

Table 4.2 Record of magnitudes M for earthquakes occurred in seismic zones 3 and 10 during period 1901-1955 [4.16]

Seismic zone	a	b	Observations
3	6.08*	0.97*	M>4.1,Eye fitting [4.6]
10	4.40*	0.76*	M>4.1,Eye fitting [4.6]
3 and 10	6.13*	0.96*	M>4.1,Eye fitting [4.6]
3	5.96 ± 1.32*	0.95 ± 0.23*	M>4.1,Least squares [4.25]
10	6.82*	1.10*	M>4.1, Maximum likelihood [4.25]
3		1.04*	M>4.1,Eye fitting [4.25]
10		0.82*	M>4.1,Eye fitting [4.25]
U.K.	4.13**	1.09**	3.25 < M < 5.5, Least squares [4.35]
Great Glen	2.9**	0.95**	3.25 < M < 5.5, Least squares [4.35]

Table 4.3 Values of a and b ($\log_{10} N = a - bM$) for different seismic zones (* period 1901-1955), (** period 1800-1970)

Seismic Source j	Number of earthquakes observed in source j	ν_j Type of Seismicity				β_j (b = 0.96)	m_{oj}	h_j (Km.)
		Observed	Assumed Low	Assumed Intermediate	Assumed High			
1			0.018	0.127	0.163	2.208	4.1	15
2	7	0.127				2.208	4.1	50
3	1	0.018				2.208	4.1	15
4	9	0.163				2.208	4.1	15
5			0.018	0.127	0.163	2.208	4.1	15
6	6	0.109				2.208	4.1	15
7			0.018	0.127	0.163	2.208	4.1	15
8 point source	1	0.018				2.208	4.1	50
9 line source	6	0.109				2.208	4.1	30

Table 4.4 Values of seismic parameters of sources shown in fig. 4.7 : average rate of earthquake occurrence per year ν_j ; β value; m_o value; depth of source h ; period of observation 1901-1955 [4.6] [4.25]^j

Number of Towers	D A T A
4	1) Height of caisson = 61 m. 2) Width of caisson = 80 m. 3) Length of tapered shape of towers = 70 m. 4) Length of parallel shape of towers = 45 m. 5) Maximum diameter of towers = 20 m. 6) Minimum diameter of towers = 12 m. 7) Maximum thickness of towers = 0.9 m. 8) Minimum thickness of towers = 0.4 m. 9) Tower spacing = 30 m.
2	From 1) to 9) (except 2)) the same as for the 4 tower platform 10) Height to bottom of platform deck = 175 m. 11) Equivalent diameter of caisson = 64 m. 12) Mass of caisson and content = 12,500 (Ton-s^2)/m. 13) Mass of deck and equipment = 1,250 (Ton-s^2)/m. 14) Mass density of reinforced concrete = 2.5 Ton/m^3 15) Mass density of sea water = 1.0 Ton/m 16) Coefficient of fluid added mass for caisson = 1.0 17) Coefficient of fluid added mass for towers = 1.0 18) Coefficient of fluid inertia = 2.0 19) Water depth = 145 m. 20) Towers filled with water up to mean sea water level

Table 8.1 Geometrical characteristics of the selected concrete gravity platform

Parameter	$(W_{19.5})_{max}$ (m/sec)	$\overline{W}_{19.5}$ (m/sec)	$\sigma W_{19.5}$ (m/sec)	$W^{+}_{19.5}$ (m/sec)	$W^{-}_{19.5}$ (m/sec)
$H_{max_{(m)}} = 26$	25.7	27.20	3.29	30.49	23.91
$(T_z)_{max_{(sec)}} = 13.4$	20.6	21.80	2.64	24.44	19.16

Table 8.2 Values of statistical estimates of wind velocity at the platform site, $W_{19.5}$, for a 12 hour storm (fully developed sea) and a return period of 50 years.

$\overline{W}_{19.5}$ = mean value of $W_{19.5}$

$\sigma W_{19.5}$ = standard deviation of $W_{19.5}$

$W^{+}_{19.5} = \overline{W}_{19.5} + \sigma W_{19.5}$

$W^{-}_{19.5} = \overline{W}_{19.5} - \sigma W_{19.5}$

Structural Response	Parameters Considered	Coefficient of Variation			
		Values of Shear Modulus, G_s (Ton/m^2)			
		5,000	7,500	10,000	15,000
u_Q	E_c	.0393	.0464	.0604	.0449
	ξ_c	.5742	.5402	.5212	.5090
	Q	.9147	.9155	.9183	.9167
	E_c, ξ_c, Q	2.9686	2.9207	2.9282	2.8519
u_W	E_c	.0977	.0908	.0830	.0705
	ξ_c	0.0	0.0	0.0	0.0
	W	.2979	.2962	.2933	.2871
	E_c, ξ_c, W	1,0147	.9996	.9807	.9479

Table 8.3 Influence of the uncertainties about E_c, ξ_c and about the seismic and wave excitations on the structural responses of the c.g.p. as measured by the coefficient of variation, C.V.

u_Q = deck displacement for seismic excitation
u_W = deck displacement for wave excitation

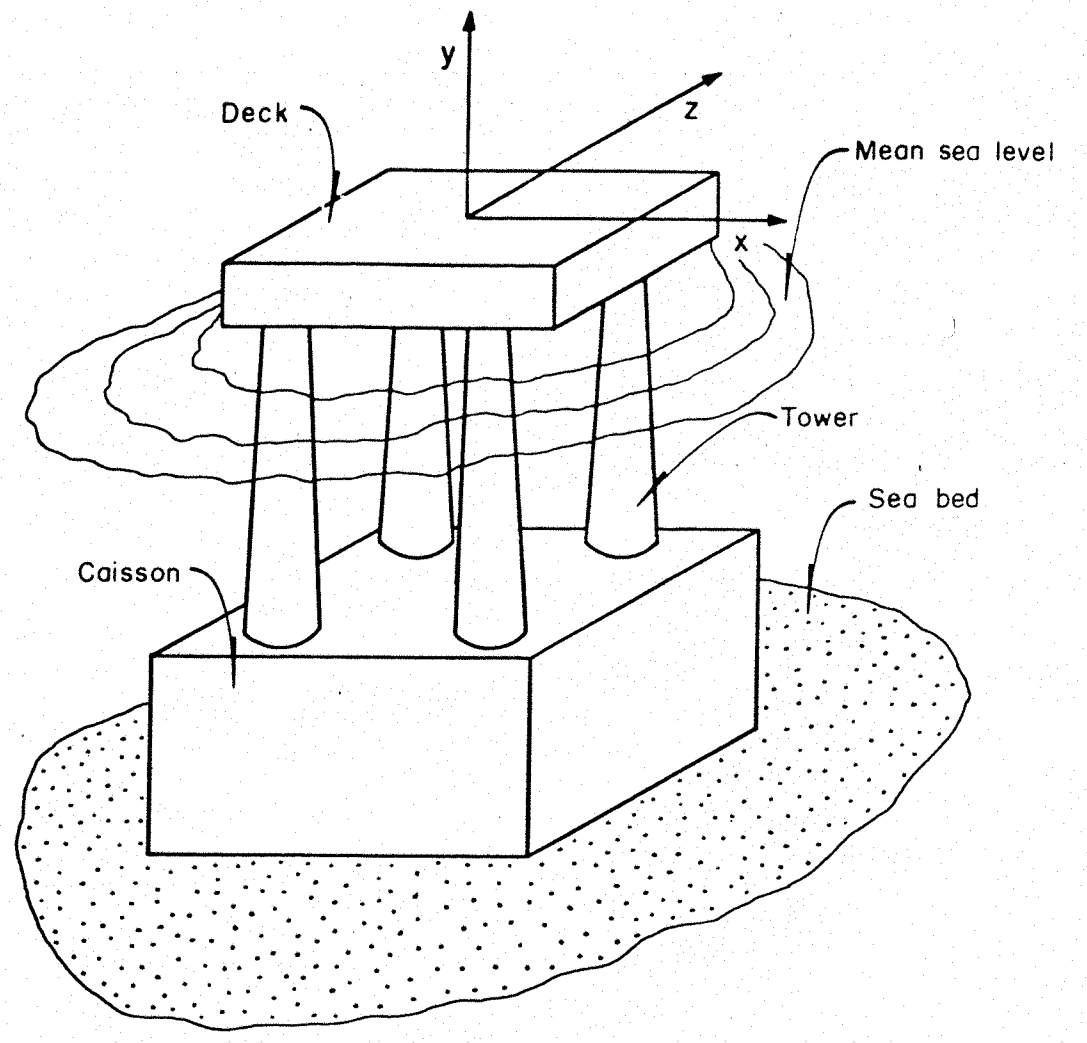

Fig. 2.1 Schematic representation of a four-tower concrete gravity platform

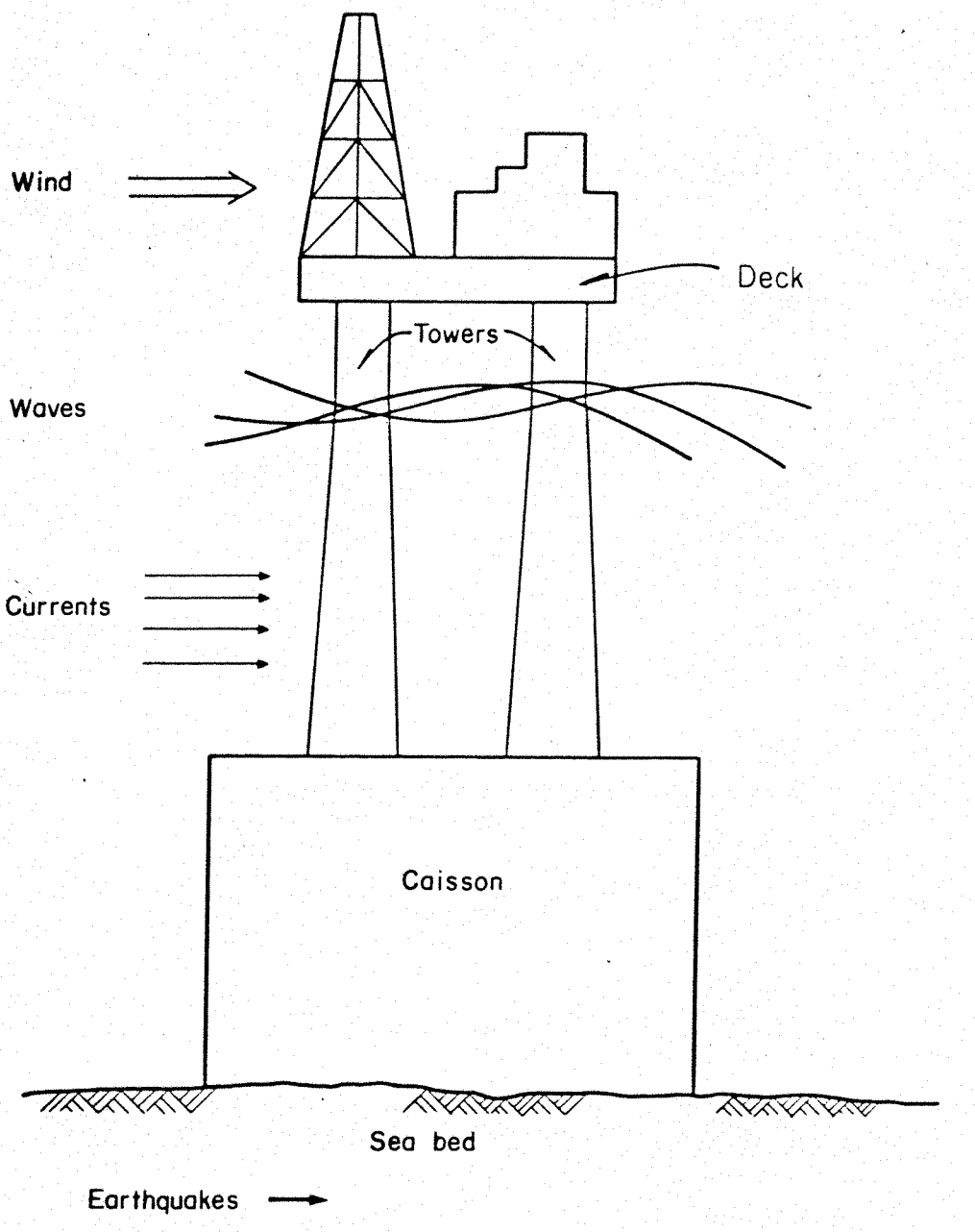

Fig. 2.2 Environmental loads acting on a concrete gravity platform

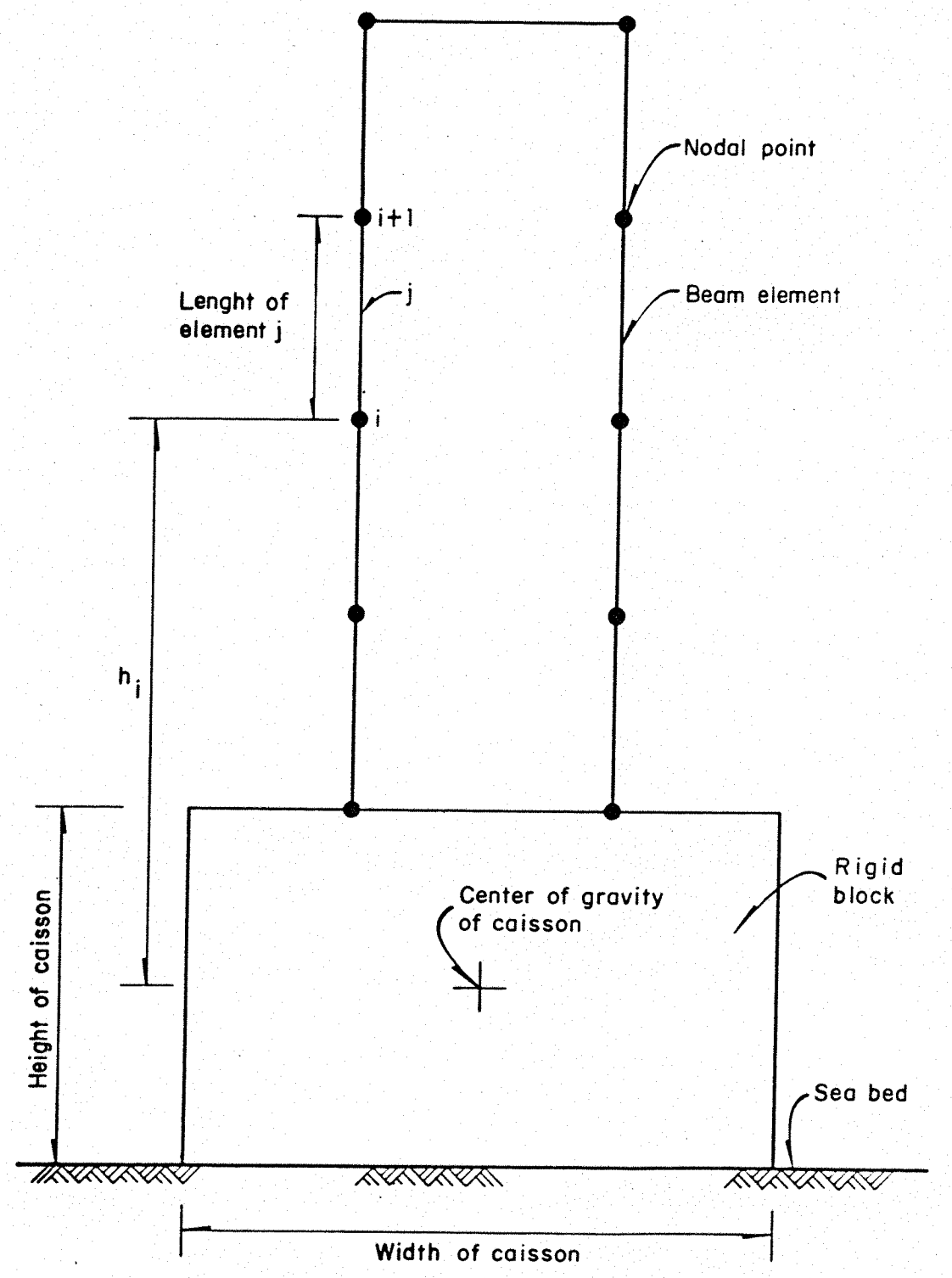

Fig. 2.3 Finite element idealization of a concrete gravity platform

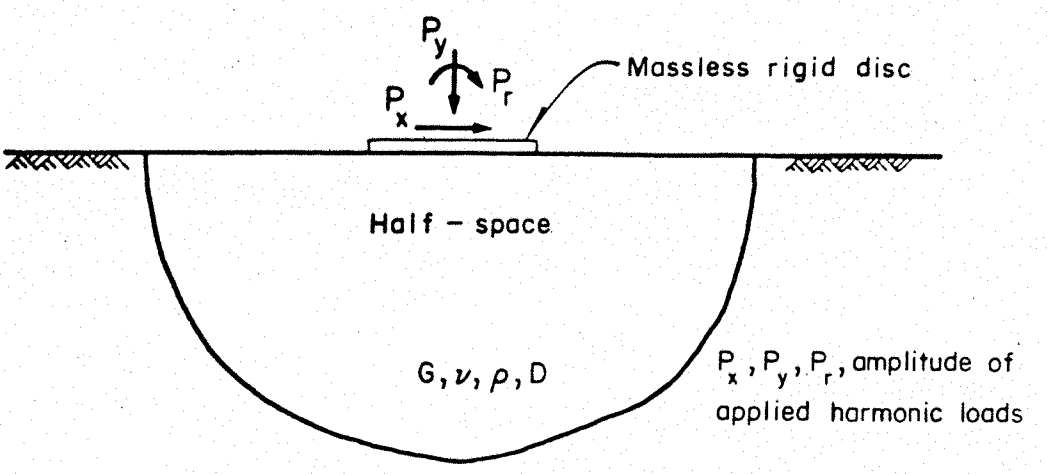

Fig. 3.1 Continuum modelling of a soil-foundation system

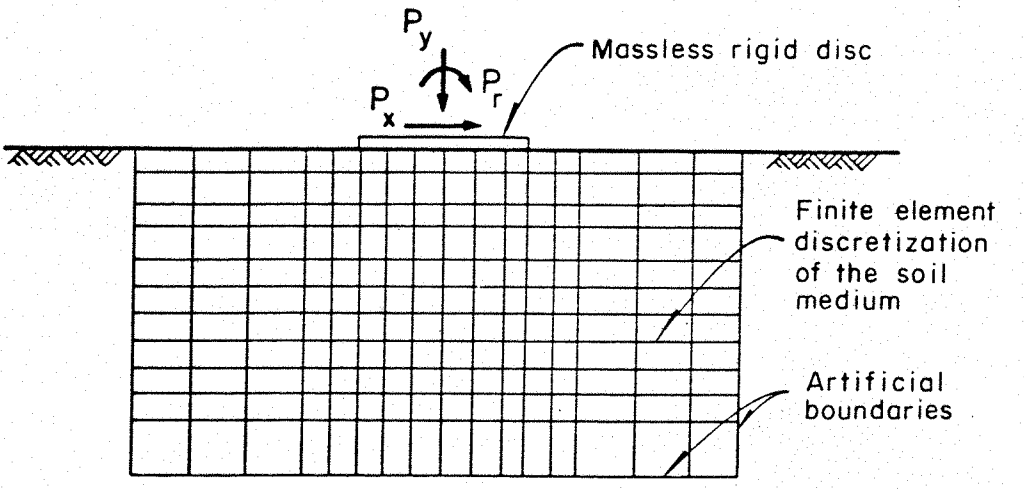

Fig. 3.2 Finite element modelling of a soil-foundation system

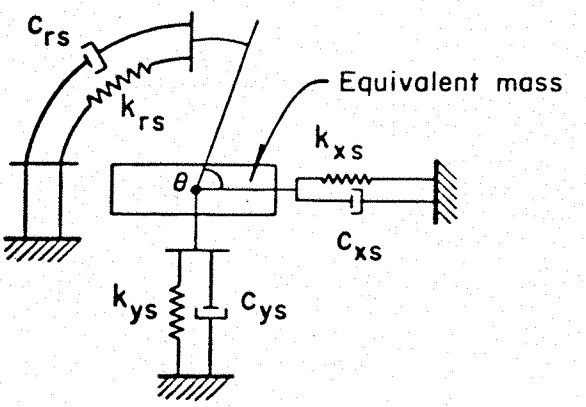

Fig. 3.3 Soil-foundation interaction model

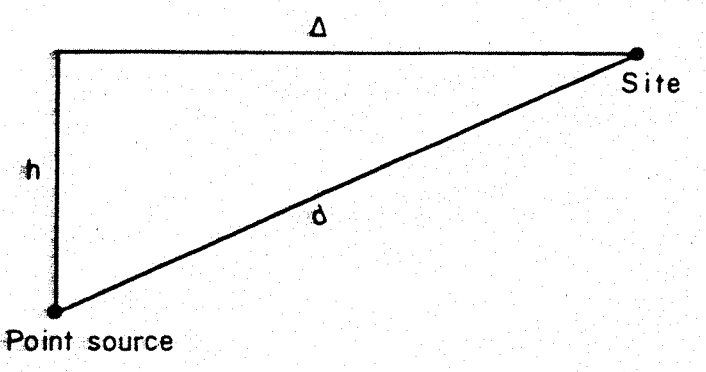

Fig. 4.1 Point source cross-section

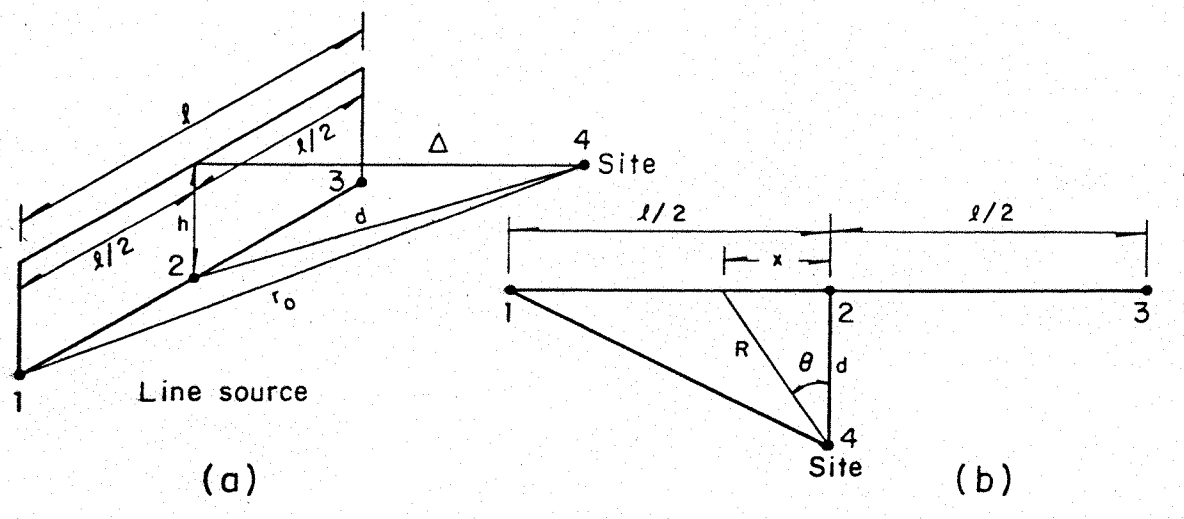

Fig. 4.2 Line source: a) perspective, b) plant

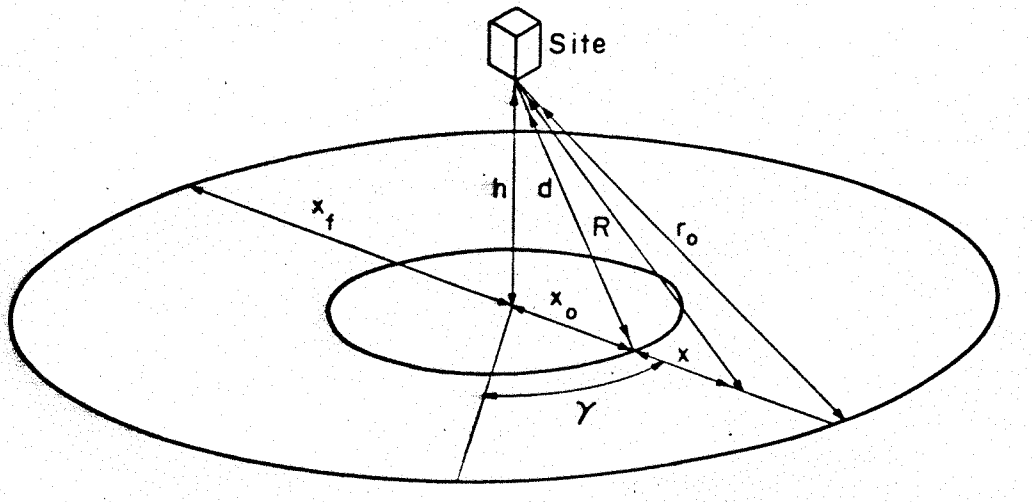

Fig. 4.3 Areal source, perspective

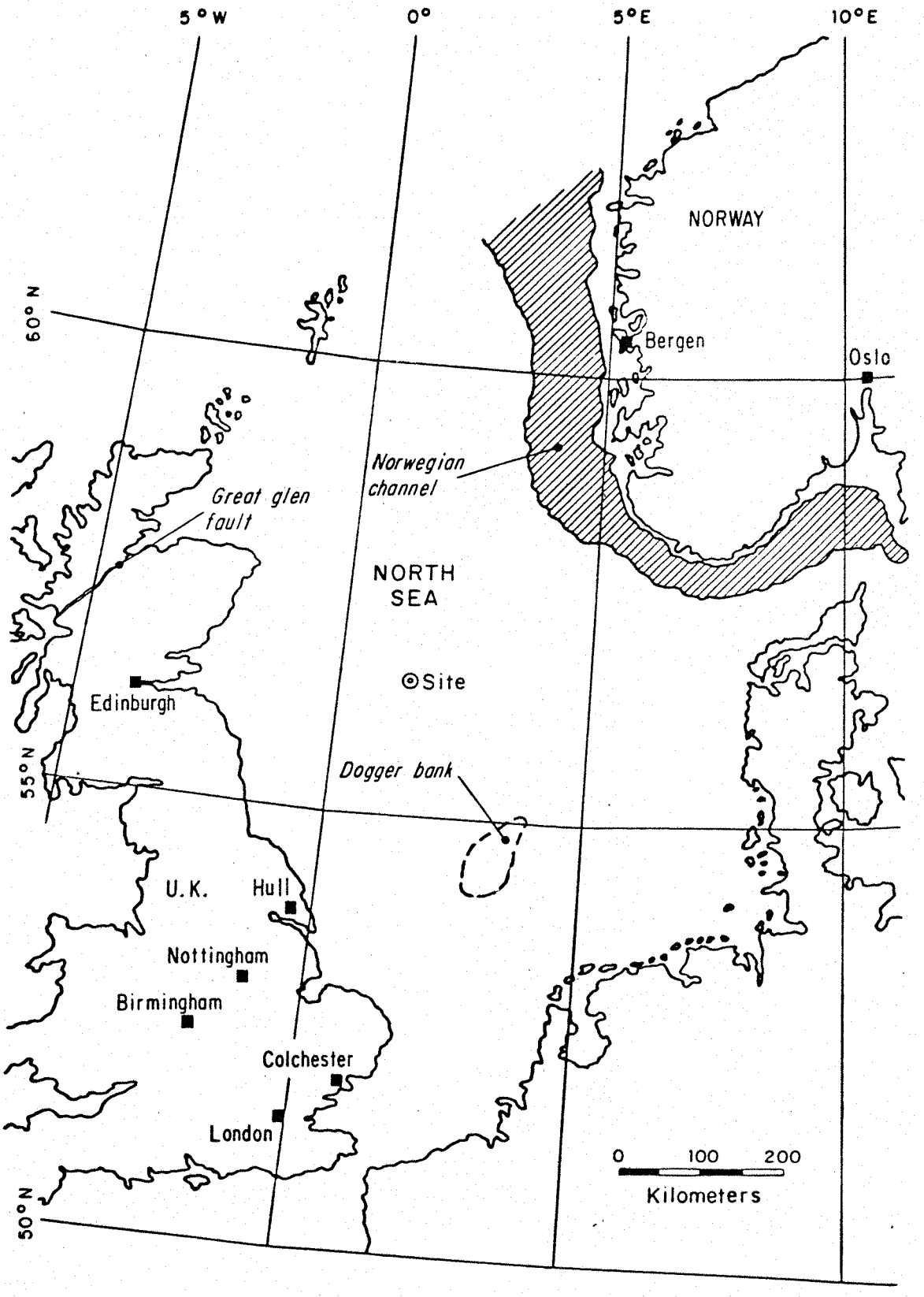

Fig. 4.4 North Sea site used for seismic risk analysis

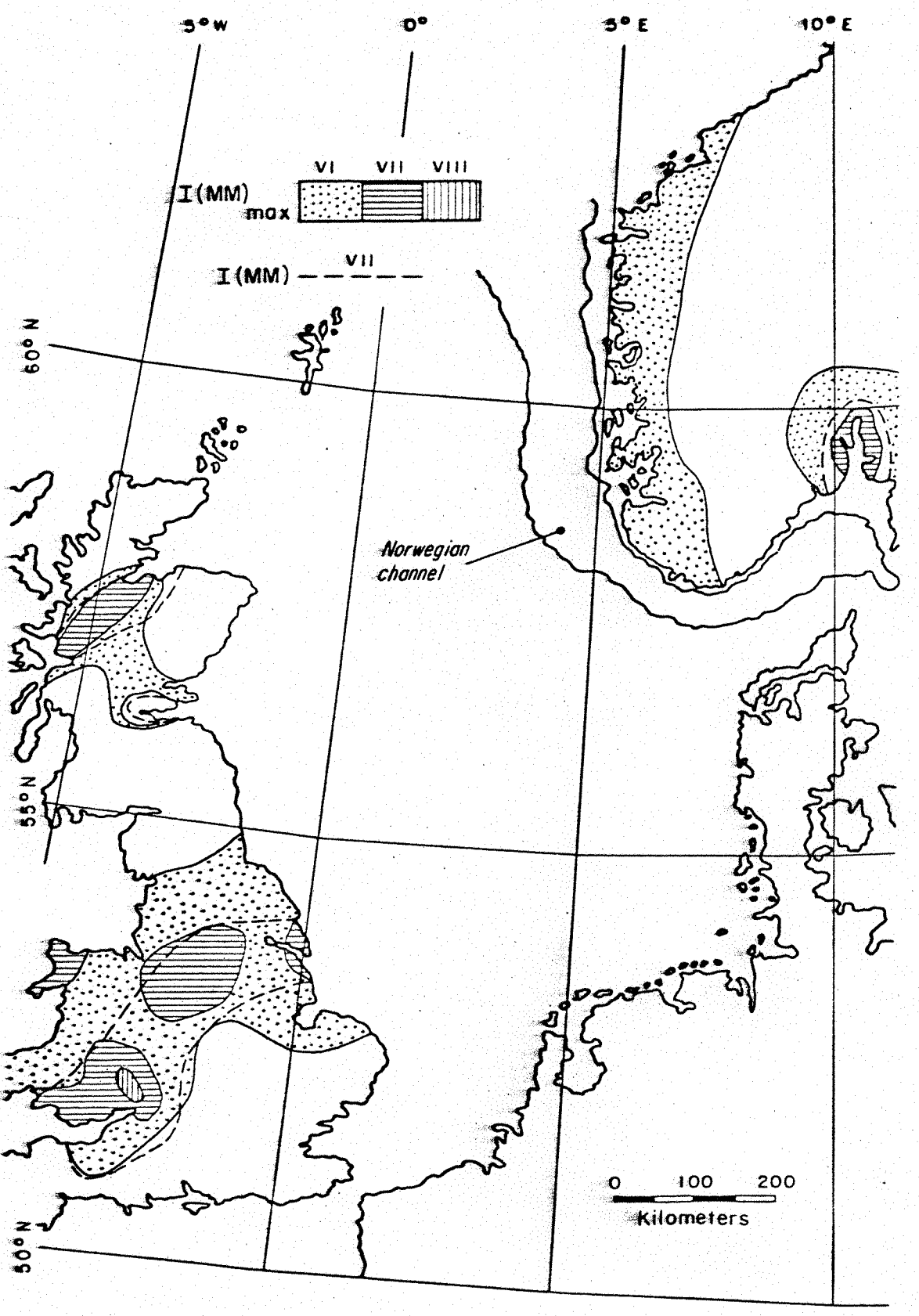

Fig. 4.5 Map of isoseismals and I(MM)max observed during the period 1901-1955 in Norway and the U.K. [4.25]

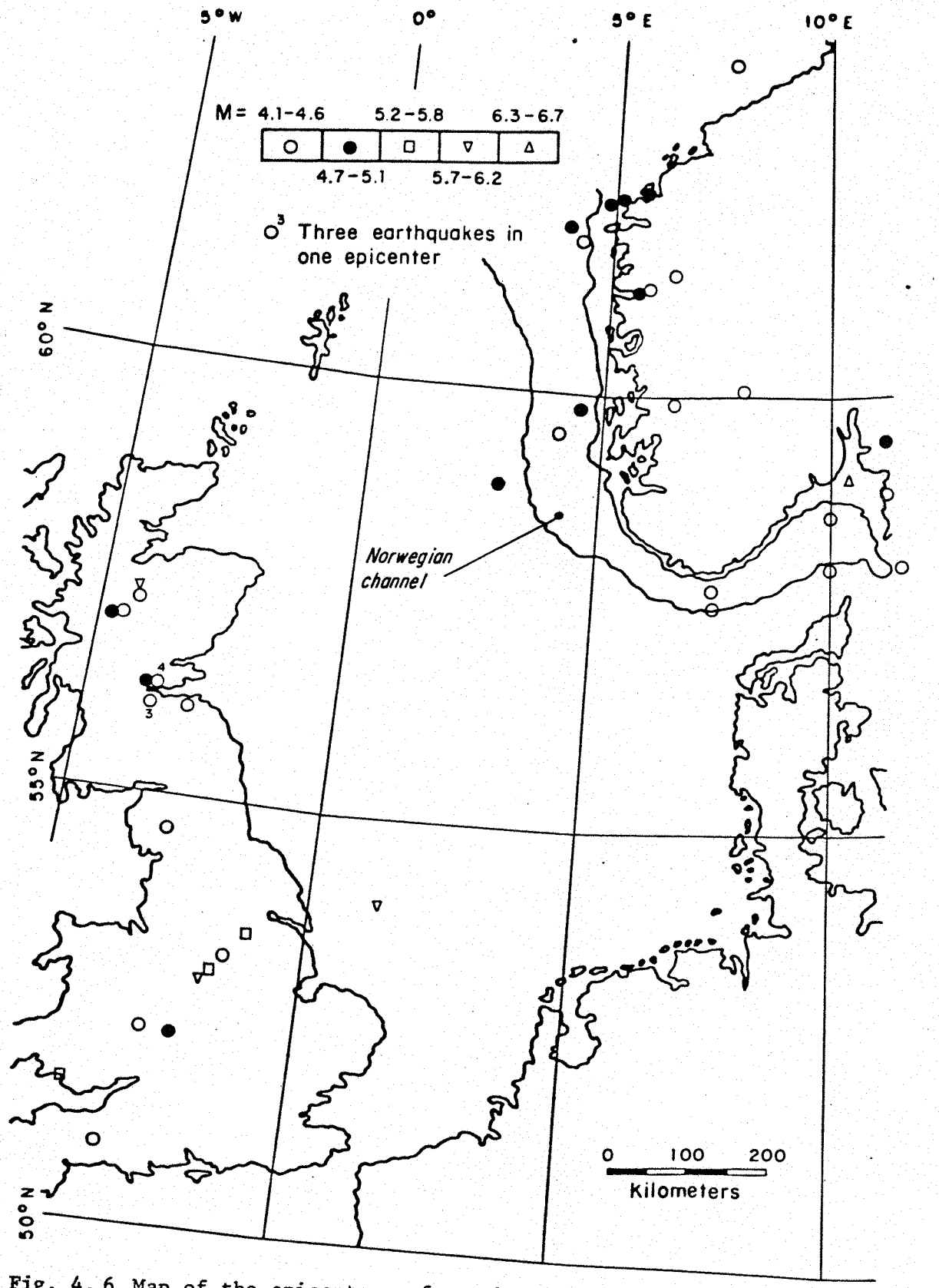

Fig. 4.6 Map of the epicenters of earthquakes observed during the period 1901–1955 in Norway, the U.K. and the North Sea [4.25]

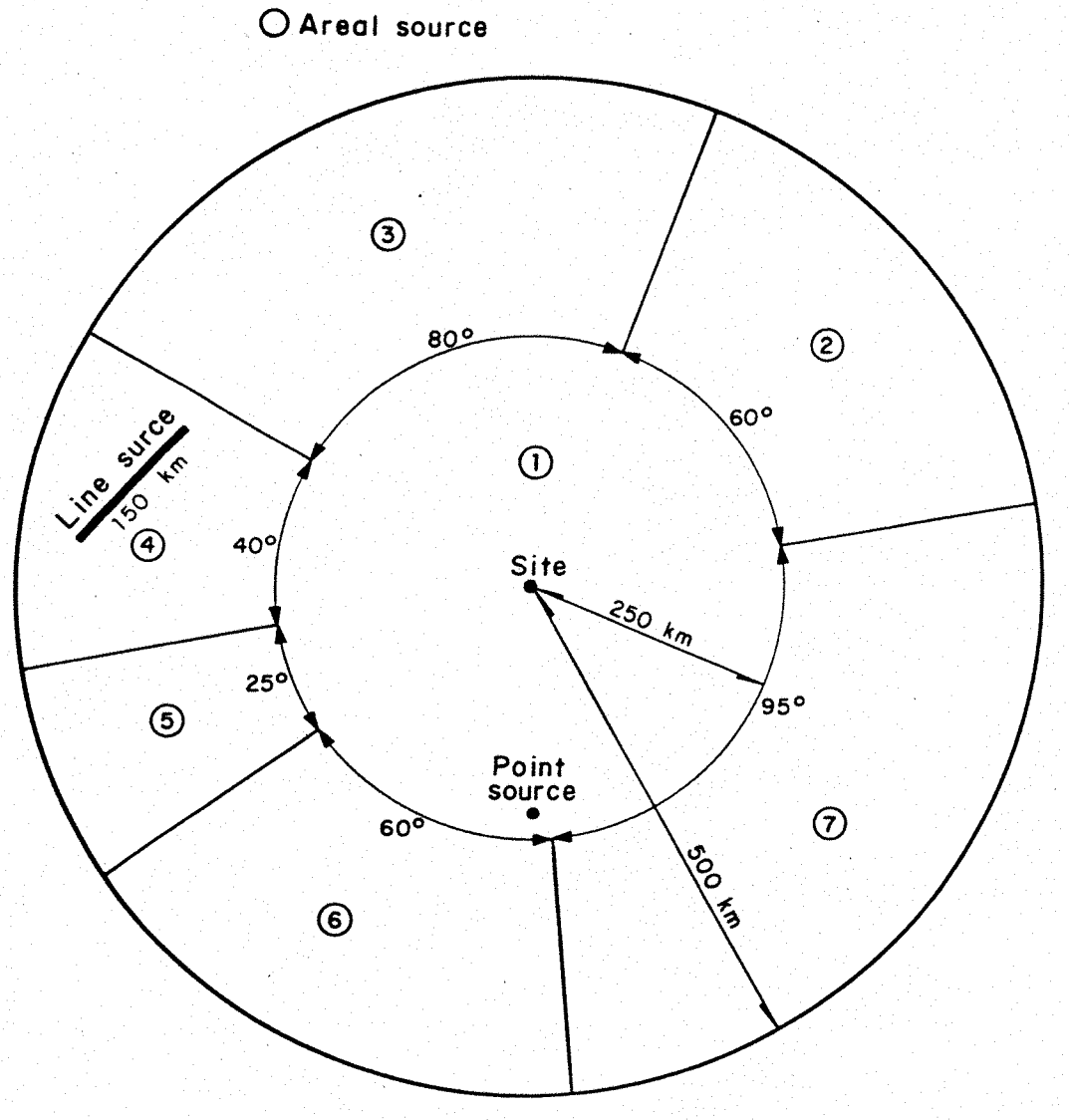

Fig. 4.7 Seismic sources contributing to the seismic risk of the site

a = wave amplitude
c = " celerity
D = " depth
H = 2a = wave height

η = wave ordinate
$\lambda = 2\pi/\kappa$ = wave length
κ = wave number
Deep waters condition $D/\lambda \geq 1/2$

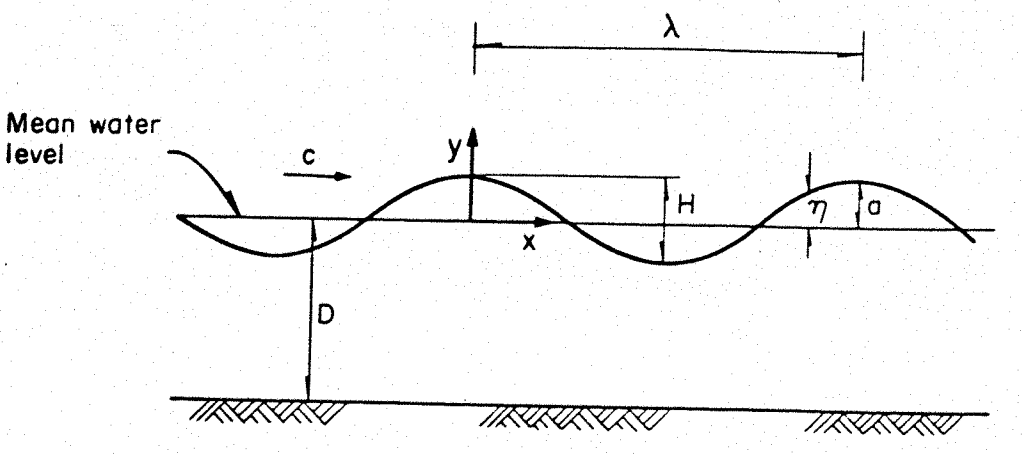

Fig. 5.1 Wave parameters used in the linear wave theory

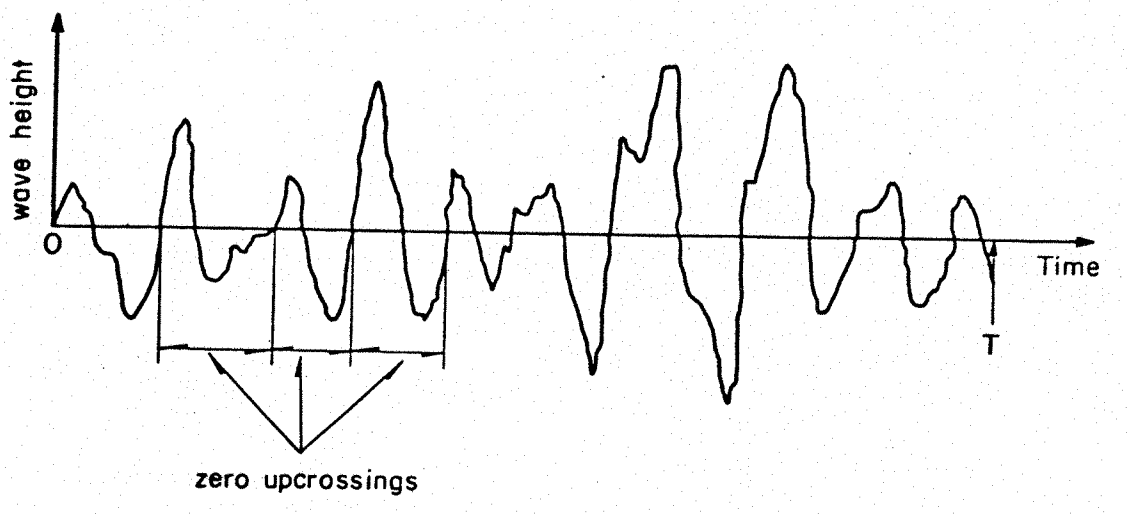

Fig. 5.2 Typical wave record

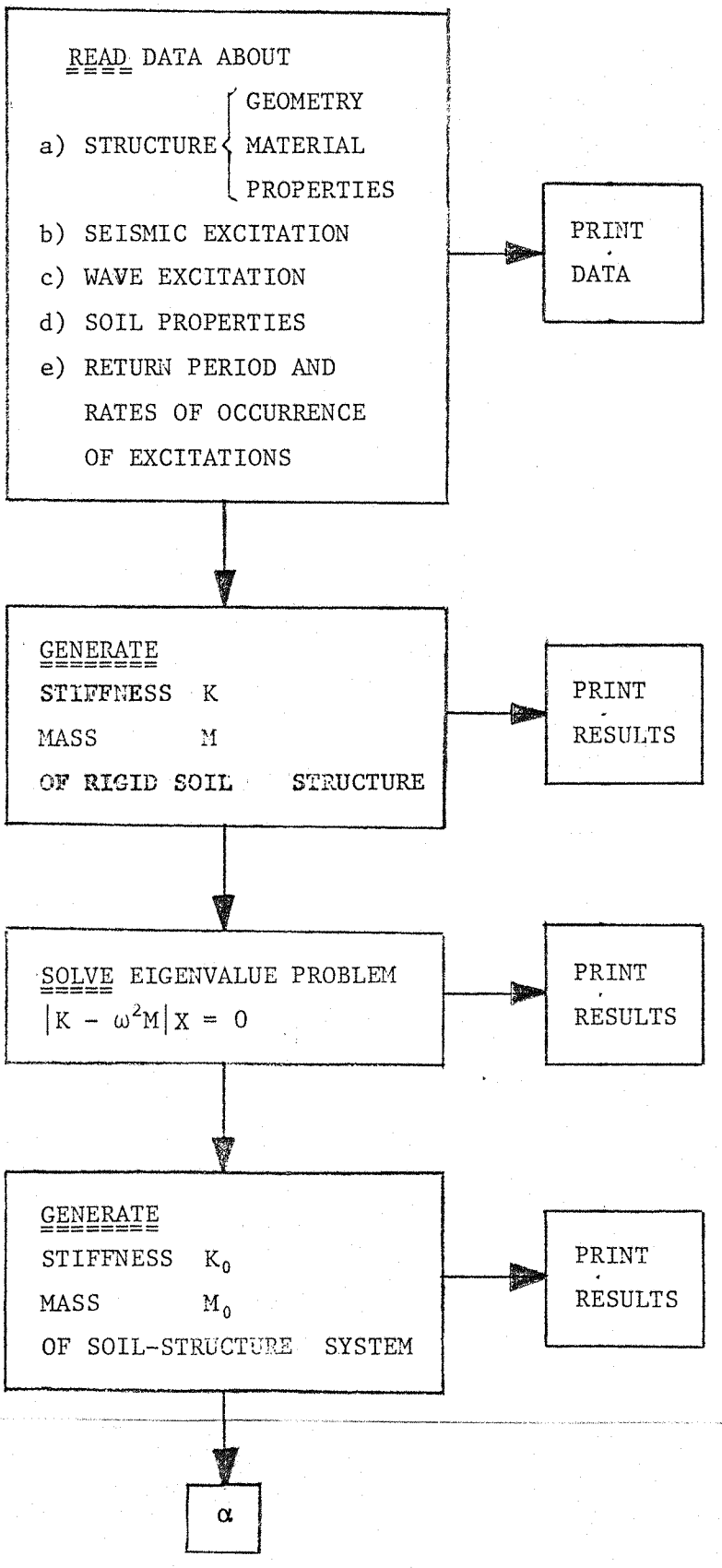

Fig. 8.1 Block diagram of computer program

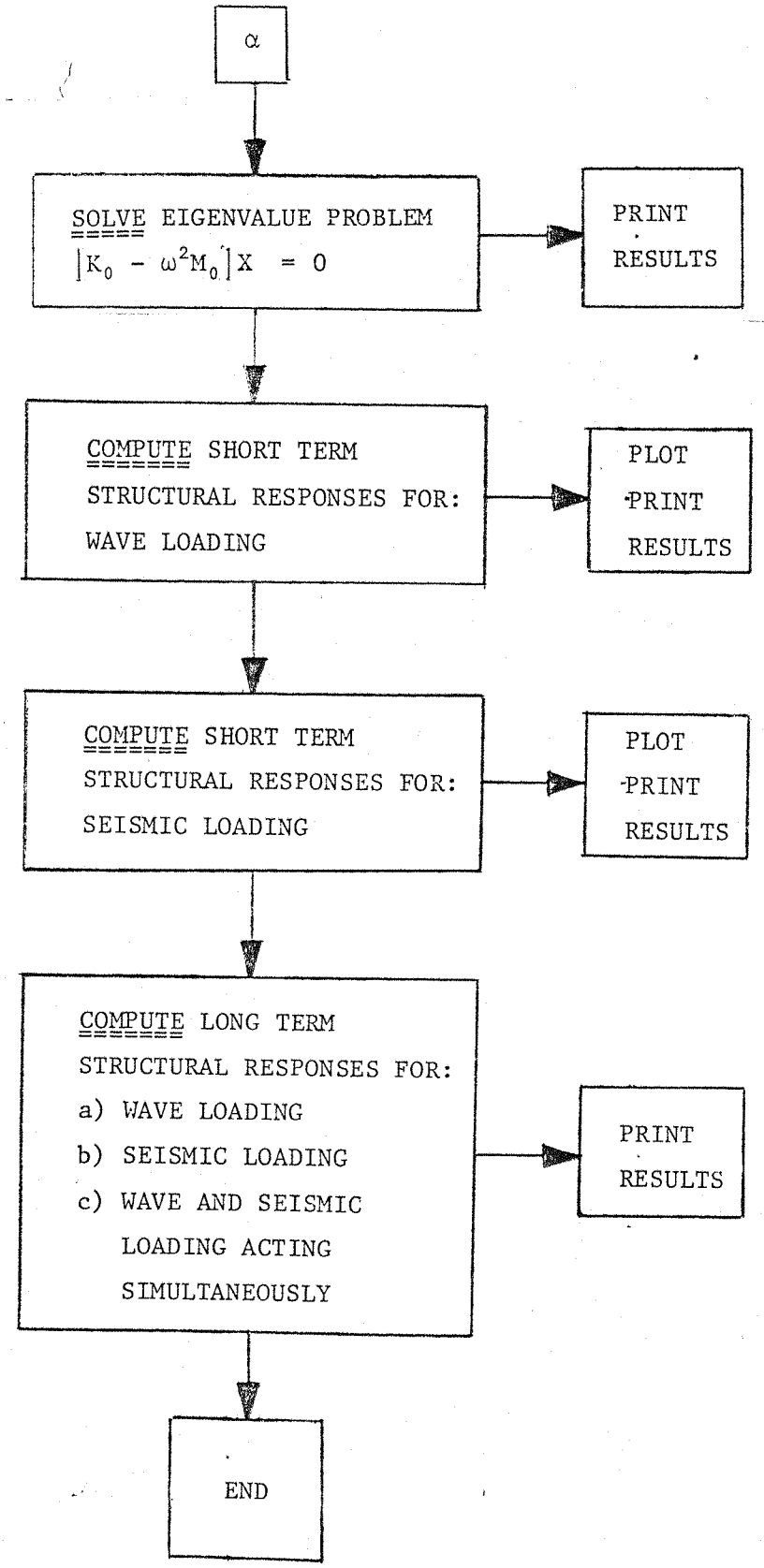
α
SOLVE EIGENVALUE PROBLEM
$[K_0 - \omega^2 M_0]X = 0$
PRINT
RESULTS
COMPUTE SHORT TERM
STRUCTURAL RESPONSES FOR:
WAVE LOADING
PLOT
PRINT
RESULTS
COMPUTE SHORT TERM
STRUCTURAL RESPONSES FOR:
SEISMIC LOADING
PLOT
PRINT
RESULTS
COMPUTE LONG TERM
STRUCTURAL RESPONSES FOR:
a) WAVE LOADING
b) SEISMIC LOADING
c) WAVE AND SEISMIC
LOADING ACTING
SIMULTANEOUSLY
PRINT
RESULTS
END

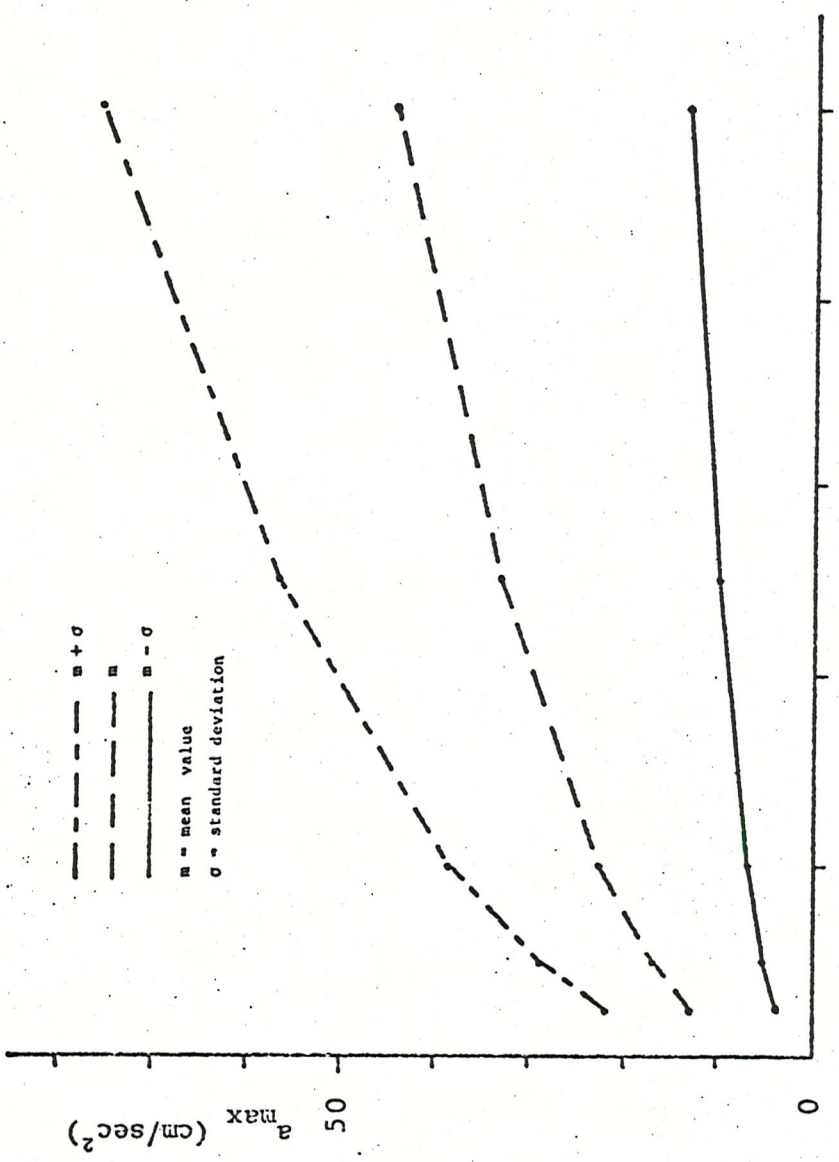

Fig. 8.2 Ground acceleration in the site, a_{max}, as a function of the return period, T_o

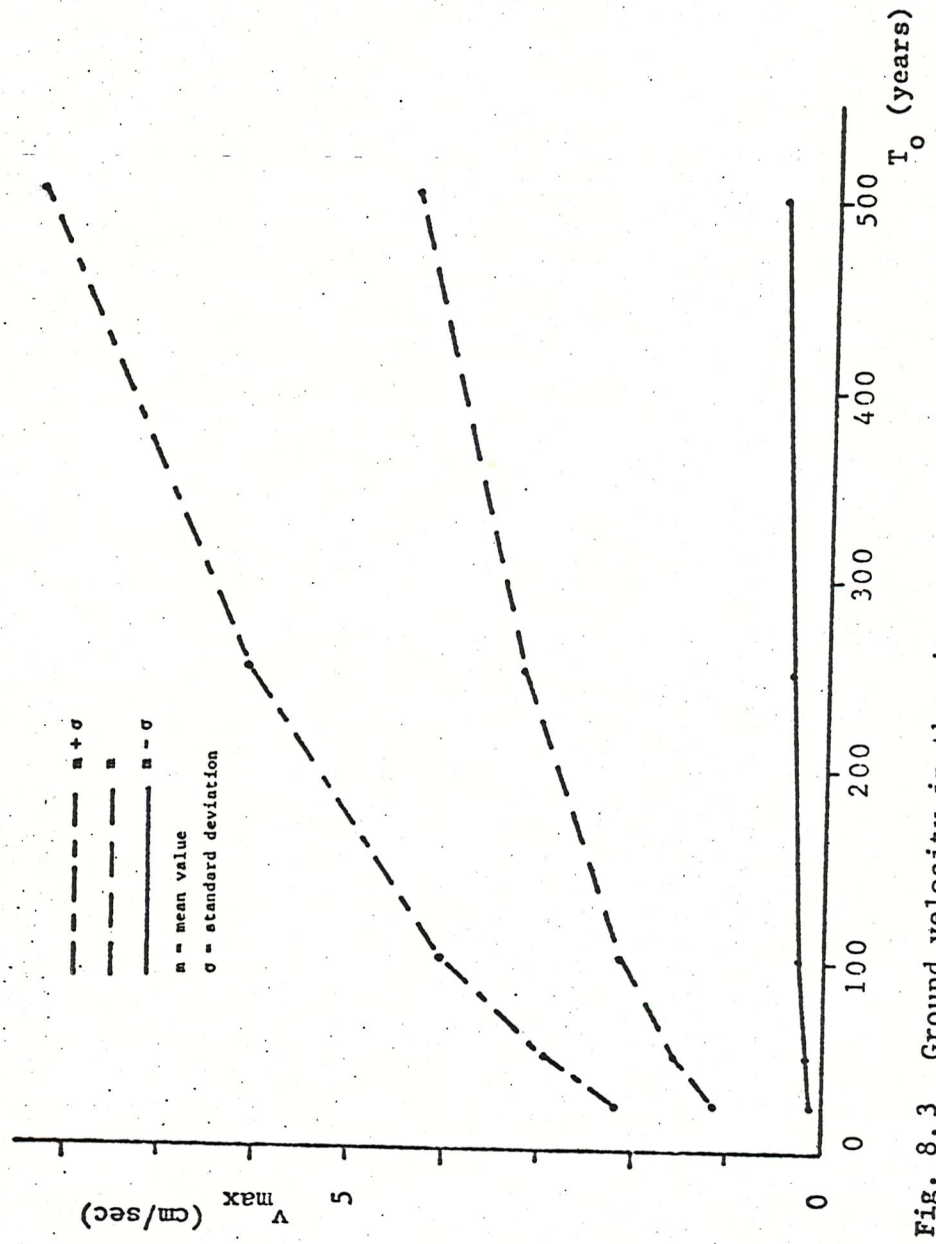

Fig. 8.3 Ground velocity in the site, v_{max} , as a function of the return period, T_o

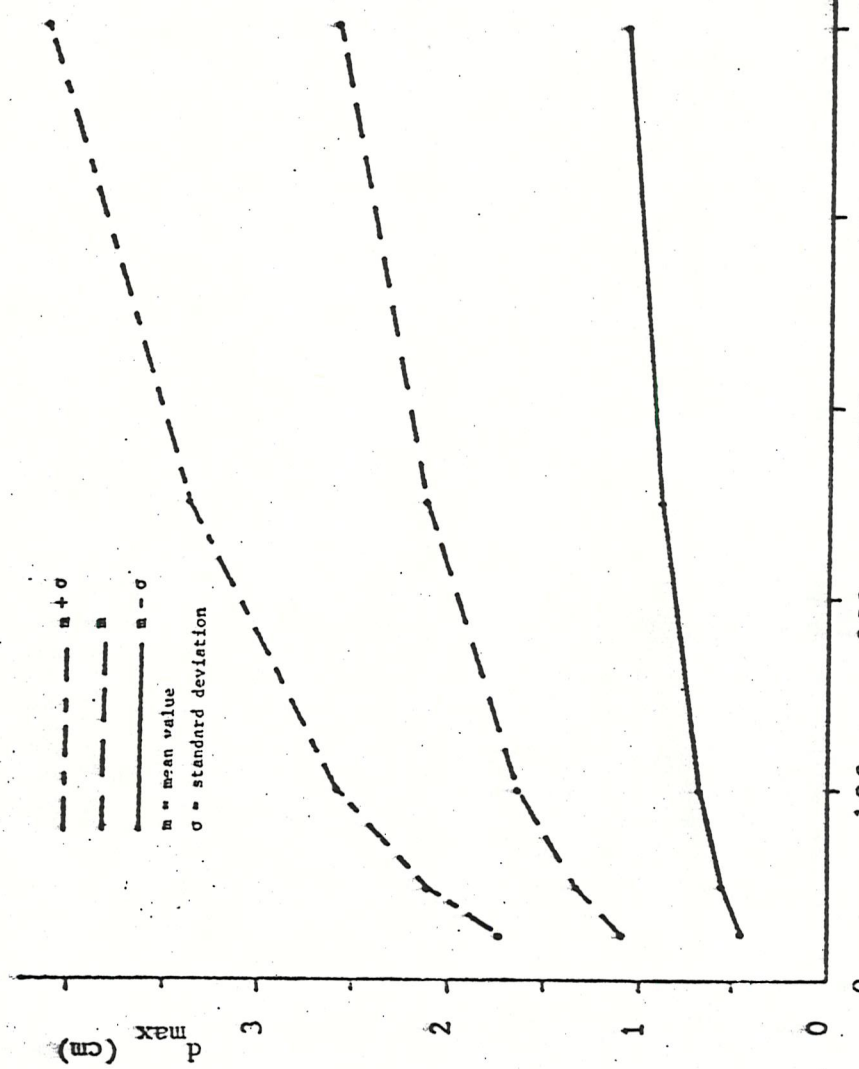

Fig. 8.4 Ground displacement in the site, d_{max}, as a function of the return period, T_o

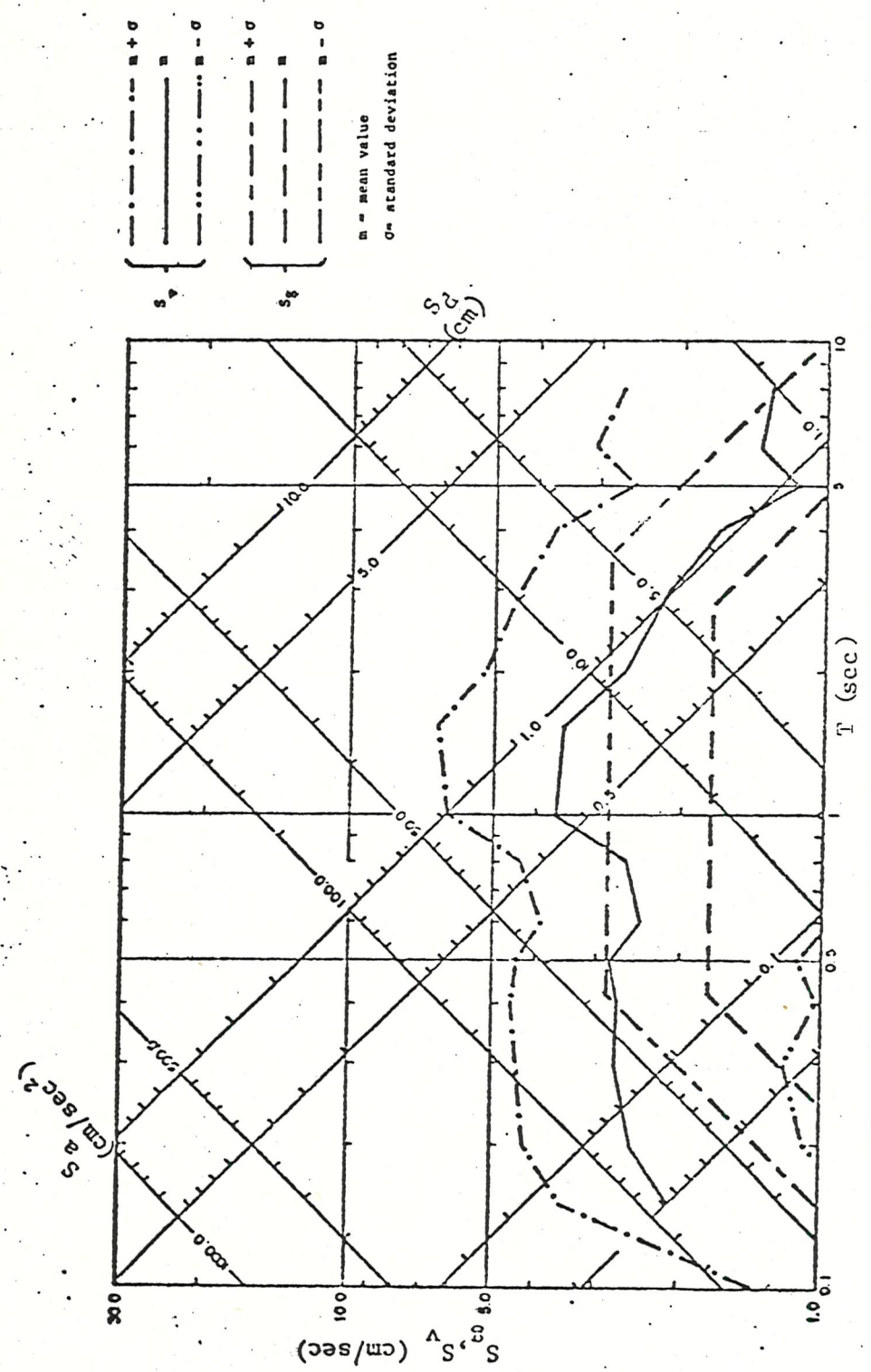

Fig. 8.5 Ground and pseudovelocity spectra, S_g , S_v , for a return period of 50 years, as a function of period, T (ξ=0.05)

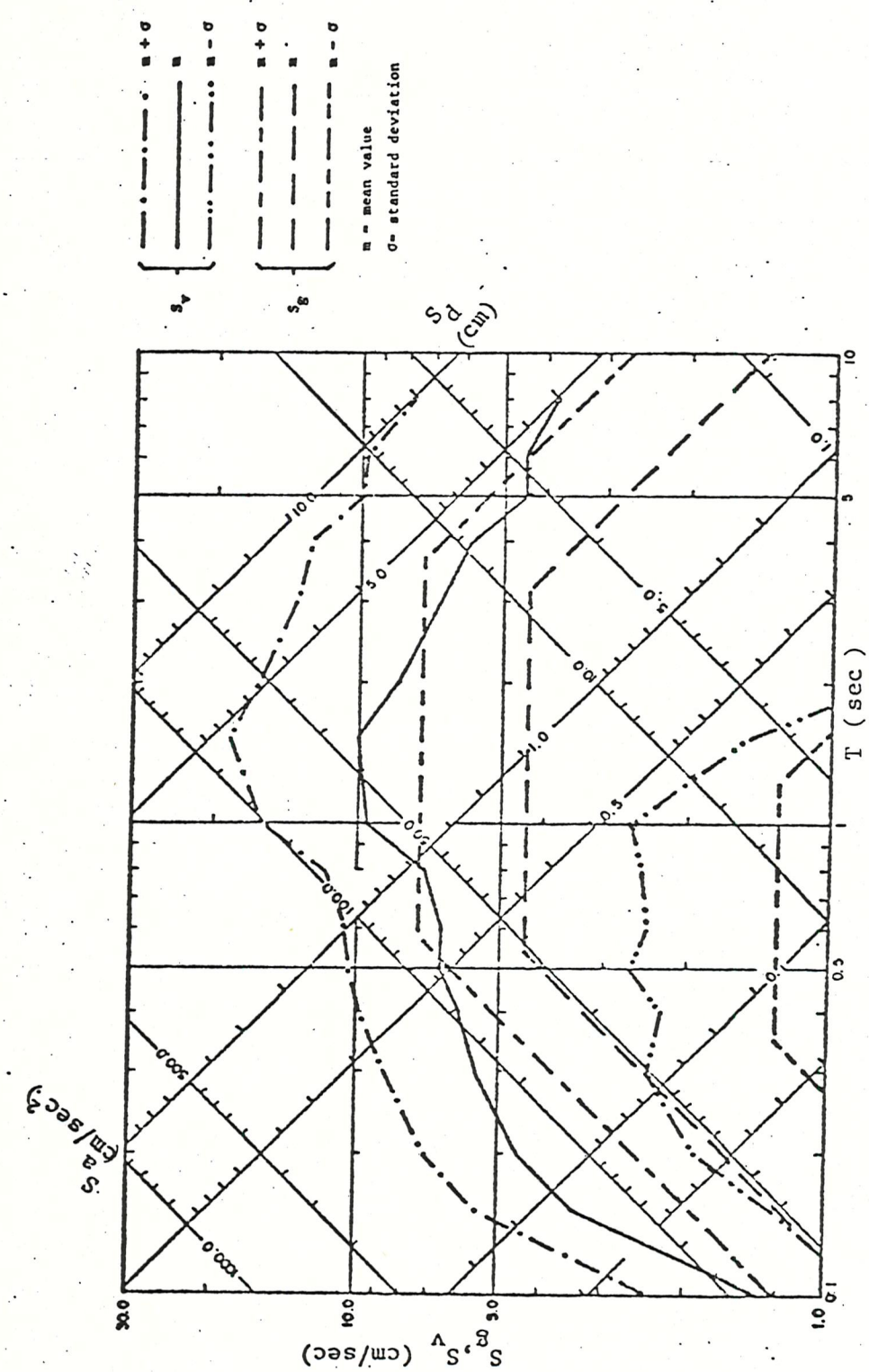

Fig. 8.6 Ground and pseudovelocity spectra, S_g , S_v , for a return period of 500 years as a function of period, T $(\xi=0.05)^g$

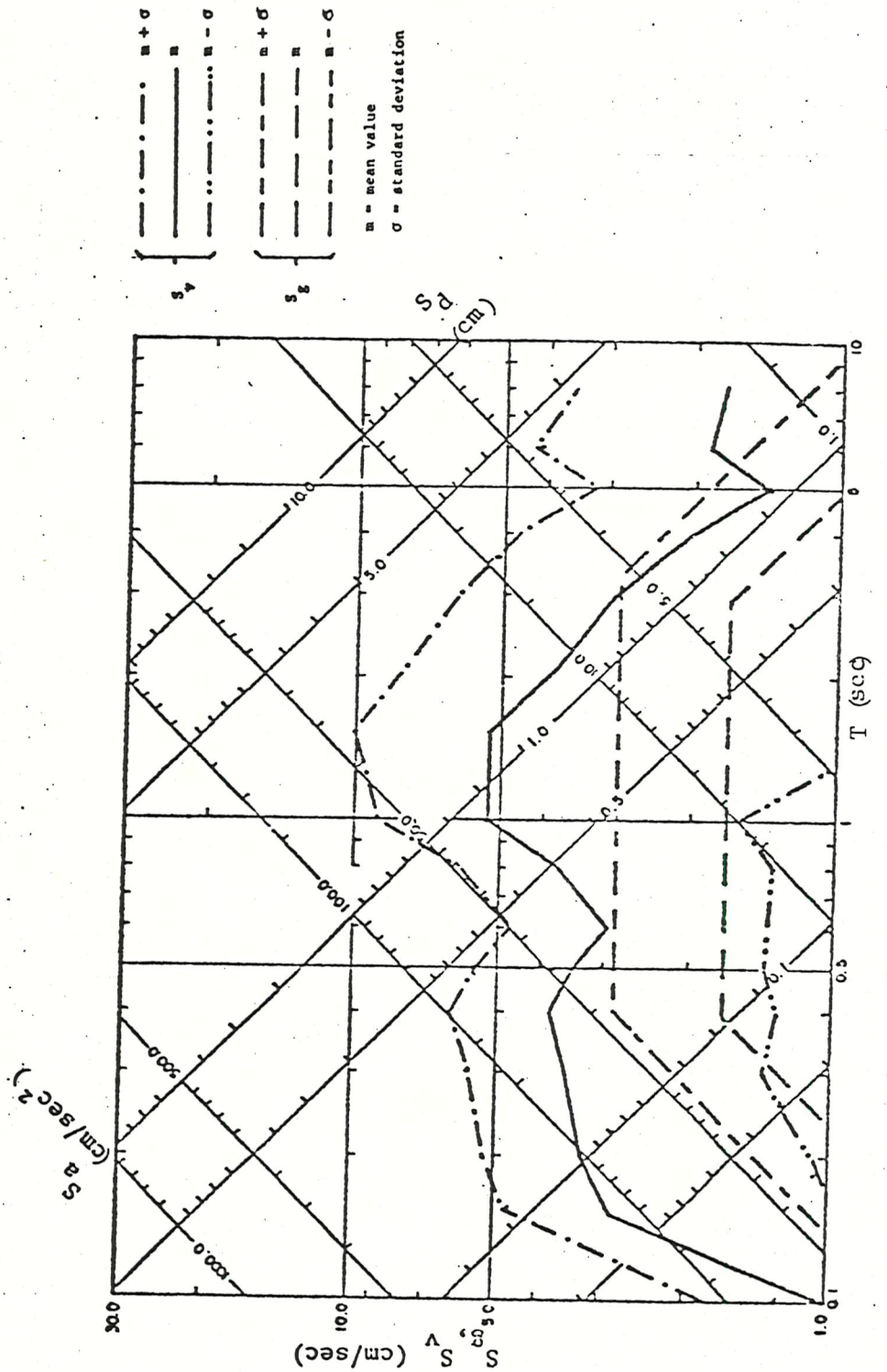

Fig. 8.7 Ground and pseudovelocity spectra, S_g , S_v , for a return period of 50 years, as a function of period, T (ξ=0.02)

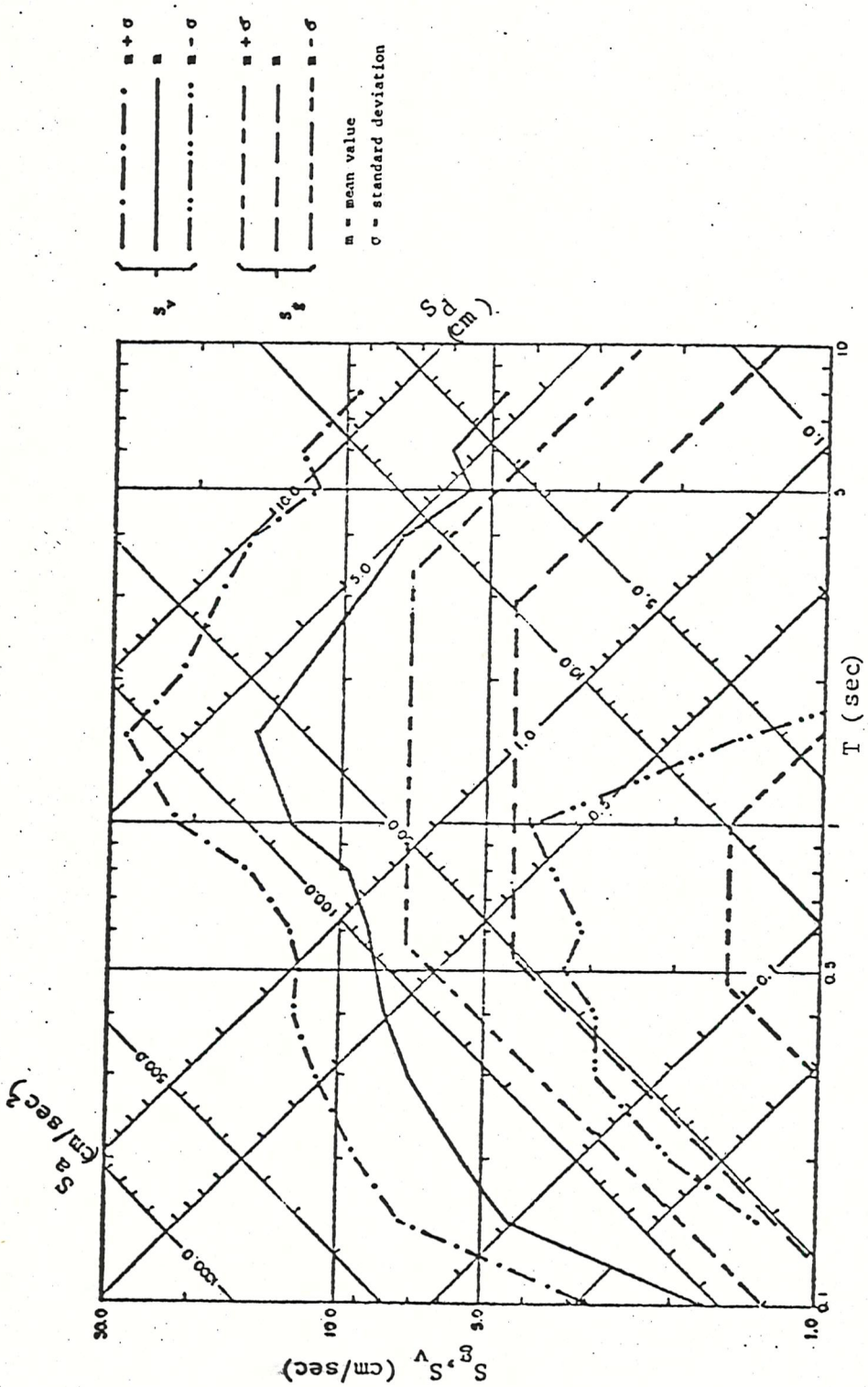

Fig. 8.8 Ground and pseudovelocity spectra, S_g , S_v , for a return period of 500 years, as a function of period, T (ξ=0.02)

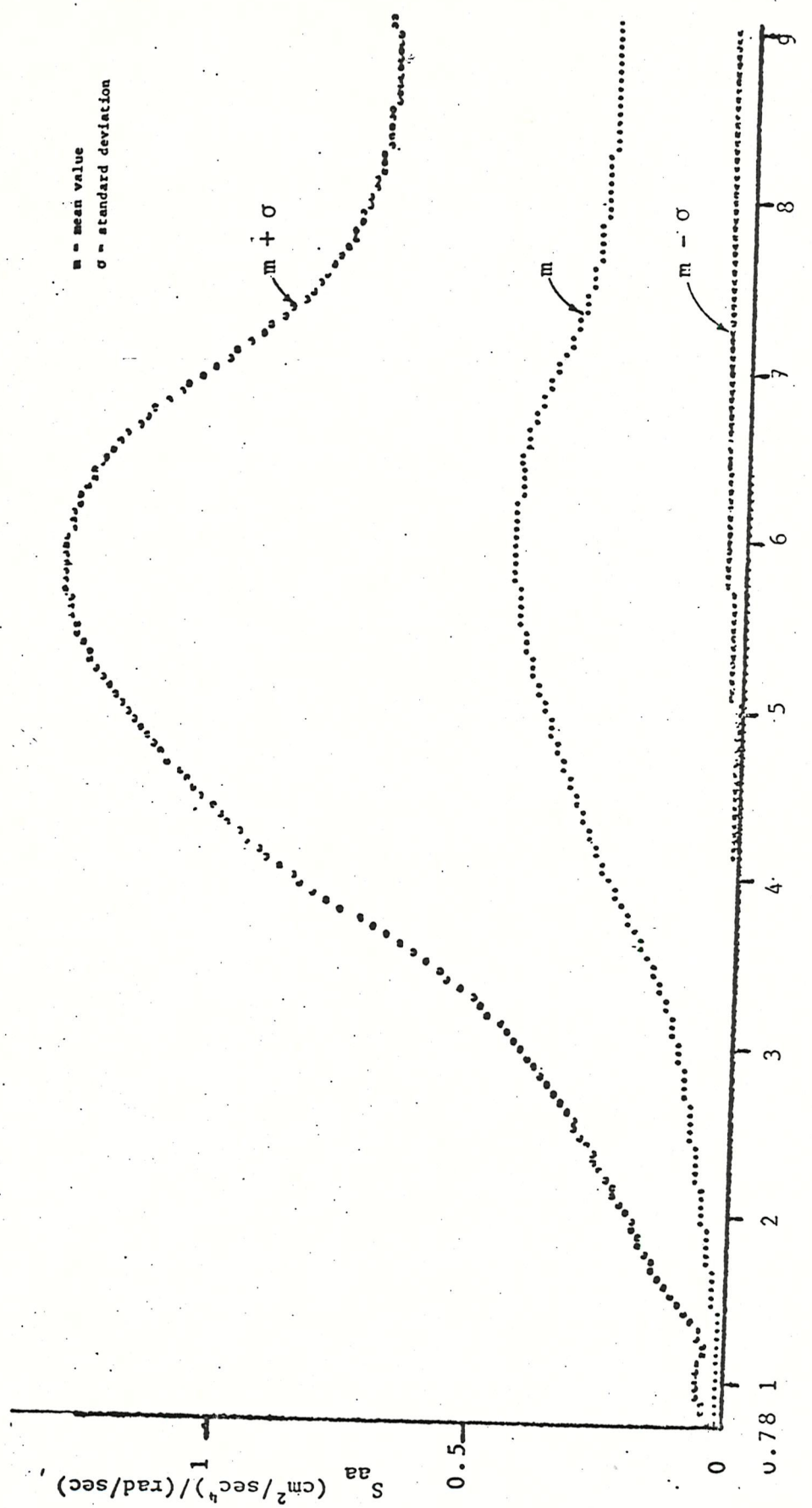

Fig. 8.9 P.s.d.f. of ground acceleration, S_{aa}, for a return period of 50 years (ξ=0.05), as a function of frequency, ω

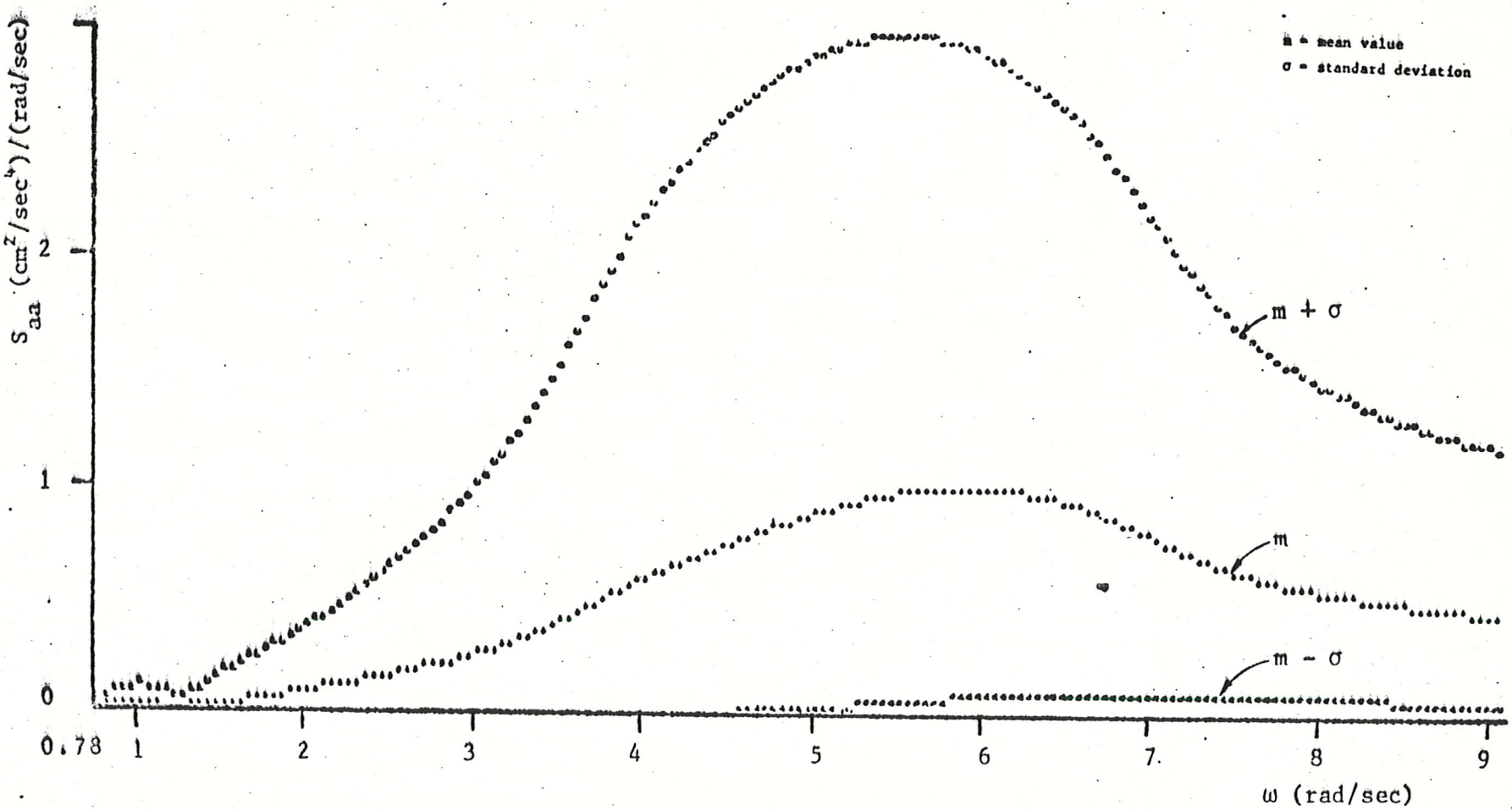

Fig. 8.10 P.s.d.f. of ground acceleration, S_{aa}, for a return period of 50 years (ξ=0.02), as a function of frequency, ω

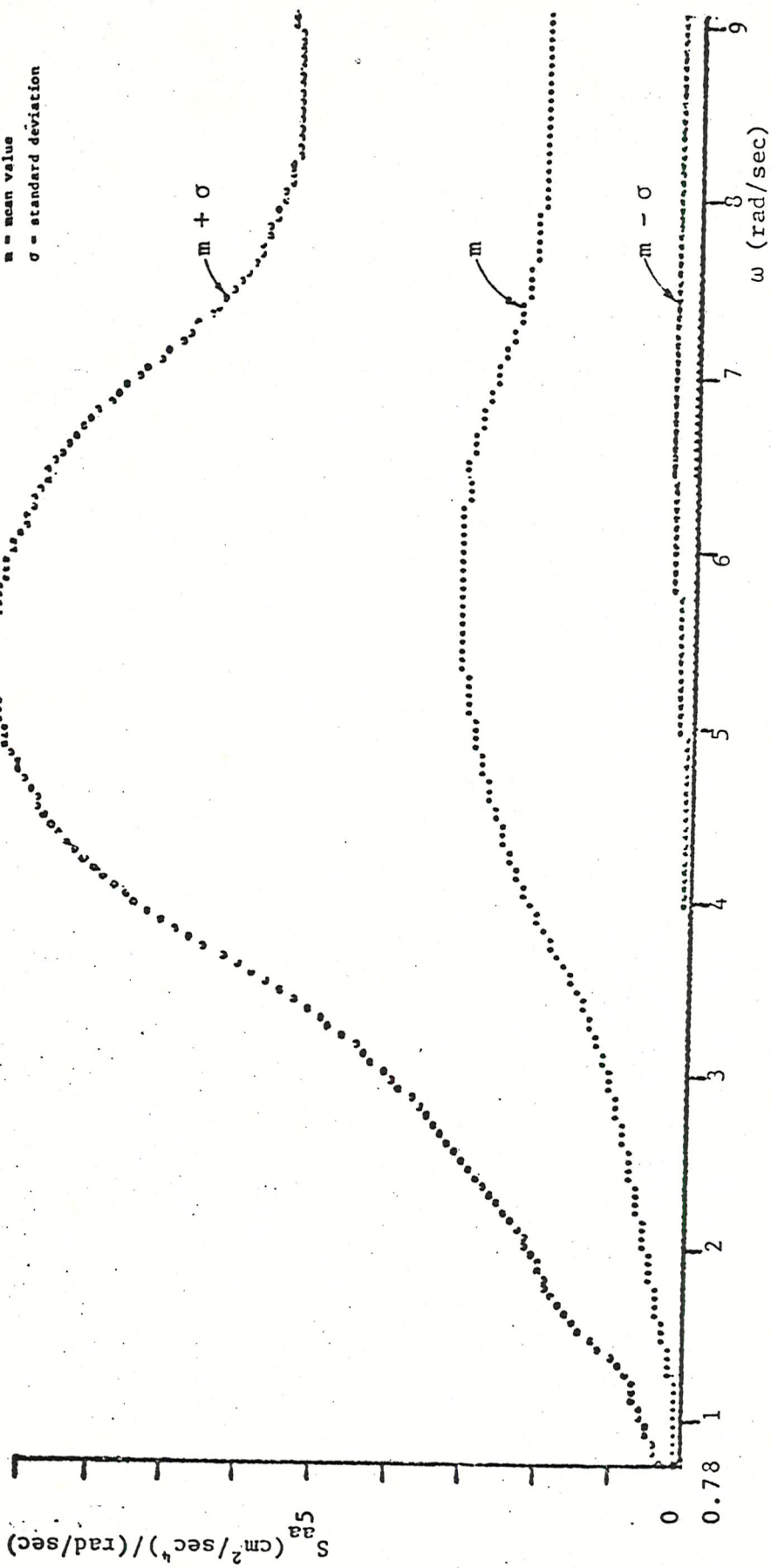

Fig. 8.11 P.s.d.f. of ground acceleration, S_{aa}, for a return period of 500 years (ξ=0.05), as a function of frequency, ω

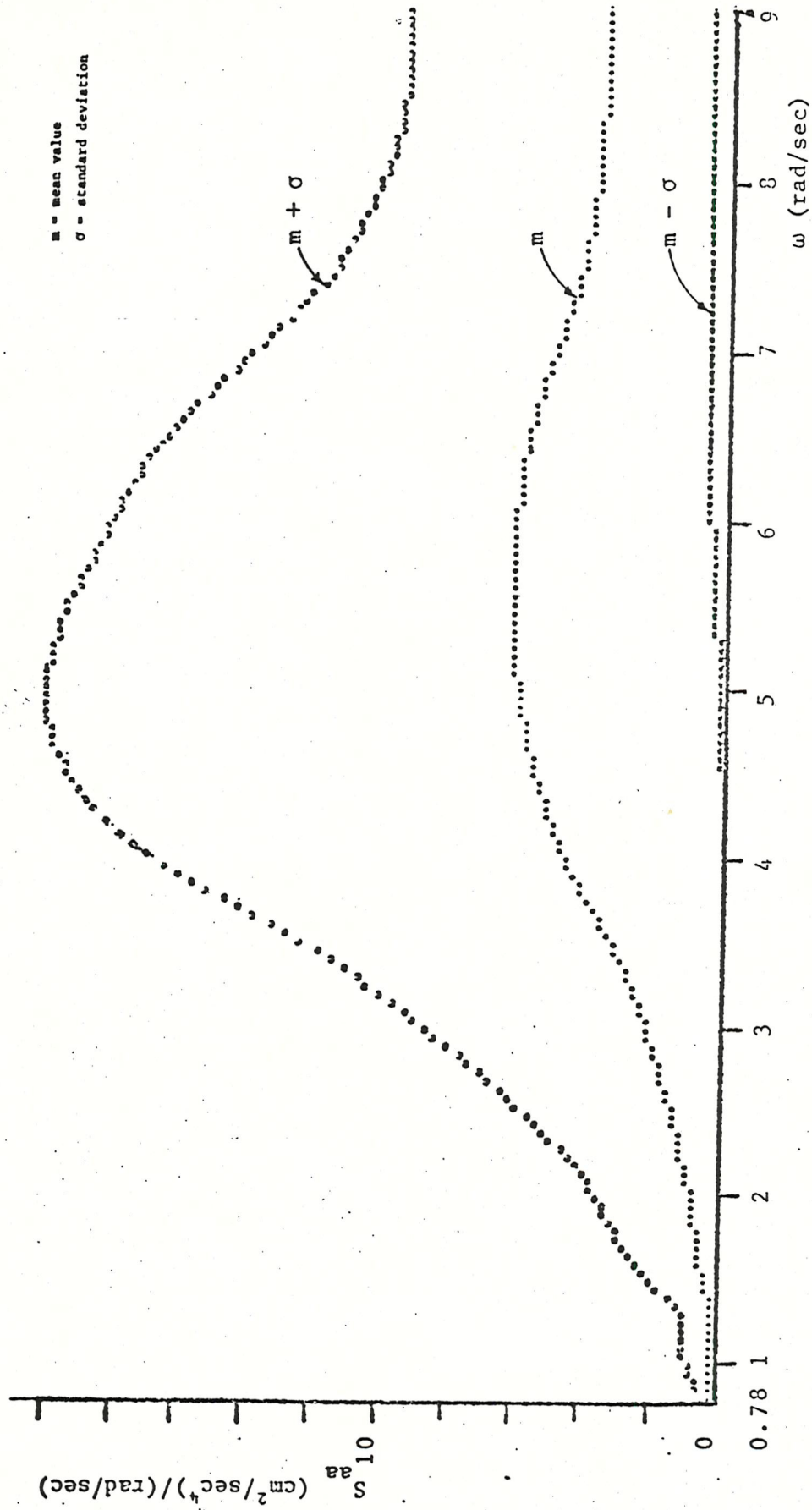

Fig. 8.12 P.s.d.f. of ground acceleration, S_{aa}, for a return period of 500 years (ξ=0.02), as a function of frequency, ω

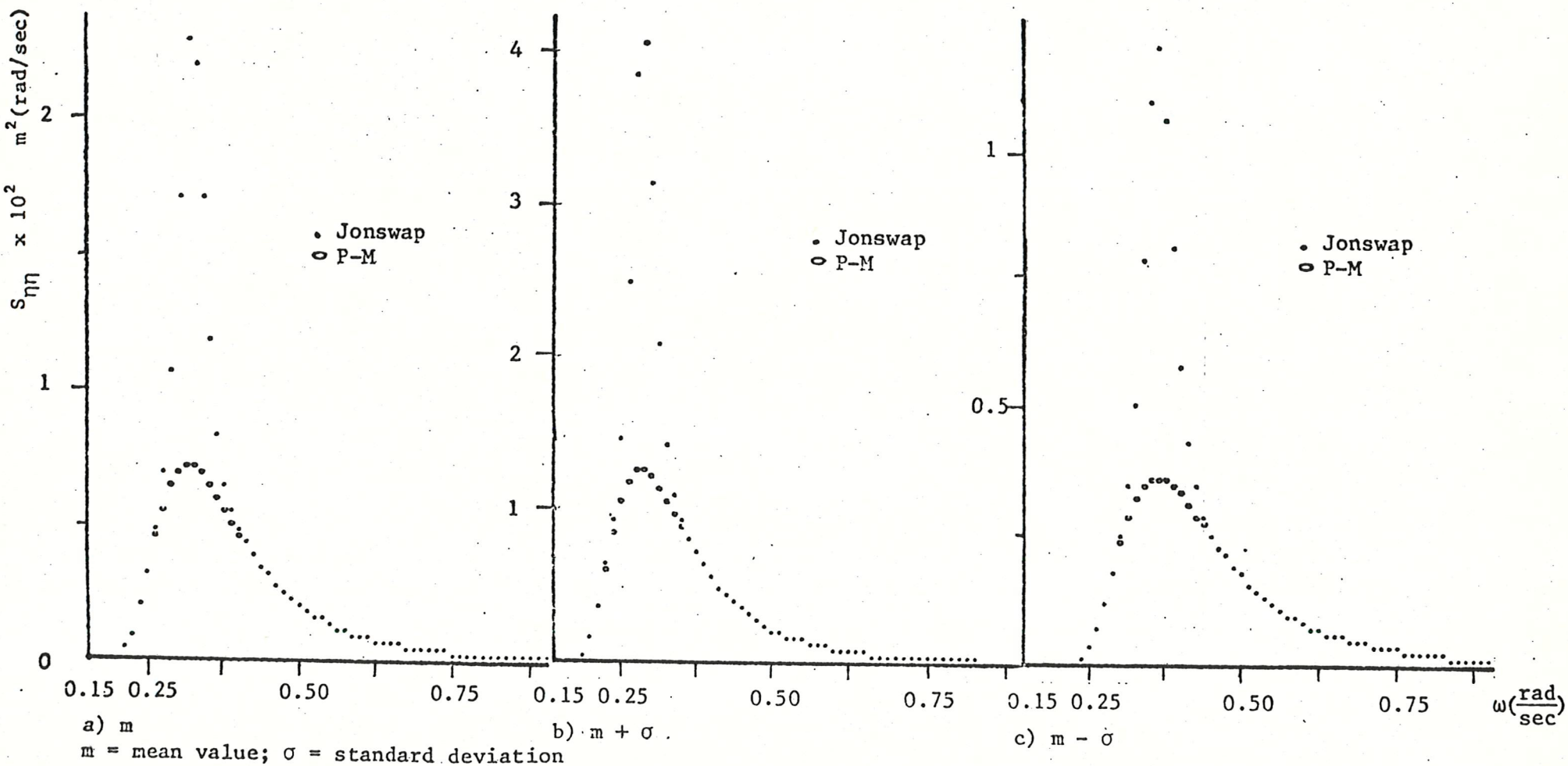

m = mean value; σ = standard deviation

Fig. 8.13 Pierson-Moskowitz, P-M, and Jonswap p.s.d. functions of wave heights, $S_{\eta\eta}$, for a return period of 50 years

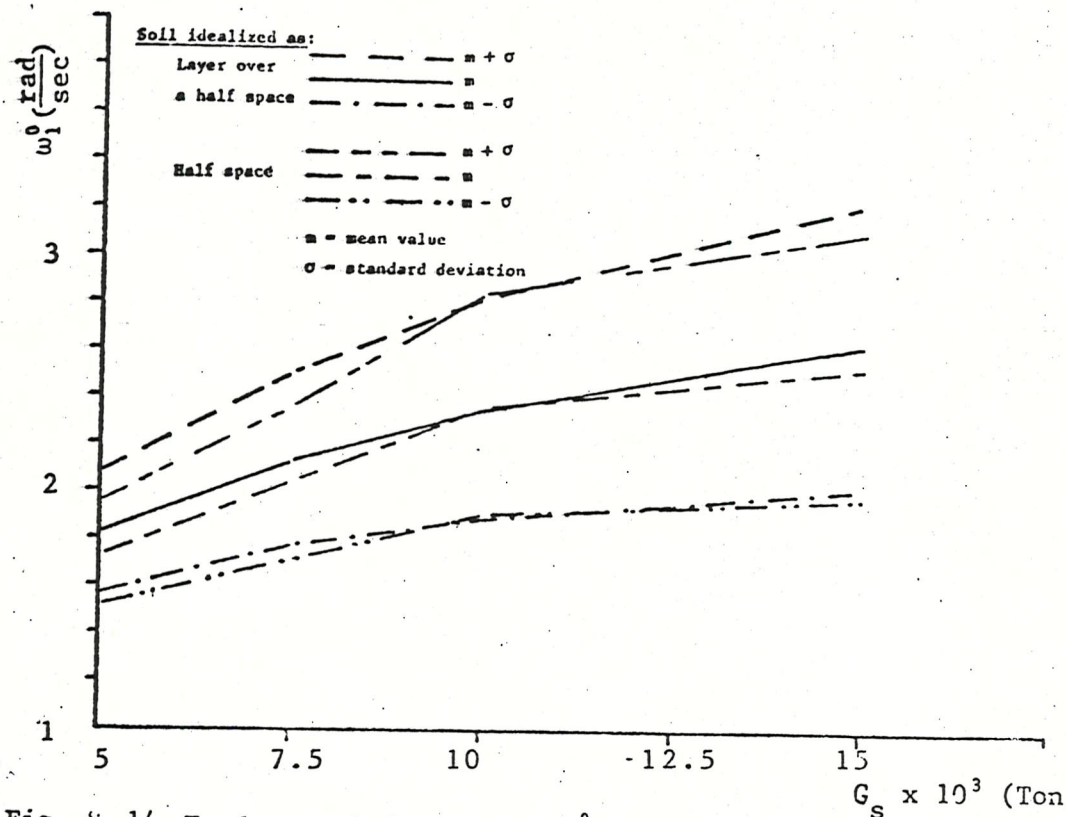

Fig. 8.14 Fundamental frequency, ω_1^0 , as a function of soil shear modulus, G_s

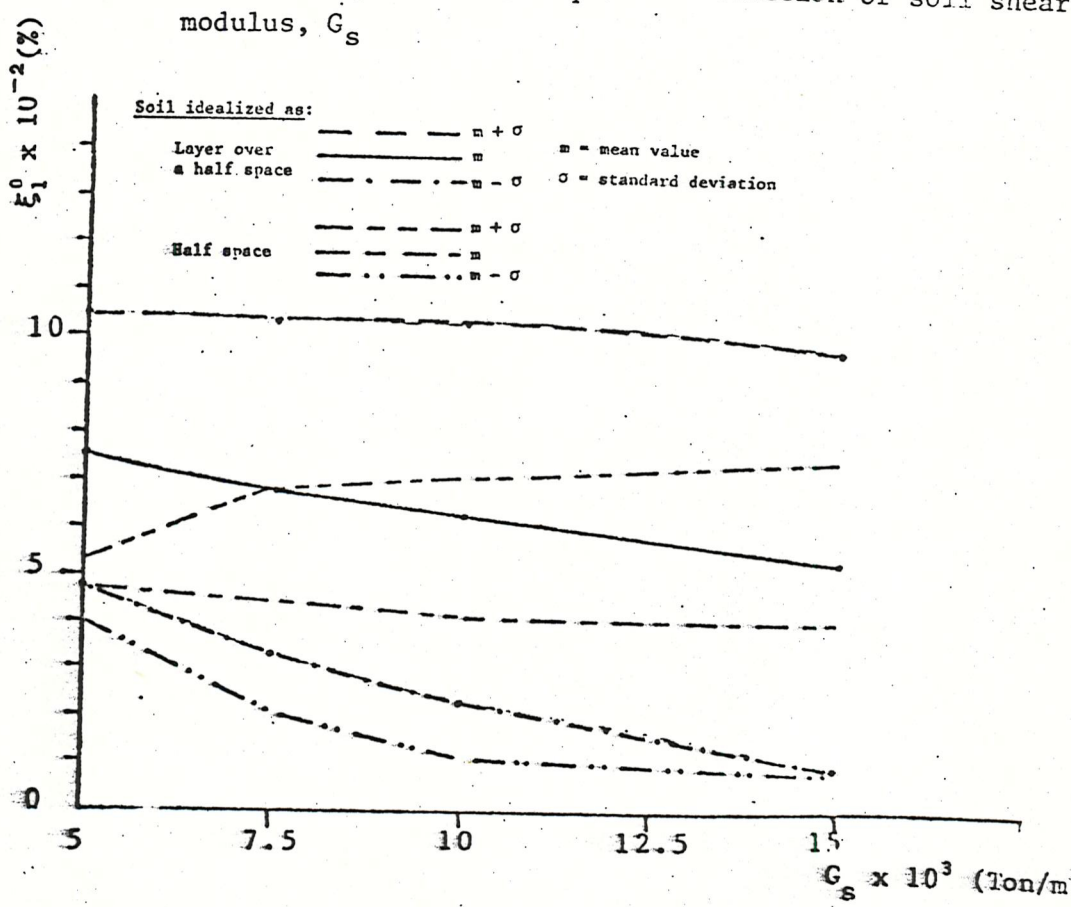

Fig. 8.15 Percentage of critical damping, ξ_1^0 , as a function of soil shear modulus, G_s

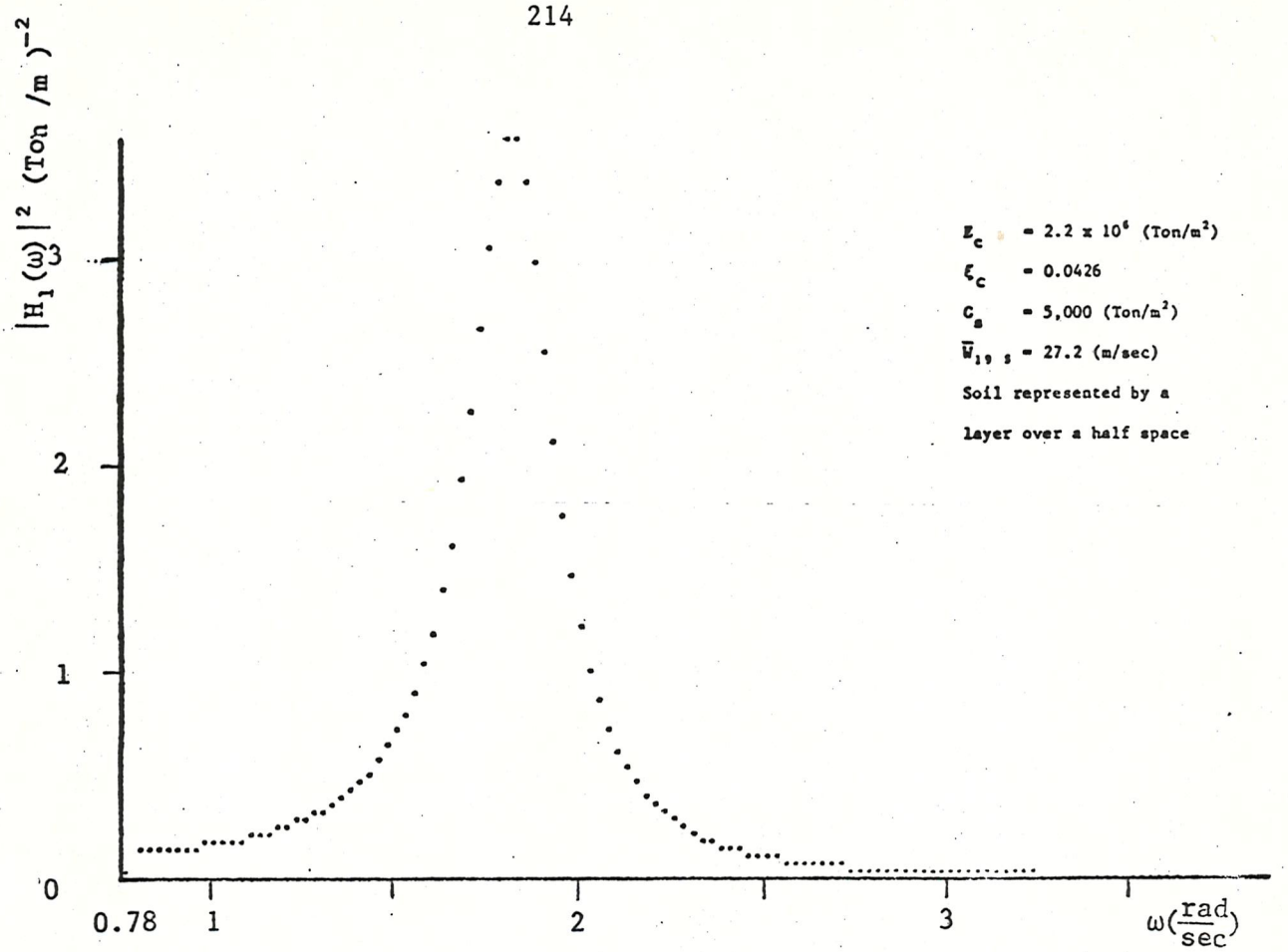

Fig. 8.16 Amplitude of complex frequency response of the first normal coordinate, $|H_1(\omega)|^2$, as a function of frequency, ω

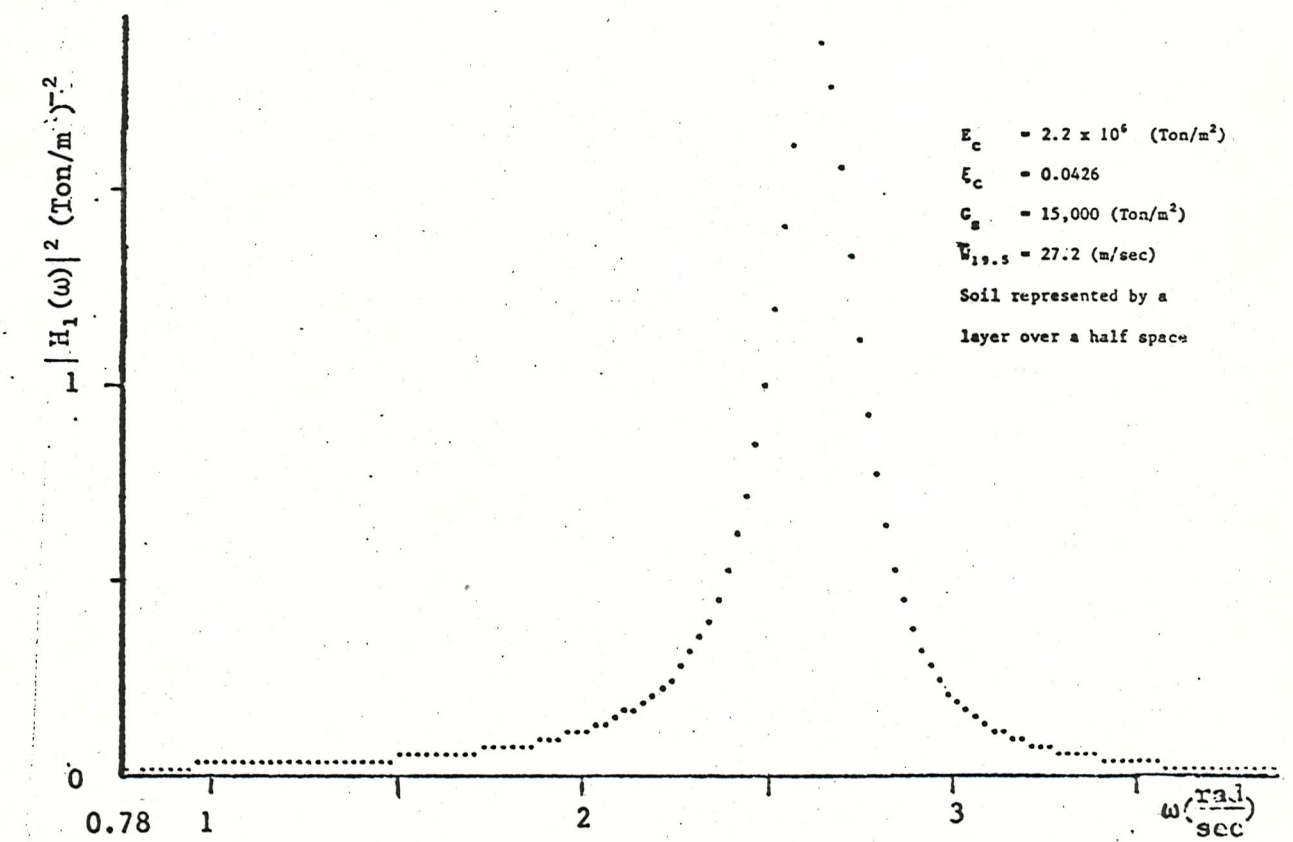

Fig. 8.17 Amplitude of complex frequency response of the first normal coordinate, $|H_1(\omega)|^2$, as a function of frequency, ω

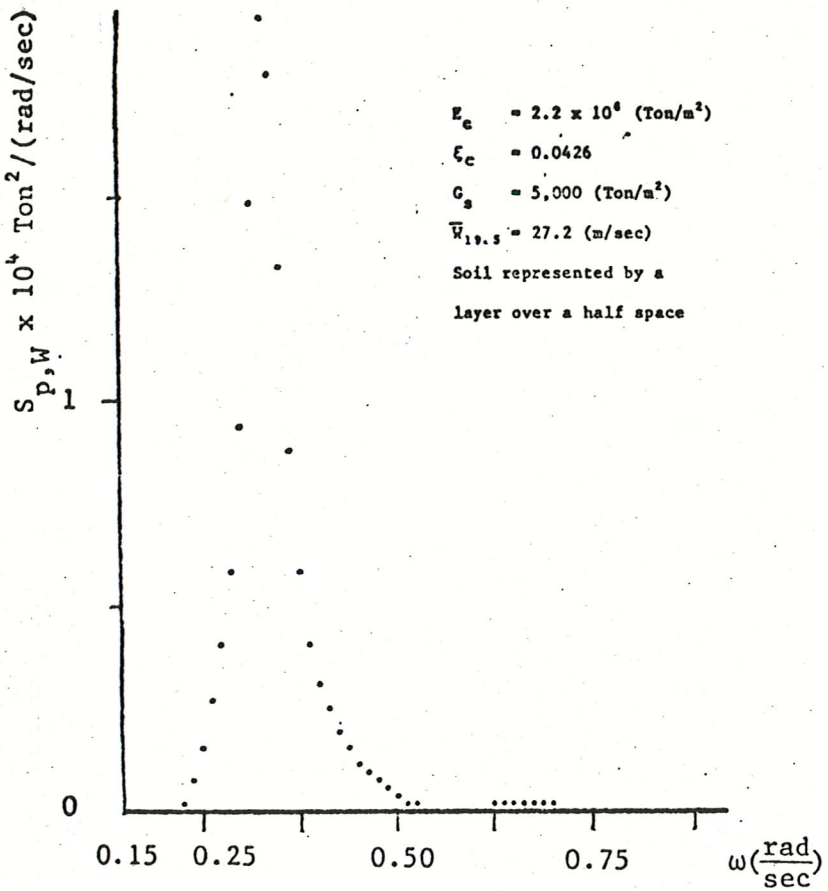

Fig. 8.18 P.s.d.f. of the first generalized load for wave excitation, $S_{p,W}$, as a function of frequency, ω

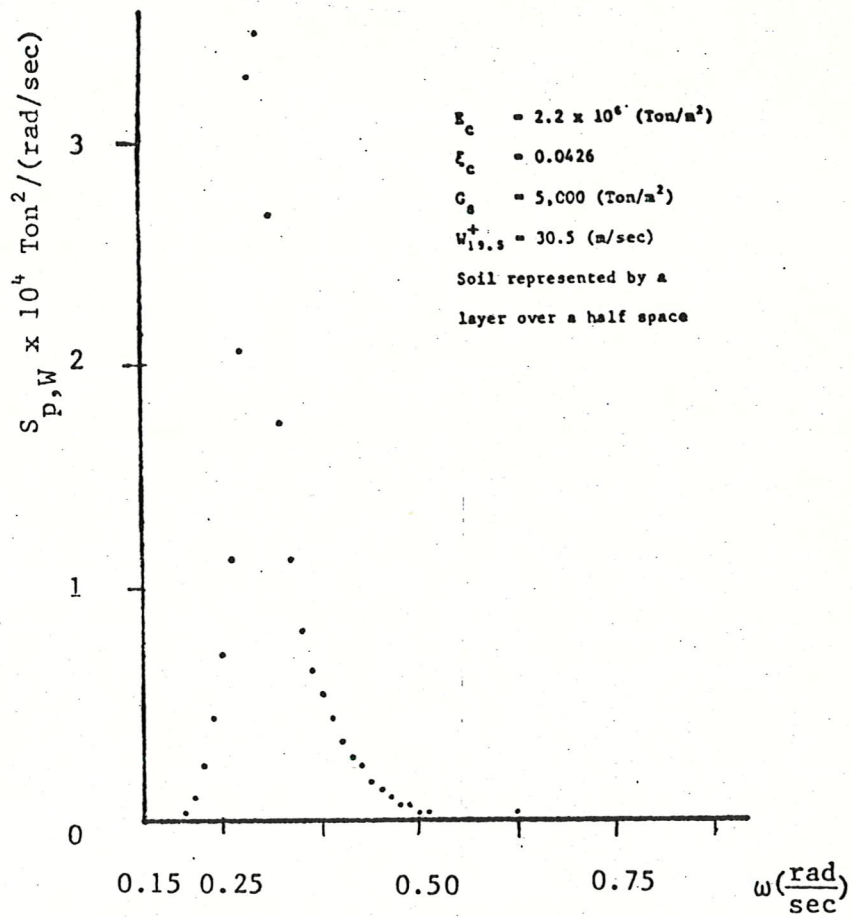

Fig. 8.19 P.s.d.f. of the first generalized load for wave excitation, $S_{p,W}$, as a function of frequency, ω

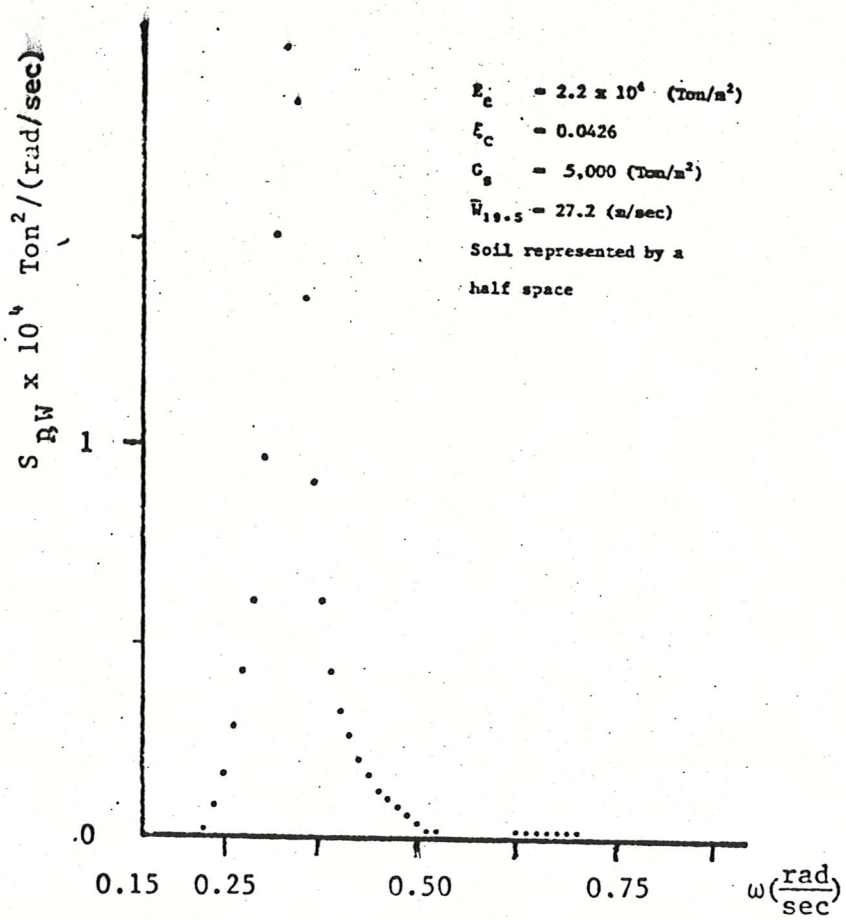

Fig. 8.20 P.s.d.f. of the first generalized coordinate for wave excitation, $S_{p,W}$, as a function of frequency, ω

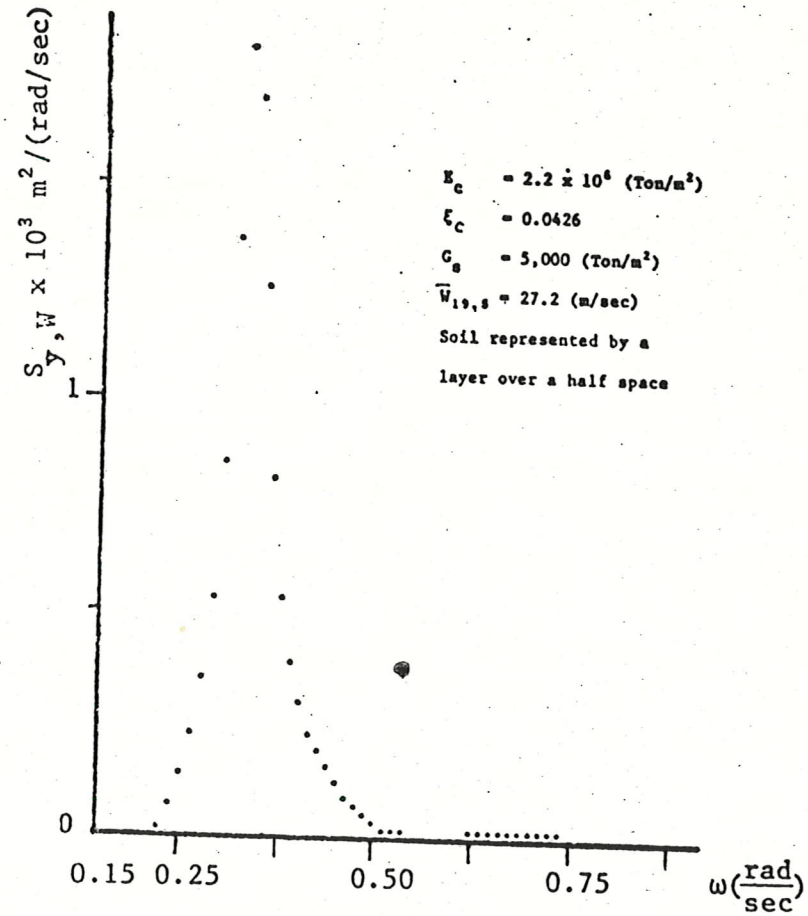

Fig. 8.21 P.s.d.f. of the first generalized coordinate for wave excitation, $S_{y,W}$, as a function of frequency, ω

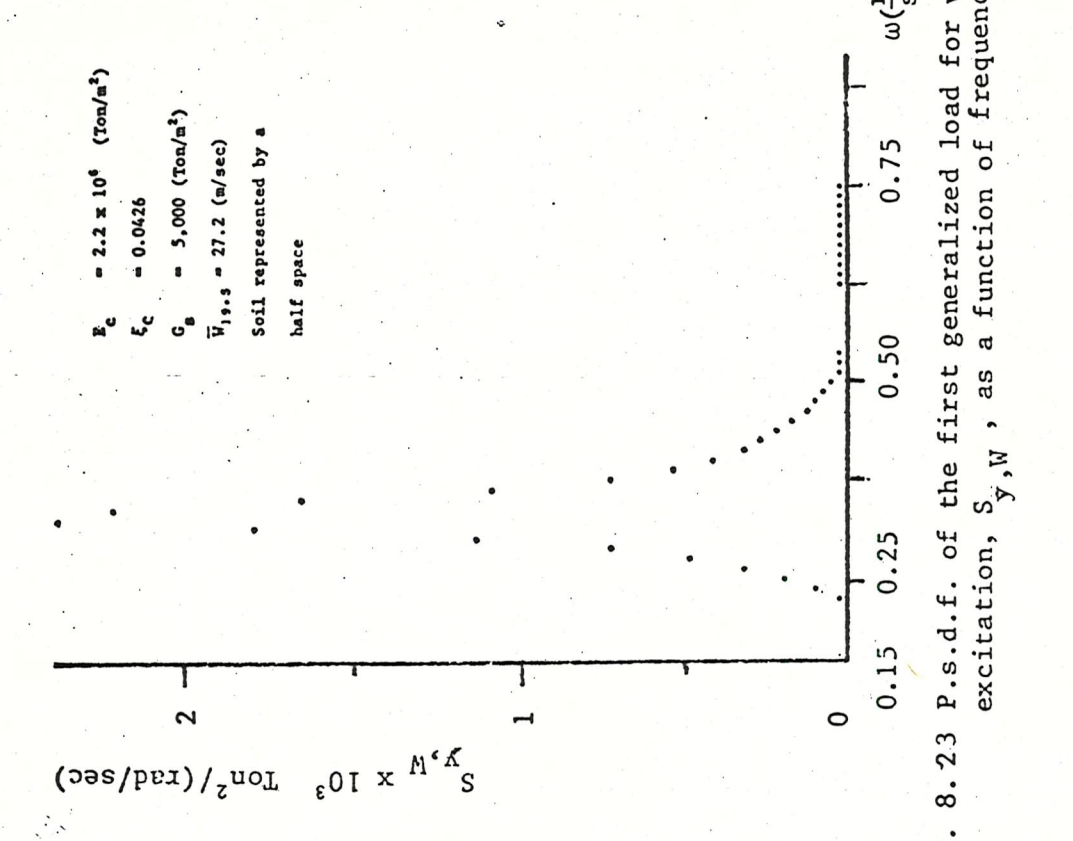

Fig. 8.23 P.s.d.f. of the first generalized load for wave excitation, $S_{y,W}$, as a function of frequency, ω

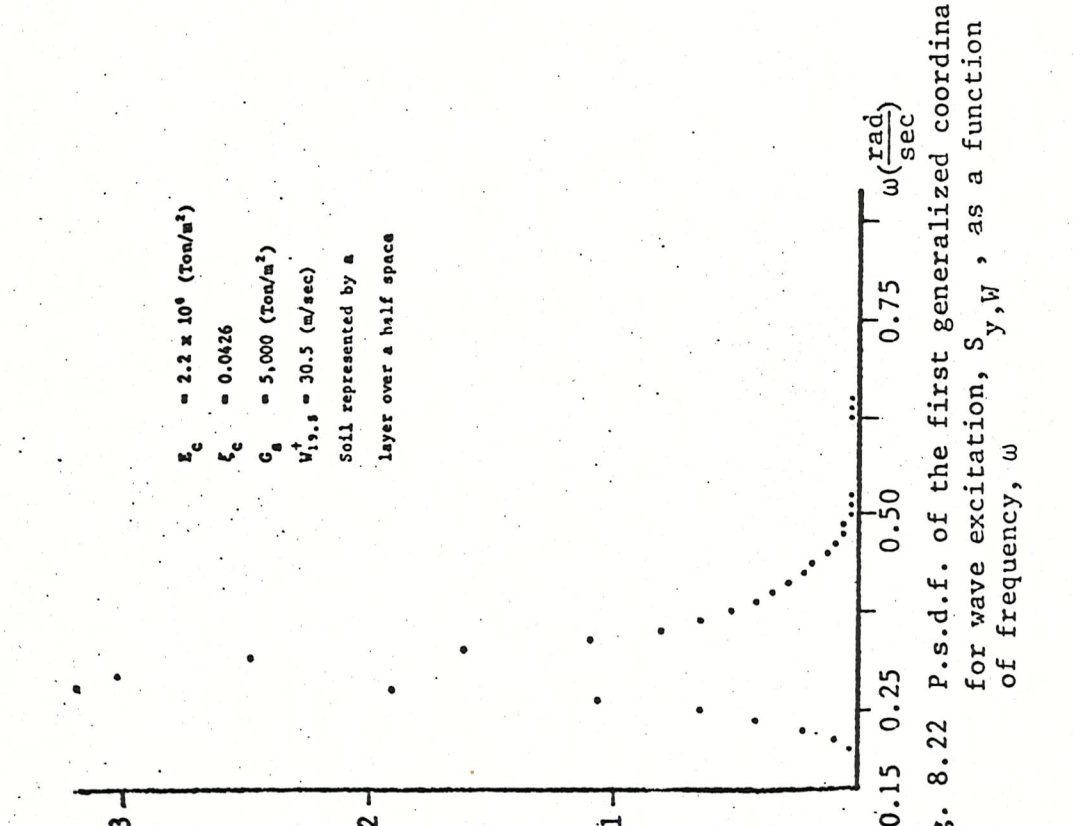

Fig. 8.22 P.s.d.f. of the first generalized coordinate for wave excitation, $S_{y,W}$, as a function of frequency, ω

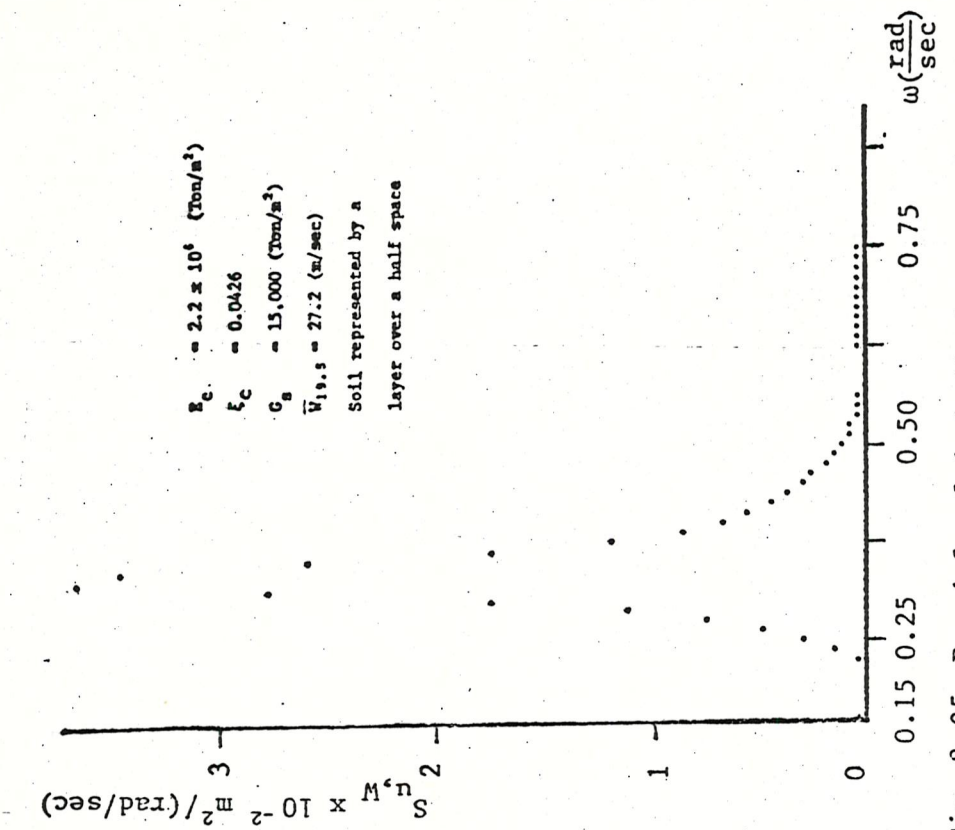

Fig. 8.25 P.s.d.f. of deck displacement for wave excitation, $S_{u,W}$, as a function of frequency, ω

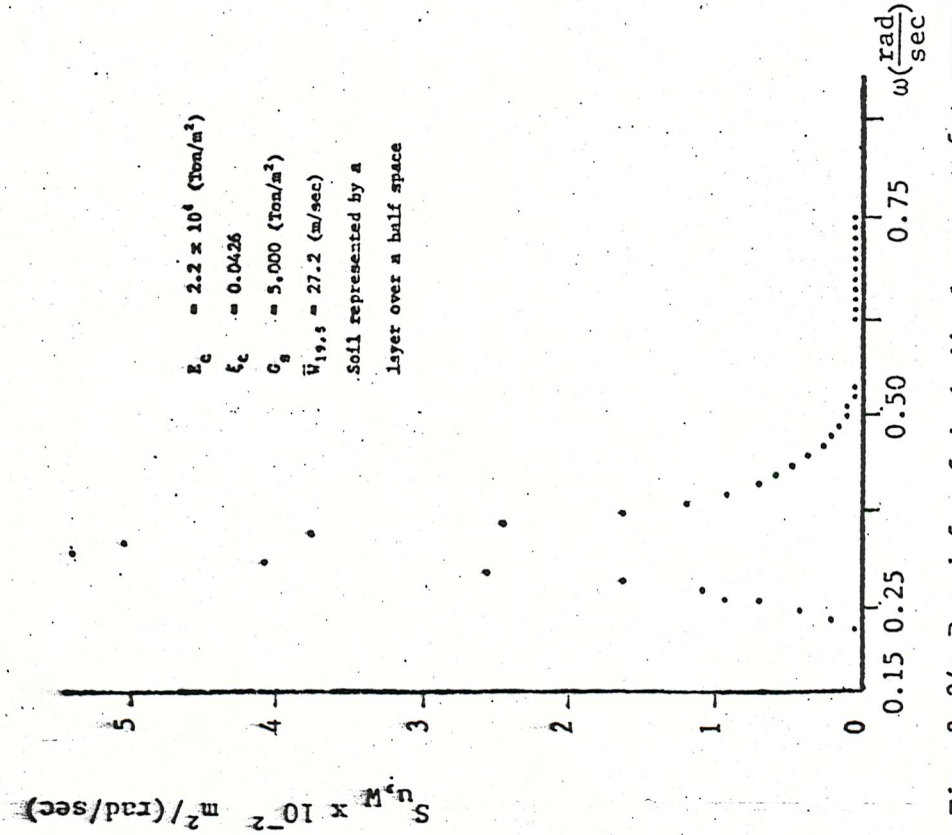

Fig. 8.24 P.s.d.f. of deck displacement for wave excitation, $S_{u,W}$, as a function of frequency, ω

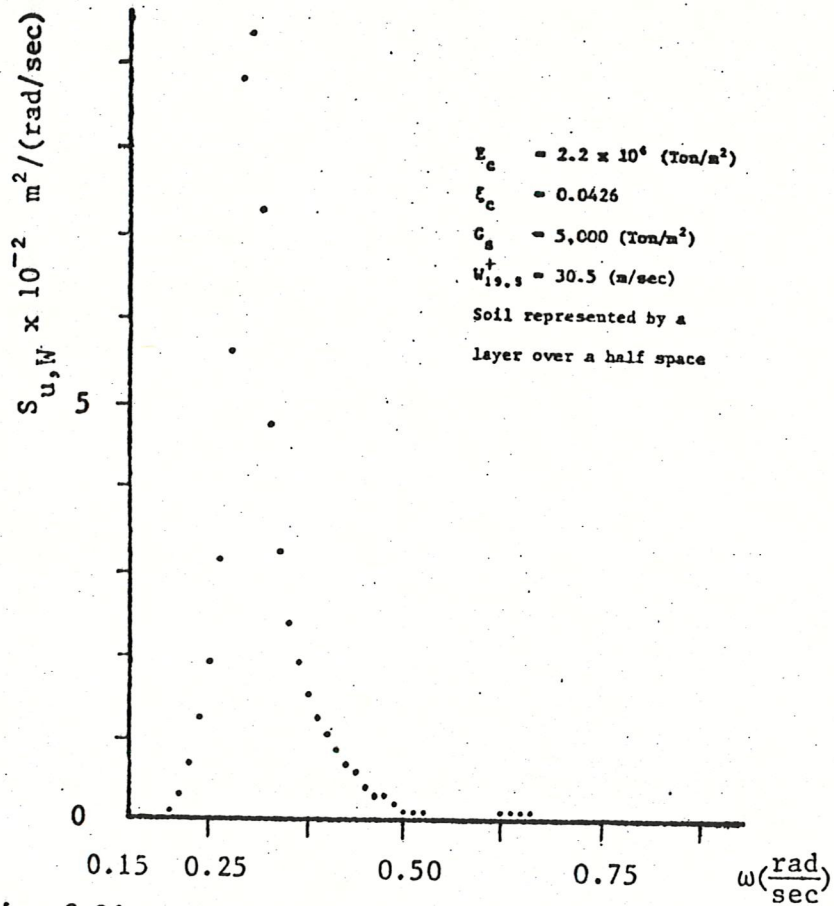

Fig. 8.26 P.s.d.f. of deck displacement for wave excitation, $S_{u,W}$, as a function of frequency, ω

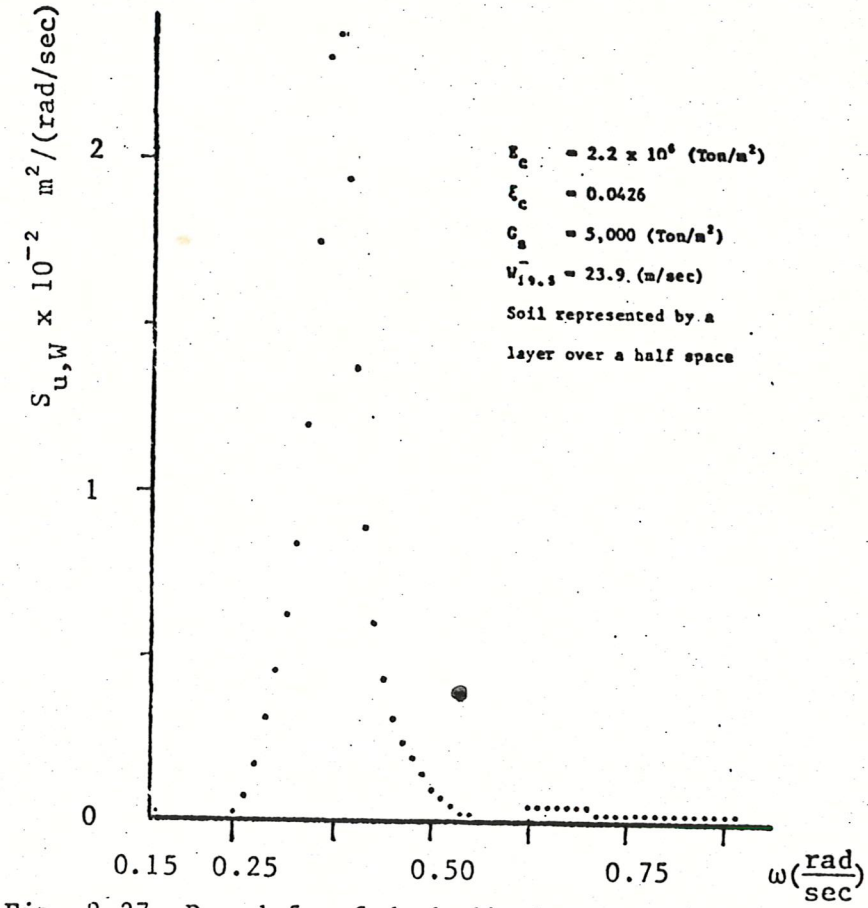

Fig. 8.27 P.s.d.f. of deck displacement for wave excitation, $S_{u,W}$, as a function of frequency, ω

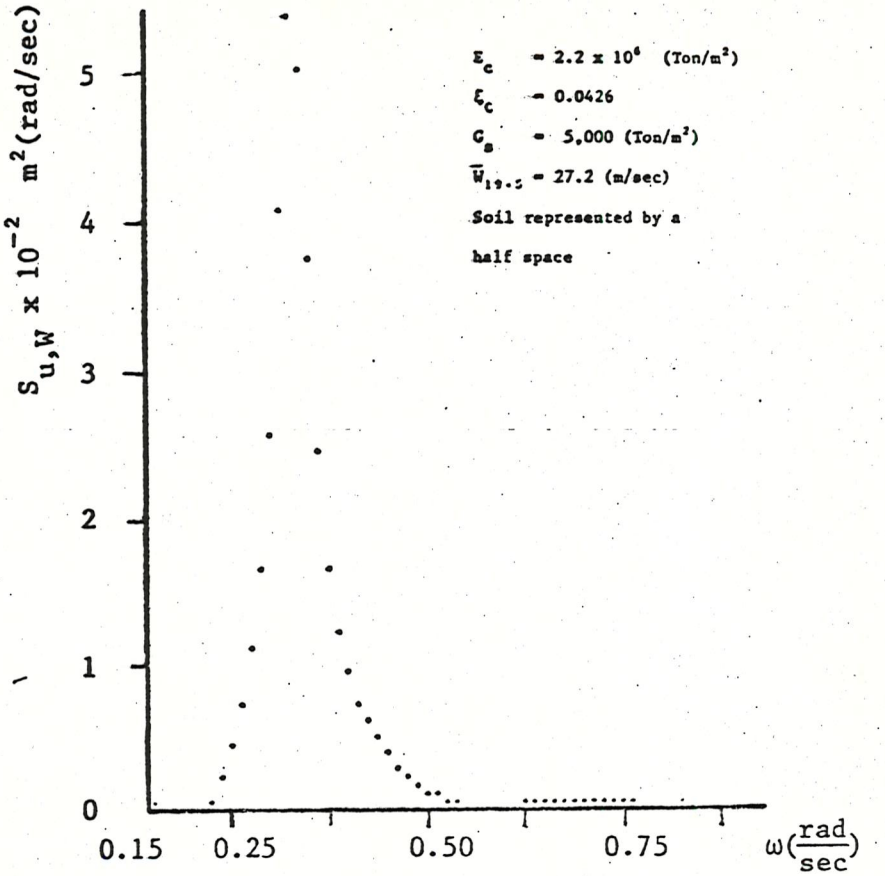

Fig. 8.28 P.s.d.f. of deck displacement for wave excitation, $S_{u,W}$, as a function of frequency, ω

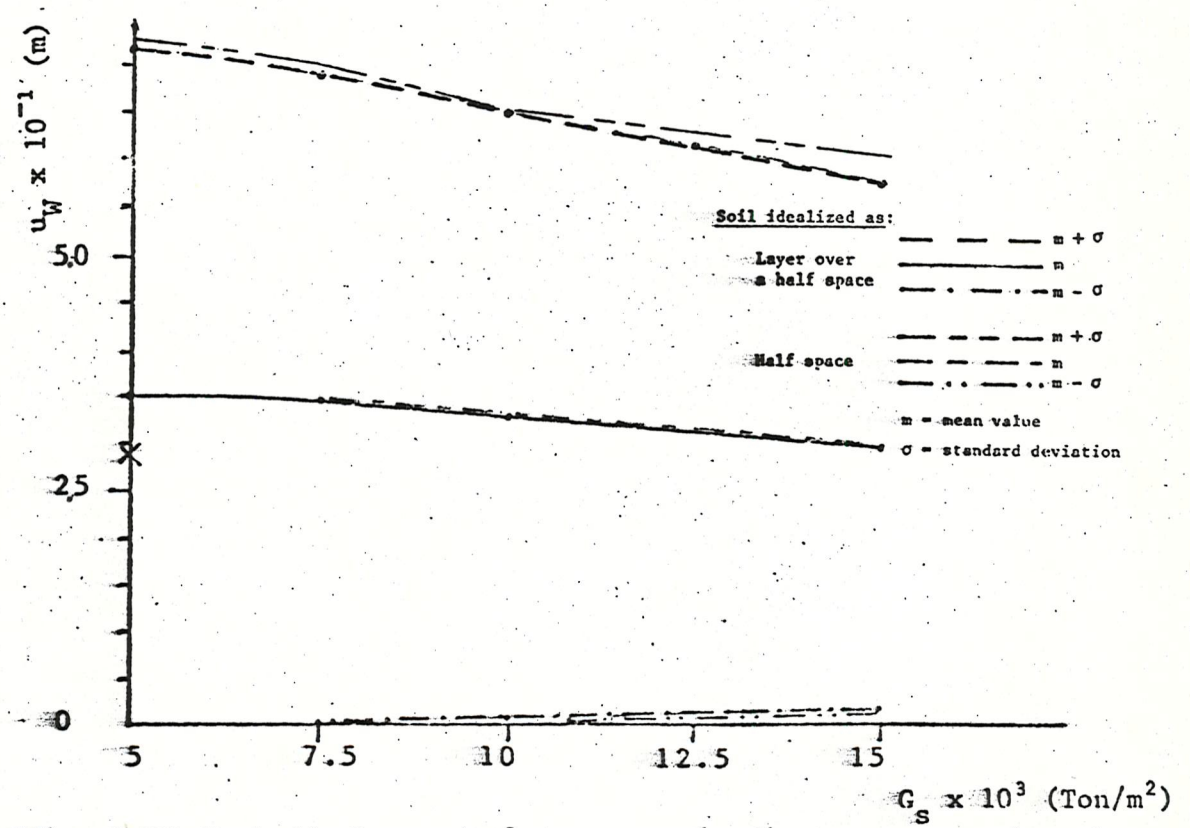

Fig. 8.29 Deck displacement for wave excitation, u_W, as a function of soil shear modulus, G_s

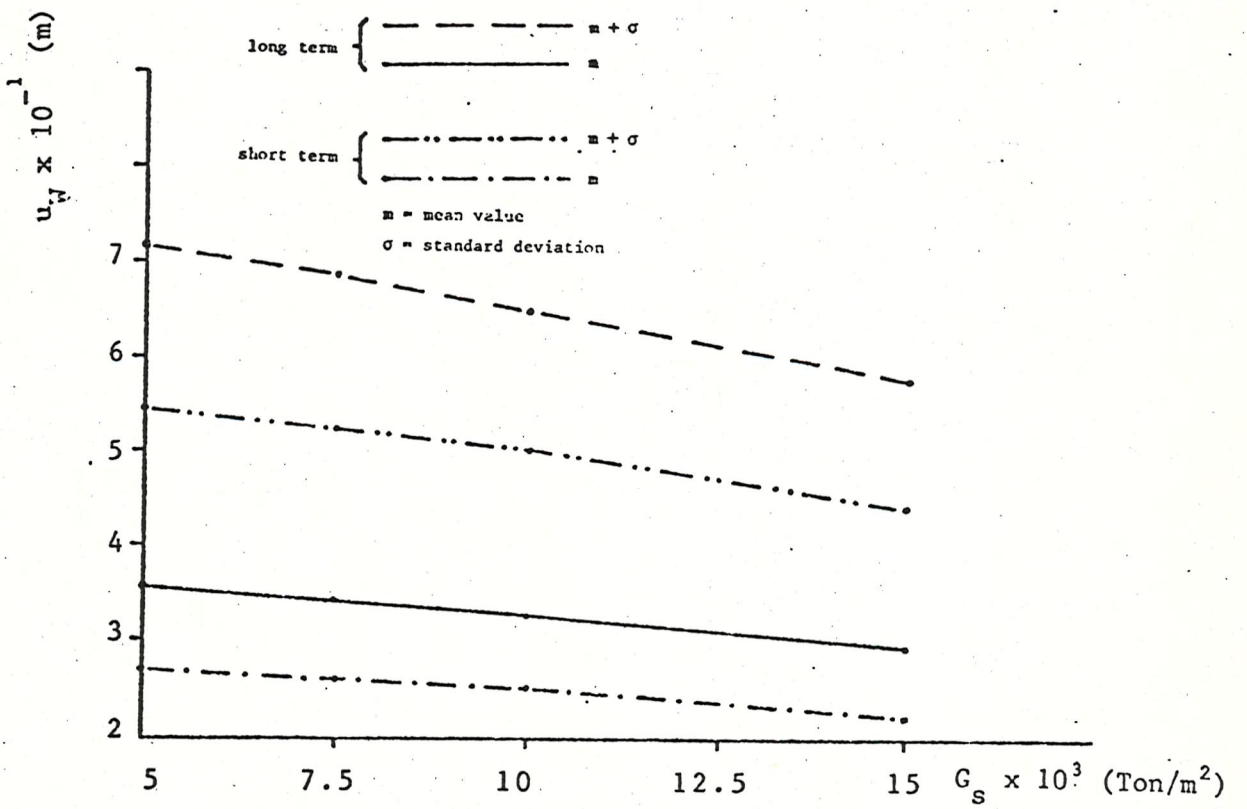

Fig. 8.30 Short and long term deck displacement for wave excitation, u_W , as a function of soil shear modulus, G_s ; soil idealized as a layer over a half space.

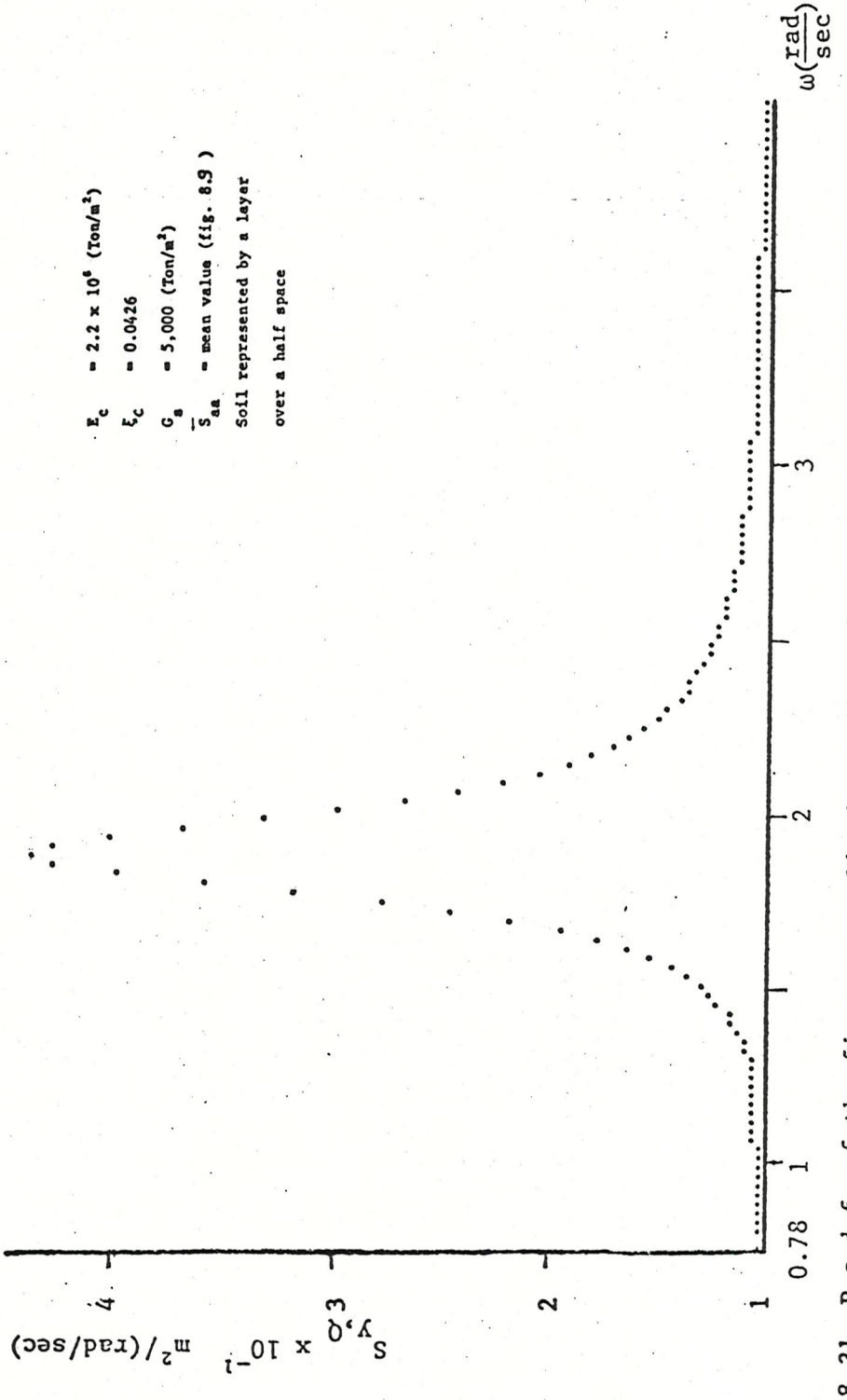

Fig. 8.31 P.s.d.f. of the first generalized coordinate for seismic excitation, $S_{y,Q}$, as a function of frequency, ω

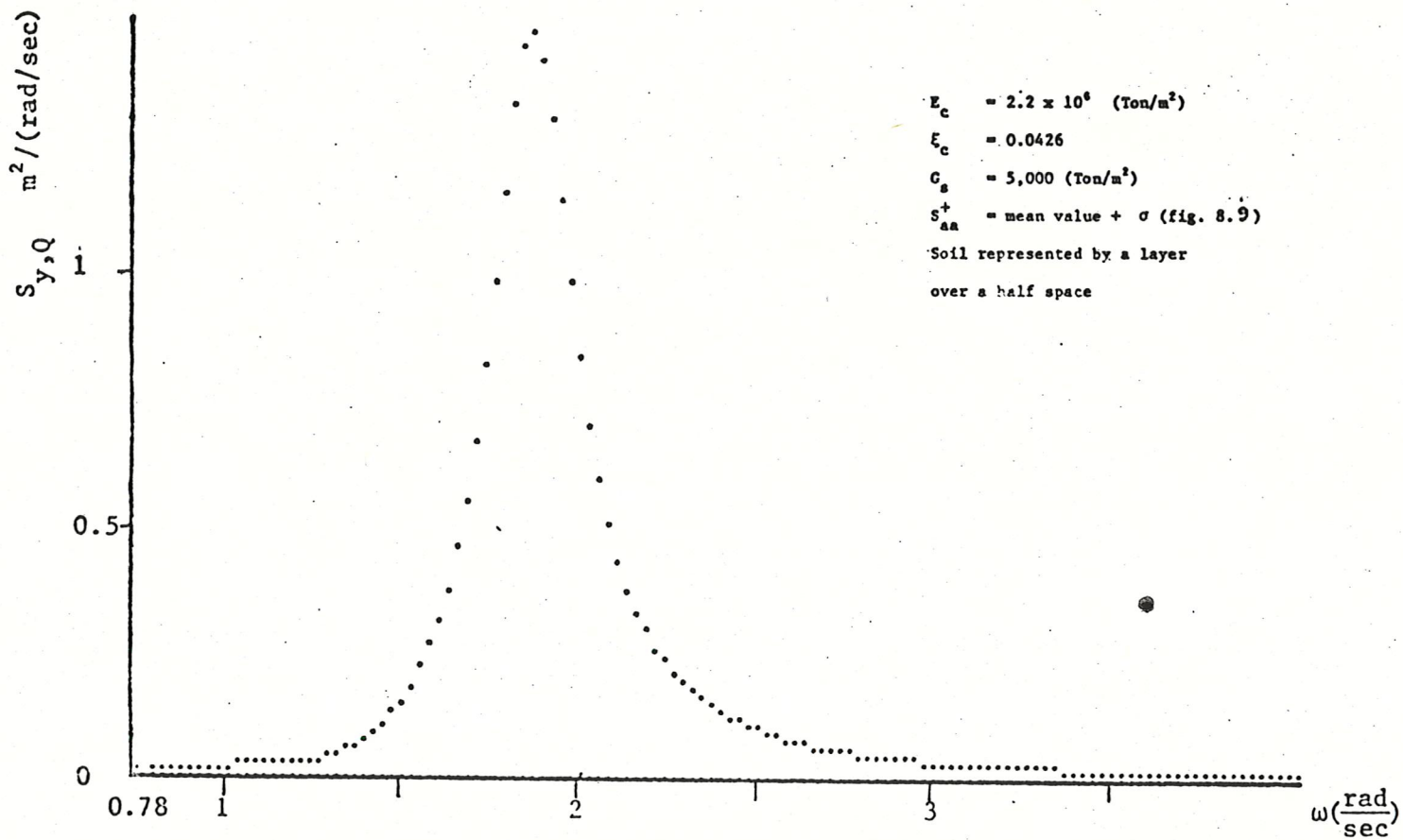

Fig. 8.32 P.s.d.f. of the first generalized coordinate for seismic excitation, $S_{y,Q}$, as a function of frequency, ω

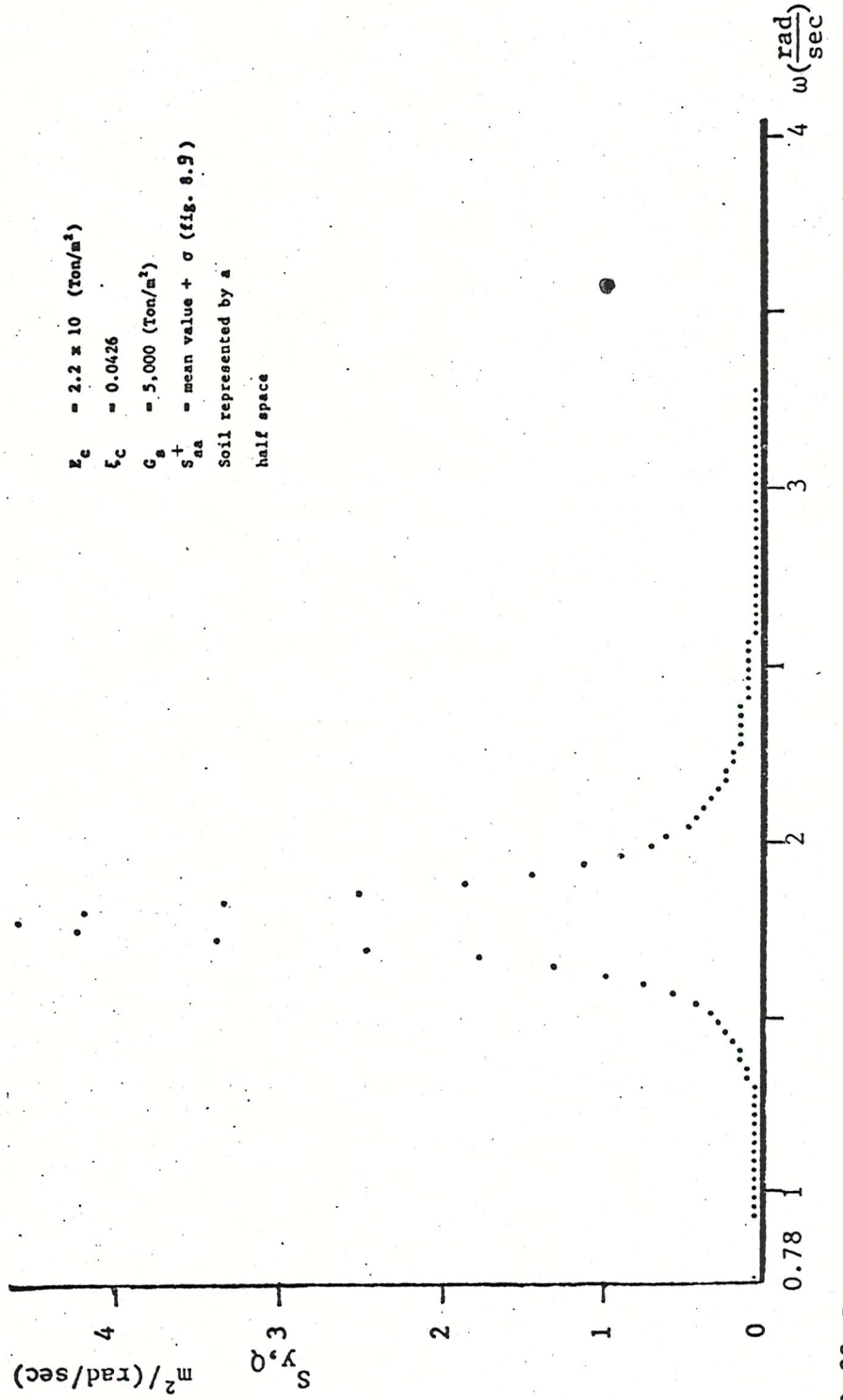

Fig. 8.33 P.s.d.f. of the first generalized coordinate for seismic excitation, $S_{y,Q}$, as a function of frequency, ω

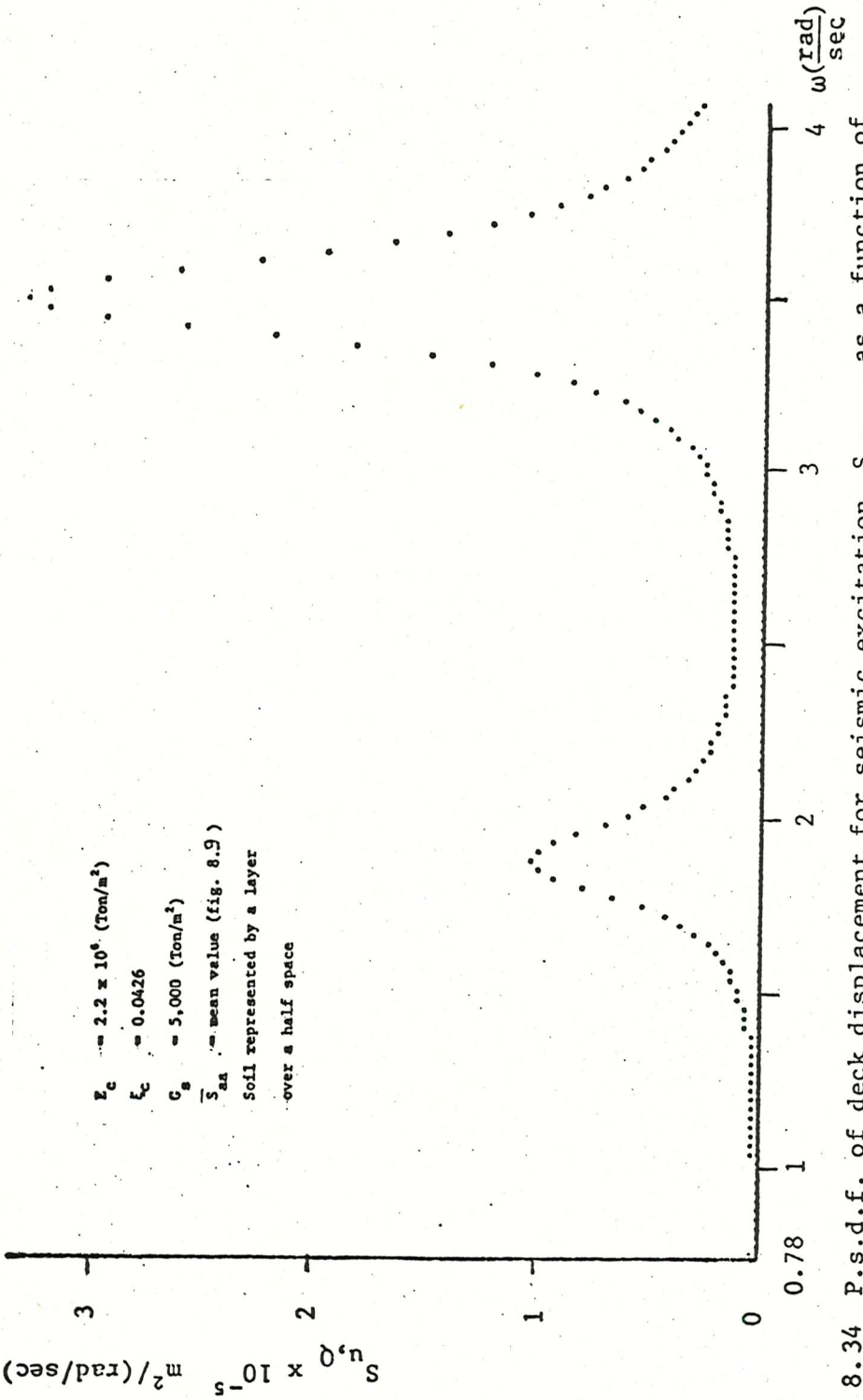

Fig. 8.34 P.s.d.f. of deck displacement for seismic excitation, $S_{u,Q}$, as a function of frequency, ω

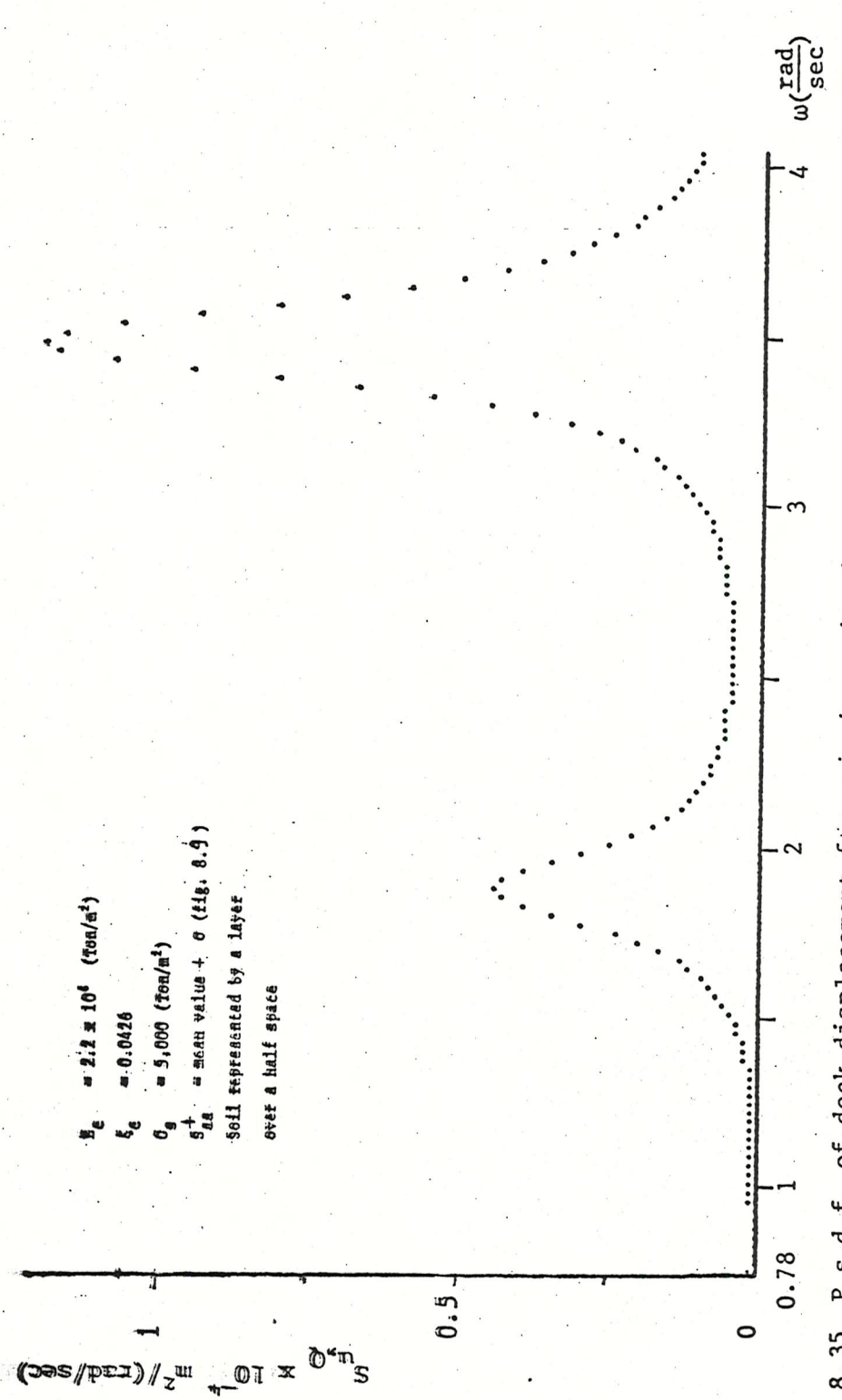

Fig. 8.35 P.s.d.f. of deck displacement for seismic excitation, $S_{u,Q}$, as a function of frequency, ω

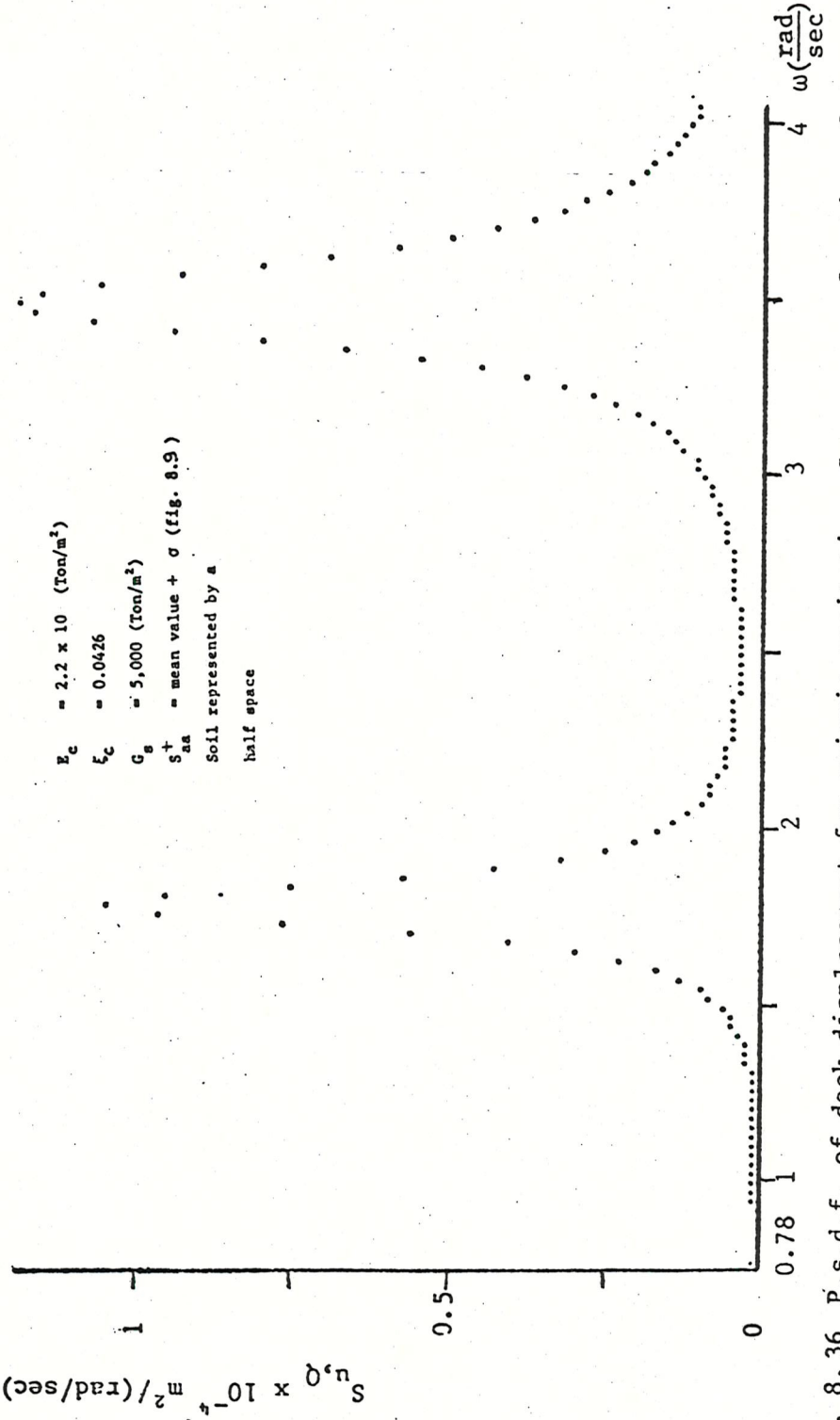

Fig. 8.36 P.s.d.f. of deck displacement for seismic excitation, $S_{u,Q}$, as a function of frequency, ω

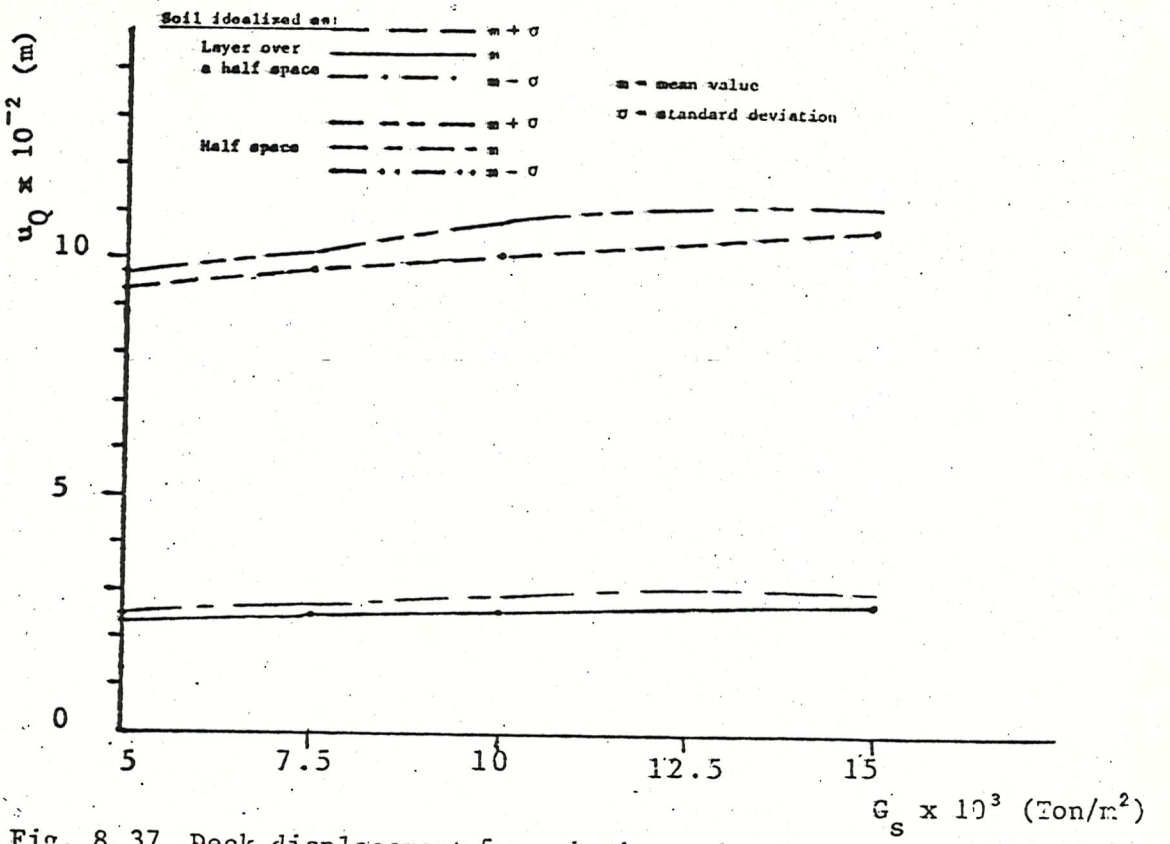

Fig. 8.37 Deck displacement for seismic excitation, u_Q, as a function of soil shear modulus, G_s

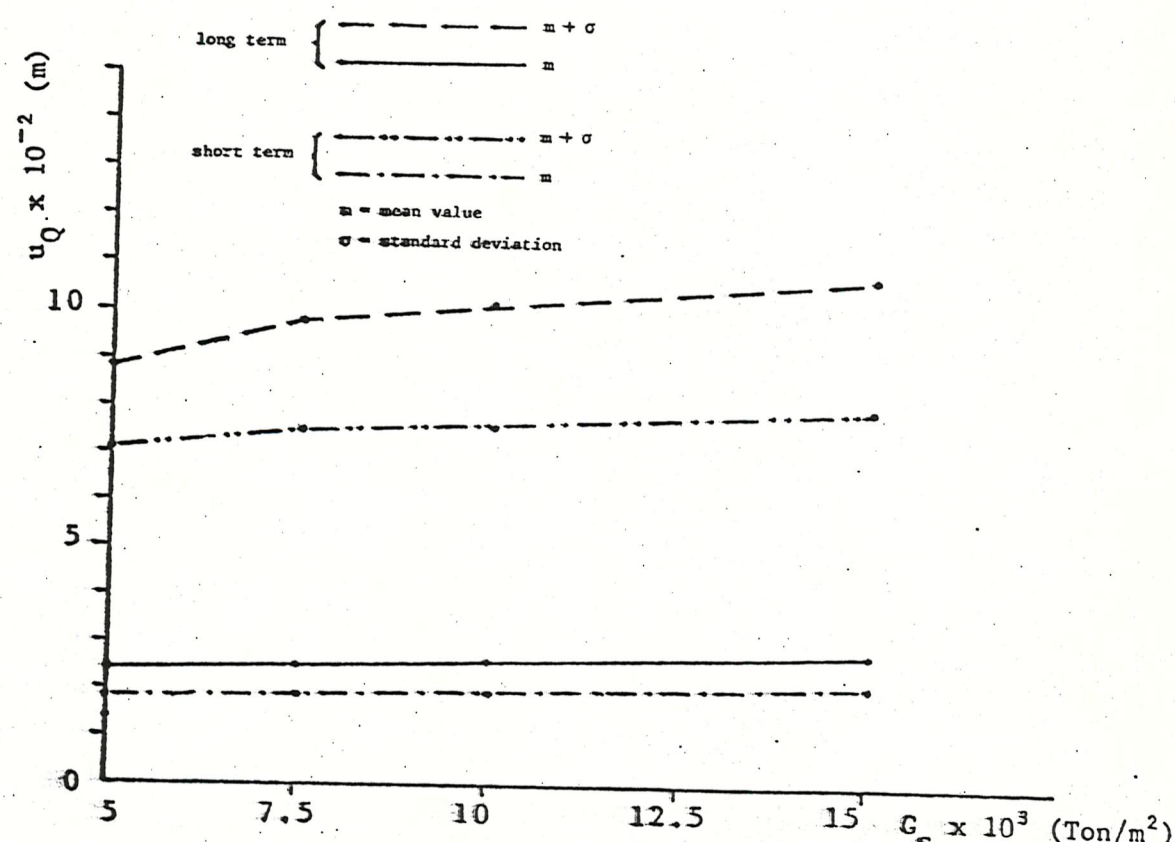

Fig. 8.38 Short and long term deck displacement for seismic excitation, u_Q, as a function of soil shear modulus, G_s; soil idealized as a layer over a half space.

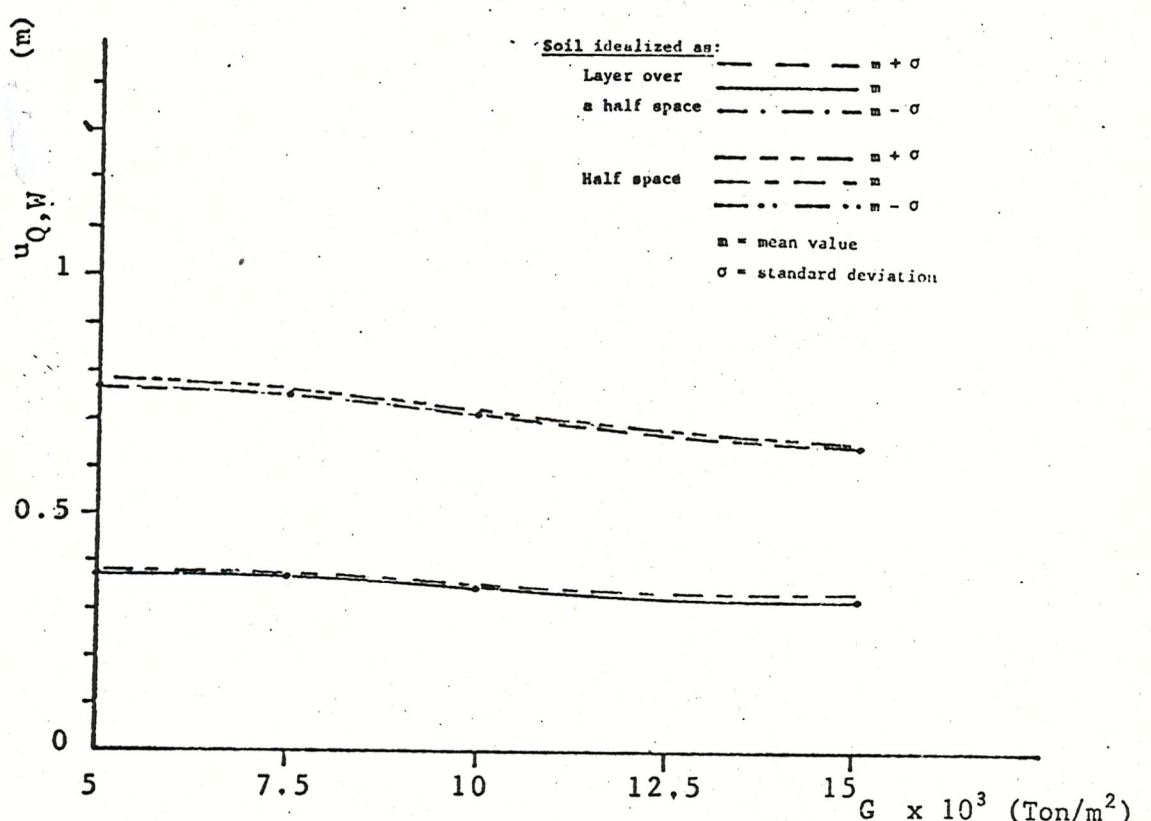

Fig. 8.39 Deck displacement for seismic and wave excitation, $u_{Q,W}$, as a function of soil shear modulus, G_s

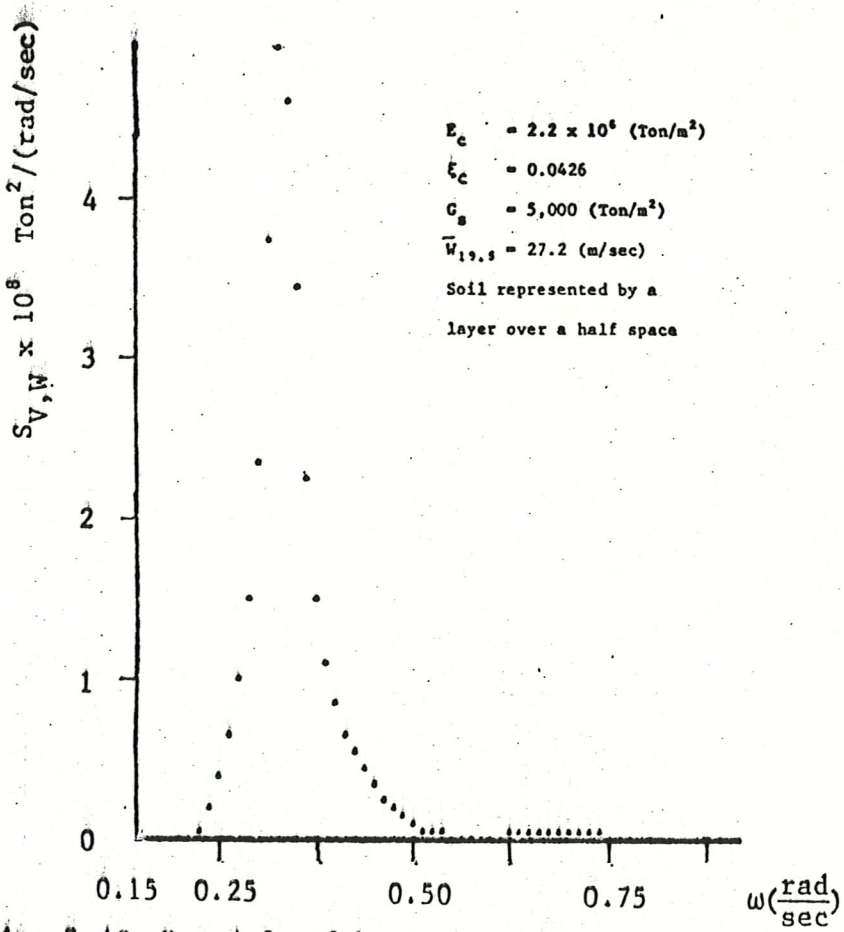

Fig. 8.40 P.s.d.f. of base shear force for wave excitation, $S_{V,W}$, as a function of frequency, ω

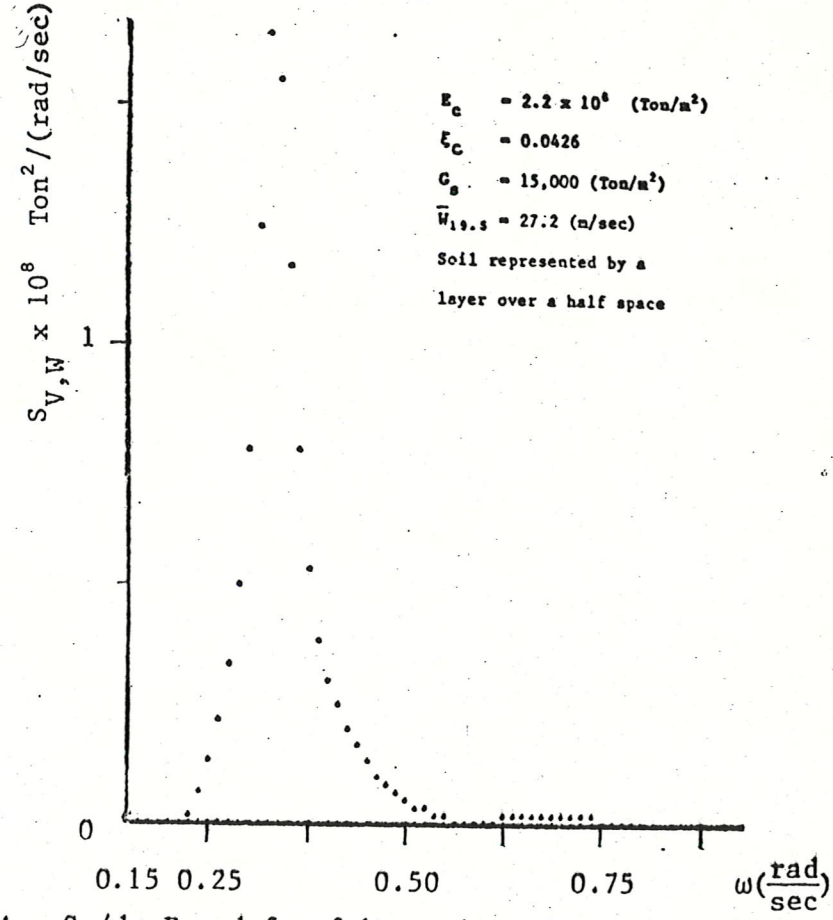

Fig. 8.41 P.s.d.f. of base shear force for wave excitation, $S_{V,W}$, as a function of frequency, ω

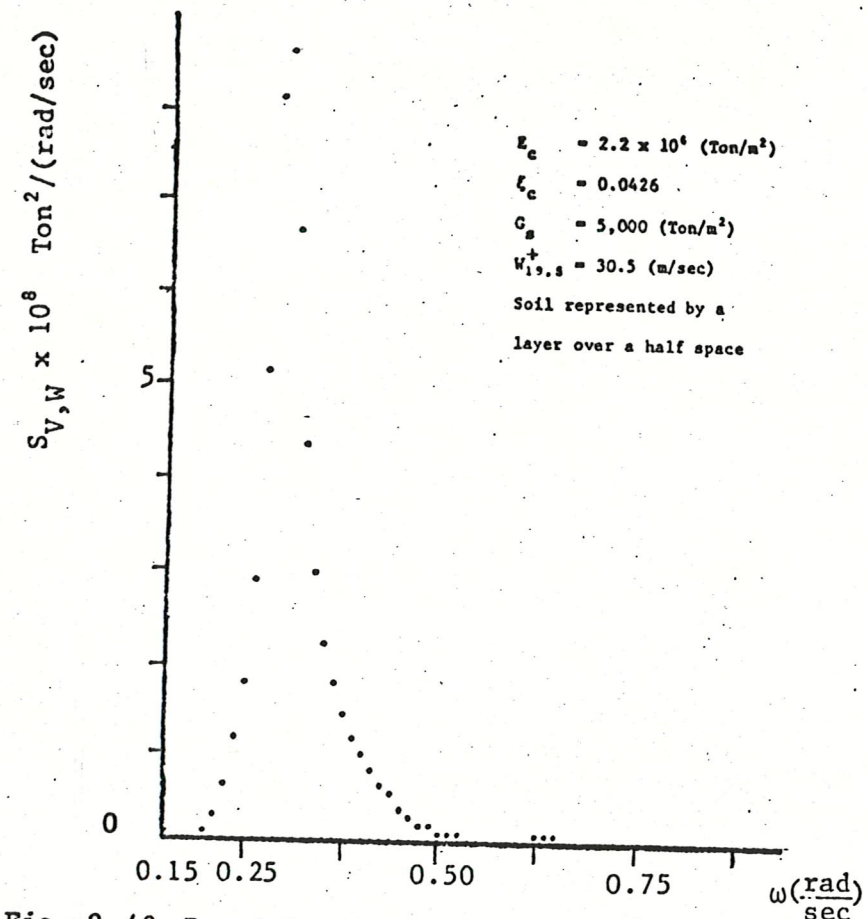

Fig. 8.42 P.s.d.f. of base shear force for wave excitation, $S_{V,W}$, as a function of frequency, ω

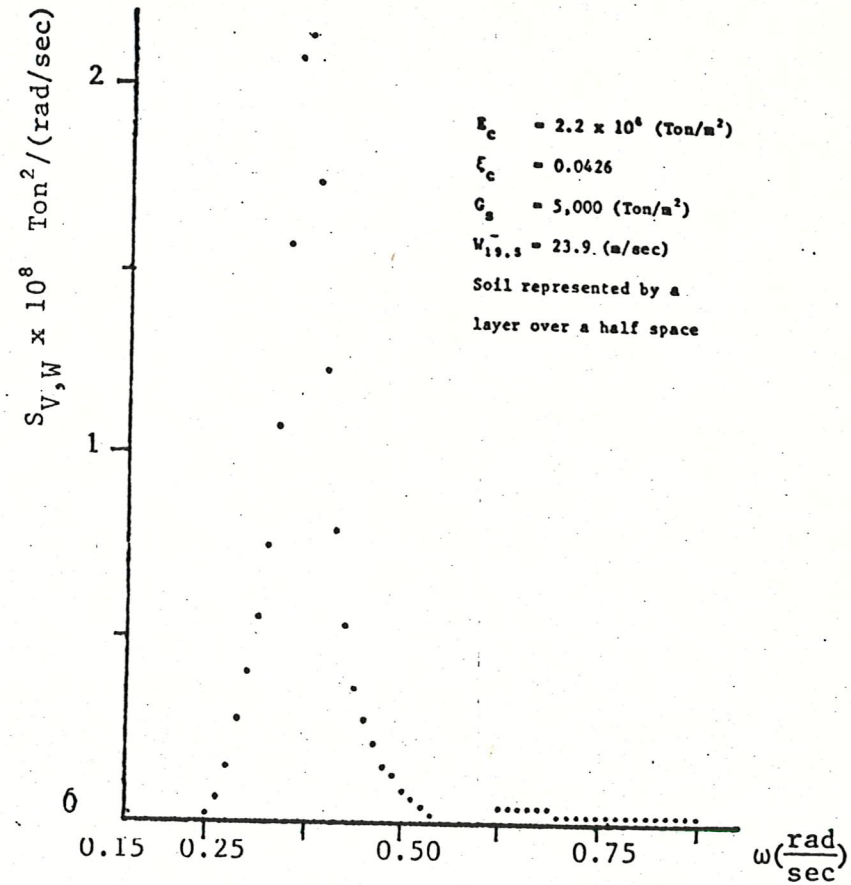

Fig. 8.43 P.s.d.f. of base shear force for wave excitation, $S_{V,W}$, as a function of frequency, ω

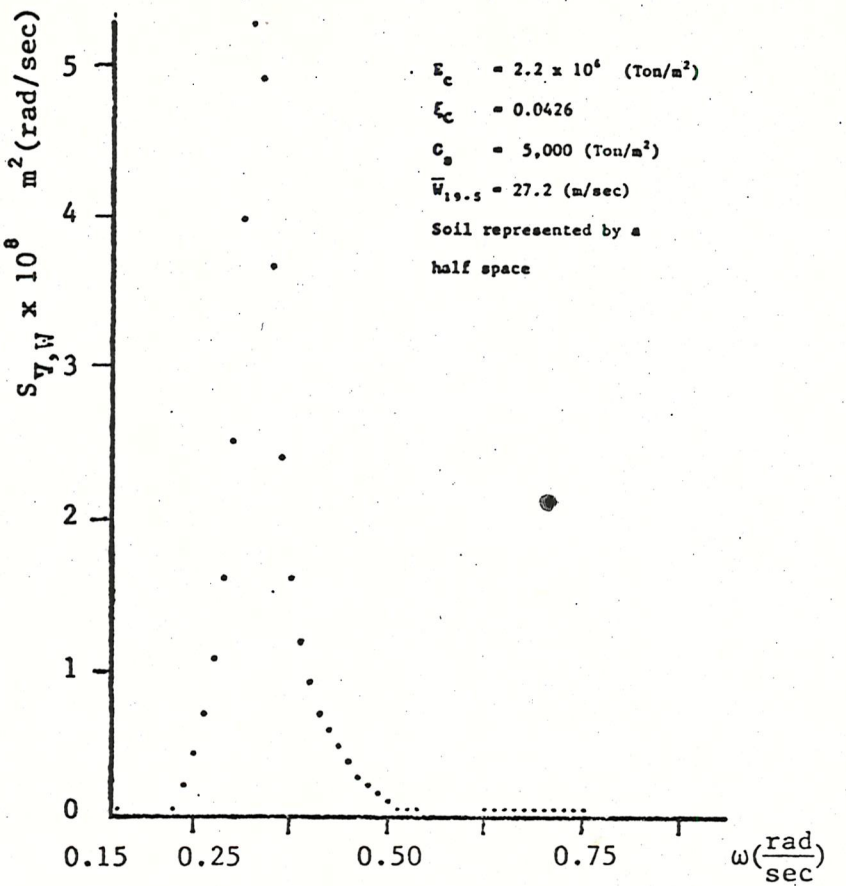

Fig. 8.44 P.s.d.f. of base shear force for wave excitation, $S_{V,W}$, as a function of frequency, ω

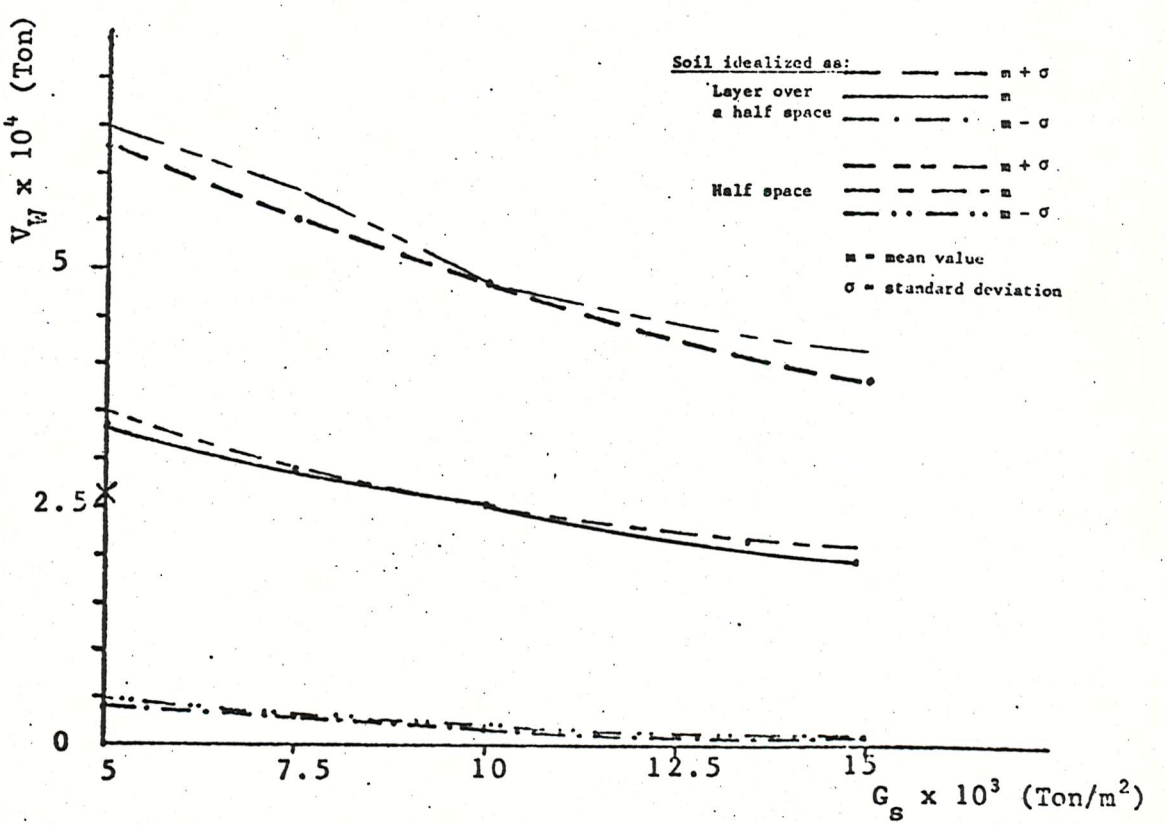

Fig. 8.45 Base shear force for wave excitation, V_W, as a function of soil shear modulus, G_s

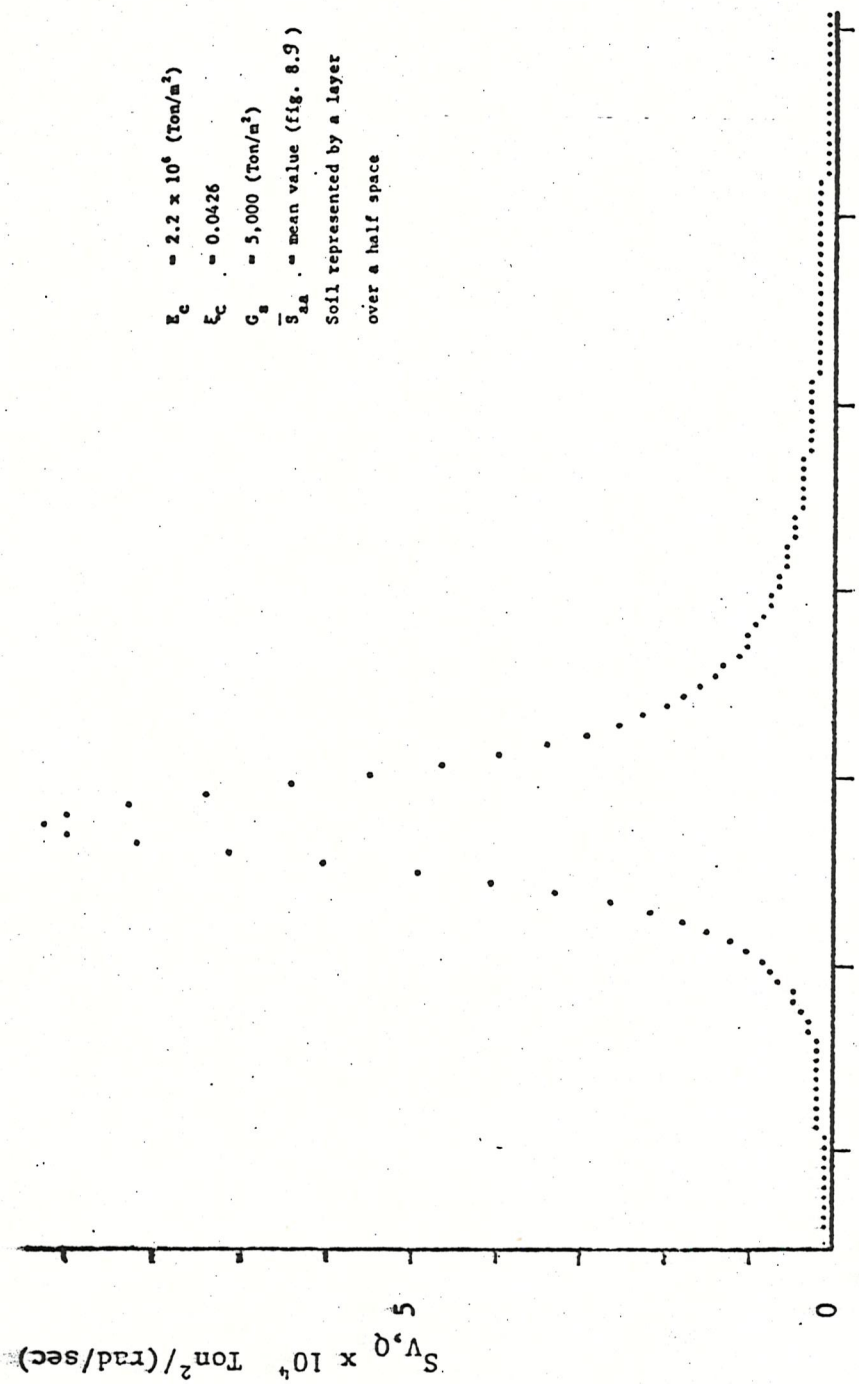

Fig. 8.46 P.s.d.f. of base shear force for seismic excitation, $S_{V,Q}$, as a function of frequency, ω

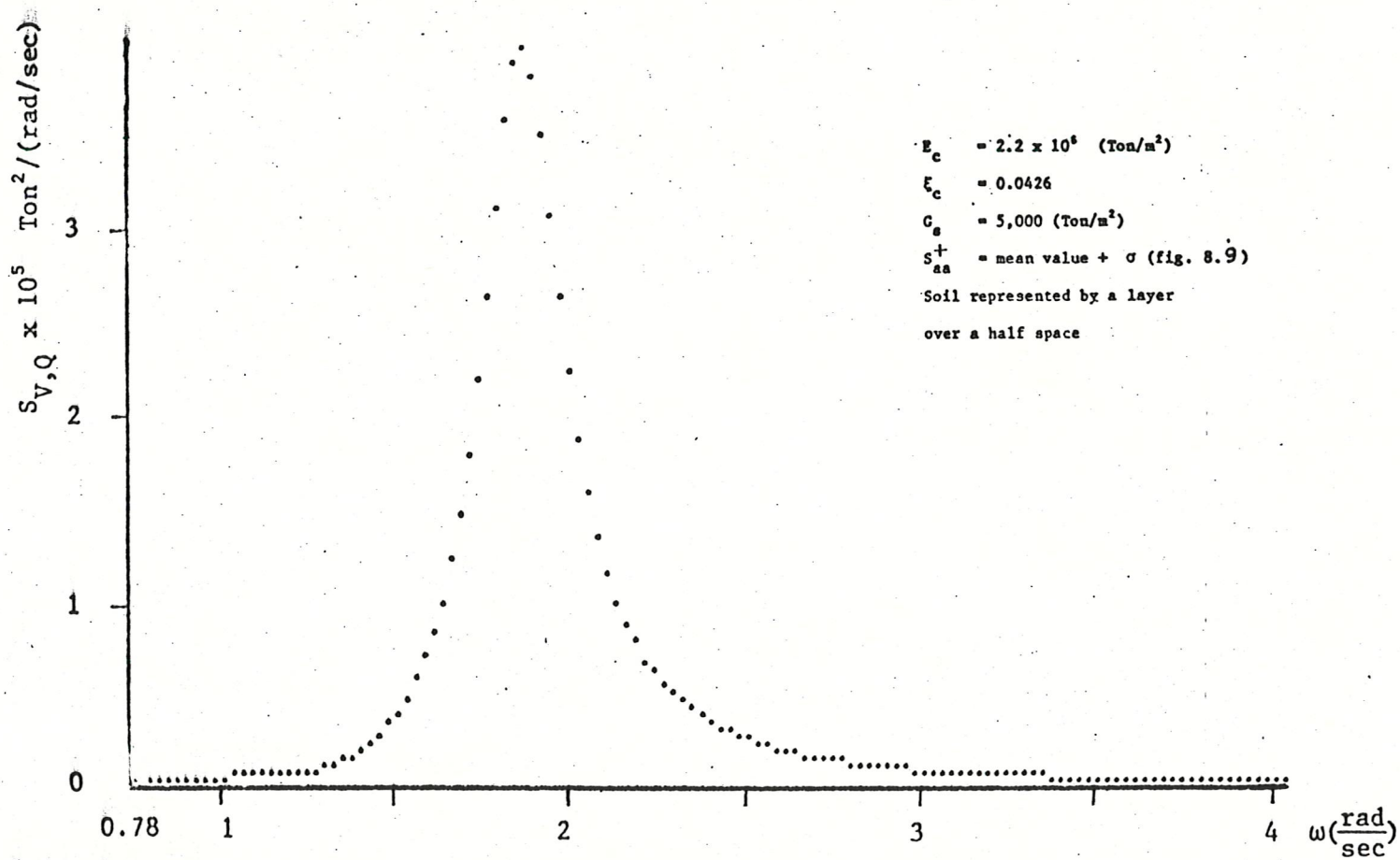

Fig. 8.47 P.s.d.f. of base shear force for seismic excitation, $S_{V,Q}$, as a function of frequency, ω

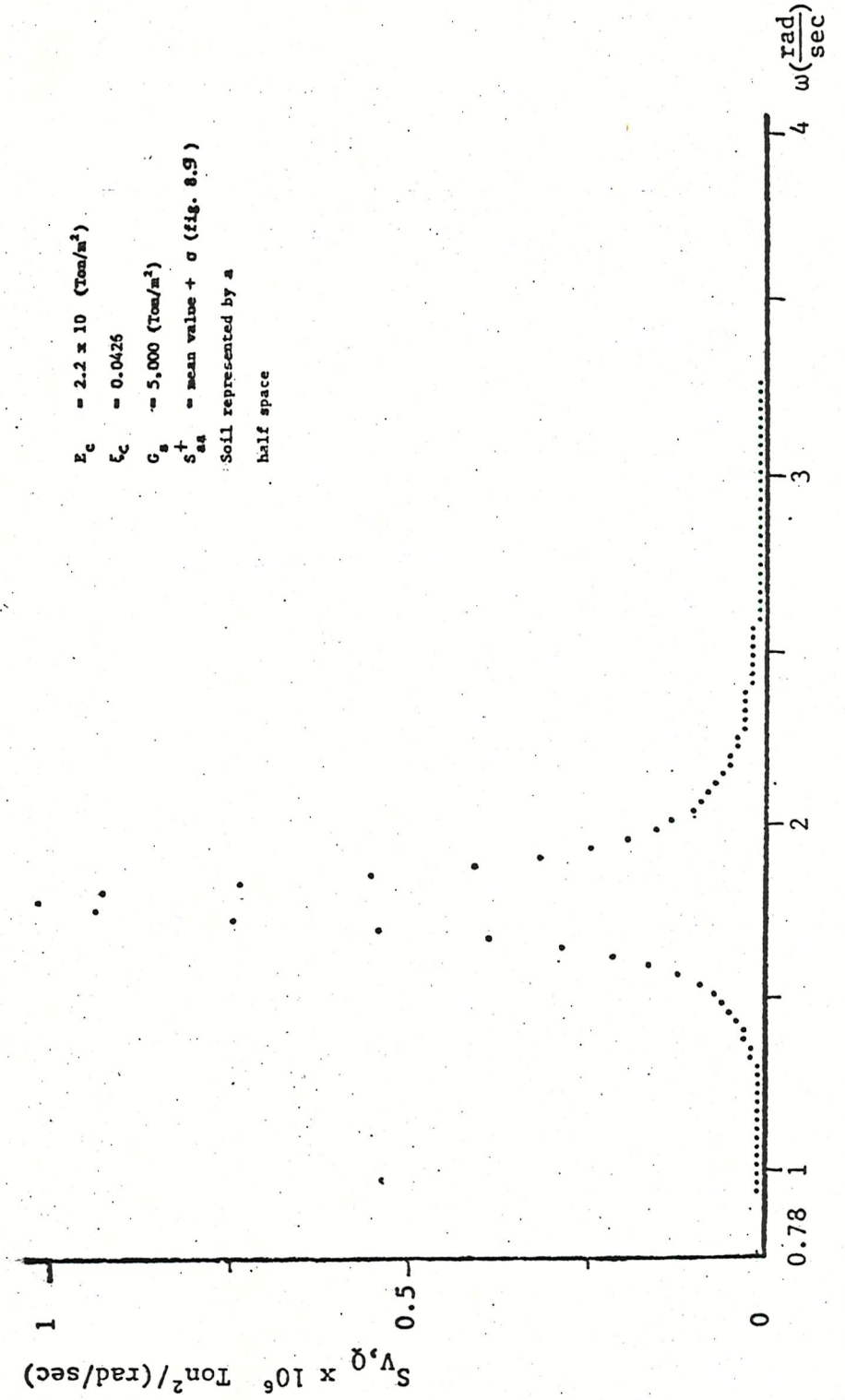

Fig. 8.48 P.s.d.f. of base shear force for seismic excitation, $S_{V,Q}$, as a function of frequency, ω

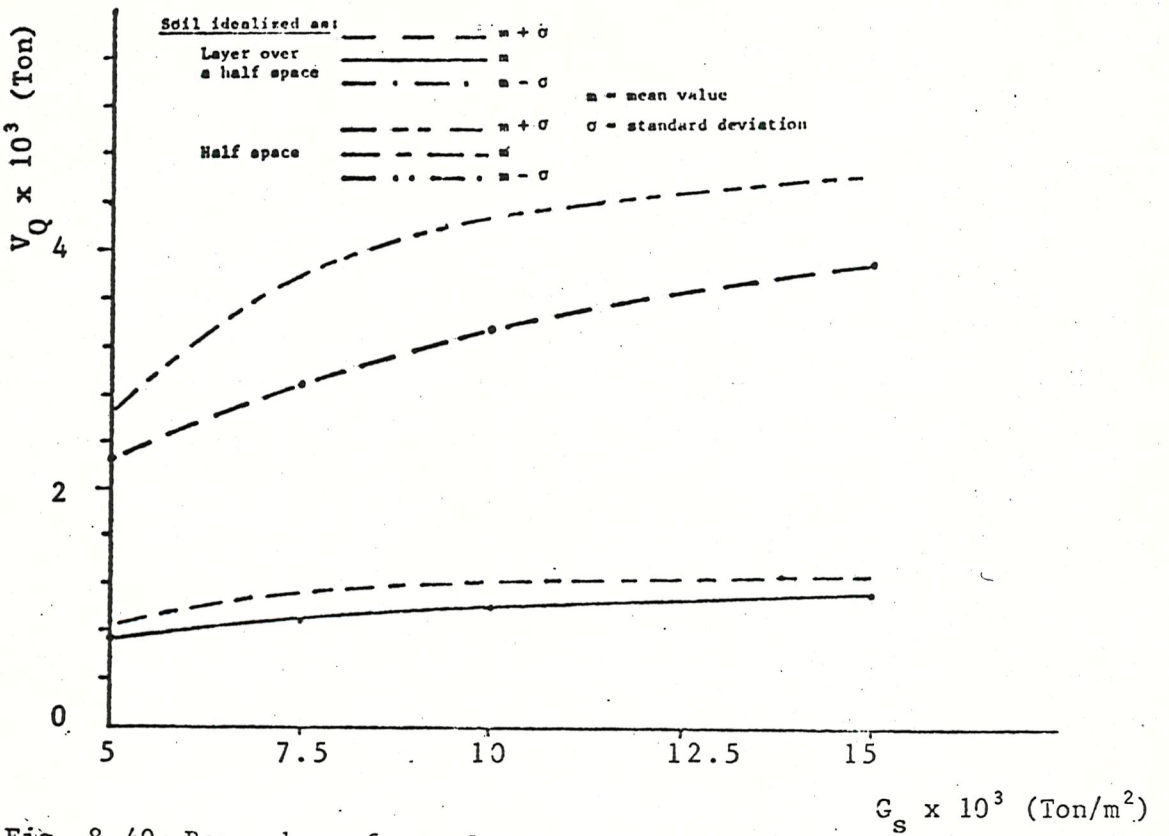

Fig. 8.49 Base shear force for seismic excitation, V_Q, as a function of soil shear modulus, G_s

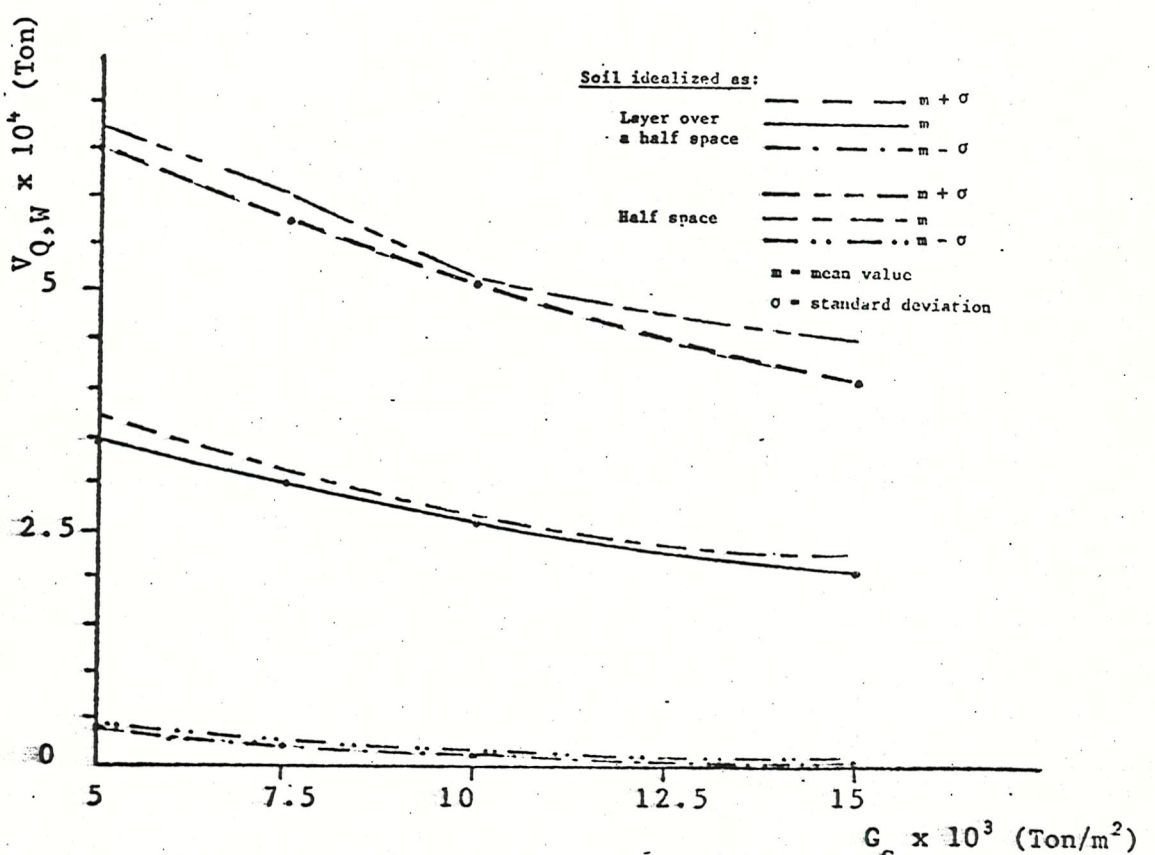

Fig. 8.50 Base shear force for seismic and wave excitation, $V_{Q,W}$, as a function of soil shear modulus, G_s

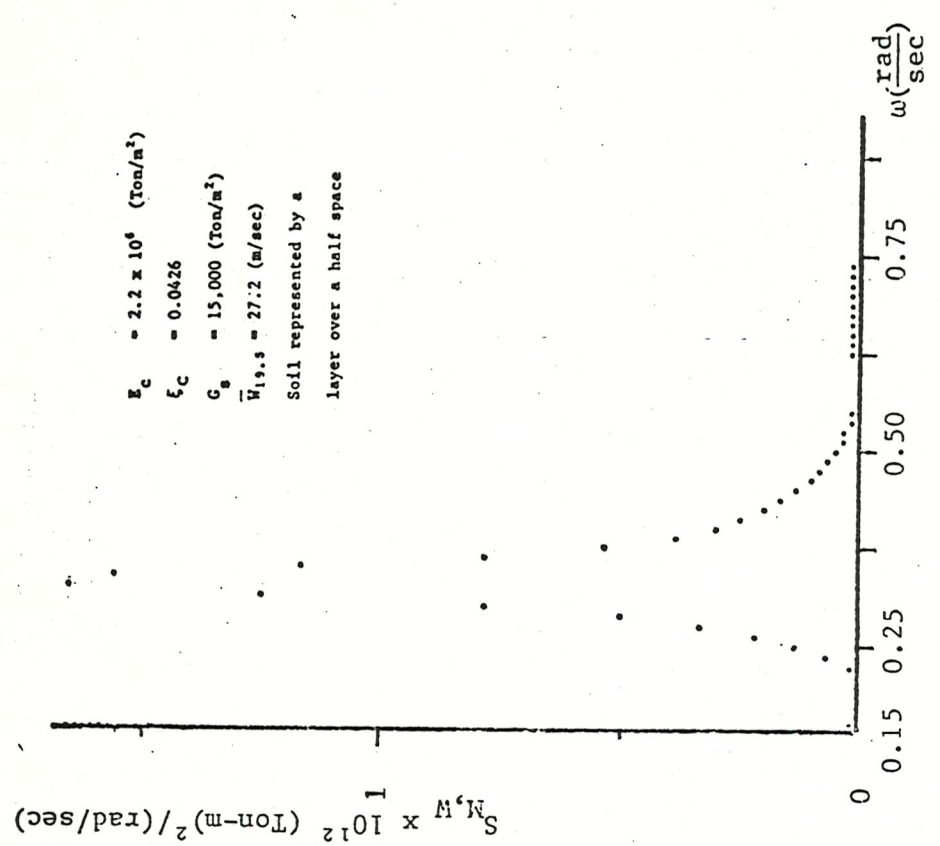

Fig. 8.52 P.s.d.f. of overturning moment for wave excitation, $S_{M,W}$, as a function of frequency, ω

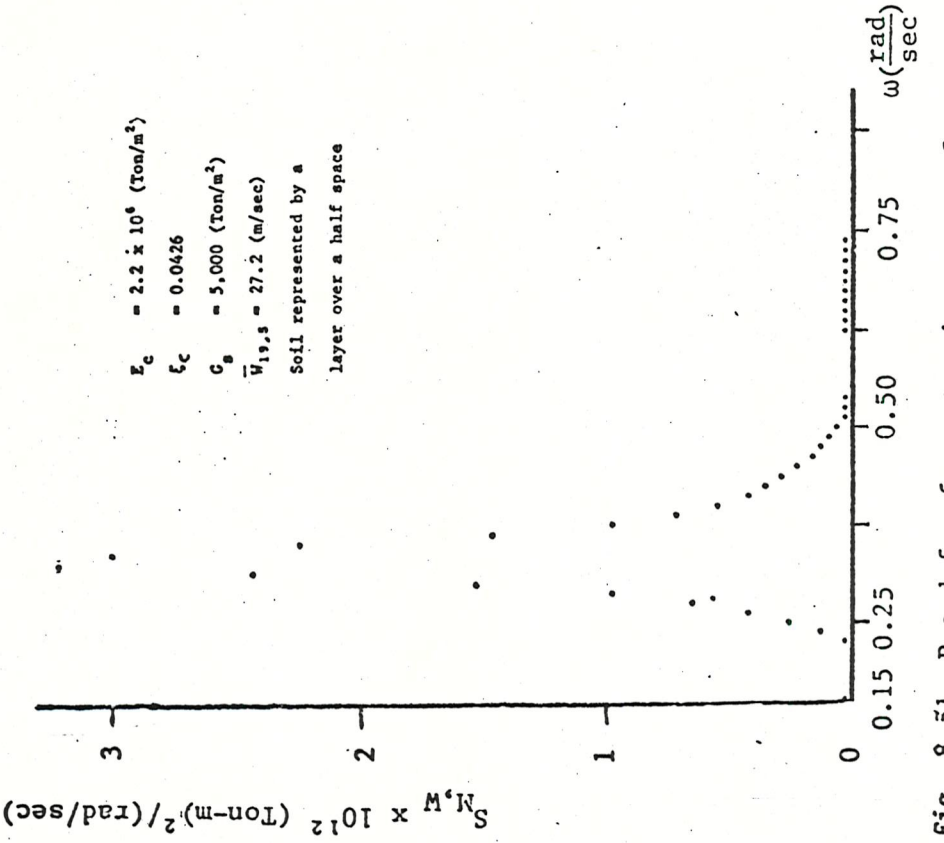

Fig. 8.51 P.s.d.f. of overturning moment for wave excitation, $S_{M,W}$, as a function of frequency, ω

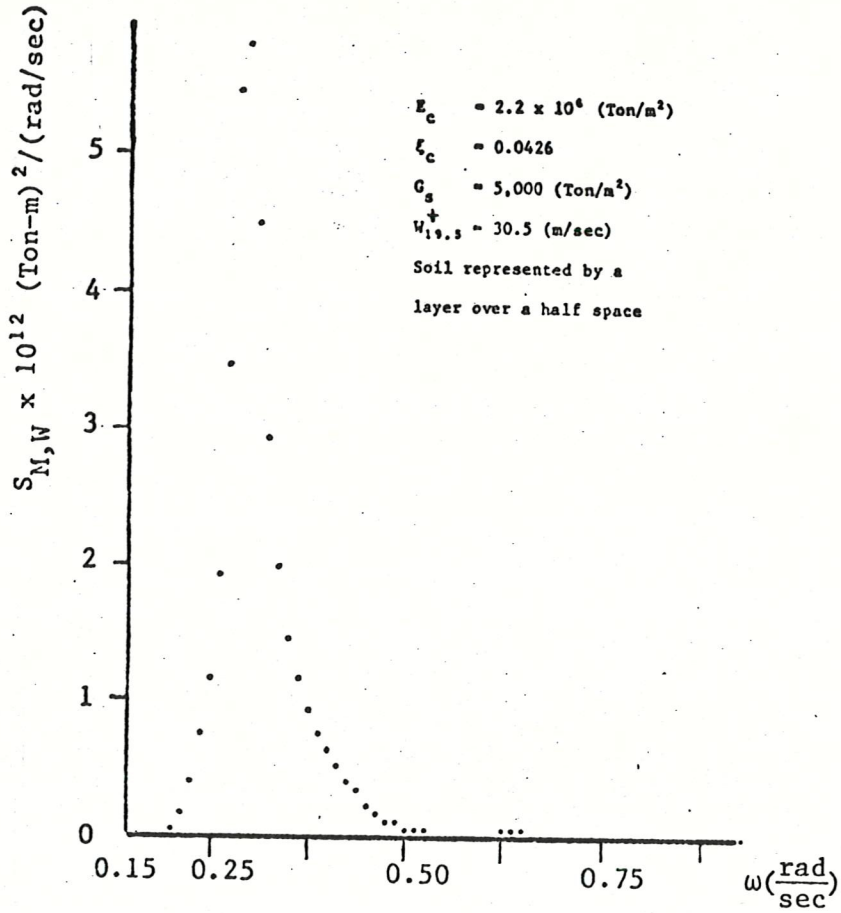

Fig. 8.53 P.s.d.f. of overturning moment for wave excitation, $S_{M,W}$, as a function of frequency, ω

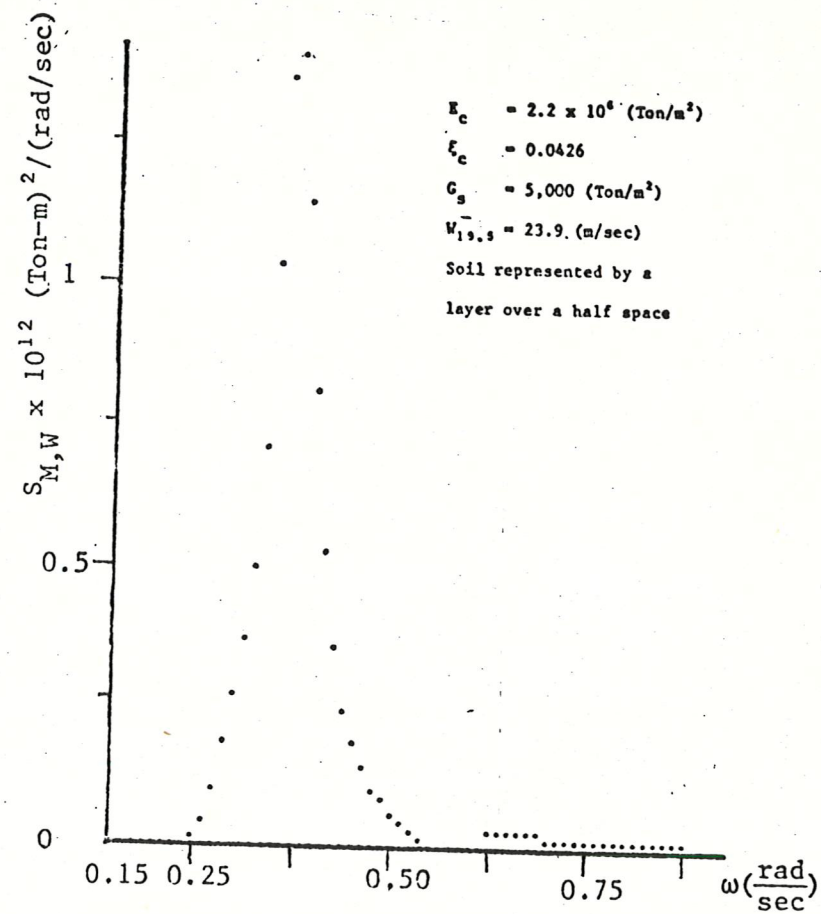

Fig. 8.54 P.s.d.f. of overturning moment for wave excitation, $S_{M,W}$, as a function of frequency, ω

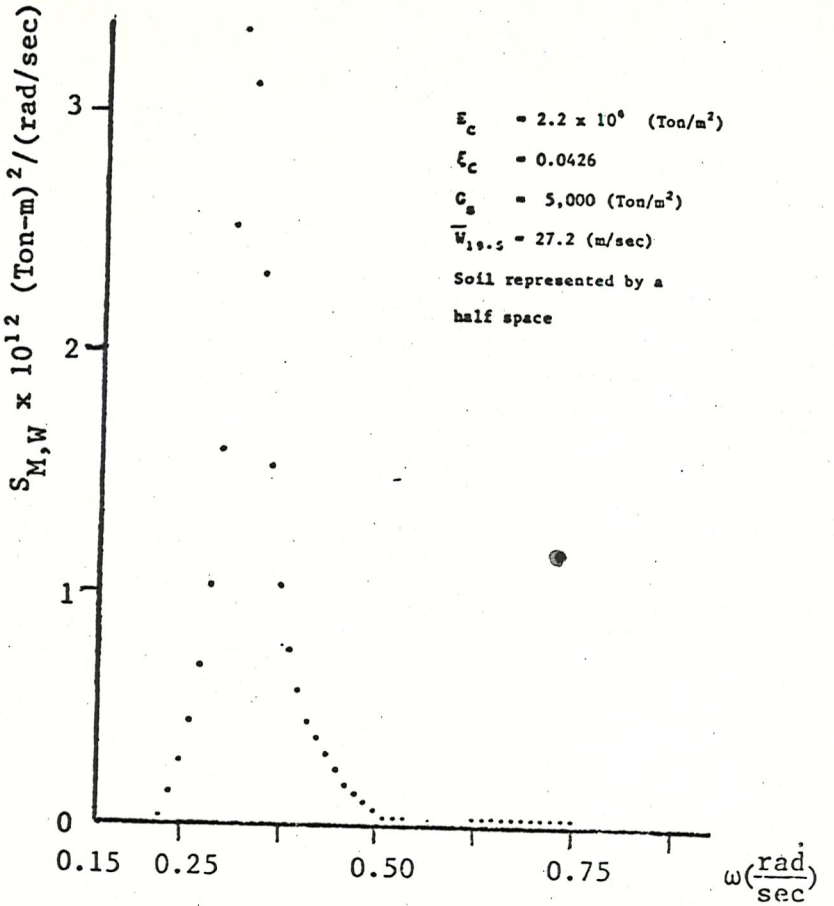

Fig. 8.55 P.s.d.f. of overturning moment for wave excitation, $S_{M,W}$, as a function of frequency, ω

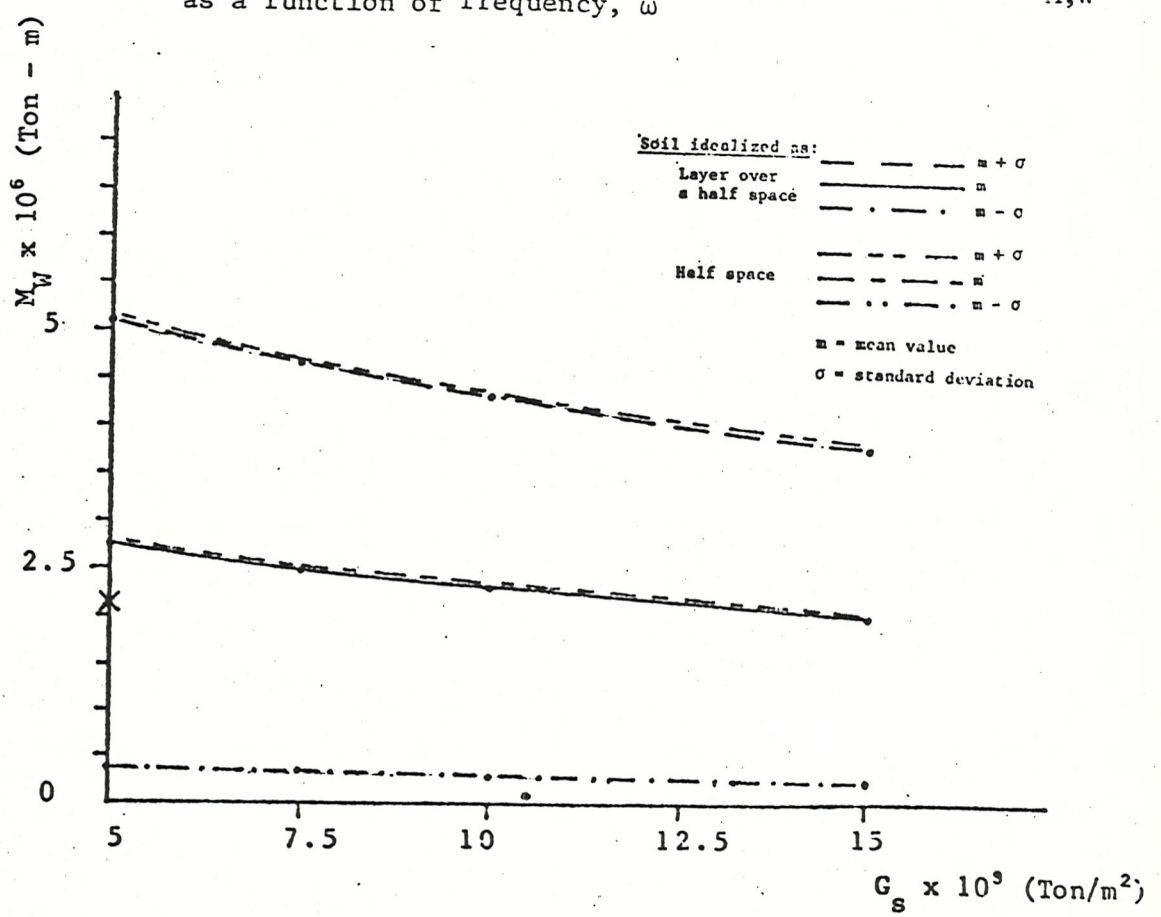

Fig. 8.56 Overturning moment for wave excitation, M_W, as a function of soil shear modulus, G_s

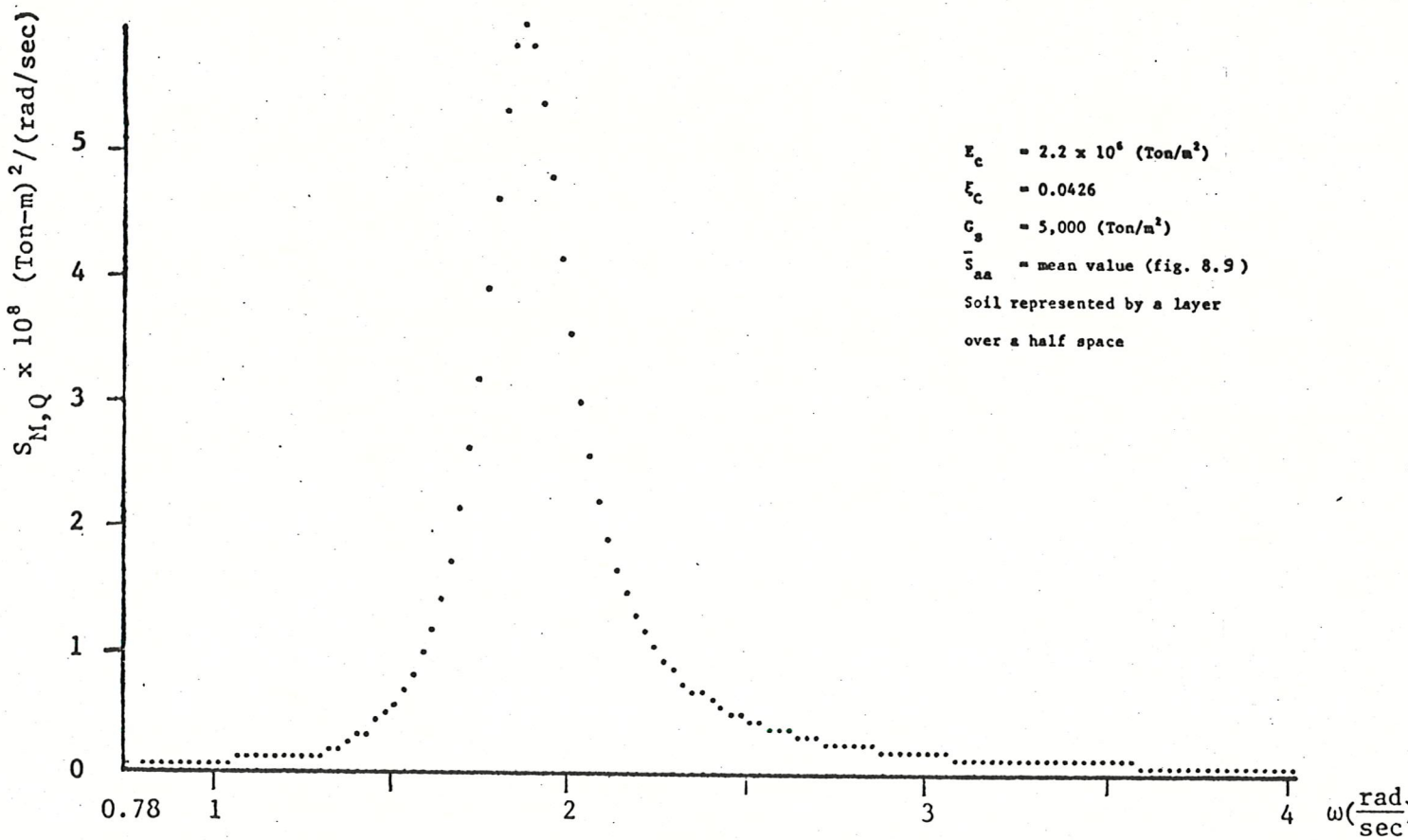

Fig. 8.57 P.s.d.f. of overturning moment for seismic excitation, $S_{M,Q}$, as a function of frequency, ω

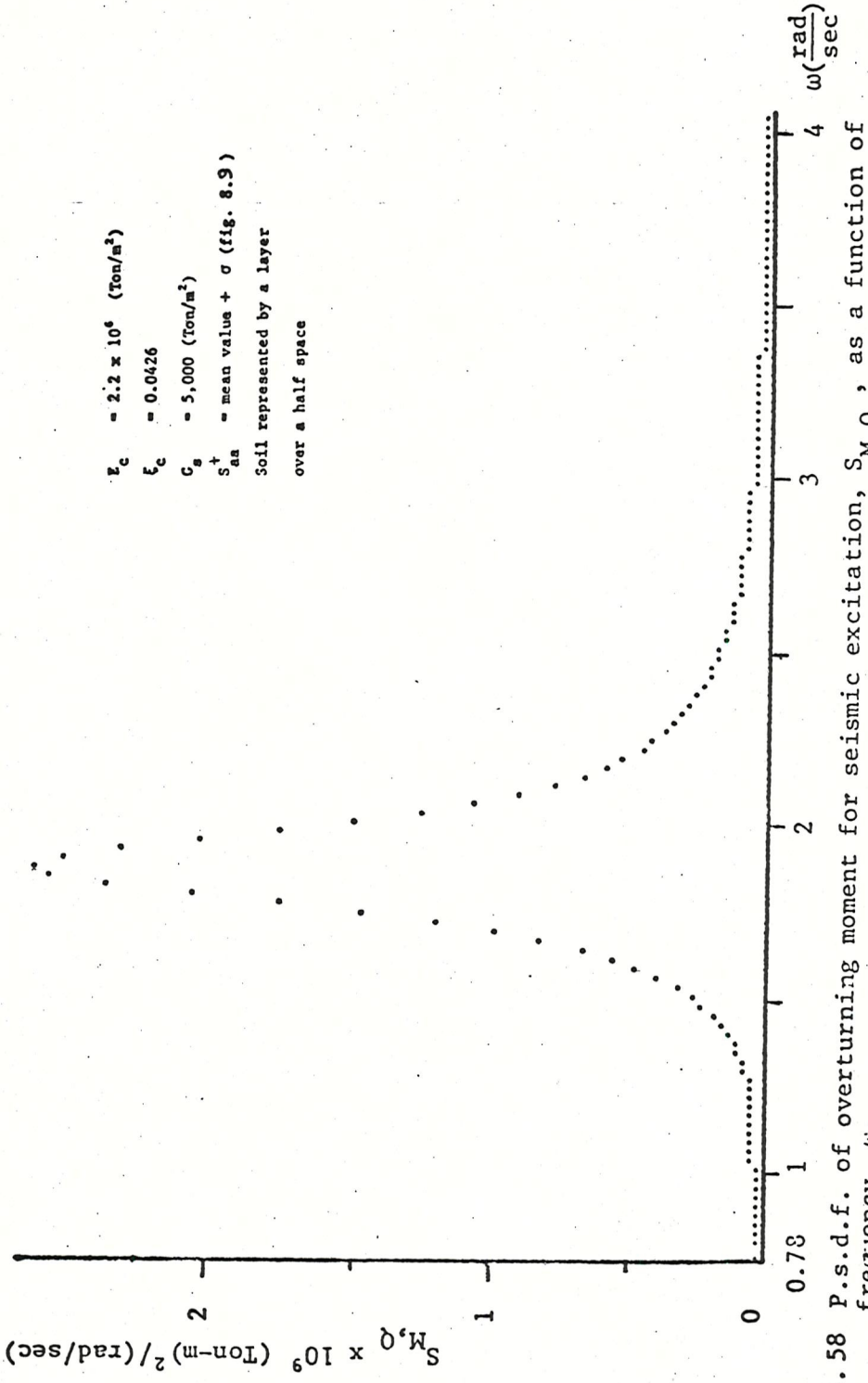

Fig. 8.58 P.s.d.f. of overturning moment for seismic excitation, $S_{M,Q}$, as a function of frequency, ω

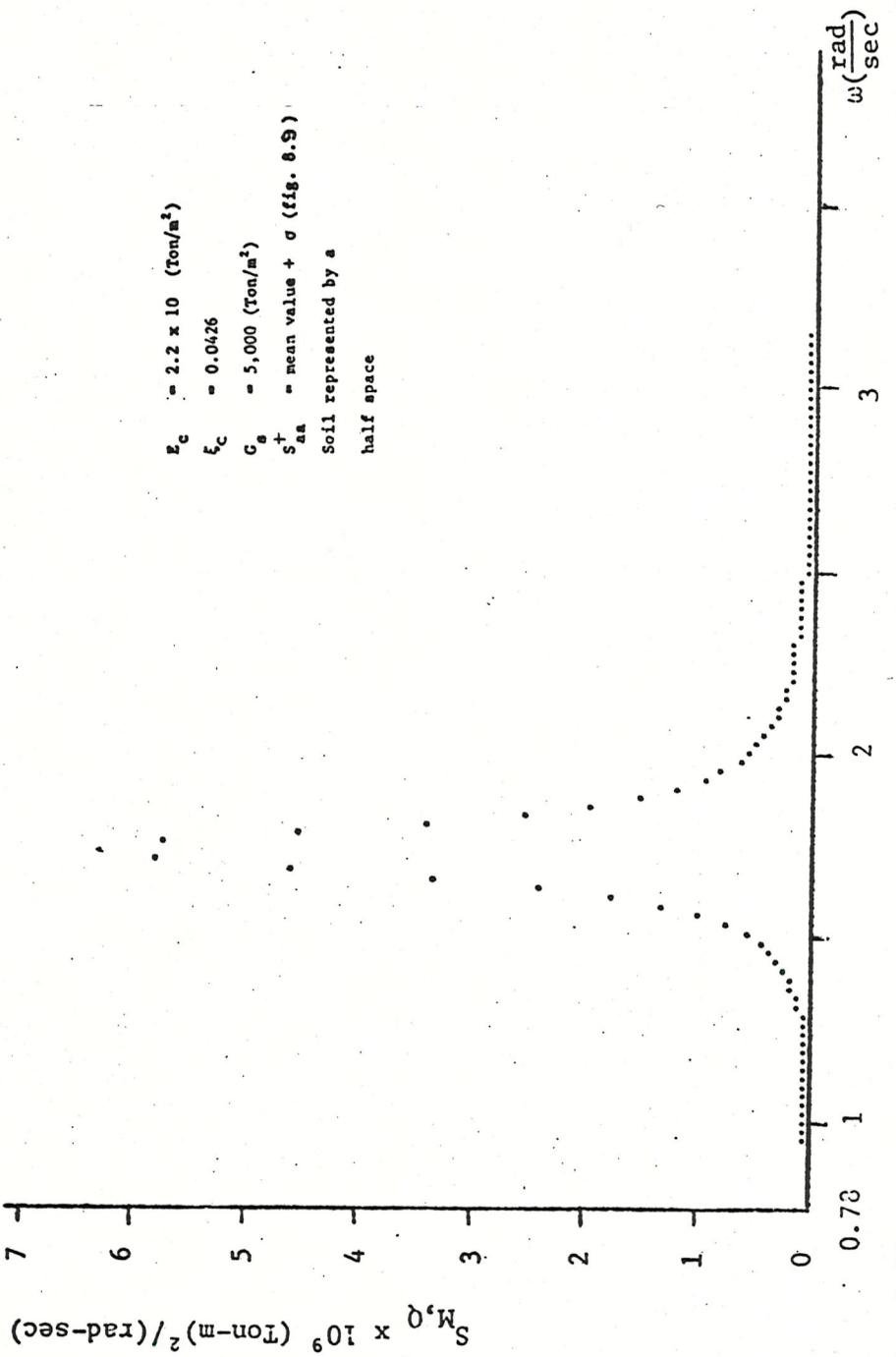

Fig. 8.59 P.s.d.f. of overturning moment for seismic excitation, $S_{M,Q}$, as a function of frequency, ω

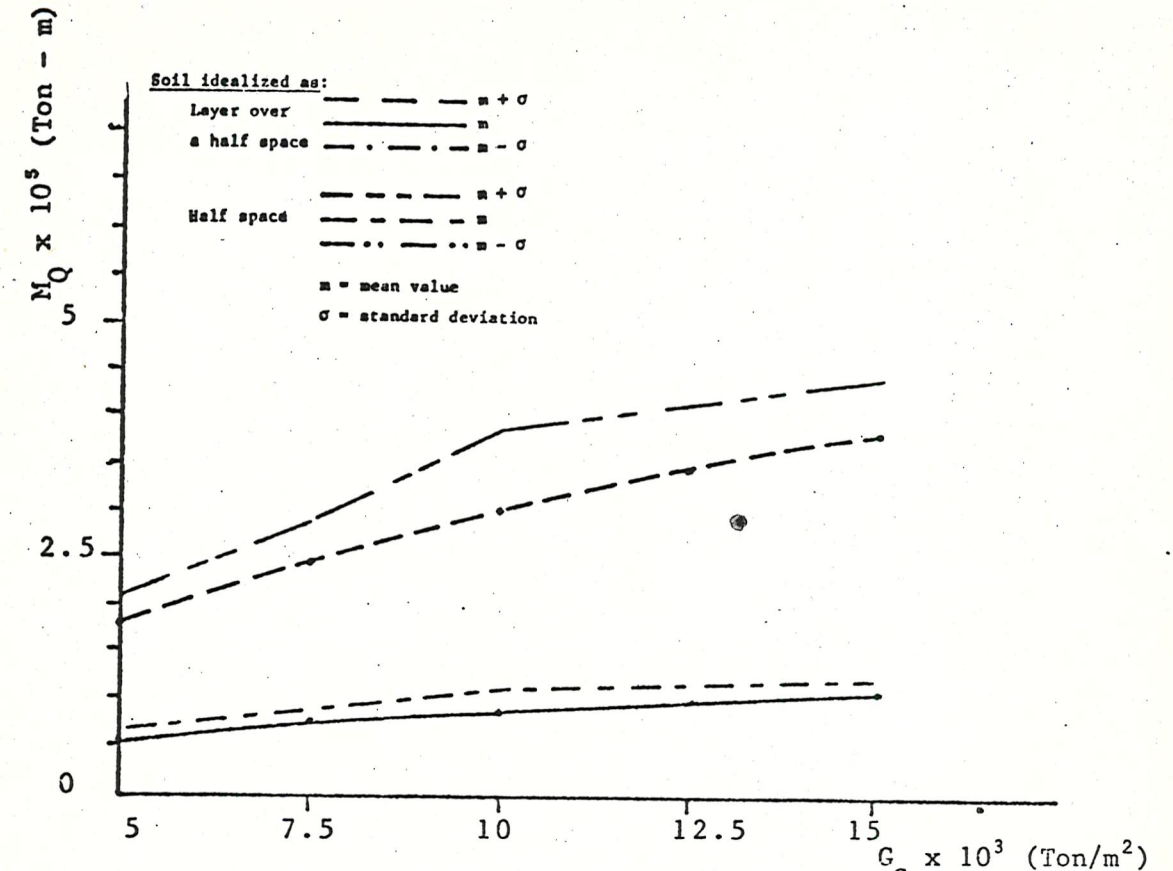

Fig. 8.60 Overturning moment for seismic excitation, M_Q, as a function of soil shear modulus, G_s

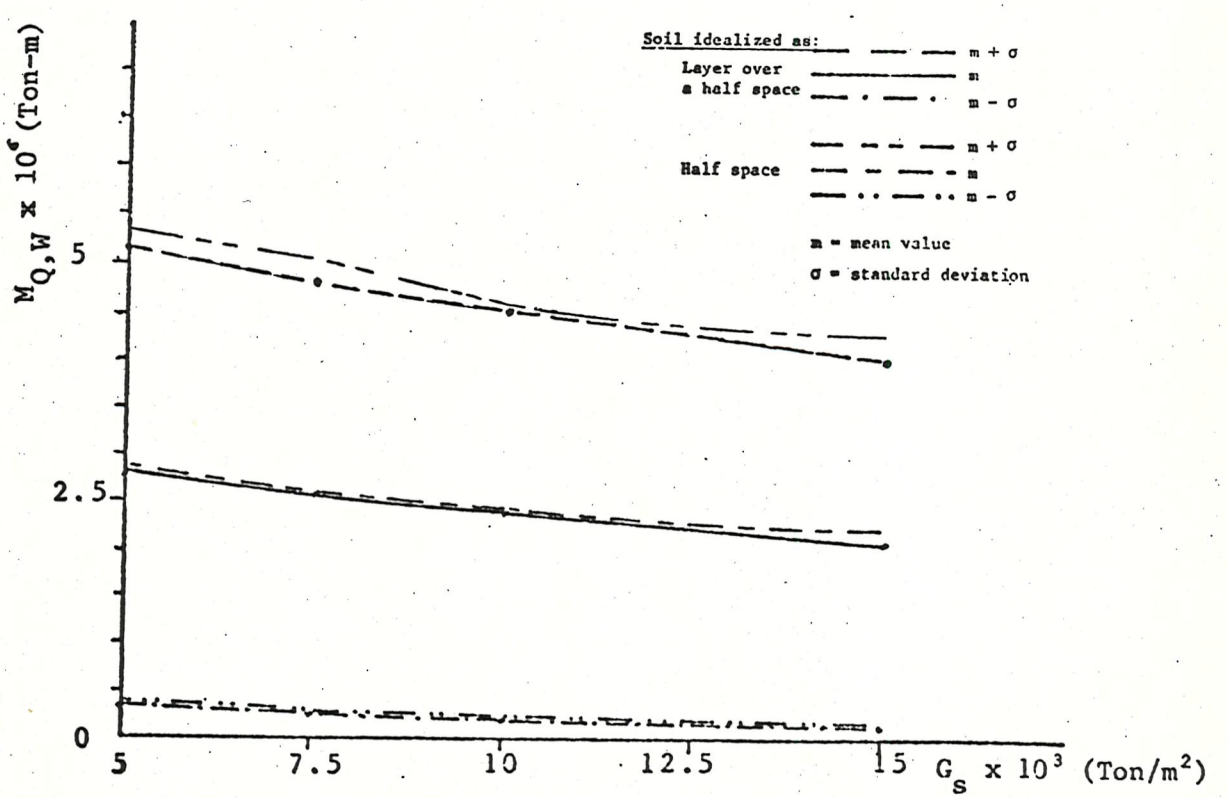

Fig. 8.61 Overturning moment for seismic and wave excitation, $M_{Q,W}$, as a function of soil shear modulus, G_s

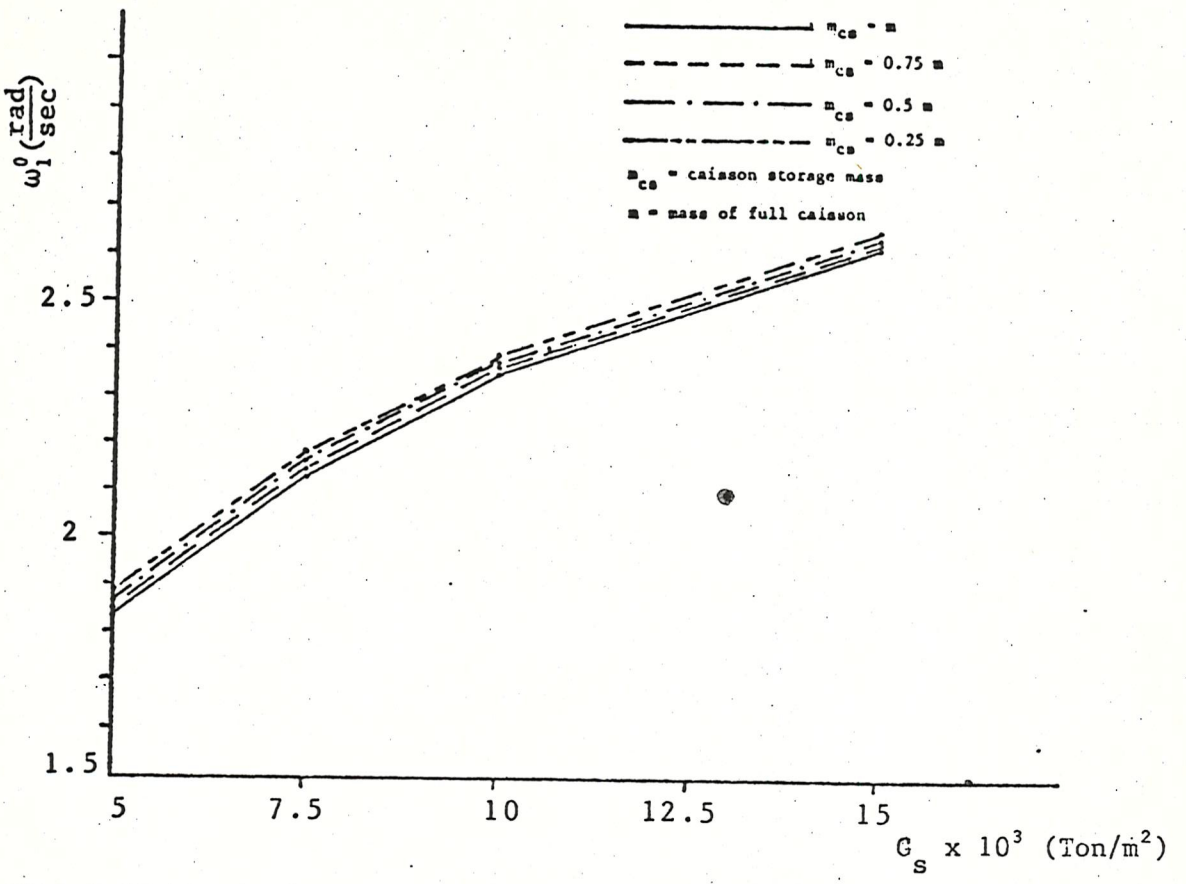

Fig. 8.62 Variation of fundamental frequency, ω_1^0 , with caisson storage mass, as a function of soil shear modulus, G_s

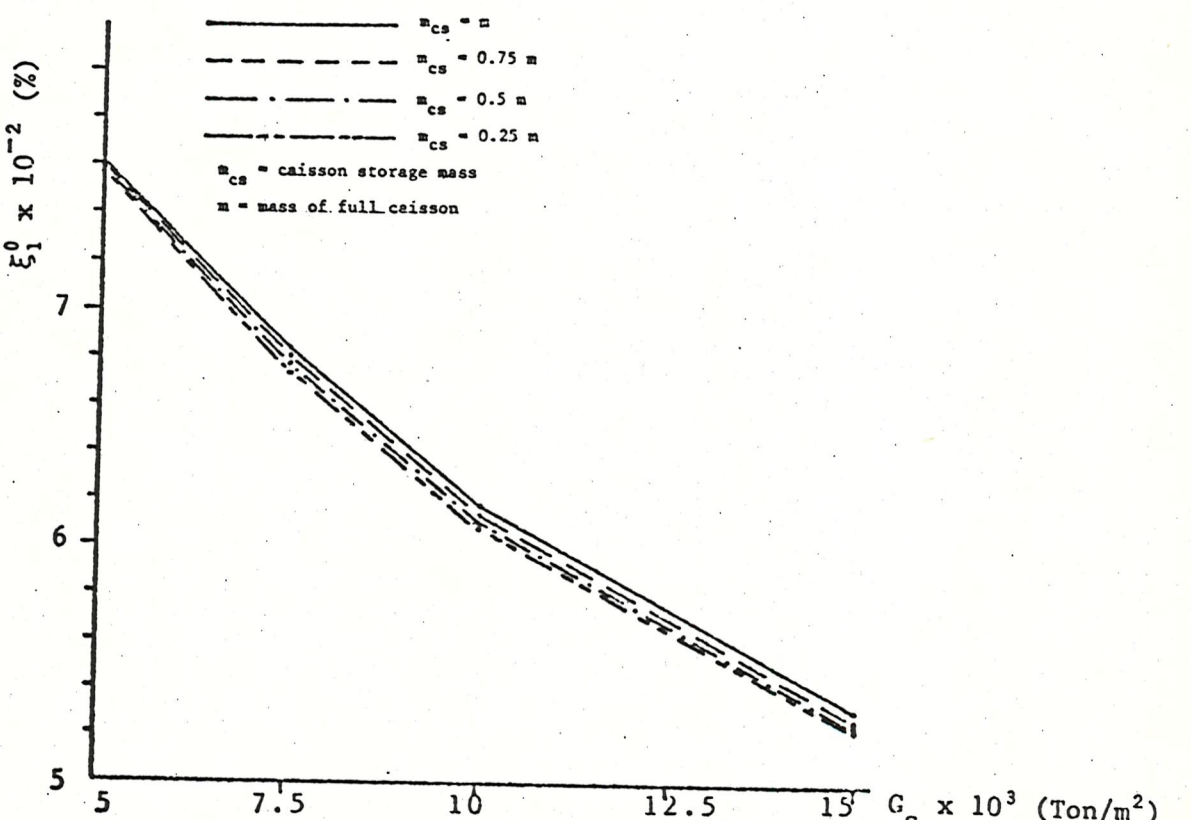

Fig. 8.63 Variation of percentage of critical damping, ξ_1^0 , with caisson storage mass, as a function of soil shear modulus, G_s

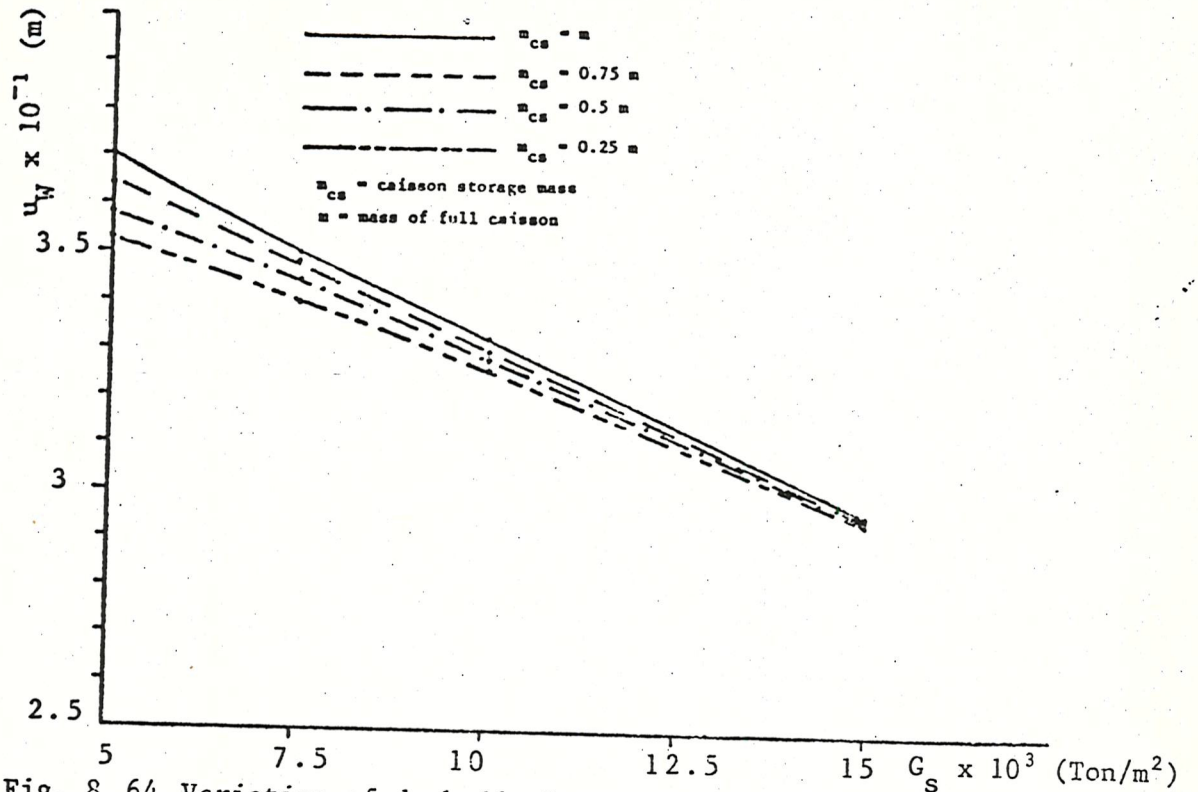

Fig. 8.64 Variation of deck displacement for wave excitation, u_W, with caisson storage mass, as a function of soil shear modulus, G_s

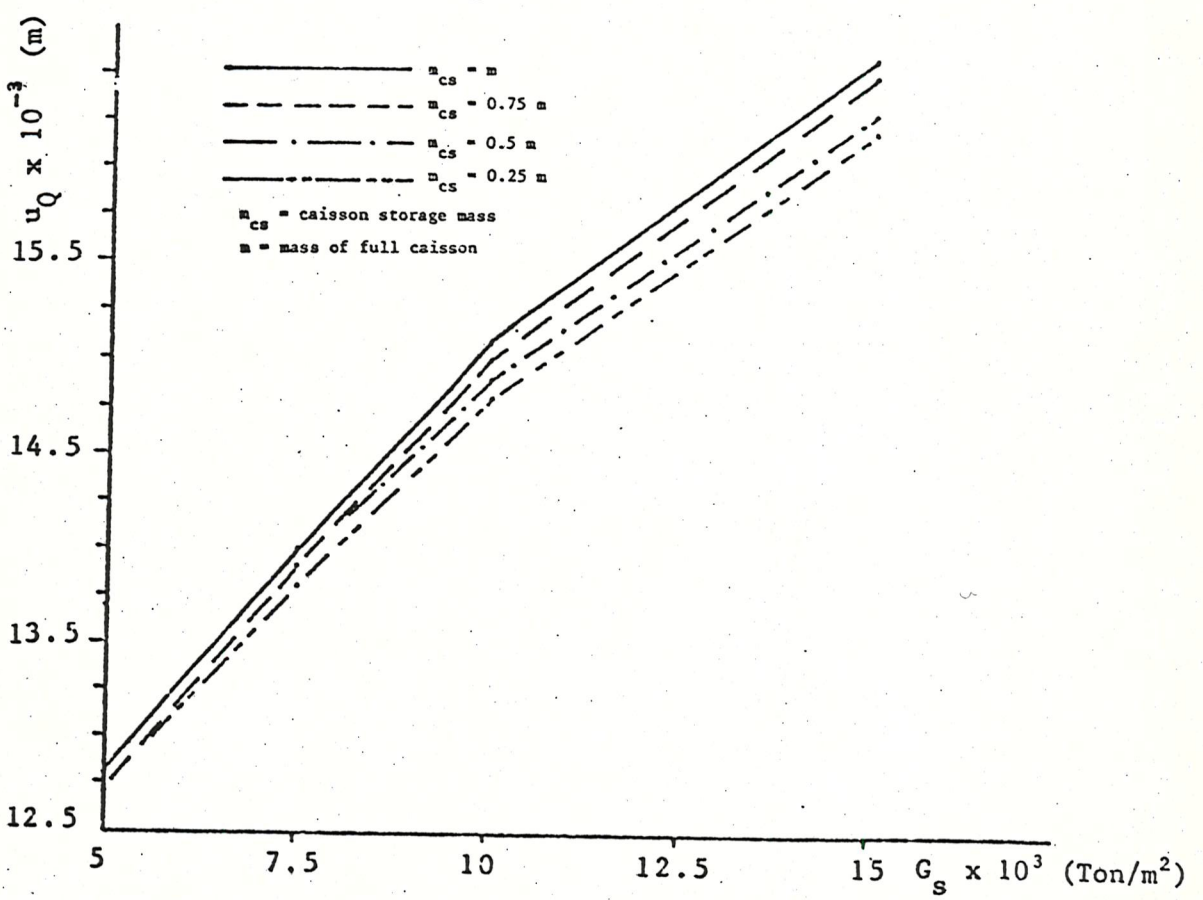

Fig. 8.65 Variation of deck displacement for seismic excitation, u_Q, with caisson storage mass, as a function of soil shear modulus, G_s

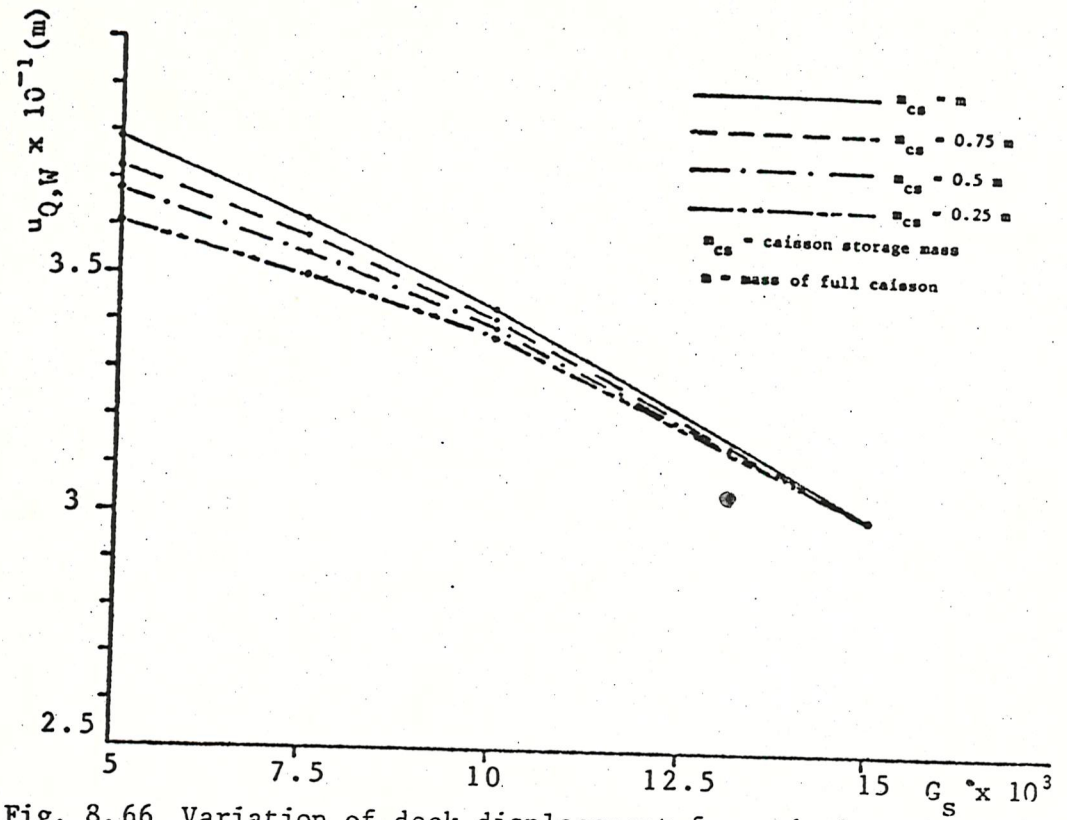

Fig. 8.66 Variation of deck displacement for seismic and wave excitation, $u_{Q,W}$, with caisson storage mass, as a function of soil shear modulus, G_s

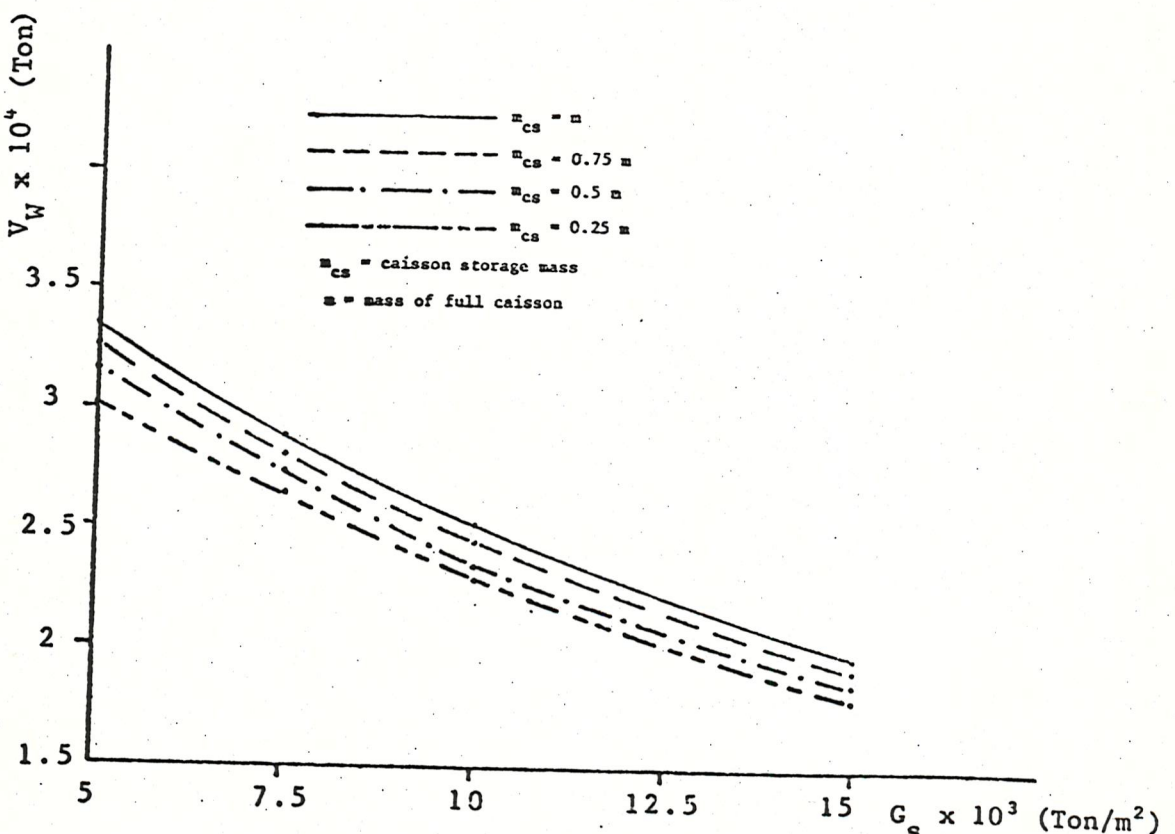

Fig. 8.67 Variation of base shear force for wave excitation, V_W, with caisson storage mass, as a function of soil shear modulus, G_s

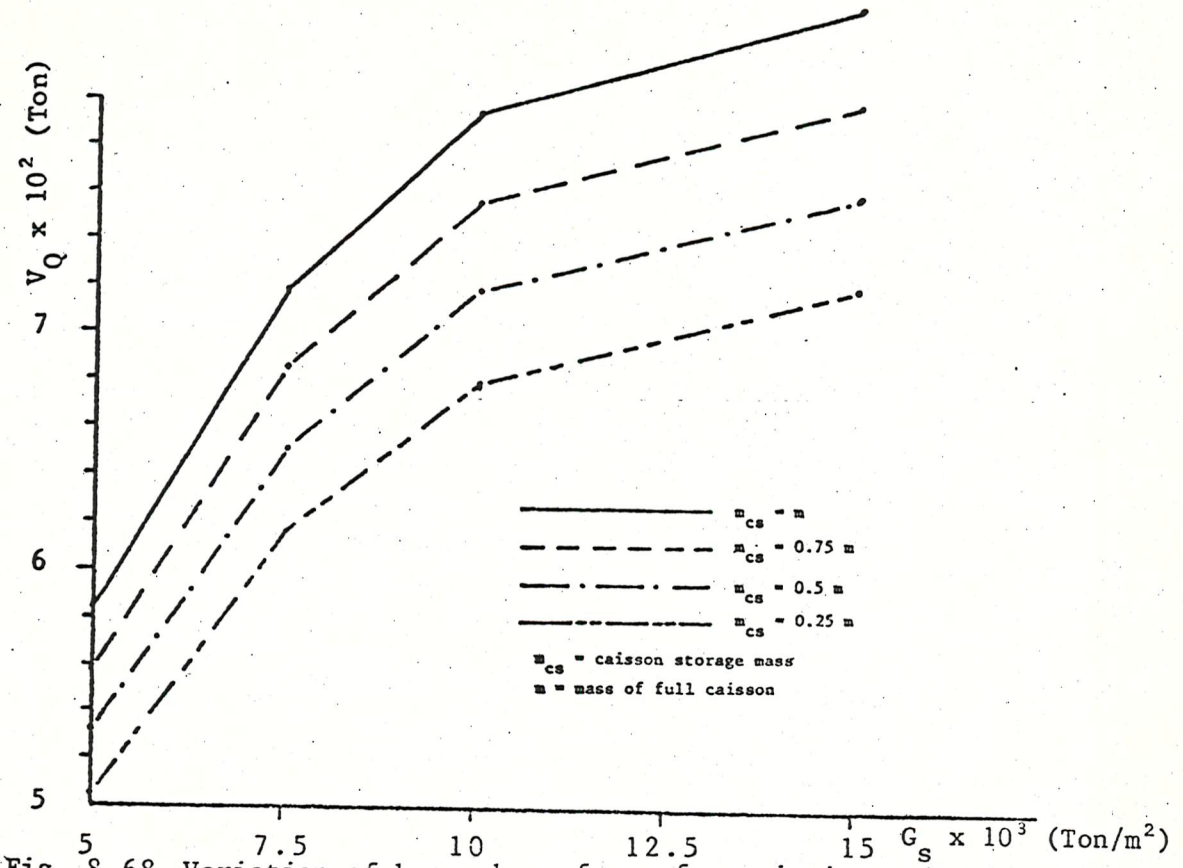

Fig. 8.68 Variation of base shear force for seismic excitation, V_Q, with caisson storage mass, as a function of soil shear modulus, G_s

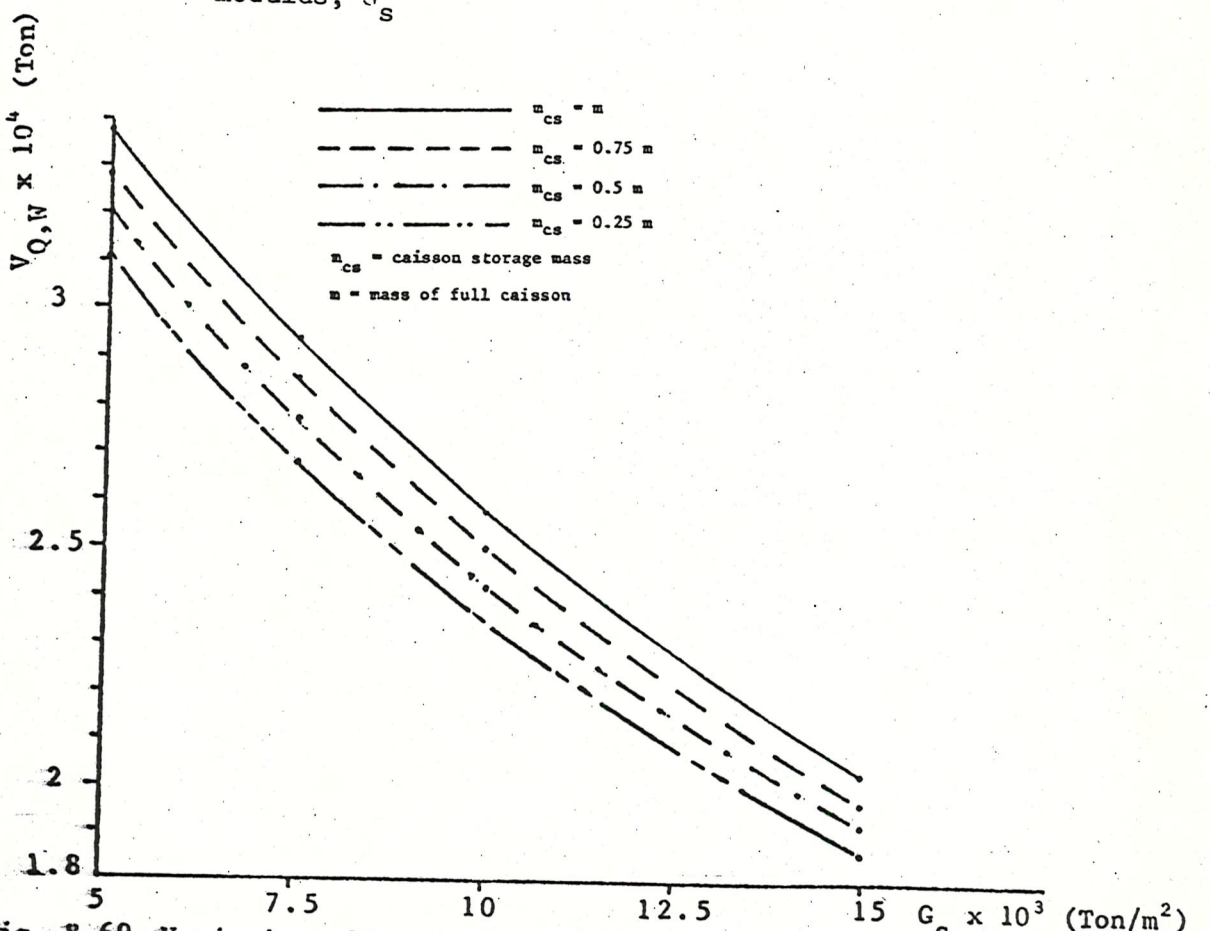

Fig. 8.69 Variation of base shear force for seismic and wave excitation, $V_{Q,W}$, with caisson storage mass, as a function of soil shear modulus, G_s

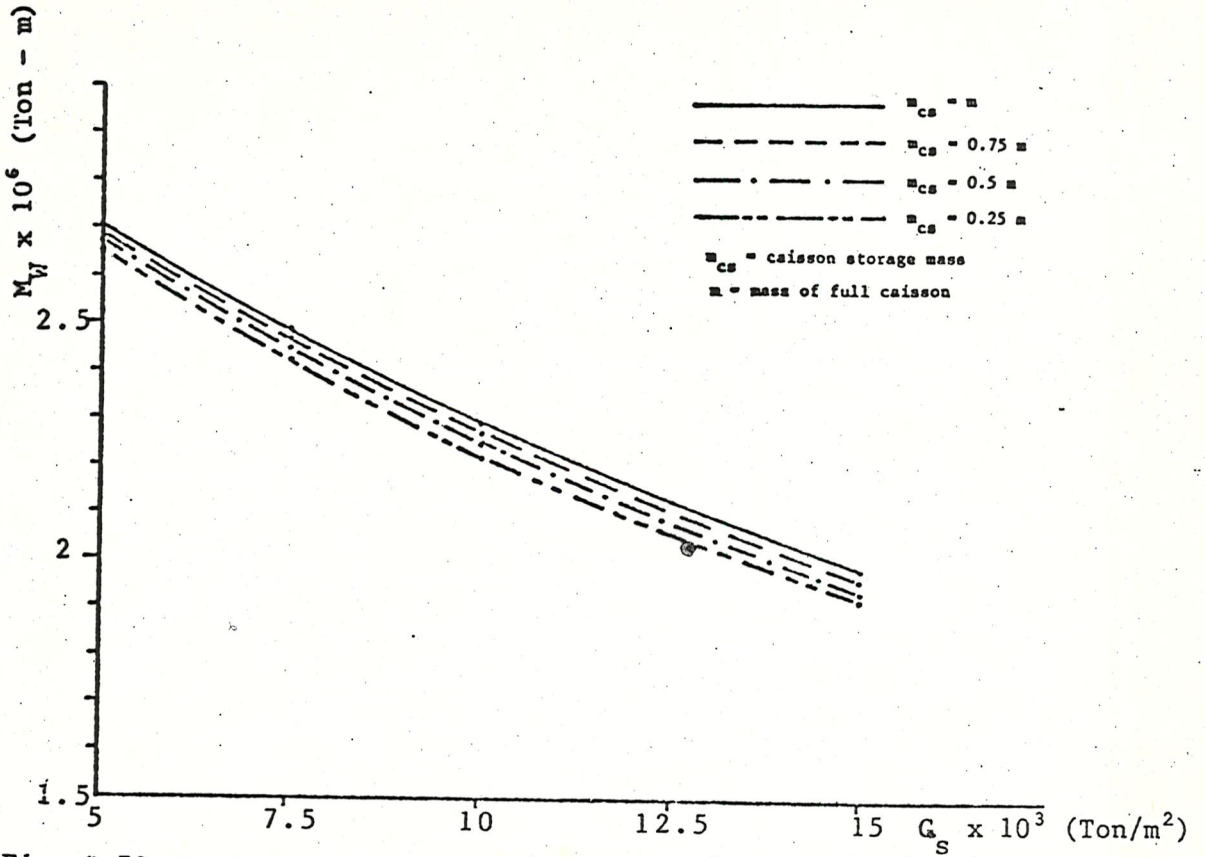

Fig. 8.70 Variation of overturning moment for wave excitation, M_W, with caisson storage mass, as a function of soil shear modulus, G_s

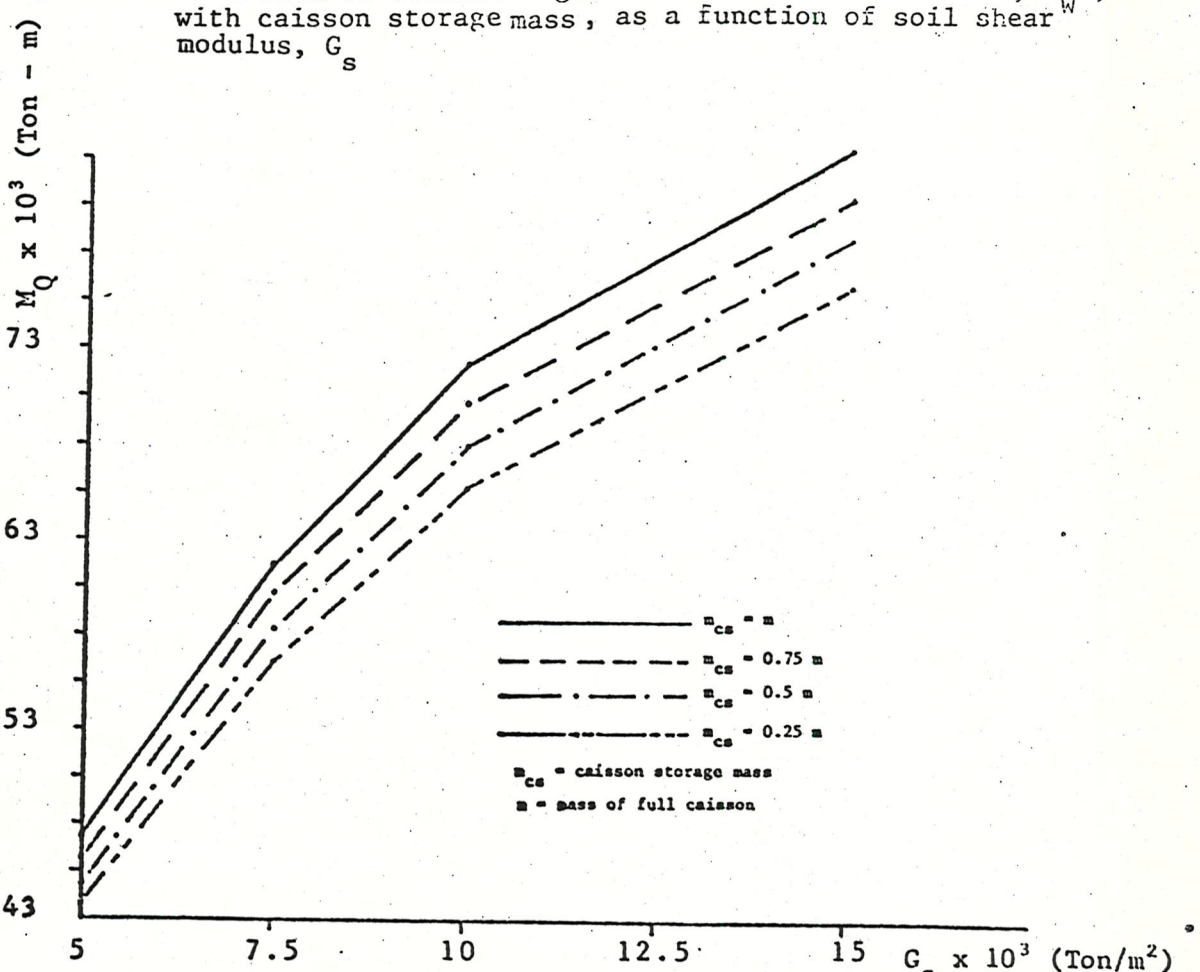

Fig. 8.71 Variation of overturning moment for seismic excitation, M_Q, with caisson storage mass, as a function of soil shear modulus, G_s

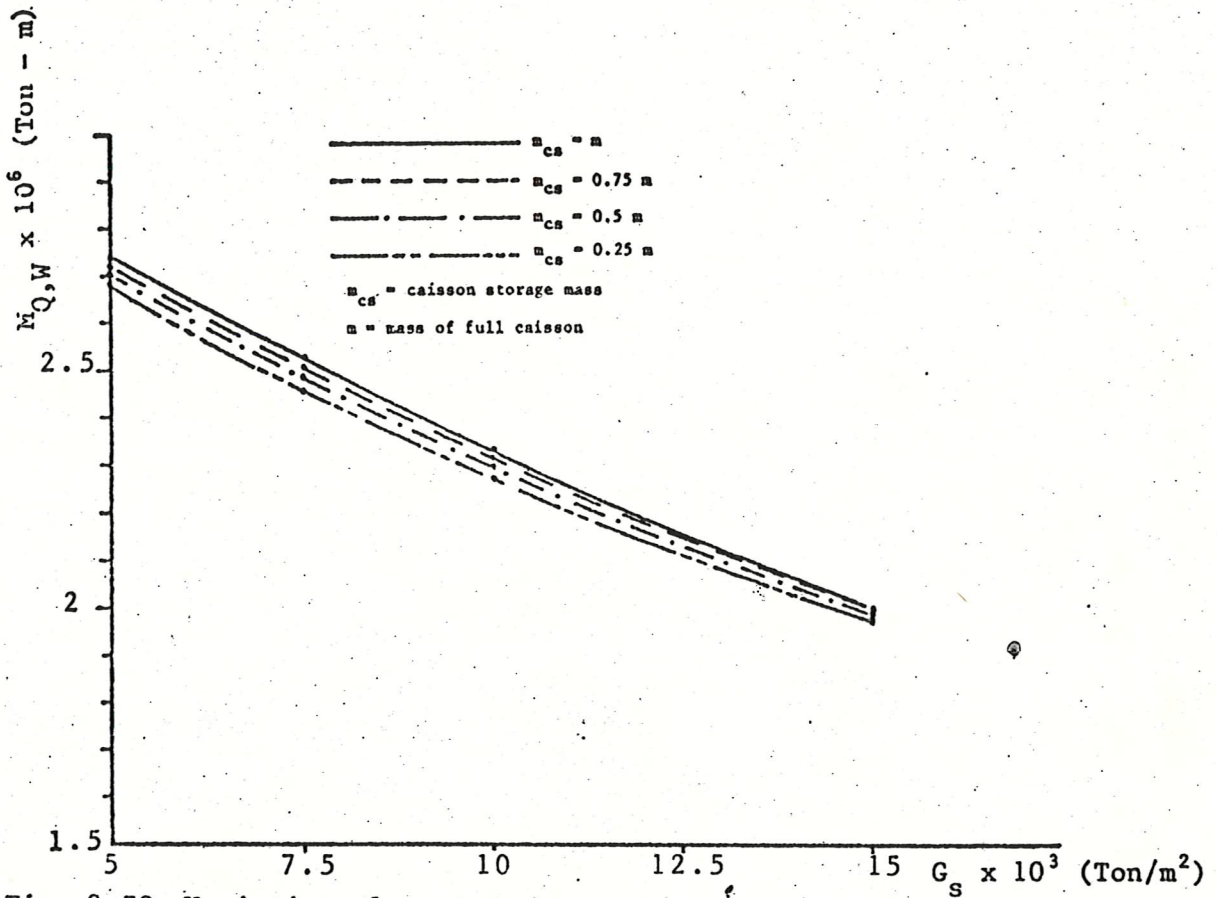

Fig. 8.72 Variation of overturning moment for seismic and wave excitation, $M_{Q,W}$, with caisson storage mass, as a function of soil shear modulus, G_s